Fall 12-20-2013

High Yield Solvothermal Synthesis of Hexaniobate Based Nanocomposites via the Capture of Preformed Nanoparticles in Scrolled Nanosheets

Shivaprasad Reddy Adireddy
University of New Orleans, sadiredd@uno.edu

High Yield Solvothermal Synthesis of Hexaniobate Based Nanocomposites via the Capture of Preformed Nanoparticles in Scrolled Nanosheets

A Dissertation

Submitted to the Graduate Faculty of the
University of New Orleans
in partial fulfillment of the
requirements for the degree of

Doctor of Philosophy
in
Chemistry

By

Shivaprasad Reddy Adireddy

B.S. Osmania University, 2005
M.S. University of New Orleans, 2011

To The People Who Make This World A Better Place

Acknowledgements

Along the journey of my Ph.D. I have been helped by several people. First I wish to express my deep gratitude and sincere thank you to my research advisor Professor John B. Wiley for his cooperation, constructive criticism, encouragement and valuable guidance during the course of my study. After joining the group, I always received enormous amount of help from my adviser in choosing my project and setting up my work space. I am truly grateful for his keen interest, responsive action, remarkable feedback and extreme support throughout the course of my research.

I also would like to thank my dissertation committee members, Prof. Mathew Tarr, Prof. Leszek Malkinski, and Prof. Steven Rick, for helpful discussions and suggestions. I am also thankful to each and every member of Department of Chemistry and Advanced Materials Research Institute for their help and support throughout my PhD. They are also acknowledged for providing an academically stimulating environment in the department.

I am thankful to my present and past group members, namely Dr. Yuan Yao, Dr. Elisha Josepha, Dr. Debasish Mohanty, Dr. Girija S. Chaubey, Mohammad Montasserasadi, Jagnyaseni Tripathy, Lea Gustin, Cecilia Carbo, Taha Rostamzade, Treva Brown, Mayra Franco and Sara Tefaghi. I remember all the great moments that I had with my group members, I am thankful for their time, and great friendship. It was an honor and great pleasure to be a part of the Wiley group.

The project work would not have been possible without the friendly support and timely help of my colleagues and friends, especially Prof. Leonard Spinu, Dr. Jose Vargas, Dr. Avijit Biswas, Dr. Jiajun Chen, Dr. Kai Wang, Dr. Bao Bao Cao, Sarah Wozny, Pramathesh Maji, Sanjeeva Dodlapati, Abhishek Srivastava, Satish Rai, Sudhendu Azad, Pinkesh Attarwala,

Sravan Burla, Vempati Satheesh, Deepak Mudili, Thilo Buck, Curt Click, Vijay Burla, Rupal Shah, Jenny Martin, Aubrie Pfirman, Jugal Shah, Thilo Buck, Rajesh Komatineni, Meet Singh, Rupa Biradar, and Sandeep Bandi.

I also want to thank my grandparents, family friends and relatives for their wishes, blessings, and help; and last, but not least, my parents, for their endless love, support, and encouragement.

Financial support from the Louisiana Board of Regents Post-Katrina Support Fund Initiative (PKSFI) is gratefully acknowledged.

Table of Contents

List of Figures

List of Tables

Abstract

The ability to encapsulate linear nanoparticle (NP) chains in scrolled nanosheets is an important advance in the formation of nanocomposites. These nanopeapods (NPPs) exhibit interesting properties that may not be achieved by individual entities. Consequently, to fully exploit the potential of NPPs, the fabrication of NPPs must focus on producing composites with unique combinations of morphologically uniform nanomaterials. Various methods can produce NPPs, but expanding these methods to a wide variety of material combinations can be difficult. Recent work in our group has resulted in the in situ formation of peapod-like structures based on chains of cobalt NPs. Building on this initial success, a more versatile approach has been developed that allows for the capture of a series of preformed NPs in NPP composites.

In the following chapters, various synthetic approaches for NPPs of various material combinations will be presented and the key roles of various reaction parameters will be discussed. Also, uniform hexaniobate nanoscrolls were fabricated via a solvothermal method induced by heating up a mixture of TBAOH, hexaniobate crystallites, and oleylamine in toluene. The interlayer spacing of the nanoscrolls was easily tuned by varying the relative amount and chain lengths of the primary alkylamines.

To fabricate NPPs, as-synthesized NPs were treated with hexaniobate crystallite in organic mixtures via solvothermal method. During solvothermal treatment, exfoliated hexaniobate nanosheets scroll around highly ordered chains of NPs to produce the target NPP structures in high yield. Reaction mixtures were held at an aging temperature for a few hours to fabricate various new NPPs (Fe_3O_4@hexaniobate, Ag@hexaniobate, Au@hexaniobate, Au-

Fe_3O_4@hexaniobate, TiO_2@hexaniobate, CdS@hexaniobate, CdSe@hexaniobate, and ZnS@hexaniobate).

This versatile method was first developed for the fabrication of magnetic peapod nanocomposites with preformed nanoparticles (NPs). This approach is effectively demonstrated on a series of ferrite NPs (≤ 14 nm) where Fe_3O_4@hexaniobate NPPs are rapidly (~ 6 h) generated in high yield. When NP samples with different sizes are reacted, clear evidence for size selectivity is seen. Magnetic dipolar interactions between ferrite NPs within the Fe_3O_4@hexaniobate samples leads to a significant rise in coercivity, increasing almost four-fold relative to free particles. Other magnetic ferrites NPPs, MFe_2O_4@hexaniobate (M = Mn, Co, Ni), can also be prepared. This synthetic approach to nanopeapods is quite versatile and should be readily extendable to other, non-ferrite NPs or NP combinations so that cooperative properties can be exploited while the integrity of the NP assemblies is maintained. Further, this approach demonstrated selectivity by encapsulating NPs according to their size.

The use of polydispersed NP systems is also possible and in this case, evidence for size and shape selectivity was observed. This behavior is significant in that it could be exploited in the purification of inhomogeneous NP samples. Other composite materials containing silver and gold NPs are accessible. Partially filled Fe_3O_4@hexaniobate NPPs were used as templates for the in situ growth of gold to produce the bi-functional Au- Fe_3O_4@hexaniobate NPPs. Encapsulation of Ag and Au NP chains with a hexaniobate nanoscroll was shifted the surface plasmon resonance to higher wavelengths.

In these composites NPs can be incorporated to form NPP structures, decorated on nanosheets before scrolling, or attached to the surfaces of the nanoscrolls. The importance of this advancement is the promise it holds for the design and assembly of active nanocomposites. One

can create important combinations of nanomaterials for potential applications in a variety of areas including catalysis, solar conversion, thermoelectrics, and multiferroics.

Keywords: Nanopeapods, nanocomposite, solvothermal synthesis, nanoparticle encapsulation, layered inorganic nanostructures, intercalation reactions, metal oxides.

Chapter 1

Introduction

1.1 Layered Materials and Nanosheets

The term ‘nano’ (derived from Greek term ‘nanos’) means one billionth (10^{-9}) of a meter. Nanoscale science and technologies can best be described as the ability to synthesize, manipulate and characterize matter at level of 100 nm or less.[1] Materials at the nanoscale behave differently from the materials at larger scales, due to the altered atomic configuration, the presence of quantum effects, and the increase in the surface area to volume ratio.[2] The fields ‘nanotechnology’ and ‘nanoscience’ are interdisciplinary and are applicable across a wide variety of technological and scientific fields respectively. The “nanoworld” requires knowledge drawn from the arenas of physics, chemistry, biology, mechanical engineering and electrical engineering.[3]

1.1 Nanotechnology

In 1974, at the Tokyo International Conference on production engineering, Nori Taniguchi introduced the term “Nanotechnology” while describing the ultrafine materials machining with nanoscale precision. Nanotechnology is increasingly attracting not only scientists and researchers but also businesses due to unique properties and huge economical potential.[4] Today, nanotechnology has many applications that have brought immediate advantages in research such as better accuracy, versatility, reliability, speed and cost-effectiveness. Custom-designed materials can be fabricated by using nanofabrication techniques that allow the controlled manipulation of atoms and molecules.[5] The chemical composition of the

nanostructure, morphology and the local density of the electronic states on the surface strongly influence the chemical reactivity and electronic, optical, mechanical and magnetic properties.[6] Such useful nanofabrication capabilities offer some extraordinary opportunities in the development of new materials including catalysts, electronic devices and magnetic data-storage media.[7]

Nanotechnology techniques are currently used in various applications, including advanced nanoelectronics, optics, enhanced automation and robotics, nanostructured chemical catalysts and textile industry, oil and gas, and so on.[8] Bionanotechnology has emerged very recently as another sub-section of nanotechnology where biology intersects with nanotechnology.[9] Applications of bionanotechnology are extremely widespread in areas including drug delivery, food packing and safety, microbial coatings in the water industry, pharmaceutical and biomedical applications, diagnosis and treatment of central nervous system, health and cosmetic products, devices that operate inside the human body at the cellular level, dentistry and so on.[3a, 3e, 6a, 10]

1.2 Nanomaterials

In the 1950's, Richard Feynman had speculated that "There is plenty of room at the bottom", in a lecture at the American Physical Society annual meeting.[11] Feynman mentioned that the electron microscope could be improved in stability and resolution, so that one would be able to characterize matter at the atomic scale. Furthermore, Feynman predicted the ability to build tiny structures by arranging the atoms within the bounds of chemical stability. K.E. Drexler advanced the idea of Feynman and proposed the concept of using nanoscale structures to fabricate larger structures in the book of *Engines of Creation*.[12] In 1981, Gerd Binnig and Heinrich Rohrer at IBM invented scanning tunneling microscope (STM), a powerful tool for

viewing surfaces at the atomic level by the quantum tunneling effect. Later on, atomic force microscope (AFM) was developed in 1985, by Gerd Binnig, Christoph Gerber and Calvin Quate, to overcome some of the basic drawbacks of STM.

During the past decade, scientists have developed various methods for synthesizing and characterizing many new materials, including nanoparticles (NPs),[1-2] nanotubes,[13] and nanosheets.[14] Nanomaterials can be formed as spheres,[15] cubes,[16] elongated rods,[17] wires,[6a] sheets,[18] tripods, tetrapods, octahedrons,[19] bipyramids,[20] prisms,[21] etc. There are two main approaches to the fabrication of nanomaterials: top-down and bottom-up. Top-down approaches begin with larger constructs and removal of material is carried out until the desired structure is achieved. Techniques such as milling, electron-beam (e-beam) lithography, focused-ion-beam (FIB) lithography, etching and laser ablation are typical top-down methods.[22] The bottom-up approach begins at the atomic scale and builds up structures. Here methods such as sol-gel, thermal decomposition, hydrothermal, solvothermal, self-assembly, and electrodeposition are good examples of the bottom-up approach.[23] Nanomaterials produced in the bottom-up approach are prepared by assembling smaller subunits on a very large scale. Both top-down and bottom-up methods have advantages and disadvantages and can be quite complimentary in the fabrication of various nanomaterials.

The synthetic techniques to fabricate nanomaterials are further classified into two types, namely, (1) physical methods and (2) chemical methods. The inert-gas evaporation technique is representative of a physical method, involving the synthesis of single-phase metals and ceramic oxides.[24] Sputtering is another physical technique to produce a wide variety of thinfilms and, involves the ejection of atoms or clusters of designed materials in an accelerated and highly focused beam of inert gas.[25] Although physical methods are useful in fabricating nanomaterials,

they often suffer from contamination problems, cost, and time consumption. In contrast, chemical methods can offer good chemical homogeneity in mixing at the molecular level and versatility in building complex nanoscale materials.[1-2, 26] Although there are certain difficulties in chemical processing such as agglomeration, complex chemistry and contamination from byproducts, chemical methods are often scalable for economically feasible bulk production.[27]

Nanomaterials characterization.

Nanomaterials characterization is an essential part of science. The development of both novel characterization tools and instruments are some of the biggest challenges in establishing a correlation between the structure, shape, and chemical composition of nanomaterials. Microscopy-based techniques such as scanning electron microscope (SEM), transmission electron microscope (TEM), scanning transmission electron microscope (STEM), electron energy loss spectroscopy (EELS), energy dispersive X-ray spectroscopy (EDS) and scanning probe microscope (SPM), are widely used in structural and morphological characterization of nanomaterials. Other techniques including powder X-ray diffraction (XRD), X-ray photoelectron spectroscopy (XPS), Raman spectroscopy, X-ray absorption near edge structure (XANES), ferromagnetic resonance (FMR), vibrating sample magnetometer (VSM), ultraviolet–visible spectroscopy (UV-Vis), thermogravimetry (TGA), differential scanning calorimetry (DSC), etc., are also extensively used in the investigation of atomic environment, chemical structure, purity, crystal structure, electrical and magnetic properties, etc.

Materials in the nanoscale often require atomic-level resolution to observe, measure, and manipulate the individual nanostructures.[28] The imaging techniques involve light, electrons, ions, or scanning probes. SEM is a powerful tool in characterizing nanomaterials.[29] The electron beam (produced with an electron gun, accelerated with a voltage between 1 KV and 30 KV) rapidly

scans over an area of the specimen while the magnetic lenses focus the beam on the sample. The topography of the sample can be imaged by collecting the low-energy secondary electrons emitted from the surface of the specimen. In TEM, electrons are accelerated to 100 KV or higher, projected into the specimen, and an image is formed by electrons that transverse the sample. The greatest advantages of TEM include higher magnification and production of a diffraction pattern from the selected area of a crystallite.[30] STEM is an invaluable technique for the systematic characterization of nanostructures.[31] In STEM mode, a fine electron probe (produced by field emission gun) scans the sample and the desired signal is collected while scanning to form an image. The high-angle annular detector captures the electrons that are inelastic and scattered to higher angles. Currently, atomic resolution compositional changes can be examined by an aberration-corrected STEM. Also, local electronic environment of single atoms can be analyzed spectroscopically by electron energy loss spectroscopy (EELS).[32]

SPM is another unique imaging technique that allows for spatially localized measurements of structure and properties. Almost any solid surface can be studied in air, in liquid, or in ultrahigh vacuum with SPM.[33] Additional techniques such as scanning tunneling microscopy (STM) and atomic force microscopy (AFM) are major members of SPM.[34] The STM technique allows the three dimensional (3D) real-space imaging of electrically conductive surfaces down to the atomic scale. Unfortunately, the technique is not useful for a non-conductive surface. This limitation is complimented by AFM, which does not require a conductive surface.

The techniques of XRD and XPS are also important tools for materials characterization. XRD is another effective technique to investigate the crystal structure of solids, including lattice constants, geometry, stresses, etc.[35] For many applications, X-ray photoelectron spectroscopy

(XPS)[36] is used for qualitative and quantitative analyses, that is, to study elemental composition of solid surfaces, densities of states, band structures, etc.

1.2.1 Zero-Dimensional (OD) Nanostructures

Over past few years, there has been an increase in research on the synthesis of zero-dimensional NPs because of their unique properties[15] that find useful applications in catalysis, magnetic data storage, solar cells, sensors, lithium ion batteries, medicine, etc.[2] Also, the technological trend towards decreasing dimensions makes them of interest to examine the correlation between the size at the nanoscale and their properties.[1]

The rational synthesis of monodispersed NPs with well-defined morphology is key for the further investigation of the size-dependent properties of nanoscale materials. The past couple of decades have witnessed a worldwide exponential growth of research activities in the field of NPs synthesis, driven by the potential hope for economic impacts and applications. The unraveling of the characteristics of these NPs is being examined. Self-assembly of these NPs by different techniques is also being pursued.[37] There are important applications (photonics, nanoelectronics, optoelectronics, etc) that would require self-assembled NPs. In addition to the morphology and quality of the NPs, the surface structure and chemical nature of the surface will play a very important role in most of their potential applications. The high surface energy accompanied by the large curvature makes the surface of a NP unstable.[38] Thus, the properties change as these NPs are used.[39]

Wet-chemical methods are widely used in the production, functionalization, purification, and assembly of NP building blocks. It is known that morphological control is a complex interplay between various experimental parameters including polarity, coordinating ability, vapor pressure and viscosity of the solvent, in addition to surfactant characteristics, reaction time and

temperature.[40] By understanding the process and controlling parameters, engineering of the growth of NPs to the desired morphology can be improved.

NPs can be synthesized at lower temperatures, using metal salts or organometallic precursors, by sol-gel[41], hydrothermal[42], solvothermal[43], combustion [44], co-precipitation[45], and microwave hydrothermal methods[46]. In general, solvothermal synthesis offers many advantages over other methods, such as simplicity and high crystallinity at relatively low temperature.[47] The liquid-solid-solution method[2] combines hydrolytic with non-hydrolytic reaction conditions to grow nanomaterials with enhanced morphological control via solvothermal treatment. The hydrolytic process possesses high rates of reaction, making it difficult to control; slight changes in kinetics may lead to dramatic changes in the morphology of the final materials; whereas non-hydrolytic conditions results in a drastic decrease in the reaction rate, leading to a slow growth process of NPs. By combining hydrolytic and non-hydrolytic processes, NPs can be synthesized with controlled morphologies and high crystallinity.[48] These NPs will be used as building blocks for the design of complex multifunctional architectures.

The controlled growth of the NPs in solution is a kinetically controlled process. Surfactants can specifically bind to a particular crystal facet and manipulate the energies of the crystallographic facets and their relative growth rates.[49] An effective strategy involves using a pair of surface agents in which one binds less tightly, permitting rapid growth, and the other binds tightly to the NP surface, hindering growth. For example, the growth rate and morphology of the NPs can be controlled by adjusting the ratio of carboxylic acid (tightly bound) and alkylphosphine (weakly bound) stabilizers.[50] The growth is arrested by quickly cooling the solution, when the NPs reach the desired size. Oleylamine (OAm), oleic acid (OAc), cetyltrimethylammonium bromide (CTAB), alkylphosphine, etc., are widely used as

surfactants.[51] In addition to the selection of surfactants and reagents, various other reaction parameters, including precursor concentration, precursor types, reaction time, temperature, etc., need to be systematically adjusted to control the size, shape, and quality of NPs.[52]

Solvothermal synthesis.

The solvothermal method has recently been extensively used in the formation of inorganic nanomaterials.[2, 53] Solvothermal synthesis is commonly performed in stainless steel pressure vessels called autoclaves within a Teflon liner; reactions are carried out under controlled temperature and/or pressure in non-aqueous solutions. Figure 1.1 shows the complete set up needed to perform solvothermal experiments.

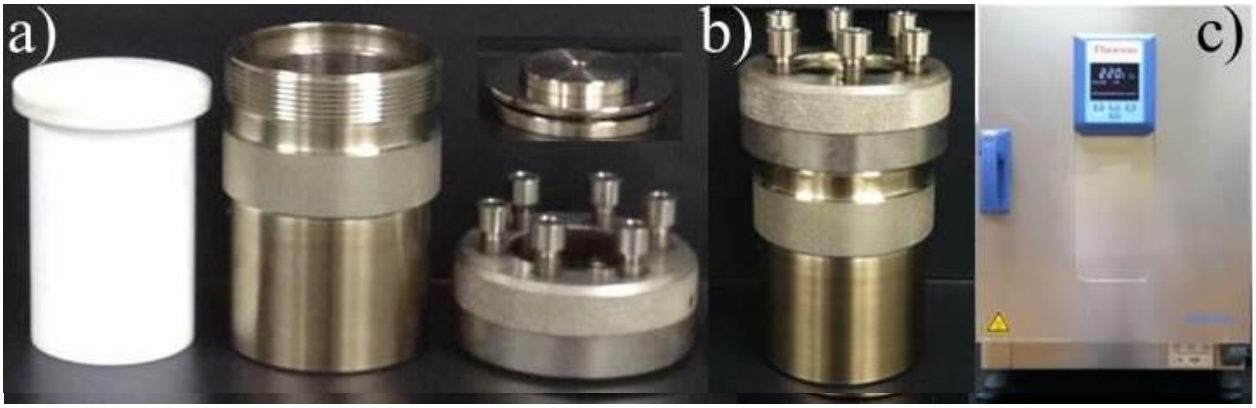

Figure 1.1. A typical set up used for solvothermal synthesis; a) parts of an autoclave (Parr bomb) such as Teflon liner (left), autoclave (stainless steel container, center), corrosion disc (top right), screw cap (lower right); b) assembled autoclave; c) Typical oven used for solvothermal experiments.

An autogeneous pressure is developed within the sealed reaction container and is found to increase dramatically with temperature under these conditions. Other experimental factors, such as the percentage fill of the vessel, temperature, any dissolved salts and the identity of organic solvents used largely determines the internal pressure produced. The pressure generated decreases when the volume of the liquid inside the vessel is increased, according to the Peng–Robinson equation of state.[53c] Therefore by decreasing the amount of reaction mixture, the

pressure generated in the reaction vessel increases, which in turn facilitates the nucleation and growth of the particle.[54]

The autogeneous pressure (p) generated within the solvothermal reaction vessel can be estimated by using given temperature (T), molar volume (V_m) of the liquid fraction in the bomb.[53c]

$$p = \left[\frac{RT}{(V_m - b)}\right] - \left[\frac{a}{(V_m^2 + 2bV_m - b^2)}\right]$$

The parameters a and b are given as:[53c]

a = $0.45724R^2T_C^2\left[1 + f_\omega(1 - T_r^{1/2})\right]^2/p_C$

b = $0.7780RT_c/P_c$

where $f_\omega = 0.37464 + 1.54226\omega - 0.26992\omega^2$.

Here, the subscript 'r' in $T_r(= T/T_C)$ refers to reduced conditions; 'C' in T_c , P_c refers to critical value; and is the acentric factor $'\omega'$ are tabulated for many different solvents in Reid et al.[133, 53c]

This method offers specific advantages over the traditional synthetic routes to inorganic solids, such as great morphological control, high crystallinity and better surface functionalization.[55] In recent years, the solvothermal method has been employed to synthesize a variety of nanomaterials with and without the aid of surfactants.[2, 56] Table 1.1 highlights different compounds that can readily be synthesized using solvothermal method and their experimental conditions.

Many groups have used the solvothermal method to prepare metal oxide NPs. For example, monodispersed TiO_2 NPs were synthesized by Wu et al.,[64] in typical procedure;

titanium isopropoxide was mixed with benzyl alcohol and OAm and kept at 180 °C for 24h. Reaction conditions can easily be tuned via solvothermal method to achieve new morphologies of NPs. For example, by introducing OAc and adjusting the concentrations of titanium isopropoxide in the reaction mixture reported by Wu et al.,[64] star shaped and dog-bone shaped TiO_2 NPs can be produced. Figure 1.2 highlights the different morphologies of TiO_2 NPs that can be readily synthesized by solvothermal method.

Table 1.1. Examples of NPs synthesized via solvothermal method.

Compound	Size (nm)	Starting materials	Solvent
$BaTiO_3$[57]	15	Ba nitrate, titanium n-butoxide	1-butanol
Bi_2Se_3[58]	25	$BiCl_3$, Se, NaI	Ethylenediamine
CdS[59]	6	Cd nitrate or sulphate, thiourea	Ethylene glycol
CdSe[60]	3	Cd stearate, Se	Toluene
CeO_2[61]	2	Ce	2-Methoxyethanol
g-Fe_2O_3, $CoFe_2O_4$[62]	7–12, 7	Co, Fe cupferron complexes	Toluene
$LiNbO_3$[54]	50	$LiNb(O\text{-}Et)_6$ in 5% w/v in ethanol	1,4-butanol
SnSe[63]	45	$SnCl_2$, Se, Na	Ethylenediamine
TiO_2[64]	11	titanium isopropoxide	benzyl alcohol
ZnSe[65]	12–16	Zn, Se	Pyridine
ZrO_2[66]	3–5	$Zr(OR)_4$	Ethanol

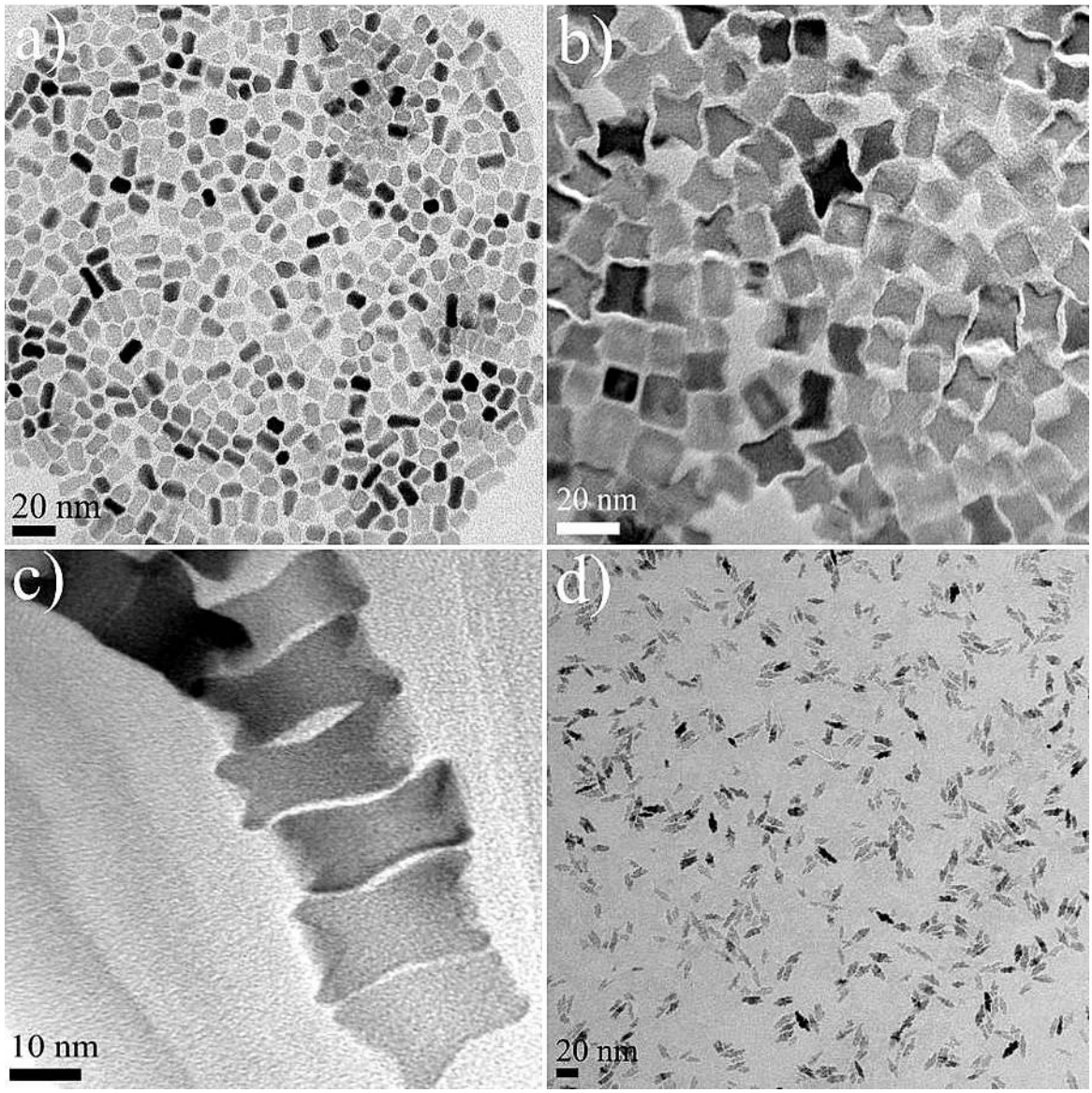

Figure 1.2. Representative TEM images of shape controlled TiO_2 NPs synthesized by solvothermal method; a) cube-like TiO_2 NPs; b) star-shaped TiO_2 NPs; c) dog-bone shaped TiO_2 NPs; d) elongated TiO_2 NPs. (Nanoparticles shown were grown in this lab by published methods)

Magnetic nanoparticles.

Magnetic NPs commonly contain elements such as manganese, iron, cobalt, nickel and zinc. Among transition metal oxide based magnetic NPs, Fe_3O_4 has been one of the most studied materials. It has been widely used in various fields, e.g., recycling of expensive catalysts, pharmaceutics, magnetic resonance imaging, drug delivery, ferrofluids, data storage and magnetics.[40b, 67] In the last few decades, there have been substantial research efforts on the synthesis of highly stable, mono-dispersed and shape-controlled magnetic NPs. Among several methods used, thermal decomposition has been one of the most common ones for the production of NPs in high yields with narrow size distribution.

In the case of magnetite, a thermal decomposition method has been successfully applied to the synthesis of NPs with different shapes. In brief, organometallic precursors [e.g., metal acetylacetonates - $Fe(acac)_3$ or $Fe(acac)_2$; metal oxides - FeO(OH) or carbonyls - $Fe(CO)_5$] are dissolved in an organic solvent with stabilizing surfactants (OAm or OAc) and heated up to 320 °C.[68] The thermal decomposition of the iron precursor will result in Fe_3O_4 NPs (Figure 1.3a). The reaction conditions can readily be extended to the preparation of other important cubic spinel ferrite NPs, such as $CoFe_2O_4$, $NiFe_2O_4$ and $MnFe_2O_4$ NPs. SiO_2 shell (Figure 1.3b) can readily be created by a protocol similar to that reported by Barnakov et al.[69] Figure 1.3c highlights the morphology of Ni NPs produced by the thermal decomposition of $Ni(acac)_2$ in presence of OAm and benzylamine at 300 °C.

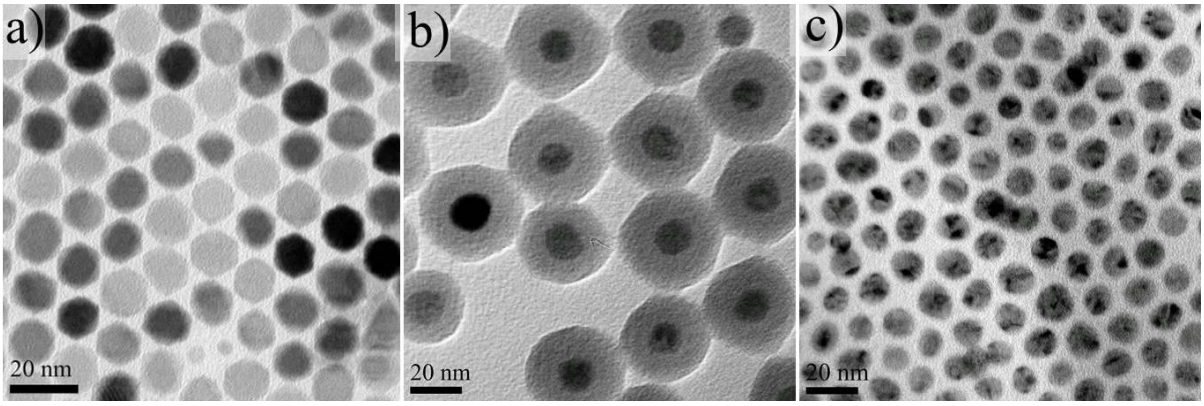

Figure 1.3. TEM images of magnetic NPs prepared by thermal decomposition of organometallic precursors in organic media at temperatures (280 – 320 °C; a) Fe_3O_4 NPs; b) Fe_3O_4@SiO_2 (core@shell) NPs; c) Spherical Ni NPs. (Nanoparticles shown were grown in this lab by published methods)

Plasmonic nanoparticles.

There has been extensive research on the synthesis and applications of noble metal NPs.[70] The property, called surface plasmon resonance, makes noble metal NPs very interesting and attractive. This strong absorption in the visible spectrum, giving rise to vivid characteristic color, has been observed and used, since centuries. Furthermore, the ability to decorate noble metal NPs on inorganic metal oxide nanostructures in various dimensions may allow for the formation of nanoarchitectures with promising applications such as surface enhanced Raman scattering (SERS), nanometer-scale optical waveguides, bio-diagnostics through the selective localized photothermal heating of cancer cells, biological and chemical sensing, optoelectronics and NP arrays for new optical band-gap materials.[71]

Free-standing, monodispersed hydrophobic noble metal NPs can be synthesized by various methods. Up until now, a number of noble metals, such as Au, Ag, Pd, Pt, and Rh have been used to generate 0D NPs, bimetallic systems and alloys with tunable and enhanced properties. Thermal decomposition and seed-mediated growth are the most common and

powerful routes to synthesize noble metal NPs. Figure 1.4 a shows the morphology of Ag NPs produced by the thermal decomposition of $AgNO_3$ in presence of OAm at 180 °C. Au NPs (Figure 1.4b) can readily be prepared by a protocol similar to that reported by Saruyama et al.[72] Pd nanoclusters can be produced by treating the $Pd(acac)_2$ in presence of OAm and benzylamine at 300 °C (Figure 1.4c).

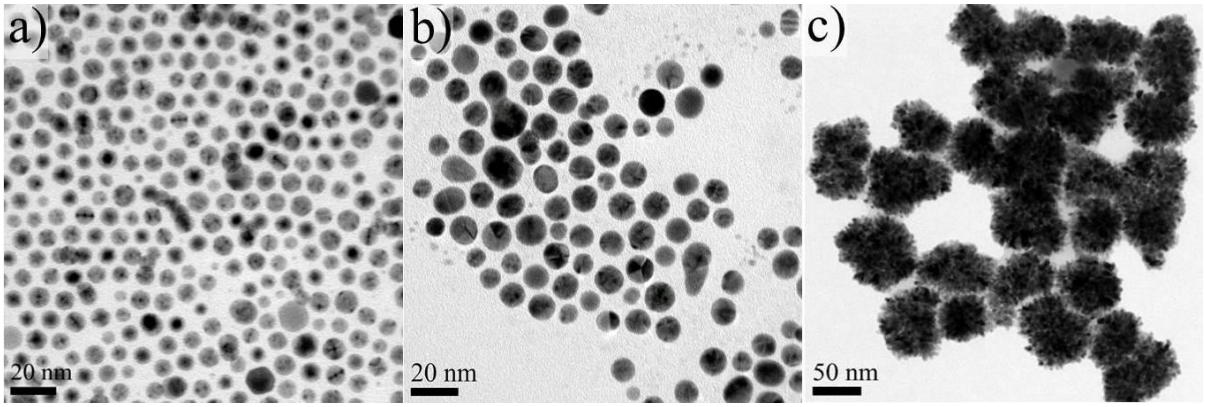

Figure 1.4. TEM images showing noble metal NPs of a) Ag NPs, b) Au NPs, and c) Pd nanoclusters. (Nanoparticles shown were grown in this lab by published methods)

Quantum dots.

Quantum dots (QDs) of various shapes have been successfully synthesized for almost two decades. The ability to generate QDs nanostructures with a variety of well-defined geometrical shapes provides a great opportunity to systematically evaluate their optical, catalytic and electrical properties. QDs, especially CdS, CdSe, etc., are promising materials for a range of various applications, including high-sensitivity infrared (IR) photodetectors, solar cells, and IR-emitting diodes and lasers.[73] The organometallic approach, based on the thermal decomposition of organometallic precursors into hot organic solvents, provides high quality QDs. Furthermore, this opens up new possibilities in the assembly of individual QDs into supercrystal structures.[74]

Figure 1.5a highlights the morphology of ZnS quantum dots produced according to Joo et al.[75] CdS quantum dots can be readily produced by the treating of $CdCl_2$ and sulfur in presence of OAm at 140 °C for 20h (Figure 1.5b). Figure 1.5c shows the morphology of CdSe quantum dots.

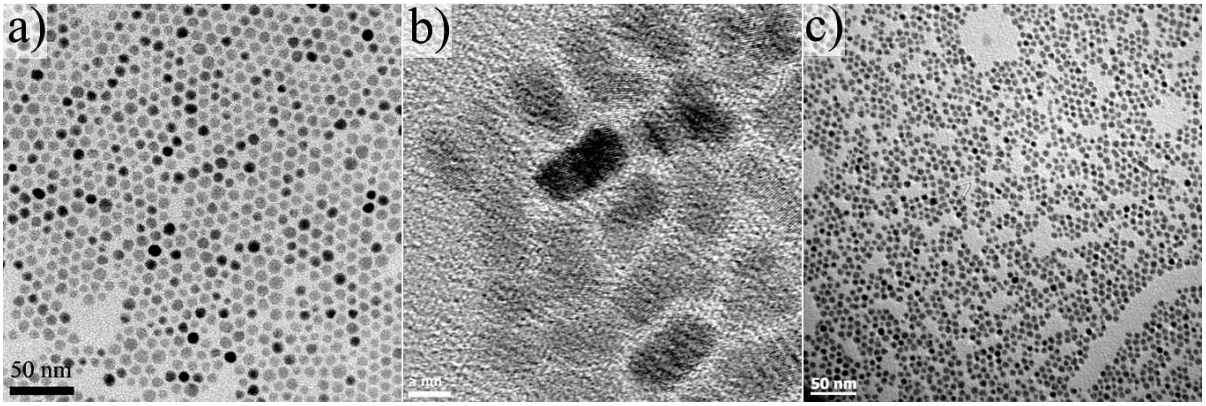

Figure 1.5. TEM images of quantum dots of a) ZnS, b) CdS, and c) CdSe. (Nanoparticles shown were grown in this lab by published methods)

Surface modification.

NPs of various compositions, sizes, and shapes are now synthetically accessible.[1, 16, 38, 76] They are synthesized in both polar and nonpolar media. NPs have a number of applications in various fields and their applications are often hindered by a lack of particles with a desired surface functionalization.[77]

The surface modification of NPs plays an essential role in achieving the particular combination of desired properties. Such properties include the chemical functionality, solubility, reactivity, stability, melting point, electronic structure.[77] The capping groups can passivate surface electronic states in NPs and stabilize NPs in solution.[78] The properties of NPs can be tailored by tuning the surface capping materials through well-established chemical substitutions such as ligand exchange.

Ligand exchange is perhaps one of the most powerful strategies that permit the facile modification of particular NP properties without affecting the morphology. Postsynthetic phase-transfer of NPs between polar and nonpolar solvents, for example, is highly desirable. Recently, several groups reported the phase-transfer of Au nanorods from CTAB-stabilized to organic solvents.[77, 79]

1.2.2 One-Dimensional (1D) Nanostructures:

One dimensional (1D) nanostructures hold great promise for a number of materials applications because of their high-aspect ratio and encapsulation potential. Structures like nanotubes, nanowires and nanoscrolls belong to the category of 1D nanostructures. These nanostructures have attracted much interest in recent years for a range of applications, including hydrogen storage, photocatalysts, and dye-sensitized solar cells.[80] In early 1990s, Martin and his co-workers pioneered a template-directed approach to preparing 1D nanomaterials by using membranes with the cylindrical pores. Iijima's discovery of carbon nanotubes (CNTs) triggered much research on various 1D nanomaterials, such as metal oxides, metals, including alloys and ceramics.[81]

Figure 1.6 shows the morphologies of various 1D nanostructures. Among 1D nanomaterials, scrolled-structured materials have shown unique properties with an interesting architecture consisting of outer, inner and interlayer surfaces. Figure 1.7 highlights the structural features of scrolled nanosheets. The scrolled type structures have asymmetric (spiraled) structure formed by convolved nanosheets. Such inorganic scrolled structures, in particular, are receiving a great deal of attention because of their potential for newly emerging applications in heterogeneous catalysis, drug-delivery systems, intercalation, ion-exchange, photodegradation, hydrogen fuel, gas sensors, and solar energy conversion.[26b, 82] The applications employ the

inherent characteristics of nanoscrolls which involve hollow core structures, atypical electron transport characteristics, enhanced mechanical strength, ultra large specific surface areas, narrow inner pore diameters, unusual confinement effects, and catalysis.[26b, 83]

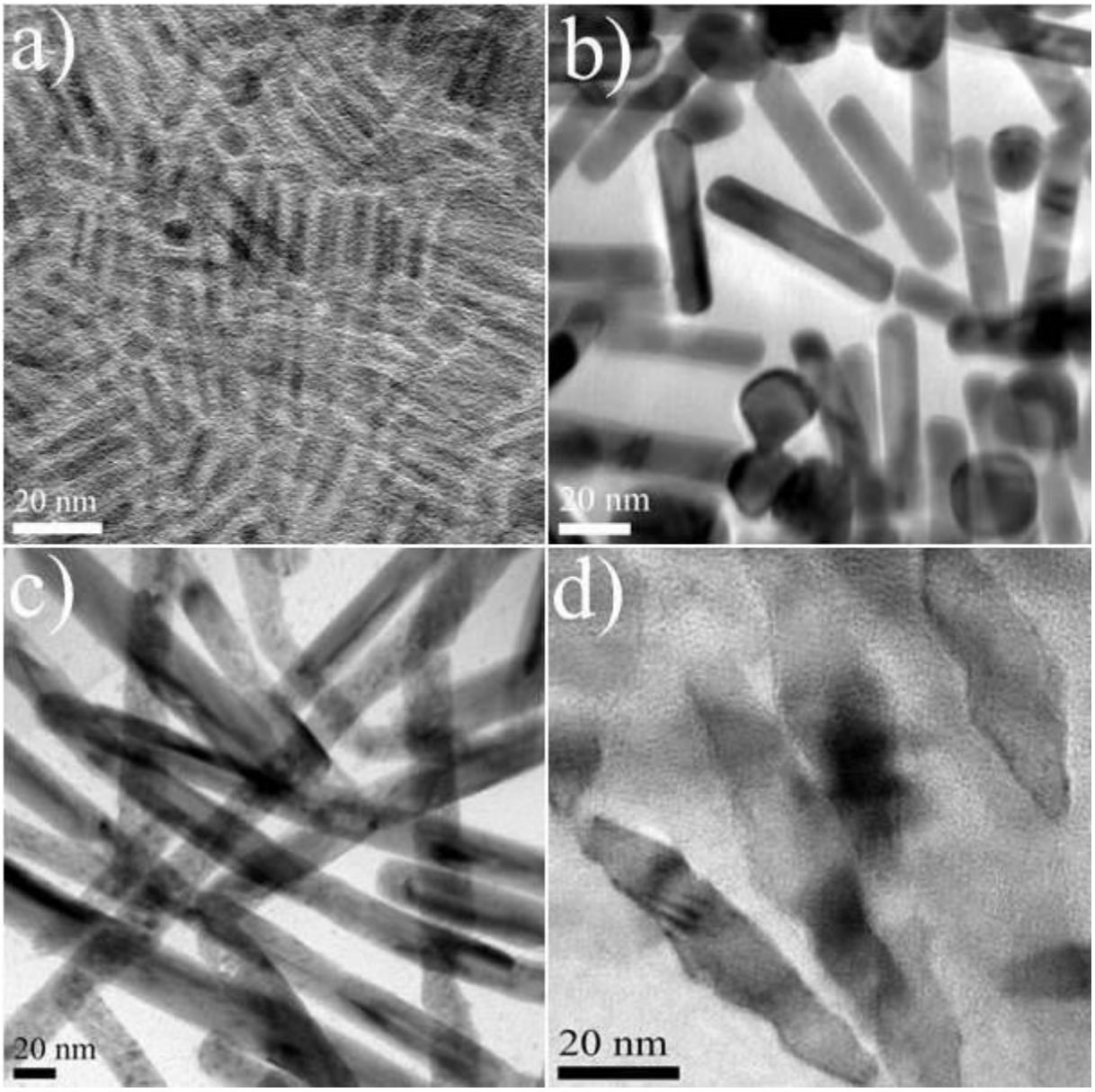

Figure 1.6. (a) TEM image showing a) Fe_3O_4 nanorods, b) Au elongated nanorods, c) Cu nanorods, and d) TiO_2 elongated nanorods. (Nanostructures shown were grown in this lab by published methods)

There are a several reports on the fabrication strategies of nanoscrolls in the literature.[26b, 83f, g, 84] Scroll forming materials include graphene,[85] BN,[83h] WS_2,[86] MoS_2,[87] TiO_2,[88] MnO_2,[89] PbO_2,[82a] $SrAl_2O_4$,[90] $K_4Nb_6O_{17}$[91] and Ruddlesden–Popper[92] and Dion–Jacobson[93] type perovskites. Saupe et al. reported that the potassium hexaniobate nanotubes are generated by the reaction of TBAOH and acid-exchanged hexaniobate at 40 °C in an aqueous-phase exfoliation and scrolling process.[91] Other template-less methods involve the spontaneous formation of oxide nanoscrolls are also known. In one instance, vanadium oxide nanoscroll form on the hydrothermal treatment of aged suspensions of V_2O_5 with dodecylamine.[94] Figure 1.8 shows the morphologies of nanoscrolls.

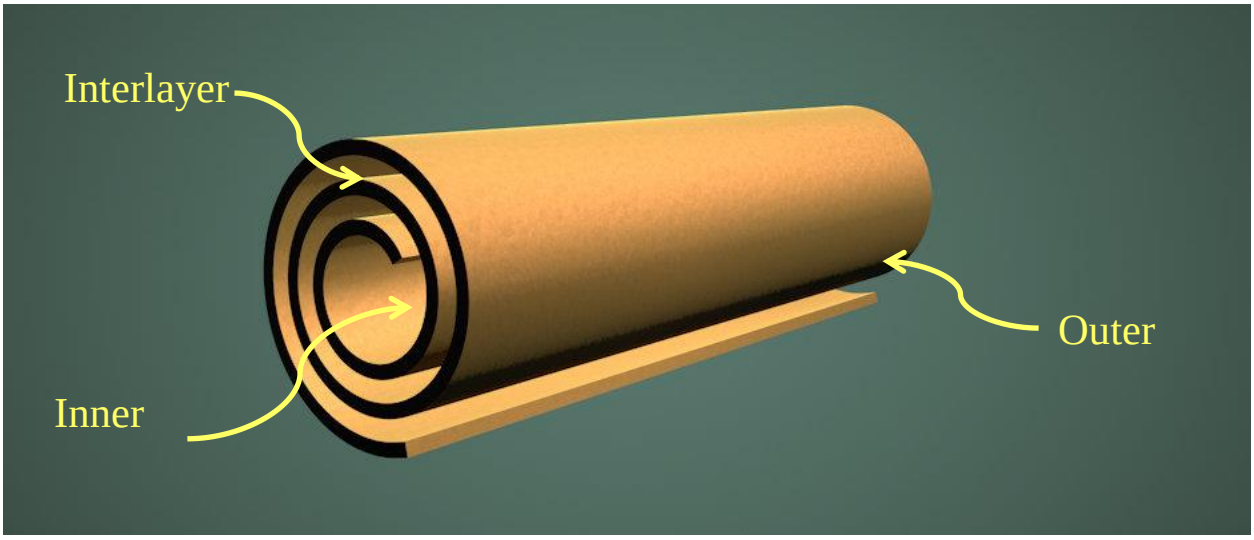

Figure 1.7. Cartoons highlight important structural features of nanoscrolls. (Nanoscroll cartoon was drawn by Cinema 4D software)

Nanoscrolls are a major focus of Chapter 2. There the focus is on the rapid large-scale fabrication of hexaniobate nanoscrolls by a non-aqueous solvothermal approach. This has several advantages over the other methods, such as facile fabrication, high yields in less than 6 hours,

and uniform morphologies of nanoscrolls. Therefore, solvothermal methods allow us to produce scroll-structured materials in high yield for future applications, such as photocatalysis.

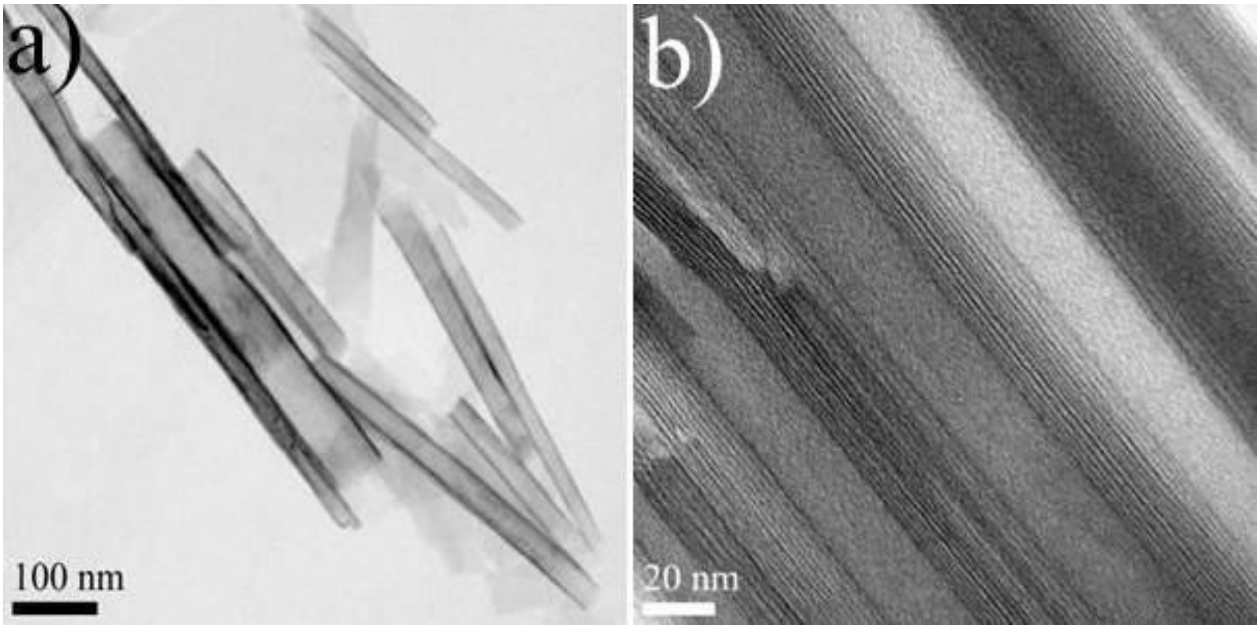

Figure 1.8. (a) TEM image showing a) simple hexaniobate nanoscrolls, b) intercalated hexaniobate nanoscrolls.

1.3 Layered Inorganic Materials

Layered inorganic structures are also important nanomaterials. Such two-dimensional (2D) nanosheets are typically produced by the liquid-phase exfoliation of layered materials.[95] This phenomenon is observed in a variety of materials including clays, metal chalcogenides, phosphates, phosphonates and oxides. An important challenge in this chemistry is processing adequately so as to achieve appropriate surface functionalization for controlled exfoliation. Exfoliated layered inorganic materials can form zero- and one-dimensional structures. Properties of the nanostructures differ significantly from the corresponding bulk materials. This behavior offers many potential applications in catalysis, rechargeable batteries, drug delivery, solar cells, and electronics.[95b-d]

Among the several families of inorganic solids, layered inorganic materials occupy an important position in view of their wide range of properties. Such properties include superconductivity, energy conversion and storage, high specific surface area, high thermal conductivity, inherent mechanical strength, colossal magnetoresistance, sensing applications, ferroelectricity, unusual electron transport characteristics, and catalytic activity.[96] Well-known examples of layered inorganic materials include graphene[97], BN[98], WS[86], MoS_2[87], TiO_2[99], $K_4Nb_6O_{17}$[91], Ruddlesden–Popper (RP)[92] type and Dion–Jacobson (DJ)[93] type. Among the various materials, graphene is one that can be altered from nanosheet to nanotube[13] or nanoscroll. This amenity is not limited to graphite and could occur in other 2D layered compounds such as exfoliated $K_4Nb_6O_{17}$ nanosheets or WS_2. Three related layered perovskite oxides, the Dion–Jacobson (DJ), Ruddlesden–Popper (RP), and Aurivillius (AV) phases are specifically important in this regard due to their ability to undergo ion-exchange, and exfoliation. The DJ, RP and AV phases have the compositions $A[A'_{n-1}B_nO_{3n+1}]$, $A_2[A'_{n-1}B_nO_{3n+1}]$ and $M_2O_2[A'_{n-1}B_nO_{3n+1}]$ respectively; A is an alkali-metal cation, A´ is an alkali-metal, alkaline earth, main group and/or rare earth, B is a transition metal, and M is a main group cation, typically Bi.[100] Figure 1.9 shows the crystal structures of various layered inorganic materials.

The synthesis of bulk layered materials has experienced a substantial growth in recent years. Traditional synthesis approaches involve high-temperature solid-state reactions of inorganic salts and binary oxides that preclude the chances of obtaining metastable members of the perovskite family. The high temperatures are necessary to overcome the small diffusion rates in these solid-state reactions. Other common methods to prepare perovskites include co-precipitation and sol-gel method[101,102], both of which are precursor methods. Another synthetic approach to solid state structures is known as topochemical reactions. Topochemical reactions

b)

are typically carried out at low temperature (< 500 °C), and they are also useful means to convert RP phases to DJ phase perovskites through ion exchange. Other topochemical manipulations such as intercalation, grafting, layer extraction, etc., can also be performed. Furthermore, host materials can be manipulated and produce compounds that cannot be readily prepared at high temperature.[100]

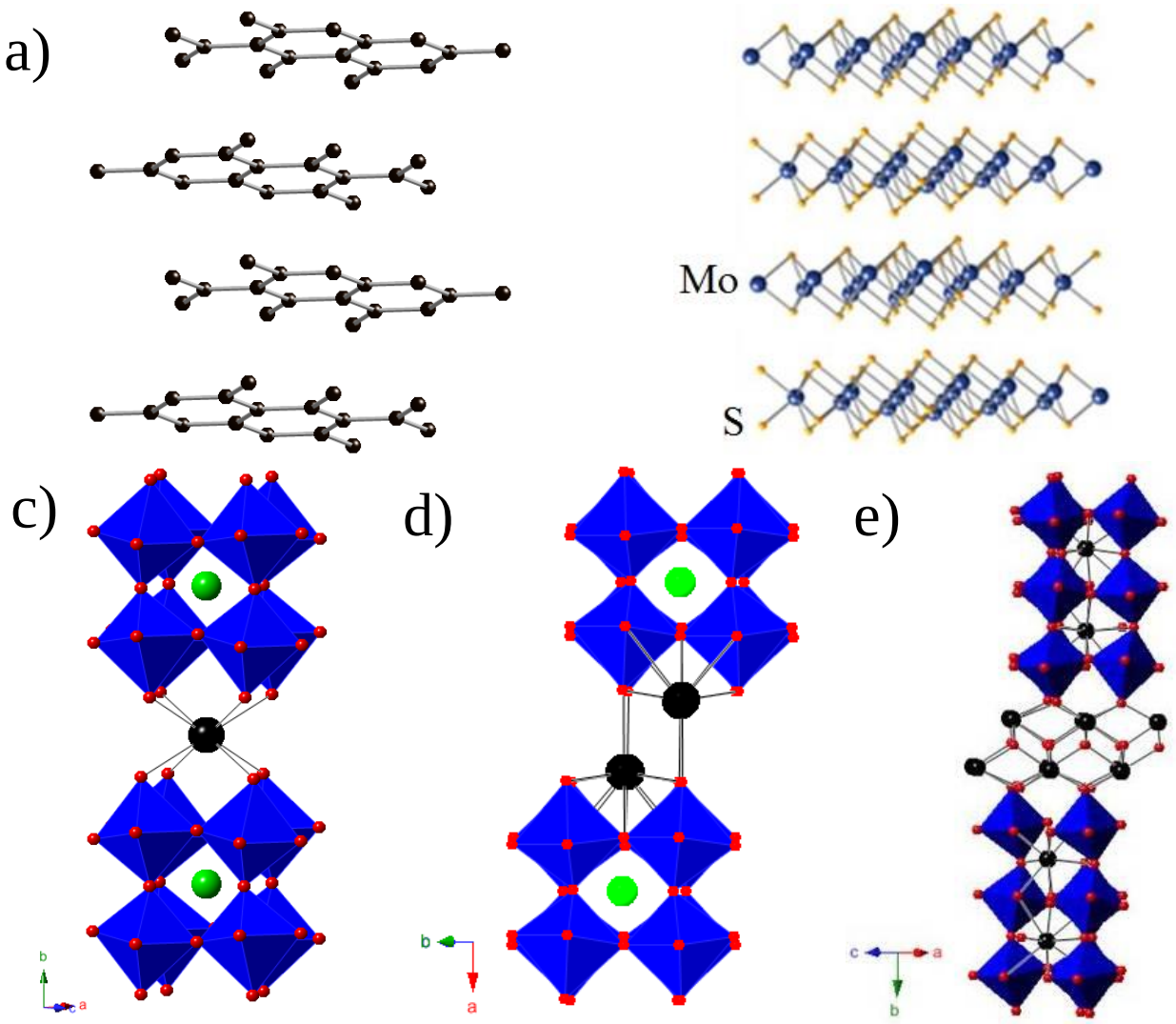

Figure 1.9. Crystal structures of layered materials (a) graphite, (b) MoS_2, (c) Dion-Jacobson, $RbLaNb_2O_7$, (d) Ruddlesden-Popper, $Rb_2LaNb_2O_7$, and (e) Aurivillius, $Bi_2O_2Bi_2Ti_3O_{10}$. (Crystal structures were drawn by CrystalMaker software)

Current research efforts are therefore directed toward developing alternate low-temperature routes that will enable the synthesis of functional layered materials.[103] Practically, the synthesis of crystalline nanostructures from quasi-isotropic compounds, for example MoS_2, WS_2, VO_x-alkylamine, titanate, GaN, In_2O_3, was accomplished.[104]

1.3.1 $K_4Nb_6O_{17}$

Layered potassium hexaniobate ($K_4Nb_6O_{17}$) has a stacked structure, which consists of negatively charged co-planar layers of corner and edge-sharing distorted NbO_6 octahedra accommodating exchangeable cations in the interlayer space[105]. Potassium hexaniobate has two distinct interlayers, designated as interlayer I and II in Figure 1.10. The ion-exchange abilities of these interlayers are different. A variety of cations, such as n-alkylammonium (C_4-C_8), methylviologen, and other guest species, can have access to the interlayer I, whereas ion-exchange within interlayer II is quite rare.

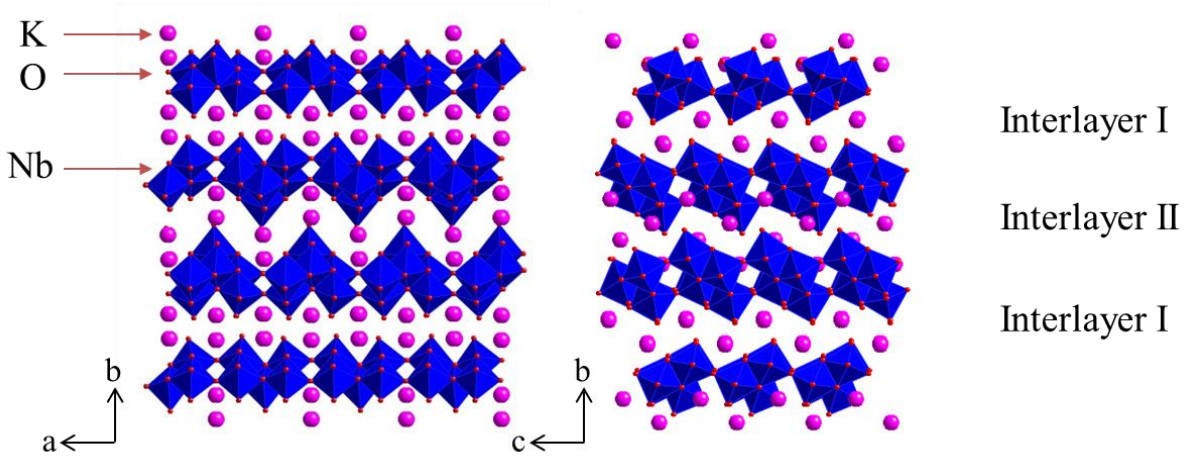

Figure 1.10. Crystal structure of $K_4Nb_6O_{17}$.[106] (Crystal structures were drawn by CrystalMaker software)

The hexaniobate has been widely used as a photocatalyst. In 1988, Onishi and coworkers observed the phenomenon of the photocatalytic splitting of water to form H_2 and O_2 over a NiO-Hexaniobate powder (1-10 μm, band gap = 3.3 eV) under the bandgap irradiation.[107] Since then, enormous efforts have been dedicated to research on hexaniobate, which has led to many promising applications in areas ranging from ion-exchangers to organic-inorganic composite materials and catalysts.[26b, 82] Also, hexaniobate was used in hydrogen (H_2) gas production under UV irradiation from pure water and aqueous methanol.[108] These applications depend not only on the properties of the material itself but also on the modifications of the hexaniobate material host (e.g., with quantum dots, noble metal and metal oxide NPs).

As an excellent photocatalyst, hexaniobate materials are expected to play an important role in helping solve many serious environmental and energy challenges, through photodegradation of toxic organics and H_2 production from water-splitting. However, the overall photocatalytic efficiency of hexaniobate is sometimes prevented by its wide band gap.[108a] The band gap of hexaniobate lies in the UV region (3.3 eV), which is only a small fraction of the sun's energy (<10%). Thus, one of the goals with these materials is to increase its optical activity by shifting the onset of the response from the UV to the visible region. One way of achieving this goal is to develop hexaniobate composite materials (e.g., with quantum dots and noble metal NPs). In this case, performance of hexaniobate materials can be improved by coupling collective oscillations of the electrons in the conduction band of metal NP surfaces to those in the conduction band of hexaniobate materials.

Another way to improve the performance of hexaniobate materials is to alter the optical properties by doping hexaniobate with others elements. The underlying electronic structure of a material determines the optical response. The electronic properties of a material are closely

determined by its physical dimensions (confinement of carriers), its atomic arrangement and chemical nature of bonds between the atoms or ions. Specifically, the metal (niobium) or the nonmetal (oxygen) component can be replaced in order to alter the material's optical properties. It appears difficult to replace the O^{2-} anion with other anions due to differences in charge states and ionic radii, and it is easier to substitute the Nb^{5+} cation in $-Nb_6O_{17}$ with other transition metals. Pian et al. synthesized TiO_2/Bi-doped hexaniobate ($TiO_2/Bi_xNb_{6-x}O_{17}$) and observed degradation of methylene blue under visible light irradiation.[109]

Another way to improve hexaniobate optical activity in the visible region is to sensitize it with other colorful inorganic or organic compounds. Various light-absorbing dyes are referred to as sensitizers. The process, where a photocurrent is generated with light energy less than that of the semiconductor band gap, is known as sensitization.[110] Hexaniobate is a wide band gap semiconductor, with optical absorption in the UV region (<400 nm). Any material with a narrower band gap or absorption in the visible or infrared regime can be used as a sensitizer for hexaniobate materials. Maeda et al. used ruthenium(II) bipyridyl complexes as visible light sensitizers, ethylenediaminetetraacetic acid (EDTA) as a sacrificial electron donor and platinum (Pt) NPs as catalysts; and thus produced H_2 photocatalytically using visible light ($\lambda > 420$ nm) with initial apparent quantum yields of 20-25%.[111] In addition, the performance of hexaniobate can be improved by modifying the surface of hexaniobate with other semiconductors which alter the charge-transfer properties between hexaniobate and the surrounding environment.

Hexaniobate nanostructures can have potential applicability in intercalation, ion-exchange and heterogeneous catalysis.[26b, 82] Also, hexaniobate nanoscrolls can be used as versatile platforms for NP encapsulation and new composite materials.[112]

The preparation of hexaniobate nanosheets has also been explored recently.[91] New physical and chemical properties emerge when the shapes of the shrinking nanomaterials change. The surface-to-volume ratio and specific surface area increase dramatically as the size of a material decrease, which largely influence to properties of materials. Acid-exchanged hexaniobate ($H_xK_{4-x}Nb_6O_{17}$) is one of the interesting materials that shows exfoliation behavior. Individual –NbO_6- layers (2D) may be exfoliated and roll into 1D nanotubular structures with the successful intercalation of large molecules[113]. To relieve built-in mechanical strain, the individual asymmetric nanosheets spontaneously scroll along [100].[114,91]To achieve nanoscrolls, first, $K_4Nb_6O_{17}$ was synthesized by the solid-state reaction of K_2CO_3 and Nb_2O_5 (in the molar ratio of 1.1:1.5) in air at 900 °C for 1h before continuing to heat at 1050 °C for another 24 h, about 1 g of which was treated with 15 mL of a 3 M HCl solution at 50 °C for 4 days.[91] The resulting acid-exchanged product was filtered, washed with water, and air-dried. The obtained protonic hexaniobate, $H_xK_{4-x}Nb_6O_{17}$, was shaken vigorously with a 20 mL of aqueous TBAOH solution (15 mM, pH = 11) at 45 °C for 10 days.

1.3.2 Hexaniobate Based Nanocomposites

Materials scientists are particularly interested in engineering functional systems at the nanometer scale to develop new and efficient ways of tailoring the structure of matter.[1, 16, 115] The layered hexaniobate is a biocompatible, nontoxic, chemically stable, and an inexpensive wide-band gap semiconductor material. Hexaniobate is used in a wide range of applications, such as photocatalysis, catalysis for degradation of toxic organics, and in dye-sensitized solar cells. Acid-exchanged hexaniobate ($H_xK_{4-x}Nb_6O_{17}$) is one of the interesting materials which shows exfoliation behavior. Hexaniobate has the unique ability to not only exfoliate but to also transform into a nanoscroll geometry to relieve built-in strain.[91] The properties of nanostructured

hexaniobate depend on their morphology, size and intercalation. The layered hexaniobate shows excellent photocatalytic activity under UV-light,[108a] though, its large band gap limits overall photocatalytic efficiency. For practical applications, it is important to design hexaniobate-based architectures with improved efficiency as far as its photocatalytic properties are concerned.

In the past, TiO_2/Bi-doped hexaniobate composites have been synthesized via a solid-state reaction and a subsequent exfoliation-restacking route.[109] Such nanocomposites showed a good photocatalytic activity in the degradation of methylene blue under visible light irradiation. However, this method results in composites without morphological uniformity and surface functionalization, leading to limited dispensability in organic solvents. Furthermore, this method generally requires a relatively long time for both the reaction and exfoliation-restacking process. Therefore, it would be beneficial to develop a controlled and rapid fabrication of hexaniobate based nanocomposites. Capturing NP chains by nanosheets is a relatively new technique for synthesizing hexaniobate based composites.[112a]

One-dimensional nanoscrolls of $K_4Nb_6O_{17}$ are mainly composed of three parts: outer surface, inner surface and interlayer region (Figure 1.8). It is reported that the interlayer region can be intercalated by metal oxides or organic molecules, improving the electric, magnetic, optical or catalytic properties of the host materials.[109, 111, 116] In addition to that, hexaniobate-magnetic multi-functional nanocomposites with hierarchical constructions may serve as important building blocks for various applications.[117] The guest magnetic 1D NP chains encapsulated in a semiconductor host nanoscroll can have significant impact on their materials properties, including chemical stability, permeability, conductivity, mechanical strength and optical properties. The fabrication of architectures of layered inorganic-noble metal alloy nanostructures provides tunable materials with enhanced photocatalytic activity via localized

surface plasmon resonance (LSPR), resulting in a strong absorbance at visible wavelengths and further improve surface area and the number of active absorption sites.[118] Furthermore, the ability to decorate hexaniobate nanostructures with noble metal NPs in various dimensions, allow the formation of nanoarchitectures for promising applications such as surface enhanced Raman scattering (SERS), nanometer-scale optical waveguides, photonics, biodiagnostics through the selective localized photothermal heating of cancer cells, biological and chemical sensing, optoelectronics and NP arrays for new optical band-gap materials.[71] Photocatalytic degradation of organic compounds by illuminated semiconductor-noble metal composites has also received increasing attention.[119] Some of the key research areas have been recognized as developing next generation photocatalysts, focusing on the loss of photoactivity during recycling and long-term storage to obtain sustained photoactivity.[120] In conclusion, development of hexaniobate-noble metal nanocomposites with higher surface states is very important to enable the broad scale preparation and utilization of photocatalysts.

1.3.3 Peapods

Nanopeapod structures represent a unique design incorporating different materials and properties into a single unit. The "pea" is most commonly a NP and the "pod" contains several peas (NPs). This class of structures have shown tremendous importance for fundamental science and technological applications, including enhanced photoresponse[121], improved electrochemical properties[122], and SERS-based chemical sensing[123]. The intrinsic properties of peapod structures can be further tuned by varying their components and achieving morphological uniformity.

In 1998, B. W. Smith reported the first C_{60}@CNT nanopeapod structure.[124] After that, a large family of nanopeapod structures with different components has been achieved by various research groups worldwide, such as Au@Ga_2O_3,[125] Au@MgO,[126] Cu@Al_2O_3,[127] Cu@TiO_2,[128]

$Ag@TiO_2$,[129] $Ni@TiO_2$,[130] $Au@Te$,[131] $Ag@SiO_2$,[123] $Ni@Ni_3S_2$,[132] and etc. Preparation methods such as atomic layer deposition (ALD), electrodeposition, Vapor-liquid-solid (VLS), Chemical-vapor-deposition (CVD), etc., have been extensively applied to synthesize nanopeapod structures. In all the above mentioned examples, outer component (pod) has always been nanotubes including SiO_2, Ga_2O_3, MgO, TiO_2, Al_2O_3, $CoAl_2O_4$, Ni_3S_2 and carbon nanotubes.[112a] In addition to nanotubes, nanoscrolls were also successfully used in the fabrication of nanopeapod structures. For examples, Yao et al. encapsulated magnetic NP chains in the hexaniobate nanoscrolls.[112a]

Although advances in synthetic strategies for nanopeapods have achieved significant success in morphological control, phase purity and crystallinity, peapod fabrication routes need much more improvement. Key challenges to improve the synthetic strategies include precise control of both pea and pod dimensions and engineering the encapsulation process. These requirements in principle could be met by developing advanced exfoliation and encapsulation techniques.

Recently, we developed a unique approach for peapod formation, where pre-formed NPs are encapsulated in scrolled hexaniobate nanosheets. This chemistry is especially flexible such that nanocomposites can be formed with a variety of NPs including metals, metal oxides and quantum dots. In addition to that, it is a low cost, rapid, scalable and versatile synthetic strategy. Chapter 3 will cover ferrite NP encapsulation and chapter 4 will cover other systems, including QD, metal oxides, and noble metals.

The importance of this advance is the promise it holds for the design and assembly of active nanocomposites. One can create very unique combinations of nanomaterials for potential applications in a variety of areas including catalysis, solar conversion, thermoelectrics, and

multiferroics.[2] Furthermore, the highly tunable nature of the composites makes them especially promising for applications in solar conversion; such properties are currently under investigation.

1.5 References

1. Daniel, M. C.; Astruc, D., Gold nanoparticles: Assembly, supramolecular chemistry, quantum-size-related properties, and applications toward biology, catalysis, and nanotechnology. *Chemical Reviews* **2004,** *104* (1), 293-346.
2. Wang, X.; Zhuang, J.; Peng, Q.; Li, Y. D., A general strategy for nanocrystal synthesis. *Nature* **2005,** *437* (7055), 121-124.
3. (a) Paul, D. R.; Robeson, L. M., Polymer nanotechnology: Nanocomposites. *Polymer* **2008,** *49* (15), 3187-3204; (b) Ferrari, M., Cancer nanotechnology: Opportunities and challenges. *Nature Reviews Cancer* **2005,** *5* (3), 161-171; (c) Sarikaya, M.; Tamerler, C.; Jen, A. K. Y.; Schulten, K.; Baneyx, F., Molecular biomimetics: nanotechnology through biology. *Nature Materials* **2003,** *2* (9), 577-585; (d) Park, C.; Yoon, J.; Thomas, E. L., Enabling nanotechnology with self assembled block copolymer patterns. *Polymer* **2003,** *44* (22), 6725-6760; (e) Hamley, I. W., Nanotechnology with soft materials. *Angewandte Chemie-International Edition* **2003,** *42* (15), 1692-1712.
4. Kamat, P. V., Quantum Dot Solar Cells. Semiconductor Nanocrystals as Light Harvesters. *J. Phys. Chem. C* **2008,** *112* (48), 18737-18753.
5. (a) Love, J. C.; Estroff, L. A.; Kriebel, J. K.; Nuzzo, R. G.; Whitesides, G. M., Self-assembled monolayers of thiolates on metals as a form of nanotechnology. *Chemical Reviews* **2005,** *105* (4), 1103-1169; (b) Tans, S. J.; Verschueren, A. R. M.; Dekker, C., Room-temperature transistor based on a single carbon nanotube. *Nature* **1998,** *393* (6680), 49-52.
6. (a) Lieber, C. M.; Wang, Z. L., Functional nanowires. *Mrs Bulletin* **2007,** *32* (2), 99-108; (b) Whang, D.; Jin, S.; Wu, Y.; Lieber, C. M., Large-scale hierarchical organization of nanowire arrays for integrated nanosystems. *Nano Letters* **2003,** *3* (9), 1255-1259; (c) Adams, D. M.; Brus, L.; Chidsey, C. E. D.; Creager, S.; Creutz, C.; Kagan, C. R.; Kamat, P. V.; Lieberman, M.; Lindsay, S.; Marcus, R. A.; Metzger, R. M.; Michel-Beyerle, M. E.; Miller, J. R.; Newton, M. D.; Rolison, D. R.; Sankey, O.; Schanze, K. S.; Yardley, J.; Zhu, X. Y., Charge transfer on the nanoscale: Current status. *Journal of Physical Chemistry B* **2003,** *107* (28), 6668-6697; (d) McEuen, P. L.; Fuhrer, M. S.; Park, H. K., Single-walled carbon nanotube electronics. *Ieee Transactions on Nanotechnology* **2002,** *1* (1), 78-85.
7. (a) Lee, J. H.; Huh, Y. M.; Jun, Y.; Seo, J.; Jang, J.; Song, H. T.; Kim, S.; Cho, E. J.; Yoon, H. G.; Suh, J. S.; Cheon, J., Artificially engineered magnetic nanoparticles for ultra-sensitive molecular imaging. *Nature Medicine* **2007,** *13* (1), 95-99; (b) O'Neal, D. P.; Hirsch, L. R.; Halas, N. J.; Payne, J. D.; West, J. L., Photo-thermal tumor ablation in mice using near infrared-absorbing nanoparticles. *Cancer Letters* **2004,** *209* (2), 171-176; (c) Berry, C. C.; Curtis, A. S. G., Functionalisation of magnetic nanoparticles for applications in biomedicine. *Journal of Physics D-Applied Physics* **2003,** *36* (13), R198-R206.
8. (a) Chau, R.; Datta, S.; Doczy, M.; Doyle, B.; Jin, J.; Kavalieros, J.; Majumdar, A.; Metz, M.; Radosavljevic, M., Benchmarking nanotechnology for high-performance and low-power logic transistor applications. *Ieee Transactions on Nanotechnology* **2005,** *4* (2), 153-158; (b) Williams, K. A.; Veenhuizen, P. T. M.; de la Torre, B. G.; Eritja, R.; Dekker, C., Nanotechnology - Carbon nanotubes with DNA recognition. *Nature* **2002,** *420* (6917), 761-

761; (c) Vettiger, P.; Cross, G.; Despont, M.; Drechsler, U.; Durig, U.; Gotsmann, B.; Haberle, W.; Lantz, M. A.; Rothuizen, H. E.; Stutz, R.; Binnig, G. K., The "millipede" - Nanotechnology entering data storage. *Ieee Transactions on Nanotechnology* **2002,** *1* (1), 39-55.

9. (a) Peppas, N. A.; Hilt, J. Z.; Khademhosseini, A.; Langer, R., Hydrogels in biology and medicine: From molecular principles to bionanotechnology. *Advanced Materials* **2006,** *18* (11), 1345-1360; (b) Langer, R.; Peppas, N. A., Advances in biomaterials, drug delivery, and bionanotechnology. *Aiche Journal* **2003,** *49* (12), 2990-3006.
10. (a) Moghimi, S. M.; Hunter, A. C.; Murray, J. C., Nanomedicine: current status and future prospects. *Faseb Journal* **2005,** *19* (3), 311-330; (b) Zhang, W. X., Nanoscale iron particles for environmental remediation: An overview. *Journal of Nanoparticle Research* **2003,** *5* (3-4), 323-332.
11. (a) Hochella, M. F., There's plenty of room at the bottom: Nanoscience in geochemistry. *Geochimica Et Cosmochimica Acta* **2002,** *66* (5), 735-743; (b) Junk, A.; Riess, F., From an idea to a vision: There's plenty of room at the bottom. *American Journal of Physics* **2006,** *74* (9), 825-830.
12. Monmaney, T., ENGINES OF CREATION - DREXLER,KE, MINSKY,M. *New York Times Book Review* **1986**, 8-8.
13. (a) Goldberger, J.; He, R. R.; Zhang, Y. F.; Lee, S. W.; Yan, H. Q.; Choi, H. J.; Yang, P. D., Single-crystal gallium nitride nanotubes. *Nature* **2003,** *422* (6932), 599-602; (b) Dai, H. J., Carbon nanotubes: Synthesis, integration, and properties. *Accounts of Chemical Research* **2002,** *35* (12), 1035-1044.
14. Stankovich, S.; Dikin, D. A.; Piner, R. D.; Kohlhaas, K. A.; Kleinhammes, A.; Jia, Y.; Wu, Y.; Nguyen, S. T.; Ruoff, R. S., Synthesis of graphene-based nanosheets via chemical reduction of exfoliated graphite oxide. *Carbon* **2007,** *45* (7), 1558-1565.
15. Kelly, K. L.; Coronado, E.; Zhao, L. L.; Schatz, G. C., The optical properties of metal nanoparticles: The influence of size, shape, and dielectric environment. *Journal of Physical Chemistry B* **2003,** *107* (3), 668-677.
16. Sun, Y. G.; Xia, Y. N., Shape-controlled synthesis of gold and silver nanoparticles. *Science* **2002,** *298* (5601), 2176-2179.
17. Jana, N. R.; Gearheart, L.; Murphy, C. J., Wet chemical synthesis of high aspect ratio cylindrical gold nanorods. *J. Phys. Chem. B* **2001,** *105* (19), 4065-4067.
18. Liu, B.; Xie, J.; Lee, J.; Ting, Y.; Chen, J. P., Optimization of high-yield biological synthesis of single-crystalline gold nanoplates. *J. Phys. Chem. B* **2005,** *109* (32), 15256-15263.
19. Zhang, J. H.; Liu, H. Y.; Wang, Z. L.; Ming, N. B., Synthesis of gold regular octahedra with controlled size and plasmon resonance. *Appl. Phys. Lett.* **2007,** *90* (16), 163122.
20. Wiley, B. J.; Xiong, Y. J.; Li, Z. Y.; Yin, Y. D.; Xia, Y. N., Right bipyramids of silver: a new shape derived from single twinned seeds. *Nano Lett* **2006,** *6* (4), 765-768.
21. Jin, R. C.; Cao, Y. W.; Mirkin, C. A.; Kelly, K. L.; Schatz, G. C.; Zheng, J. G., Photoinduced conversion of silver nanospheres to nanoprisms. *Science* **2001,** *294* (5548), 1901-1903.
22. Wang, X. R.; Dai, H. J., Etching and narrowing of graphene from the edges. *Nature Chemistry* **2010,** *2* (8), 661-665.
23. Altman, M.; Shukla, A. D.; Zubkov, T.; Evmenenko, G.; Dutta, P.; van der Boom, M. E., Controlling structure from the bottom-up: Structural and optical properties of layer-by-layer assembled palladium coordination-based multilayers. *J. Am. Chem. Soc.* **2006,** *128* (22), 7374-7382.

24. Helmersson, U.; Lattemann, M.; Bohlmark, J.; Ehiasarian, A. P.; Gudmundsson, J. T., Ionized physical vapor deposition (IPVD): A review of technology and applications. *Thin Solid Films* **2006,** *513* (1-2), 1-24.
25. Carcia, P. F.; McLean, R. S.; Reilly, M. H.; Nunes, G., Transparent ZnO thin-film transistor fabricated by rf magnetron sputtering. *Applied Physics Letters* **2003,** *82* (7), 1117-1119.
26. (a) Hiramatsu, H.; Osterloh, F. E., A simple large-scale synthesis of nearly monodisperse gold and silver nanoparticles with adjustable sizes and with exchangeable surfactants. *Chemistry of Materials* **2004,** *16* (13), 2509-2511; (b) Viculis, L. M.; Mack, J. J.; Kaner, R. B., A chemical route to carbon nanoscrolls. *Science* **2003,** *299* (5611), 1361-1361.
27. (a) Gao, J. H.; Gu, H. W.; Xu, B., Multifunctional Magnetic Nanoparticles: Design, Synthesis, and Biomedical Applications. *Accounts of Chemical Research* **2009,** *42* (8), 1097-1107; (b) West, J. L.; Halas, N. J., Engineered nanomaterials for biophotonics applications: Improving sensing, imaging, and therapeutics. *Annual Review of Biomedical Engineering* **2003,** *5*, 285-292.
28. (a) Scholl, J. A.; Garcia-Etxarri, A.; Koh, A. L.; Dionne, J. A., Observation of Quantum Tunneling between Two Plasmonic Nanoparticles. *Nano Letters* **2013,** *13* (2), 564-569; (b) Petralia, R. S.; Yokotani, N.; Wenthold, R. J., LIGHT AND ELECTRON-MICROSCOPE DISTRIBUTION OF THE NMDA RECEPTOR SUBUNIT NMDAR1 IN THE RAT NERVOUS-SYSTEM USING A SELECTIVE ANTIPEPTIDE ANTIBODY. *Journal of Neuroscience* **1994,** *14* (2), 667-696; (c) Batson, P. E., SIMULTANEOUS STEM IMAGING AND ELECTRON-ENERGY-LOSS SPECTROSCOPY WITH ATOMIC-COLUMN SENSITIVITY. *Nature* **1993,** *366* (6457), 727-728.
29. Elliott, S. L.; Broom, R. F.; Humphreys, C. J., Dopant profiling with the scanning electron microscope - A study of Si. *Journal of Applied Physics* **2002,** *91* (11), 9116-9122.
30. Nitzan, A., Electron transmission through molecules and molecular interfaces. *Annual Review of Physical Chemistry* **2001,** *52*, 681-750.
31. Muller, D. A.; Kourkoutis, L. F.; Murfitt, M.; Song, J. H.; Hwang, H. Y.; Silcox, J.; Dellby, N.; Krivanek, O. L., Atomic-scale chemical imaging of composition and bonding by aberration-corrected microscopy. *Science* **2008,** *319* (5866), 1073-1076.
32. Berger, S. D.; McKenzie, D. R.; Martin, P. J., EELS ANALYSIS OF VACUUM ARC-DEPOSITED DIAMOND-LIKE FILMS. *Philosophical Magazine Letters* **1988,** *57* (6), 285-290.
33. Dai, H. J.; Hafner, J. H.; Rinzler, A. G.; Colbert, D. T.; Smalley, R. E., Nanotubes as nanoprobes in scanning probe microscopy. *Nature* **1996,** *384* (6605), 147-150.
34. Maltezopoulos, T.; Bolz, A.; Meyer, C.; Heyn, C.; Hansen, W.; Morgenstern, M.; Wiesendanger, R., Wave-function mapping of InAs quantum dots by scanning tunneling spectroscopy. *Physical Review Letters* **2003,** *91* (19).
35. (a) Guzelian, A. A.; Banin, U.; Kadavanich, A. V.; Peng, X.; Alivisatos, A. P., Colloidal chemical synthesis and characterization of InAs nanocrystal quantum dots. *Applied Physics Letters* **1996,** *69* (10), 1432-1434; (b) Hatchard, T. D.; Dahn, J. R., In situ XRD and electrochemical study of the reaction of lithium with amorphous silicon. *Journal of the Electrochemical Society* **2004,** *151* (6), A838-A842.
36. Powell, C. J., Improvements in the reliability of X-ray photoelectron spectroscopy for surface analysis. *Journal of Chemical Education* **2004,** *81* (12), 1734-1750.
37. (a) Kalsin, A. M.; Fialkowski, M.; Paszewski, M.; Smoukov, S. K.; Bishop, K. J. M.; Grzybowski, B. A., Electrostatic self-assembly of binary nanoparticle crystals with a

diamond-like lattice. *Science* **2006,** *312* (5772), 420-424; (b) Zeng, H.; Li, J.; Liu, J. P.; Wang, Z. L.; Sun, S. H., Exchange-coupled nanocomposite magnets by nanoparticle self-assembly. *Nature* **2002,** *420* (6914), 395-398.
38. Sun, S. H.; Murray, C. B.; Weller, D.; Folks, L.; Moser, A., Monodisperse FePt nanoparticles and ferromagnetic FePt nanocrystal superlattices. *Science* **2000,** *287* (5460), 1989-1992.
39. (a) Lin, Y.; Boker, A.; He, J. B.; Sill, K.; Xiang, H. Q.; Abetz, C.; Li, X. F.; Wang, J.; Emrick, T.; Long, S.; Wang, Q.; Balazs, A.; Russell, T. P., Self-directed self-assembly of nanoparticle/copolymer mixtures. *Nature* **2005,** *434* (7029), 55-59; (b) Kotov, N. A.; Dekany, I.; Fendler, J. H., LAYER-BY-LAYER SELF-ASSEMBLY OF POLYELECTROLYTE-SEMICONDUCTOR NANOPARTICLE COMPOSITE FILMS. *Journal of Physical Chemistry* **1995,** *99* (35), 13065-13069.
40. (a) Grzelczak, M.; Perez-Juste, J.; Mulvaney, P.; Liz-Marzan, L. M., Shape control in gold nanoparticle synthesis. *Chemical Society Reviews* **2008,** *37* (9), 1783-1791; (b) Katz, E.; Willner, I., Integrated nanoparticle-biomolecule hybrid systems: Synthesis, properties, and applications. *Angewandte Chemie-International Edition* **2004,** *43* (45), 6042-6108; (c) O'Brien, S.; Brus, L.; Murray, C. B., Synthesis of monodisperse nanoparticles of barium titanate: Toward a generalized strategy of oxide nanoparticle synthesis. *J. Am. Chem. Soc.* **2001,** *123* (48), 12085-12086.
41. Frey, M. H.; Payne, D. A., SYNTHESIS AND PROCESSING OF BARIUM-TITANATE CERAMICS FROM ALKOXIDE SOLUTIONS AND MONOLITHIC GELS. *Chemistry of Materials* **1995,** *7* (1), 123-129.
42. (a) Asiaie, R.; Zhu, W. D.; Akbar, S. A.; Dutta, P. K., Characterization of submicron particles of tetragonal BaTiO3. *Chemistry of Materials* **1996,** *8* (1), 226-234; (b) Dutta, P. K.; Asiaie, R.; Akbar, S. A.; Zhu, W. D., HYDROTHERMAL SYNTHESIS AND DIELECTRIC-PROPERTIES OF TETRAGONAL BATIO3. *Chemistry of Materials* **1994,** *6* (9), 1542-1548.
43. Wei, X.; Xu, G.; Ren, Z. H.; Wang, Y. G.; Shen, G.; Han, G. R., Synthesis of highly dispersed barium titanate nanoparticles by a novel solvothermal method. *Journal of the American Ceramic Society* **2008,** *91* (1), 315-318.
44. Martirosyan, K. S.; Nawarathna, D.; Claycomb, J. R.; Miller, J. H.; Luss, D., Complex dielectric behaviour during formation of BaTiO3 by combustion synthesis. *Journal of Physics D-Applied Physics* **2006,** *39* (16), 3689-3694.
45. Li, X. P.; Shih, W. H., Size effects in barium titanate particles and clusters. *Journal of the American Ceramic Society* **1997,** *80* (11), 2844-2852.
46. Sun, W. A.; Pang, Y.; Li, J. Q.; Ao, W. Q., Particle coarsening II: Growth kinetics of hydrothermal BaTiO3. *Chemistry of Materials* **2007,** *19* (7), 1772-1779.
47. Rebolledo, A. F.; Fuertes, A. B.; Gonzalez-Carreno, T.; Sevilla, M.; Valdes-Solis, T.; Tartaj, P., Signatures of clustering in superparamagnetic colloidal nanocomposites of an inorganic and hybrid nature. *Small* **2008,** *4* (2), 254-261.
48. Dinh, C. T.; Nguyen, T. D.; Kleitz, F.; Do, T. O., Shape-Controlled Synthesis of Highly Crystalline Titania Nanocrystals. *Acs Nano* **2009,** *3* (11), 3737-3743.
49. (a) Tao, A. R.; Habas, S.; Yang, P. D., Shape control of colloidal metal nanocrystals. *Small* **2008,** *4* (3), 310-325; (b) Perez-Juste, J.; Pastoriza-Santos, I.; Liz-Marzan, L. M.; Mulvaney, P., Gold nanorods: Synthesis, characterization and applications. *Coordination Chemistry Reviews* **2005,** *249* (17-18), 1870-1901.

50. Sun, S. H., Recent advances in chemical synthesis, self-assembly, and applications of FePt nanoparticles. *Advanced Materials* **2006,** *18* (4), 393-403.
51. (a) Yin, Y.; Alivisatos, A. P., Colloidal nanocrystal synthesis and the organic-inorganic interface. *Nature* **2005,** *437* (7059), 664-670; (b) Wen, P. H.; Itoh, H.; Tang, W. P.; Feng, Q., Single nanocrystals of anatase-type TiO2 prepared from layered titanate nanosheets: Formation mechanism and characterization of surface properties. *Langmuir* **2007,** *23* (23), 11782-11790.
52. Bonnemann, H.; Richards, R. M., Nanoscopic metal particles - Synthetic methods and potential applications. *European Journal of Inorganic Chemistry* **2001,** (10), 2455-2480.
53. (a) Deng, Z. X.; Li, L. B.; Li, Y. D., Novel inorganic-organic-layered structures: Crystallographic understanding of both phase and morphology formations of one-dimensional CdE (E = S, Se, Te) nanorods in ethylenediamine. *Inorganic Chemistry* **2003,** *42* (7), 2331-2341; (b) Wang, C.; Deng, Z. X.; Zhang, G. H.; Fan, S. S.; Li, Y. D., Synthesis of nanocrystalline TiO2 in alcohols. *Powder Technology* **2002,** *125* (1), 39-44; (c) Rajamathi, M.; Seshadri, R., Oxide and chalcogenide nanoparticles from hydrothermal/solvothermal reactions. *Current Opinion in Solid State & Materials Science* **2002,** *6* (4), 337-345.
54. Mohanty, D.; Chaubey, G. S.; Yourdkhani, A.; Adireddy, S.; Caruntu, G.; Wiley, J. B., Synthesis and piezoelectric response of cubic and spherical LiNbO3 nanocrystals. *Rsc Advances* **2012,** *2* (5), 1913-1916.
55. (a) Li, H. X.; Bian, Z. F.; Zhu, J.; Zhang, D. Q.; Li, G. S.; Huo, Y. N.; Li, H.; Lu, Y. F., Mesoporous titania spheres with tunable chamber stucture and enhanced photocatalytic activity. *J. Am. Chem. Soc.* **2007,** *129* (27), 8406-+; (b) Rao, C. N. R.; Deepak, F. L.; Gundiah, G.; Govindaraj, A., Inorganic nanowires. *Progress in Solid State Chemistry* **2003,** *31* (1-2), 5-147; (c) Chen, W.; Wang, J. Y.; Chen, C.; Yue, Q.; Yuan, H. M.; Chen, J. S.; Wang, S. N., Photoluminescent metal-organic polymer constructed from trimetallic clusters and mixed carboxylates. *Inorganic Chemistry* **2003,** *42* (4), 944-946; (d) Patzke, G. R.; Krumeich, F.; Nesper, R., Oxidic nanotubes and nanorods - Anisotropic modules for a future nanotechnology. *Angewandte Chemie-International Edition* **2002,** *41* (14), 2446-2461; (e) Cao, R.; Sun, D. F.; Liang, Y. C.; Hong, M. C.; Tatsumi, K.; Shi, Q., Syntheses and characterizations of three-dimensional channel-like polymeric lanthanide complexes constructed by 1,2,4,5-benzenetetracarboxylic acid. *Inorganic Chemistry* **2002,** *41* (8), 2087-2094.
56. (a) Walton, R. I., Subcritical solvothermal synthesis of condensed inorganic materials. *Chemical Society Reviews* **2002,** *31* (4), 230-238; (b) Qian, Y. T., Solvothermal synthesis of nanocrystalline III-V semiconductors. *Advanced Materials* **1999,** *11* (13), 1101-+.
57. Adireddy, S.; Lin, C. K.; Cao, B. B.; Zhou, W. L.; Caruntu, G., Solution-Based Growth of Monodisperse Cube-Like BaTiO3 Colloidal Nanocrystals. *Chemistry of Materials* **2010,** *22* (6), 1946-1948.
58. Wang, W. Z.; Geng, Y.; Qian, Y. T.; Xie, Y.; Liu, X. M., Synthesis and characterization of nanocrystalline Bi2Se3 by solvothermal method. *Materials Research Bulletin* **1999,** *34* (1), 131-134.
59. Yu, S. H.; Yang, J.; Han, Z. H.; Zhou, Y.; Yang, R. Y.; Qian, Y. T.; Zhang, Y. H., Controllable synthesis of nanocrystalline CdS with different morphologies and particle sizes by a novel solvothermal process. *Journal of Materials Chemistry* **1999,** *9* (6), 1283-1287.
60. Gautam, U. K.; Rajamathi, M.; Meldrum, F.; Morgan, P. E. D.; Seshadri, R., A solvothermal route to capped CdSe nanoparticles. *Chemical Communications* **2001,** (7), 629-630.

61. Inoue, M.; Kimura, M.; Inui, T., Transparent colloidal solution of 2 nm ceria particles. *Chemical Communications* **1999,** (11), 957-958.
62. Thimmaiah, S.; Rajamathi, M.; Singh, N.; Bera, P.; Meldrum, F.; Chandrasekhar, N.; Seshadri, R., A solvothermal route to capped nanoparticles of gamma-Fe2O3 and CoFe2O4. *Journal of Materials Chemistry* **2001,** *11* (12), 3215-3221.
63. Wang, W. Z.; Geng, Y.; Qian, Y. T.; Wang, C.; Liu, X. M., A convenient, low temperature route to nanocrystalline SnSe. *Materials Research Bulletin* **1999,** *34* (3), 403-406.
64. Wu, B. H.; Guo, C. Y.; Zheng, N. F.; Xie, Z. X.; Stucky, G. D., Nonaqueous Production of Nanostructured Anatase with High-Energy Facets. *J. Am. Chem. Soc.* **2008,** *130* (51), 17563-17567.
65. Li, Y. D.; Ding, Y.; Qian, Y. T.; Zhang, Y.; Yang, L., A solvothermal elemental reaction to produce nanocrystalline ZnSe. *Inorganic Chemistry* **1998,** *37* (12), 2844-2845.
66. Zhao, J. P.; Fan, W. H.; Wu, D.; Sun, Y. H., Stable nanocrystalline zirconia sols prepared by a novel method: Alcohol thermal synthesis. *Journal of Materials Research* **2000,** *15* (2), 402-406.
67. (a) Farokhzad, O. C.; Langer, R., Impact of Nanotechnology on Drug Delivery. *Acs Nano* **2009,** *3* (1), 16-20; (b) Kang, Y. S.; Risbud, S.; Rabolt, J. F.; Stroeve, P., Synthesis and characterization of nanometer-size Fe3O4 and gamma-Fe2O3 particles. *Chem. Mat.* **1996,** *8* (9), 2209-&; (c) Yu, H.; Chen, M.; Rice, P. M.; Wang, S. X.; White, R. L.; Sun, S. H., Dumbbell-like bifunctional Au-Fe3O4 nanoparticles. *Nano Lett.* **2005,** *5* (2), 379-382; (d) Yavuz, C. T.; Mayo, J. T.; Yu, W. W.; Prakash, A.; Falkner, J. C.; Yean, S.; Cong, L. L.; Shipley, H. J.; Kan, A.; Tomson, M.; Natelson, D.; Colvin, V. L., Low-field magnetic separation of monodisperse Fe3O4 nanocrystals. *Science* **2006,** *314* (5801), 964-967; (e) Wang, J.; Chen, Q. W.; Zeng, C.; Hou, B. Y., Magnetic-field-induced growth of single-crystalline Fe3O4 nanowires. *Adv. Mater.* **2004,** *16* (2), 137-+; (f) Taberna, L.; Mitra, S.; Poizot, P.; Simon, P.; Tarascon, J. M., High rate capabilities Fe3O4-based Cu nano-architectured electrodes for lithium-ion battery applications. *Nature Materials* **2006,** *5* (7), 567-573; (g) Bazylinski, D. A.; Heywood, B. R.; Mann, S.; Frankel, R. B., FE3O4 AND FE3S4 IN A BACTERIUM. *Nature* **1993,** *366* (6452), 218-218.
68. Yu, W. W.; Falkner, J. C.; Yavuz, C. T.; Colvin, V. L., Synthesis of monodisperse iron oxide nanocrystals by thermal decomposition of iron carboxylate salts. *Chemical Communications* **2004,** (20), 2306-2307.
69. Barnakov, Y. A.; Yu, M. H.; Rosenzweig, Z., Manipulation of the magnetic properties of magnetite-silica nanocomposite materials by controlled Stober synthesis. *Langmuir* **2005,** *21* (16), 7524-7527.
70. Cobley, C. M.; Chen, J. Y.; Cho, E. C.; Wang, L. V.; Xia, Y. N., Gold nanostructures: a class of multifunctional materials for biomedical applications. *Chem. Soc. Rev.* **2011,** *40* (1), 44-56.
71. (a) Skrabalak, S. E.; Chen, J. Y.; Sun, Y. G.; Lu, X. M.; Au, L.; Cobley, C. M.; Xia, Y. N., Gold Nanocages: Synthesis, Properties, and Applications. *Accounts Chem. Res.* **2008,** *41* (12), 1587-1595; (b) Haes, A. J.; Zou, S. L.; Schatz, G. C.; Van Duyne, R. P., A nanoscale optical biosensor: The long range distance dependence of the localized surface plasmon resonance of noble metal nanoparticles. *J. Phys. Chem. B* **2004,** *108* (1), 109-116.
72. Saruyama, M.; Kanehara, M.; Teranishi, T., Drastic Structural Transformation of Cadmium Chalcogenide Nanoparticles Using Chloride Ions and Surfactants. *J. Am. Chem. Soc.* **2010,** *132* (10), 3280-+.

73. (a) Alivisatos, A. P., Semiconductor clusters, nanocrystals, and quantum dots. *Science* **1996,** *271* (5251), 933-937; (b) Lewis, N. S., Toward cost-effective solar energy use. *Science* **2007,** *315* (5813), 798-801.
74. (a) Rogach, A. L.; Talapin, D. V.; Shevchenko, E. V.; Kornowski, A.; Haase, M.; Weller, H., Organization of matter on different size scales: Monodisperse nanocrystals and their superstructures. *Advanced Functional Materials* **2002,** *12* (10), 653-664; (b) Murray, C. B.; Kagan, C. R.; Bawendi, M. G., Synthesis and characterization of monodisperse nanocrystals and close-packed nanocrystal assemblies. *Annual Review of Materials Science* **2000,** *30*, 545-610; (c) Brus, L., Chemical approaches to semiconductor nanocrystals. *Journal of Physics and Chemistry of Solids* **1998,** *59* (4), 459-465.
75. Joo, J.; Na, H. B.; Yu, T.; Yu, J. H.; Kim, Y. W.; Wu, F. X.; Zhang, J. Z.; Hyeon, T., Generalized and facile synthesis of semiconducting metal sulfide nanocrystals. *J. Am. Chem. Soc.* **2003,** *125* (36), 11100-11105.
76. Bruchez, M.; Moronne, M.; Gin, P.; Weiss, S.; Alivisatos, A. P., Semiconductor nanocrystals as fluorescent biological labels. *Science* **1998,** *281* (5385), 2013-2016.
77. Goulet, P. J. G.; Bourret, G. R.; Lennox, R. B., Facile Phase Transfer of Large, Water-Soluble Metal Nanoparticles to Nonpolar Solvents. *Langmuir* **2012,** *28* (5), 2909-2913.
78. Fang, X. L.; Chen, C.; Jin, M. S.; Kuang, Q.; Xie, Z. X.; Xie, S. Y.; Huang, R. B.; Zheng, L. S., Single-crystal-like hematite colloidal nanocrystal clusters: synthesis and applications in gas sensors, photocatalysis and water treatment. *Journal of Materials Chemistry* **2009,** *19* (34), 6154-6160.
79. Khanal, B. P.; Zubarev, E. R., Rings of nanorods. *Angewandte Chemie-International Edition* **2007,** *46* (13), 2195-2198.
80. (a) Hagfeldt, A.; Boschloo, G.; Sun, L. C.; Kloo, L.; Pettersson, H., Dye-Sensitized Solar Cells. *Chemical Reviews* **2010,** *110* (11), 6595-6663; (b) Tian, B. Z.; Zheng, X. L.; Kempa, T. J.; Fang, Y.; Yu, N. F.; Yu, G. H.; Huang, J. L.; Lieber, C. M., Coaxial silicon nanowires as solar cells and nanoelectronic power sources. *Nature* **2007,** *449* (7164), 885-U8; (c) Law, M.; Greene, L. E.; Johnson, J. C.; Saykally, R.; Yang, P. D., Nanowire dye-sensitized solar cells. *Nature Materials* **2005,** *4* (6), 455-459; (d) Hagfeldt, A.; Gratzel, M., Molecular photovoltaics. *Accounts of Chemical Research* **2000,** *33* (5), 269-277.
81. (a) Ajayan, P. M., Nanotubes from carbon. *Chemical Reviews* **1999,** *99* (7), 1787-1799; (b) Baughman, R. H.; Zakhidov, A. A.; de Heer, W. A., Carbon nanotubes - the route toward applications. *Science* **2002,** *297* (5582), 787-792.
82. (a) Shi, L.; Xu, Y. M.; Li, Q., Controlled growth of lead oxide nanosheets, scrolled nanotubes, and nanorods. *Crystal Growth & Design* **2008,** *8* (10), 3521-3525; (b) Lieber, C. M., One-dimensional nanostructures: Chemistry, physics & applications. *Solid State Communications* **1998,** *107* (11), 607-616; (c) Feng, S. H.; Xu, R. R., New materials in hydrothermal synthesis. *Accounts of Chemical Research* **2001,** *34* (3), 239-247.
83. (a) Xing, J.; Fang, W. Q.; Zhao, H. J.; Yang, H. G., Inorganic Photocatalysts for Overall Water Splitting. *Chemistry-an Asian Journal* **2012,** *7* (4), 642-657; (b) Townsend, T. K.; Sabio, E. M.; Browning, N. D.; Osterloh, F. E., Improved Niobate Nanoscroll Photocatalysts for Partial Water Splitting. *Chemsuschem* **2011,** *4* (2), 185-190; (c) Abe, R., Recent progress on photocatalytic and photoelectrochemical water splitting under visible light irradiation. *Journal of Photochemistry and Photobiology C-Photochemistry Reviews* **2010,** *11* (4), 179-209; (d) Sarahan, M. C.; Carroll, E. C.; Allen, M.; Larsen, D. S.; Browning, N. D.; Osterloh, F. E., K4Nb6O17-derived photocatalysts for hydrogen evolution from water: Nanoscrolls

versus nanosheets. *Journal of Solid State Chemistry* **2008,** *181* (7), 1678-1683; (e) Lin, H. Y.; Lee, T. H.; Sie, C. Y., Photocatalytic hydrogen production with nickel oxide intercalated K4Nb6O17 under visible light irradiation. *International Journal of Hydrogen Energy* **2008,** *33* (15), 4055-4063; (f) Xie, X.; Ju, L.; Feng, X. F.; Sun, Y. H.; Zhou, R. F.; Liu, K.; Fan, S. S.; Li, Q. L.; Jiang, K. L., Controlled Fabrication of High-Quality Carbon Nanoscrolls from Monolayer Graphene. *Nano Letters* **2009,** *9* (7), 2565-2570; (g) Golberg, D., NANOMATERIALS Exfoliating the inorganics. *Nature Nanotechnology* **2011,** *6* (4), 200-201; (h) Hamilton, E. J. M.; Dolan, S. E.; Mann, C. M.; Colijn, H. O.; McDonald, C. A.; Shore, S. G., PREPARATION OF AMORPHOUS BORON-NITRIDE AND ITS CONVERSION TO A TURBOSTRATIC, TUBULAR FORM. *Science* **1993,** *260* (5108), 659-661.

84. (a) Cao, J.; Musfeldt, J. L.; Mazumdar, S.; Chernova, N. A.; Whittingham, M. S., Pinned low-energy electronic excitation in metal-exchanged vanadium oxide nanoscrolls. *Nano Letters* **2007,** *7* (8), 2351-2355; (b) Maeda, K.; Eguchi, M.; Youngblood, W. J.; Mallouk, T. E., Niobium Oxide Nanoscrolls as Building Blocks for Dye-Sensitized Hydrogen Production from Water under Visible Light Irradiation. *Chemistry of Materials* **2008,** *20* (21), 6770-6778.
85. Saito, R.; Fujita, M.; Dresselhaus, G.; Dresselhaus, M. S., ELECTRONIC-STRUCTURE OF GRAPHENE TUBULES BASED ON C-60. *Physical Review B* **1992,** *46* (3), 1804-1811.
86. Li, Y. D. D.; Li, X. L. L.; He, R. R. R.; Zhu, J.; Deng, Z. X. X., Artificial lamellar mesostructures to WS2 nanotubes. *Journal of the American Chemical Society* **2002,** *124* (7), 1411-1416.
87. Feldman, Y.; Wasserman, E.; Srolovitz, D. J.; Tenne, R., HIGH-RATE, GAS-PHASE GROWTH OF MOS2 NESTED INORGANIC FULLERENES AND NANOTUBES. *Science* **1995,** *267* (5195), 222-225.
88. Richter, C.; Schmuttenmaer, C. A., Exciton-like trap states limit electron mobility in TiO2 nanotubes. *Nature Nanotechnology* **2010,** *5* (11), 769-772.
89. Ma, R. Z.; Bando, Y.; Sasaki, T., Directly rolling nanosheets into nanotubes. *Journal of Physical Chemistry B* **2004,** *108* (7), 2115-2119.
90. Ye, C. H.; Bando, Y.; Shen, G. Z.; Golberg, D., Formation of crystalline SrAl2O4 nanotubes by a roll-up and post-annealing approach. *Angewandte Chemie-International Edition* **2006,** *45* (30), 4922-4926.
91. Saupe, G. B.; Waraksa, C. C.; Kim, H. N.; Han, Y. J.; Kaschak, D. M.; Skinner, D. M.; Mallouk, T. E., Nanoscale tubules formed by exfoliation of potassium hexaniobate. *Chemistry of Materials* **2000,** *12* (6), 1556-1562.
92. Schaak, R. E.; Mallouk, T. E., Prying apart Ruddlesden-Popper phases: Exfoliation into sheets and nanotubes for assembly of perovskite thin films. *Chem. Mat.* **2000,** *12* (11), 3427-3434.
93. Uma, S.; Raju, A. R.; Gopalakrishnan, J., BRIDGING THE RUDDLESDEN-POPPER AND THE DION-JACOBSON SERIES OF LAYERED PEROVSKITES - SYNTHESIS OF LAYERED OXIDES, A2-XLA2TI3-XNBXO10 (A=K, RB), EXHIBITING ION-EXCHANGE. *Journal of Materials Chemistry* **1993,** *3* (7), 709-713.
94. Corr, S. A.; Grossman, M.; Furman, J. D.; Melot, B. C.; Cheetham, A. K.; Heier, K. R.; Seshadri, R., Controlled Reduction of Vanadium Oxide Nanoscrolls: Crystal Structure, Morphology, and Electrical Properties. *Chemistry of Materials* **2008,** *20* (20), 6396-6404.

95. (a) Sun, Y. Q.; Wu, Q. O.; Shi, G. Q., Graphene based new energy materials. *Energy & Environmental Science* **2011,** *4* (4), 1113-1132; (b) Cui, X.; Zhang, C. Z.; Hao, R.; Hou, Y. L., Liquid-phase exfoliation, functionalization and applications of graphene. *Nanoscale* **2011,** *3* (5), 2118-2126; (c) Chen, D.; Tang, L. H.; Li, J. H., Graphene-based materials in electrochemistry. *Chemical Society Reviews* **2010,** *39* (8), 3157-3180; (d) Dias, A. S.; Lima, S.; Carriazo, D.; Rives, V.; Pillinger, M.; Valente, A. A., Exfoliated titanate, niobate and titanoniobate nanosheets as solid acid catalysts for the liquid-phase dehydration of D-xylose into furfural. *Journal of Catalysis* **2006,** *244* (2), 230-237.
96. (a) Takagi, S.; Eguchi, M.; Tryk, D. A.; Inoue, H., Porphyrin photochemistry in inorganic/organic hybrid materials: Clays, layered semiconductors, nanotubes, and mesoporous materials. *Journal of Photochemistry and Photobiology C-Photochemistry Reviews* **2006,** *7* (2-3), 104-126; (b) Mao, J. G.; Wang, Z. K.; Clearfield, A., New lead inorganic-organic hybrid microporous and layered materials: Synthesis, properties, and crystal structures. *Inorganic Chemistry* **2002,** *41* (23), 6106-6111; (c) Shimojima, A.; Sugahara, Y.; Kuroda, K., Inorganic-organic layered materials derived via the hydrolysis and polycondensation of trialkoxy(alkyl)silanes. *Bulletin of the Chemical Society of Japan* **1997,** *70* (11), 2847-2853; (d) Kanatzidis, M. G.; Tonge, L. M.; Marks, T. J.; Marcy, H. O.; Kannewurf, C. R., INSITU INTERCALATIVE POLYMERIZATION OF PYRROLE IN FEOCL - A NEW CLASS OF LAYERED, CONDUCTING POLYMER INORGANIC HYBRID MATERIALS. *J. Am. Chem. Soc.* **1987,** *109* (12), 3797-3799.
97. Kosynkin, D. V.; Higginbotham, A. L.; Sinitskii, A.; Lomeda, J. R.; Dimiev, A.; Price, B. K.; Tour, J. M., Longitudinal unzipping of carbon nanotubes to form graphene nanoribbons. *Nature* **2009,** *458* (7240), 872-U5.
98. Chopra, N. G.; Luyken, R. J.; Cherrey, K.; Crespi, V. H.; Cohen, M. L.; Louie, S. G.; Zettl, A., BORON-NITRIDE NANOTUBES. *Science* **1995,** *269* (5226), 966-967.
99. Kasuga, T.; Hiramatsu, M.; Hoson, A.; Sekino, T.; Niihara, K., Formation of titanium oxide nanotube. *Langmuir* **1998,** *14* (12), 3160-3163.
100. Sanjaya Ranmohotti, K. G.; Josepha, E.; Choi, J. L.; Zhang, J. X.; Wiley, J. B., Topochemical manipulation of perovskites: low-temperature reaction strategies for directing structure and properties. *Adv. Mater.* **2011,** *23* (4), 442-460.
101. Sato, M.; Abo, J.; Jin, T., Structure examination of $NaLaNb_2O_7$ synthesized by soft chemistry. *Solid State Ionics* **1992,** *57* (3-4), 285-293.
102. (a) Hernandez, B. A.; Chang, K. S.; Fisher, E. R.; Dorhout, P. K., Sol-gel template synthesis and characterization of $BaTiO_3$ and $PbTiO_3$ nanotubes. *Chem. Mater.* **2002,** *14* (2), 480-482; (b) Hu, M. Z. C.; Miller, G. A.; Payzant, E. A.; Rawn, C. J., Homogeneous (co) precipitation of inorganic salts for synthesis of monodispersed barium titanate particles. *J. Mater. Sci.* **2000,** *35* (12), 2927-2936.
103. Rapoport, L.; Fleischer, N.; Tenne, R., Applications of WS2 (MoS2) inorganic nanotubes and fullerene-like nanoparticles for solid lubrication and for structural nanocomposites. *Journal of Materials Chemistry* **2005,** *15* (18), 1782-1788.
104. (a) Vurgaftman, I.; Meyer, J. R.; Ram-Mohan, L. R., Band parameters for III-V compound semiconductors and their alloys. *Journal of Applied Physics* **2001,** *89* (11), 5815-5875; (b) Strite, S.; Morkoc, H., GAN, AIN, AND INN - A REVIEW. *Journal of Vacuum Science & Technology B* **1992,** *10* (4), 1237-1266.

105. Domen, K.; Kudo, A.; Shibata, M.; Tanaka, A.; Maruya, K.; Onishi, T., NOVEL PHOTOCATALYSTS, ION-EXCHANGED K4NB6O17, WITH A LAYER STRUCTURE. *J. Chem. Soc.-Chem. Commun.* **1986,** (23), 1706-1707.
106. Gasperin, M.; Le Bihan, M. T., Mecanisme d'hydratation des niobates alcalins lamellaires de formule $A_4Nb_6O_{17}$ (A=K, Rb, Cs). *J. Solid State Chem.* **1982,** *43* (3), 346-353.
107. Kudo, A.; Tanaka, A.; Domen, K.; Maruya, K.; Aika, K.; Onishi, T., PHOTOCATALYTIC DECOMPOSITION OF WATER OVER NIO-K4NB6O17 CATALYST. *Journal of Catalysis* **1988,** *111* (1), 67-76.
108. (a) Kudo, A.; Sayama, K.; Tanaka, A.; Asakura, K.; Domen, K.; Maruya, K.; Onishi, T., NICKEL-LOADED K4NB6O17 PHOTOCATALYST IN THE DECOMPOSITION OF H2O INTO H-2 AND O-2 - STRUCTURE AND REACTION-MECHANISM. *J. Catal.* **1989,** *120* (2), 337-352; (b) Domen, K.; Ebina, Y.; Sekine, T.; Tanaka, A.; Kondo, J.; Hirose, C., ION-EXCHANGEABLE LAYERED NIOBATES AS PHOTOCATALYSTS. *Catal. Today* **1993,** *16* (3-4), 479-486.
109. Pian, X. T.; Lin, B. Z.; Chen, Y. L.; Kuang, J. D.; Zhang, K. Z.; Fu, L. M., Pillared Nanocomposite TiO2/Bi-Doped Hexaniobate with Visible-Light Photocatalytic Activity. *J. Phys. Chem. C* **2011,** *115* (14), 6531-6539.
110. Gratzel, M., Photoelectrochemical cells. *Nature* **2001,** *414* (6861), 338-344.
111. Maeda, K.; Eguchi, M.; Lee, S. H. A.; Youngblood, W. J.; Hata, H.; Mallouk, T. E., Photocatalytic Hydrogen Evolution from Hexaniobate Nanoscrolls and Calcium Niobate Nanosheets Sensitized by Ruthenium(II) Bipyridyl Complexes. *J. Phys. Chem. C* **2009,** *113* (18), 7962-7969.
112. (a) Yao, Y.; Chaubey, G. S.; Wiley, J. B., Fabrication of Nanopeapods: Scrolling of Niobate Nanosheets for Magnetic Nanoparticle Chain Encapsulation. *J. Am. Chem. Soc.* **2012,** *134* (5), 2450-2452; (b) Kobayashi, Y.; Hata, H.; Salama, M.; Mallouk, T. E., Scrolled sheet precursor route to niobium and tantalum oxide nanotubes. *Nano Letters* **2007,** *7* (7), 2142-2145.
113. Bizeto, M. A.; Shiguihara, A. L.; Constantino, V. R. L., Layered niobate nanosheets: building blocks for advanced materials assembly. *J. Mater. Chem.* **2009,** *19* (17), 2512-2525.
114. Du, G. H.; Chen, Q.; Yu, Y.; Zhang, S.; Zhou, W. Z.; Peng, L. M., Synthesis, modification and characterization of K4Nb6O17-type nanotubes. *Journal of Materials Chemistry* **2004,** *14* (9), 1437-1442.
115. (a) Hoffmann, M. R.; Martin, S. T.; Choi, W. Y.; Bahnemann, D. W., ENVIRONMENTAL APPLICATIONS OF SEMICONDUCTOR PHOTOCATALYSIS. *Chemical Reviews* **1995,** *95* (1), 69-96; (b) Hernandez, Y.; Nicolosi, V.; Lotya, M.; Blighe, F. M.; Sun, Z. Y.; De, S.; McGovern, I. T.; Holland, B.; Byrne, M.; Gun'ko, Y. K.; Boland, J. J.; Niraj, P.; Duesberg, G.; Krishnamurthy, S.; Goodhue, R.; Hutchison, J.; Scardaci, V.; Ferrari, A. C.; Coleman, J. N., High-yield production of graphene by liquid-phase exfoliation of graphite. *Nat. Nanotechnol.* **2008,** *3* (9), 563-568.
116. Bizeto, M. A.; Constantino, V. R. L., Porphyrin inclusion into hexaniobate nanoscrolls. *Microporous and Mesoporous Materials* **2005,** *83* (1-3), 212-218.
117. (a) Boeve, H.; Bruynseraede, C.; Das, J.; Dessein, K.; Borghs, G.; De Boeck, J.; Sousa, R. C.; Melo, L. V.; Freitas, P. P., Technology assessment for the implementation of magnetoresistive elements with semiconductor components in magnetic random access memory (MRAM) architectures. *Ieee Transactions on Magnetics* **1999,** *35* (5), 2820-2825; (b) Jun, Y. W.; Jung, Y. Y.; Cheon, J., Architectural control of magnetic semiconductor

nanocrystals. *J. Am. Chem. Soc.* **2002,** *124* (4), 615-619; (c) Redl, F. X.; Cho, K. S.; Murray, C. B.; O'Brien, S., Three-dimensional binary superlattices of magnetic nanocrystals and semiconductor quantum dots. *Nature* **2003,** *423* (6943), 968-971; (d) Kim, J.; Lee, J. E.; Lee, J.; Yu, J. H.; Kim, B. C.; An, K.; Hwang, Y.; Shin, C. H.; Park, J. G.; Hyeon, T., Magnetic fluorescent delivery vehicle using uniform mesoporous silica spheres embedded with monodisperse magnetic and semiconductor nanocrystals. *J. Am. Chem. Soc.* **2006,** *128* (3), 688-689.

118. (a) Willets, K. A.; Van Duyne, R. P., Localized surface plasmon resonance spectroscopy and sensing. In *Annual Review of Physical Chemistry*, 2007; Vol. 58, pp 267-297; (b) Hutter, E.; Fendler, J. H., Exploitation of localized surface plasmon resonance. *Adv. Mater.* **2004,** *16* (19), 1685-1706; (c) Anker, J. N.; Hall, W. P.; Lyandres, O.; Shah, N. C.; Zhao, J.; Van Duyne, R. P., Biosensing with plasmonic nanosensors. *Nature Materials* **2008,** *7* (6), 442-453.
119. (a) Rajeshwar, K.; de Tacconi, N. R.; Chenthamarakshan, C. R.; Wampler, W.; Carlson, T.; Lin, W. Y., FUEL 69-New generation carbon-oxide semiconductor-noble metal catalysts for PEM fuel cell applications. *Abstracts of Papers of the American Chemical Society* **2007,** *234*; (b) Yang, J.; Levina, L.; Sargent, E. H.; Kelley, S. O., Heterogeneous deposition of noble metals on semiconductor nanoparticles in organic or aqueous solvents. *Journal of Materials Chemistry* **2006,** *16* (41), 4025-4028.
120. Centi, G.; Perathoner, S., Catalysis: Role and Challenges for a Sustainable Energy. *Topics in Catalysis* **2009,** *52* (8), 948-961.
121. Hu, M. S.; Chen, H. L.; Shen, C. H.; Hong, L. S.; Huang, B. R.; Chen, K. H.; Chen, L. C., Photosensitive gold-nanoparticle-embedded dielectric nanowires. *Nat. Mater.* **2006,** *5* (2), 102-106.
122. Wang, Y.; Zhang, H. J.; Lu, L.; Stubbs, L. P.; Wong, C. C.; Lin, J., Designed functional systems from peapod-like Co@carbon to Co_3O_4@carbon nanocomposites. *Acs Nano* **2010,** *4* (8), 4753-4761.
123. Hunyadi, S. E.; Murphy, C. J., Tunable one-dimensional silver-silica nanopeapod architectures. *J. Phys. Chem. B* **2006,** *110* (14), 7226-7231.
124. Smith, B. W.; Monthioux, M.; Luzzi, D. E., Encapsulated C_{60} in carbon nanotubes. *Nature* **1998,** *396* (6709), 323-324.
125. (a) Hsieh, C. H.; Chou, L. J.; Lin, G. R.; Bando, Y.; Golberg, D., Nanophotonic switch: gold-in-Ga_2O_3 peapod nanowires. *Nano Lett.* **2008,** *8* (10), 3081-3085; (b) Chen, P. H.; Hsieh, C. H.; Chen, S. Y.; Wu, C. H.; Wu, Y. J.; Chou, L. J.; Chen, L. J., Direct observation of Au/Ga_2O_3 peapodded nanowires and their plasmonic behaviors. *Nano Lett.* **2010,** *10* (9), 3267-3271.
126. (a) Lai, Y. F.; Chaudouët, P.; Charlot, F.; Matko, I.; Dubourdieu, C., Magnesium oxide nanowires synthesized by pulsed liquid-injection metal organic chemical vapor deposition. *Appl. Phys. Lett.* **2009,** *94* (2), 022904; (b) Zhou, W. W.; Sun, L.; Yu, T.; Zhang, J. X.; Gong, H.; Fan, H. J., The morphology of Au@ MgO nanopeapods. *Nanotechnology* **2009,** *20* (45), 455603.
127. Qin, Y.; Lee, S. M.; Pan, A.; Gösele, U.; Knez, M., Rayleigh-instability-induced metal nanoparticle chains encapsulated in nanotubes produced by atomic layer deposition. *Nano Lett.* **2008,** *8* (1), 114-118.
128. Qin, Y.; Liu, L. F.; Yang, R. B.; Gösele, U.; Knez, M., General assembly method for linear metal nanoparticle chains embedded in nanotubes. *Nano Lett.* **2008,** *8* (10), 3221-3225.

129. Sioss, J. A.; Keating, C. D., Batch preparation of linear Au and Ag nanoparticle chains via wet chemistry. *Nano Lett.* **2005,** *5* (9), 1779-1783.
130. Zhu, W.; Wang, G. Z.; Hong, X.; Shen, X. S.; Li, D. P.; Xie, X., Metal nanoparticle chains embedded in TiO_2 nanotubes prepared by one-step electrodeposition. *Electrochim. Acta* **2009,** *55* (2), 480-484.
131. Hangarter, C. M.; Lee, Y. I.; Hernandez, S. C.; Choa, Y. H.; Myung, N. V., Nanopeapods by galvanic displacement reaction. *Angew. Chem. Int. Ed.* **2010,** *49* (39), 7081-7085.
132. Zhou, W.; Chen, W. M.; Nai, J. W.; Yin, P. G.; Chen, C. P.; Guo, L., Selective synthesis of peapodlike Ni/Ni_3S_2 nanochains and nickel sulfide hollow chains and their magnetic properties. *Adv. Funct. Mater.* **2010,** *20* (21), 3678-3683.
133. Reid, R. C.; Prausnitz J.M.; Poling B. E., The properties of liquids and gases, 4th edition. Singapore: McGraw-Hill **1986**.

Chapter 2

Rapid Large-scale Fabrication of Hexaniobate Nanoscrolls*

2.1 Introduction

Nanoscrolls have emerged as an interesting low-dimensional construct with potential applications in advanced materials and assembly.[1] Well-known examples of compounds that scroll include graphene,[2] BN,[3] WS_2,[4] MoS_2,[5] TiO_2,[6] MnO_2,[7] PbO_2,[8] $SrAl_2O_4$,[9] $K_4Nb_6O_{17}$[10] and Ruddlesden–Popper[11] and Dion–Jacobson[12] type perovskites. Such 1D nanomaterials can be significant due to enhanced mechanical strength, unusual confinement effects, and atypical electron transport characteristics as well as potential applicability in intercalation, ion-exchange, heterogeneous catalysis and organic-inorganic composite materials.[1a, 8, 13] Further, the act of scrolling may be utilized in nanoscale mechanical devices or in the controlled capture of specific guest species for production of new materials with enhanced properties.[14]

The scroll-forming layered oxide, potassium hexaniobate ($K_4Nb_6O_{17}$), has been extensively studied for use as a UV-light driven photocatalyst in water splitting.[5, 15] Its structure consists of negatively charged layers of edge- and corner-sharing NbO_6 octahedra with exchangeable potassium cations in the interlayer space.[16] Individual Nb_6O_{17} layers can be exfoliated and, following the intercalation of tetraalkylammonium ions, spontaneously convolve into nanoscrolls along [100] to relieve mechanical strain intrinsic to the asymmetric layers.[10, 17]

*This chapter was adapted from: Adireddy, S.; Yao, Y.; He, J.; Wiley, J. B., Rapid Solvothermal Fabrication of Hexaniobate Nanoscrolls. *Materials Research Bulletin* **2013,** *48* (9), 3236-3241.

Gasperin and Le Bihan reported that anhydrous $K_4Nb_6O_{17}$ has unit cell dimensions as a = 7.83Å, b = 33.21 Å, c = 6.46 Å, and represent an orthorhombic crystal structure with the space group $P21nb$.[18]

Recently, several groups have reported synthetic routes to nanostructures of hexaniobate.[19] A common preparative procedure for nanostructured hexaniobate materials involves the tetraalkylammonium hydroxide treatment of acid-exchanged hexaniobate precursor at room temperature. Mallouk and coworkers have shown that individual Nb_6O_{17} layers can be exfoliated and, following the intercalation of tetraalkylammonium ions, spontaneously form nanoscrolls.[10] Du et al. investigated reactions with various alkylamines ($C_nH_{2n+1}NH_2$, $n \geq 3$) to tune the interlayer spacing of multiwalled nanoscrolls, where the individual layers of the nanoscrolls are clearly defined.[19a, 20] Transmission electron microscopy (TEM) images confirmed the scroll-like nature of these nanoscrolls, where the amine molecules act as intercalants between successive hexaniobate sheets. It has also been demonstrated that sizeable cations such as tetramethylpyridylphorphyrin (TMPyP) can also be inserted into hexaniobate nanoscrolls.[19g]

Solvothermal synthesis is a versatile technique for the fabrication of a variety of materials.[21] Nanomaterials for example can be readily produced with high crystallinity and great morphological control,[21a] various reaction parameters (solvent, surfactant, temperature, etc.) can be systematically tuned to achieve the desired morphology. Further, the confined conditions (sealed autoclave) available with this approach allows access to high reaction pressures and temperatures and the exclusion of unwanted impurities (e.g. water) in a variety of low boiling organic solvents. In recent years, this technique has been extensively employed to synthesize nanomaterials with and without the aid of surfactants.[21b-d, 22] Examples include the preparation of carbon nanotubes, metal nanoparticles, and $CdWO_4$ nanowires and nanorods.[21a, 23]

While there have been several reports on effective methods for the synthesis of hexaniobate nanoscrolls, these often require extended reaction times, have low yields, and can produce scrolls with irregular structures.[19a, 19f, 24] Here, we report an effective route for the fabrication of bulk quantities of both simple (SNS) and intercalated nanoscrolls (INS). In addition to that, we demonstrate a systematic study of the effect of alkylamine chain length on hexaniobate nanoscrolls under solvothermal conditions. This solvothermal approach lends itself well to the large scale production of high quality nanoscrolls with tunable interlayer dimensions. A complete morphological transition from a nanosheet to a nanoscroll occurs at ~220 °C under solvothermal conditions. The utility of oxide nanoscrolls in known applications as well as the development of new nanocomposite materials based on these structures would benefit from rapid, high yield methods of nanoscroll production.[19c, 19f, 25] These morphological transitions, with their associated interlayer manipulations, make hexaniobate very attractive candidate for a wide variety of catalytic applications, including use as UV-light driven photocatalysts in water splitting and degradation of toxic substances.[5, 15] Furthermore, this act of scrolling is important in the controlled capture of specific guest species (nanoparticles) for the production of new nanomaterials with directed or enhanced properties.[5] We have exploited this approach specifically in the production of nanopeapod structures – this work is presented in later chapters.

2.2 Experimental

Materials. K_2CO_3 (Alfa Aesar, 99%) and Nb_2O_5 (Alfa Aesar, 99%), tetrabutylammonium hydroxide 30-hydrate (TBAOH, Sigma Aldrich), oleylamine (Aldrich 70%), oleic acid (Aldrich, 90%), propylamine (Aldrich, 99%), benzylamine (Aldrich, 99%), octylamine (Aldrich, 99%), (1- hexadecyl)trimethylammonium bromide (CTAB, Alfa, 98%),

toluene (Aldrich, anhydrous, 99.8%), octyl ether (Aldrich, 99%), ethanol (200 Proof, absolute) and milli-Q water (18.2 $M\Omega^{-cm}$, Millipore).

2.2.1 Preparation of Niobate Nanoscrolls

$K_4Nb_6O_{17}$.

$K_4Nb_6O_{17}$ was synthesized by the solid-state reaction of K_2CO_3 and Nb_2O_5 (in the molar ratio of 1.1:1.5) in air at 900 °C for 1h before continuing to heat at 1050 ^oC for another 24 h.[10] A slight excess of K_2CO_3 was used to compensate for the loss of volatile potassium oxide species. The product was washed 2 times with *ca.* 200 mL milli-Q water and 50 mL acetone and dried overnight at 80 °C.

Acid-exchange and conventional exfoliation of $K_4Nb_6O_{17}$.

Experimental conditions were used similar to Saupe et al.[10] The proton-exchange form of hexaniobate, $H_xK_{4-x}Nb_6O_{17}$ was obtained by treating 0.15 g of $K_4Nb_6O_{17}$ powder with 15 mL of a 3 M HCl solution at 50 °C for 4 days. As-synthesized product was thoroughly washed 2 times with *ca.* 200 mL of milli-Q water and 50 mL acetone and dried overnight at 80 °C. $TBA_xH_{4-x}Nb_6O_{17}$ nanoscrolls were prepared by stirring the 0.1 g of $H_xK_{4-x}Nb_6O_{17}$ powder in 20 mL of aqueous TBAOH solution (15 mM, pH = 11) at 45 °C for 10 days.

Solvothermal preparation of simple nanoscrolls (SNS).

A reaction solution was prepared by mixing $H_xK_{4-x}Nb_6O_{17}$ (0.10 g), 0.15 g (0.19 mmol) TBAOH, 0.17 mL (~0.52 mmol) oleylamine, and 0.15 mL (~0.48 mmol) oleic acid in 13 mL of toluene. This mixture was magnetically stirred for 1 hour and transferred into a Teflon-lined stainless steel autoclave (Parr, model 4749, 1800 psig, 23 mL). The autoclave was maintained at 220 °C for 6 h and then cooled down to room temperature. The resulting white precipitate was

washed with 50 mL ethanol and centrifuged for 5 min to remove excess intercalating agents. Hexane can also be used in place of toluene for this reaction.

Solvothermal preparation of intercalated multi-walled nanoscrolls (INS).

The reaction solution was prepared by mixing $H_xK_{4-x}Nb_6O_{17}$ (0.10 g), 0.15 g (0.19 mmol) TBAOH and 5 mL oleylamine (~15 mmol) in 8 mL of toluene. (Reactions can readily be scaled up to 0.50 g.) For CTAB – INS, 0.02g of CTAB (~0.05 mmol) in 7 mL milli-Q water and 7 mL absolute ethanol. This mixture was magnetically stirred for 1 hour and transferred into a Teflon-lined stainless steel autoclave (Parr, model 4749, 1800 psig, 23 mL). The autoclave was maintained at 220 °C for 6 h and then cooled down to room temperature. The resulting white precipitate was washed with 50 mL ethanol and centrifuged for 5 min to remove excess intercalating agents. Similar reactions can also be carried out where oleylamine is replaced by propylamine, benzylamine, or octylamine.

Preparation of the water-soluble hexaniobate colloidal suspensions.

In a typical process, 0.05 g of SNS or INS were added to 10 mL of ethanol solution of tetrabutylammonium hydroxide (TBAOH) (0.15g) at room temperature. The resulting mixture was stirred for at least 3 days at 45 °C to produce a stable colloidal suspension. After centrifugation to remove the supernatant, white nanoscroll products were purified by two successive cycles of ultrasonic treatment and centrifugation in 20 mL ethanol before being redispersed in milli-Q water.

2.2.2 Characterization

Transmission electron microscopy (TEM) images were taken at JEOL 2010 high-resolution microscope at operating voltage 200 keV and equipped with a Gatan slow scan charge-coupled device camera for image recording. The nanoscrolls were also characterized by

high-resolution TEM (HRTEM) and selected area electron diffraction (SAED) using FEI TECNAI G2 F30 FEG TEM (300 kV) at nearby facility (Tulane University). For TEM analysis, a dilute toluene dispersion of nanoscrolls was drop casted onto a carbon film coated fine mesh copper grid. The phase purity and crystal structure of the nanopeapods was investigated on a Philips X-Pert PW 3020 MPD equipped with a curved graphite monochromator, with accelerating voltage and current of 40 kV and 40 mA, respectively. The surface composition of the hexaniobate nanoscrolls was studied with a Thermo Nicolet Omnic FT-IR spectrometer in the attenuated total reflection mode. The wavelength range was from 4000 to 500 cm^{-1}. X-ray photoelectron spectra (XPS) were collected by Kratos AXIS 165 instrument by Dr. Dongmei Cao at Louisiana State University. X-ray absorption near-edge spectroscopy (XANES) measurements were carried out at the variable line spacing plane grating monochromator (VLSPGM) beamline with an operational photon energy range between 200 eV and 1000 eV at the Center for Advanced Microstructures & Devices (CAMD) synchrotron with the help of Dr. Eizi Morikawa. Thermogravimetric analysis (TGA)-differential thermal analysis (DTA) was performed on a TA thermal analysis system. For each scan, 3-4 mg of sample was used. The heating profile consisted of two cycles of heating from 20 to 1000 °C and then cooling from 1000 to 20 °C at a rate of 5 °C/min.

2.3 Results

In the conventional aqueous method, exfoliation and scroll formation are relatively slow, several days or more, and the scrolls often possess a less rigid morphology. TEM images (Figure 2.1) highlight some of the structural features seen in these samples; nanoscrolls can show a variation in diameter along their length (a), an undulation (b), and a twisting behavior (c).

Nanoscroll production would be greatly improved by a new method that allows for the formation of well-formed scrolls, rapidly and in high yield.

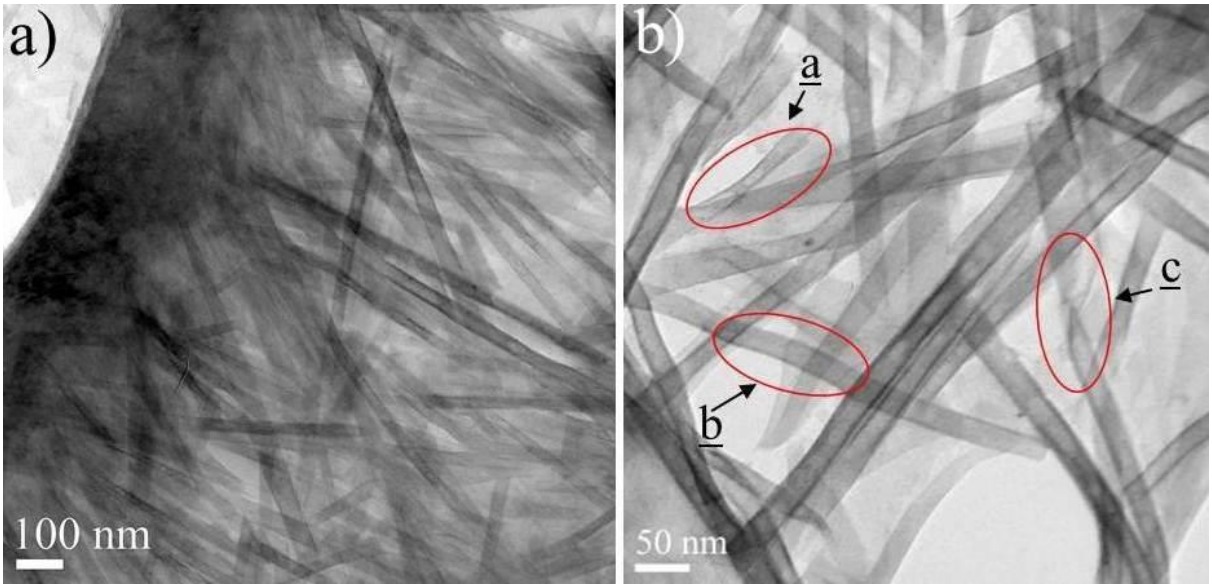

Figure 2.1. (a) TEM micrograph of nanoscrolls obtained in the conventional aqueous method at 45 °C for 5 days and 9 days respectively. (b) TEM image highlight some of the structural features seen in these samples; nanoscrolls can show a variation in diameter along their length (a), an undulation (b), and a twisting behavior (c).

2.3.1 Solvothermal Synthesis

We have developed a new method for the rapid synthesis of SNS and INS hexaniobate nanoscrolls by a solvothermal synthetic route. In typical syntheses, $H_xK_{4-x}Nb_6O_{17}$, TBAOH and oleylamine were combined in toluene and heat treated at 220 °C for 6 h in a Teflon-lined stainless steel autoclave. Hexaniobate nanoscrolls were readily obtained after centrifugation and purification. All reactions gave complete conversion of bulk $H_xK_{4-x}Nb_6O_{17}$ to nanoscrolls and, depending on the concentration of OAm, either SNS (0.5 mM) or INS (15 mM) were obtained. Figure 2.2 highlights the reaction scheme used in the formation of both simple (SNS) and intercalated nanoscrolls (INS) sets of scrolls.

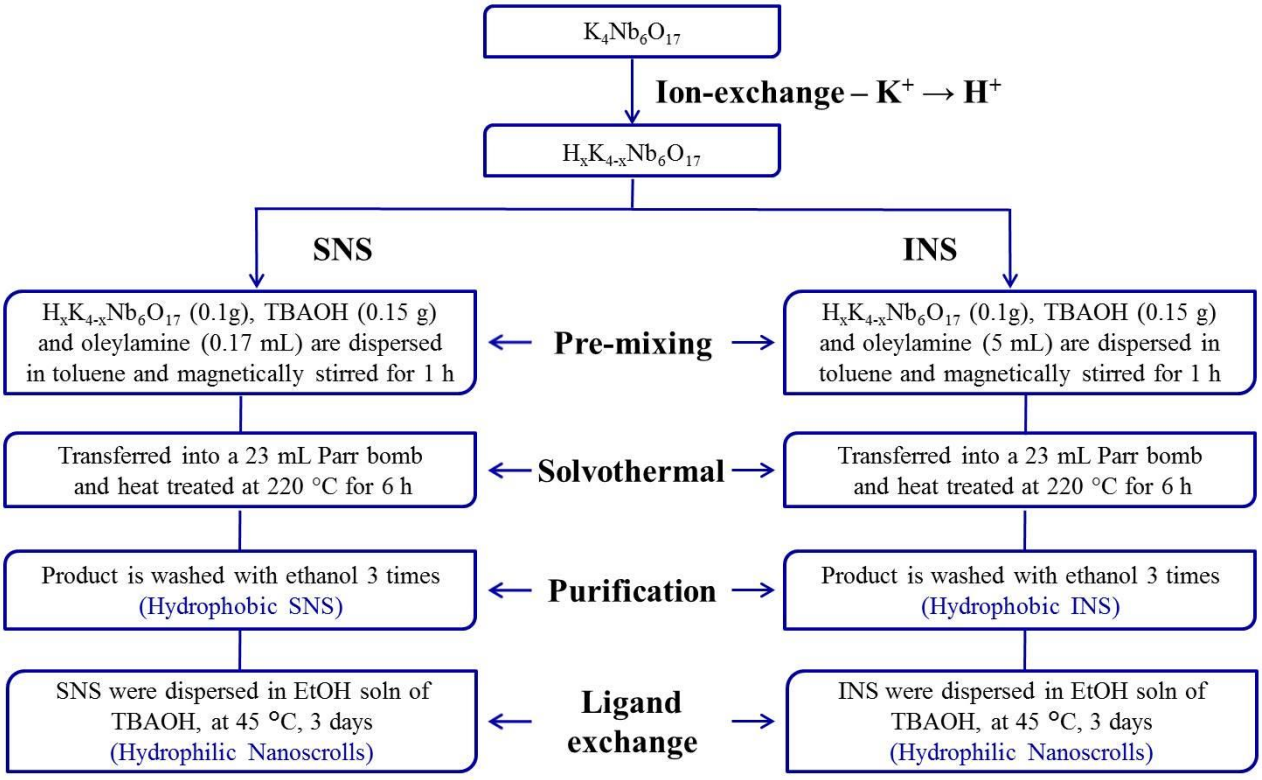

Figure 2.2. Procedure to fabricate hydrophobic and hydrophilic hexaniobate nanoscrolls.

Solvothermally prepared hexaniobate scrolls differ in structure with variations in the concentration of OAm. TEM investigations show that when 0.5 mM of OAm is used, SNS form (Figure 2.3). The nanoscrolls have a wall thickness of about 3 nm with outer and inner diameters in the ranges of 25-55 nm and 20-45 nm, respectively. High-resolution TEM (HRTEM) of a typical SNS shows two sets of lattice fringes from the scroll edge with spacings of 3.9 Å and 8.3 Å that are almost perpendicular to each other. The lattice fringes are attributed to the (200) and (040) spacings of $K_4Nb_6O_{17}$-type structure, respectively, and are in good agreement with the results reported by Du and co-workers.[19a]

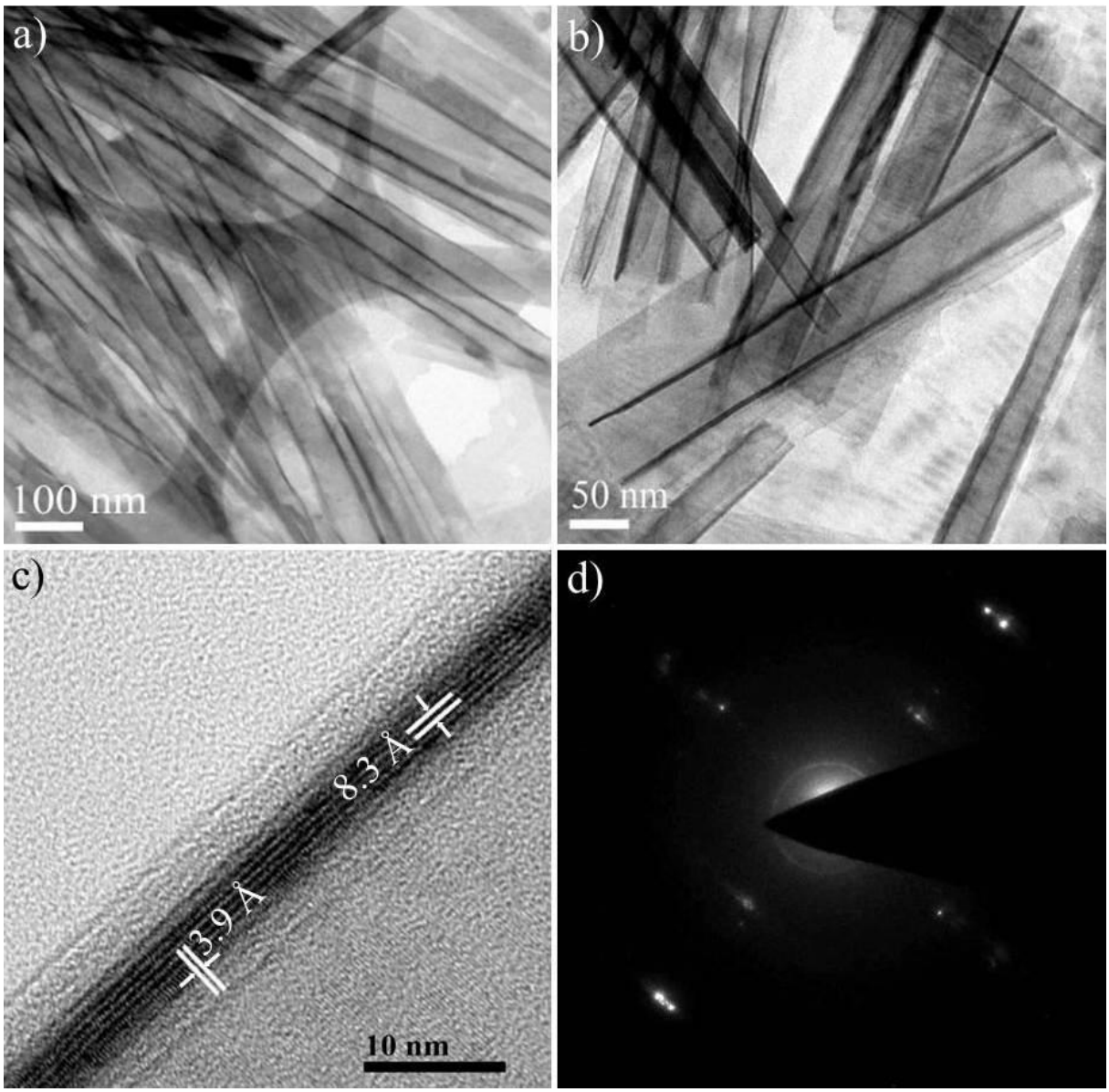

Figure 2.3. (a, b) TEM micrographs of SNS obtained in the typical synthesis at 220 °C for 6h, (c) HRTEM, and (d) SAED patterns of SNS.

Oleylamine was found to be essential in maintaining the morphological uniformity of the nanoscrolls. By increasing the amount of oleylamine to 15 mM, nanoscroll interlayer dimensions were manipulated and well-defined multi-walled nanoscroll structures (INS) were induced (Figure 2.4). This results in the formation of INS consisting of 2 to 6 layers with a wall thicknesses varying between 7-12 nm and an interlayer spacing of ~3.2 nm (Figure 2.4c). The

outer and inner scroll diameters range from 30-55 nm and 12-25 nm (Figure 2.4), respectively. Further, selected area electron diffraction (SAED) patterns of SNS and INS (Figures 2.3d and 2.4d) show a variation in the nanoscroll architecture (Table 2.1). The greater number of diffuse reflections and rings in the INS results from a less well-defined registry between the set of scrolled layers.

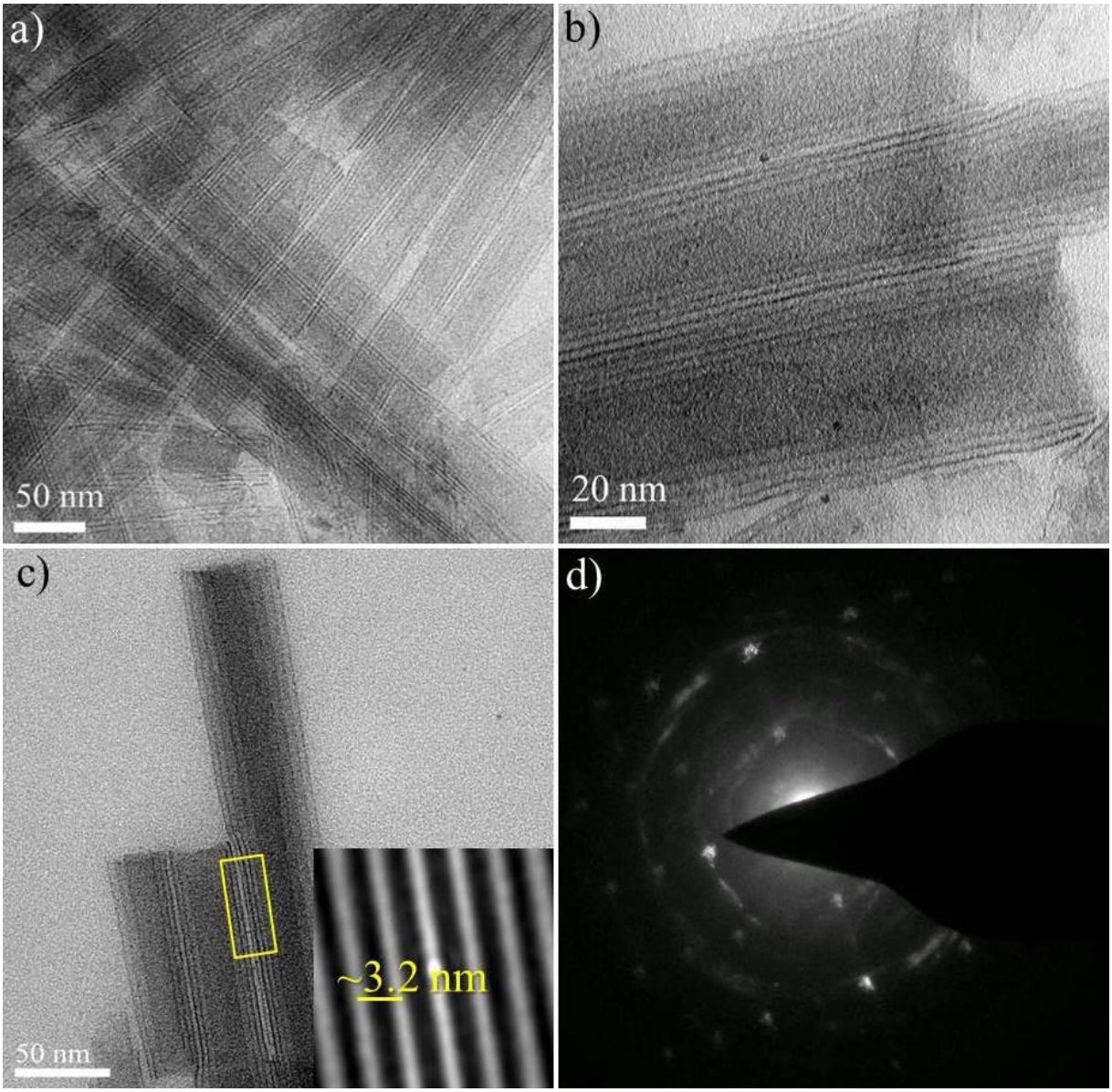

Figure 2.4. (a, b) TEM micrographs of INS, (c) TEM image (Inset: digital micrograph auto-correlation image, showing multi-walled architecture with constant interlayer spacing), and (d) SAED pattern of INS.

Table 2.1. Nanoscroll dimensions.

Dimension (nm)	SNS	INS
Wall thickness	2.5 - 3.5	7 - 12
Internal diameter	20 - 45	12 - 20
Overall diameter	25 – 55	30 - 55

2.3.2 Factors Influencing Nanoscroll Formation and Architecture

Alkyl amines are often used as exfoliating agents for the layered hexaniobate crystallites.[20] Based on the experimental results presented in Table 2.2, it is clear that there are several factors which influence the morphology of nanoscrolls.

Table 2.2. Reaction parameters for different designed experiments.

Sample	Niobate (g)	TBAOH (g)	OAm (mL)	Solvent (mL)	Temp -Time	Morphology
1	0.05	0.15	0.15	13	220 °C - 6h	SNS (Hydrophobic)
2	0.05	0.15	5	8	220 °C - 6h	INS (Hydrophobic)
3	0.05	0.15	0	13	220 °C - 6h	Scrolls with poor morphology (Hydrophilic)
4	0.05	0	5	8	220 °C - 6h	Scrolls (≤20% yields) (Hydrophobic)
5	0.05	0	0	13	220 °C - 6h	No scrolls (crystallites)

Our experiments showed that the morphology of the resulting nanostructures was sensitive to a series of reaction parameters such as the amount of TBAOH, the amount of oleylamine, temperature, and time. TBAOH acts as exfoliating agent and oleylamine plays a dual

role as intercalant and surfactant. It was observed that the chemisorption of the surfactant on exfoliated hexaniobate layers results in high quality 1D-intercalated hexaniobate nanoscrolls (INS). To better understand the fabrication process, samples were collected at different reaction times (1.5 h, 3h, 6h and 12h).

Controlled experiments were performed to investigate the role of TBAOH on the nanoscroll morphology. When TBAOH and oleylamine were used, regularly shaped nanoscrolls were observed (sample 1 & 2, Table 2.2; Figures 2.3 and 2.4). In the absence of oleylamine (sample 3, Table 2.2; Figure 2.5a), the nanosheets were found to be exfoliated and scrolled in the presence of TBAOH (boiling point, ~100 °C). As-synthesized nanoscrolls had irregular morphologies. By introducing the oleylamine without using TBAOH in the reaction mixture, control over morphologies of nanoscrolls was achieved; yet, the delamination of hexaniobate slabs found to be very slow, causing low yields of nanoscrolls (Figure 2.5b). In the absence of TBAOH and oleylamine, no scrolls were found (Figure 2.5c).

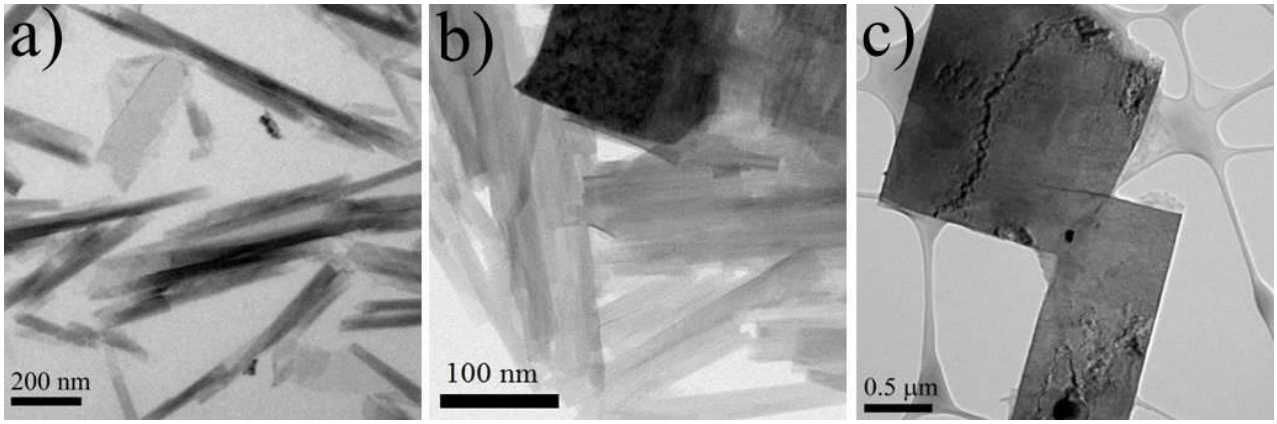

Figure 2.5. TEM images supporting the mechanism. (a) nanoscrolls after 6h solvothermal treatment in the absence of oleylamine (sample 4, Table 2.2); (b) nanoscrolls after 6h solvothermal treatment in the absence of TBAOH (Sample 5, Table 2.2); (c) Hexaniobate crystallites after 6h solvothermal treatment without TBAOH and oleylamine (Sample 6, Table 2.2)

Experiments were conducted to investigate the effect of the reaction temperature and times on the exfoliation of hexaniobate crystallites at a fixed reaction composition. At 120 °C, no single sheets were found before 6h. For a reaction time of 12 h at 120 °C, nanoscrolls started appearing with non-uniform morphologies (Figure 2.6a). These experiments confirmed that the exfoliation and scrolling of hexaniobate are temperature and time dependent. To better understand this phenomenon, experiments were performed at 150 °C and 180 °C for 12 h; both sets of conditions resulted in better yields (≤ 80%; Figures 2.6b and c, respectively).

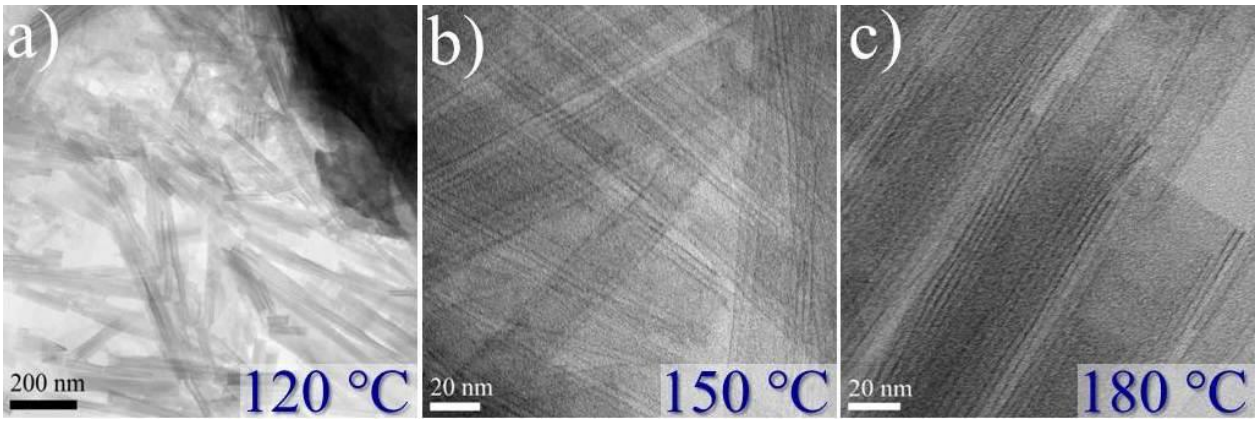

Figure 2.6. TEM images showing the effect of temperature on the morphology of the nanoscrolls; (a, b, c) nanoscrolls after 12h solvothermal treatment at 120 °C, 150 °C, and 180 °C respectively.

To better understand the scrolling process, experiments were performed at different reaction times at a fixed temperature of 220 °C (Figure 2.7). Based on TEM analysis (Figure 2.7a), hexaniobate crystallites start to exfoliate after 90 minutes. Exfoliated nanosheets break at the certain crystallographic planes and convolve into nanoscrolls (Figure 2.7b). This transformation of nanosheets into complete nanoscrolls takes 4 to 6 h (Figure 2.7c and d). At 220 °C for 12h, high-quality hexaniobate nanoscrolls with the yields of ≥95% were observed (Figure 2.7d). TEM images suggest that nanoscrolls have better morphological features at longer reaction

times (12h or more) but scroll structures do not vary after longer reaction times (Figure 2.7e and f).

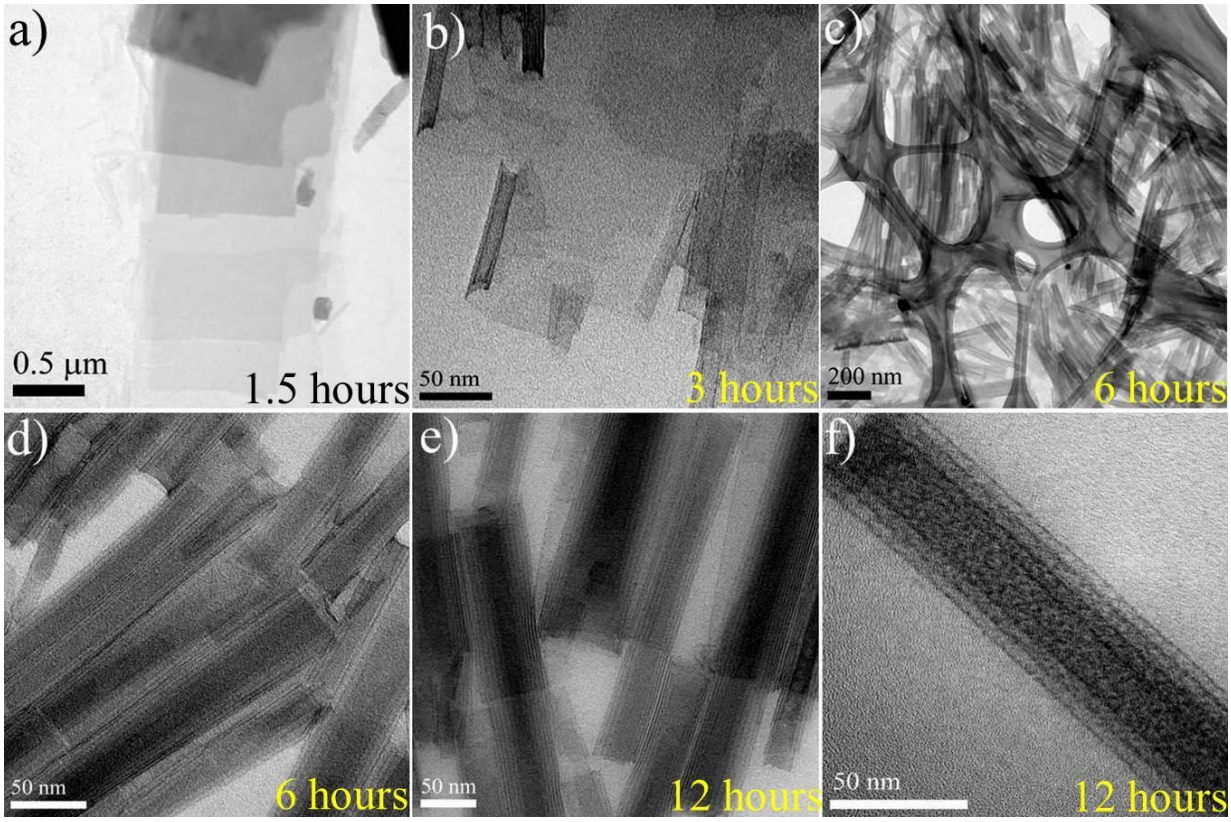

Figure 2.7. TEM images supporting the mechanism. (a) Exfoliation of hexaniobate crystallites after 1.5 h solvothermal treatment at 220 °C; (b) nanosheets during the scrolling event (3 h); (c, d) nanoscrolls after 6 h, (e, f) nanoscrolls after12 h of solvothermal treatment at 220 °C.

2.3.3 Other Intercalants

To demonstrate the versatility of this synthetic method, we have also extended this synthetic approach to a series of alkylamines and found that the intercalated hexaniobate nanoscrolls can be fabricated with tunable interlayer spacings. Figure 2.8 highlights some INS made by using CTAB (Figures 2.8a and b) where well-formed nanoscroll structures have been prepared in high yields by this approach in 6 h at 220 °C. The intercalants such as propylamine,

benzylamine and octylamine were also used in nanoscroll fabrication and found that interlayer of the nanoscrolls has been tuned. As expected, alkylamine molecules with smaller chain lengths produce nanoscrolls with smaller interlayer spacings. The spacings were found to be 3.75 nm (CTAB, Figure 2.8a and b), 1.92 nm (propylamine, Figure 2.8c), 2.5 nm (benzylamine, Figure 2.8d), 2.8 nm (octylamine, Figure 2.8e) respectively, and are in good agreement with the results reported by Du and co-workers.[26]

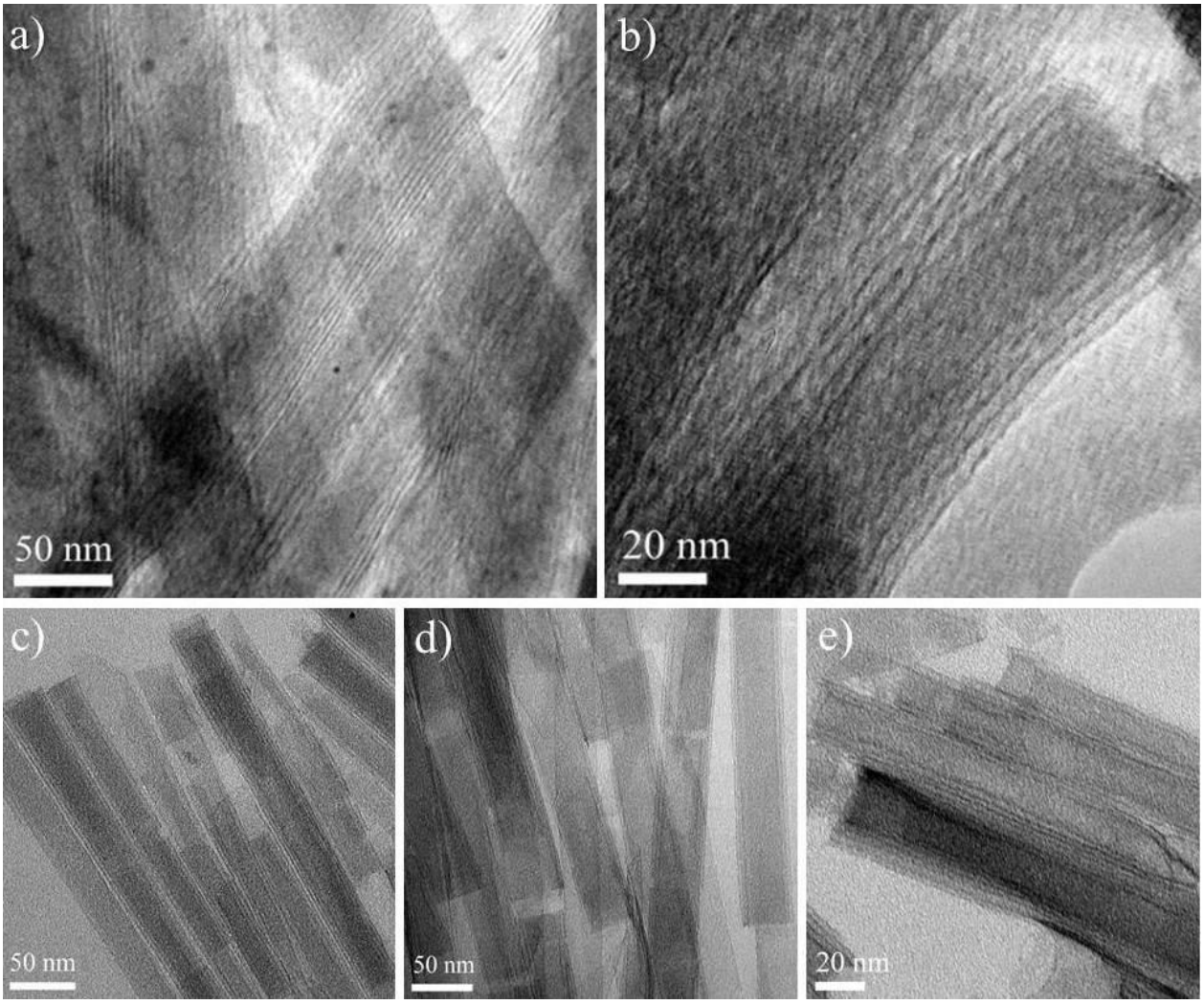

Figure 2.8. TEM images represent the multi-walled hexaniobate nanoscrolls in the presence of (a, b) CTAB; (c) propylamine; (d) benzylamine, and (e) octylamine**.**

2.3.4 Dispersion in Different Solvents

The utilization of nanoscrolls in various applications will be bolstered if they can be readily dispersed in different solvents. The OAm surface groups in the as-prepared SNS allow these materials to be readily dispersed in non-polar solvents (e.g. toluene). If samples are treated with TBAOH in ethanol solution using methods similar to Wu et al.,[27] the hydrophobic OAm surface groups are displaced by TBA^+, allowing the nanoscrolls to be suspended in various hydrophilic solutions (Figure 2.9).

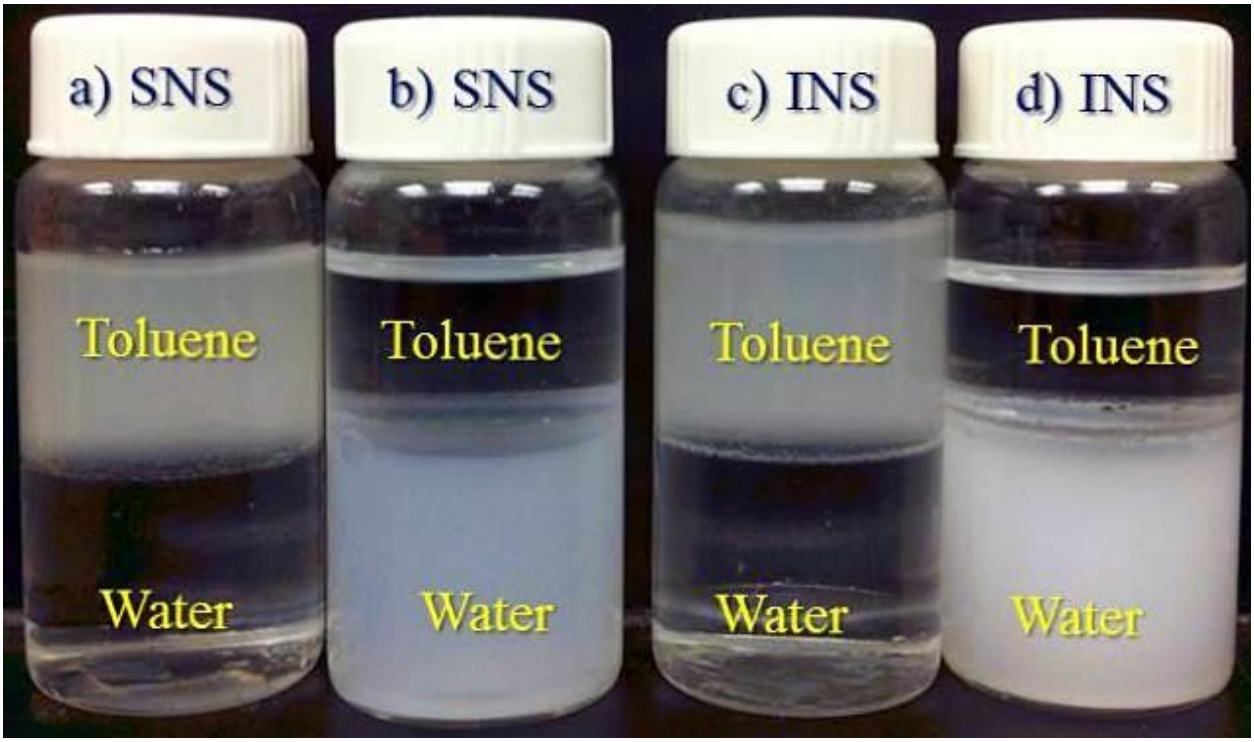

Figure 2.9. Surface functionalized nanoscrolls in non-polar and polar solvents. SNS dispersions in (a) toluene and (b) water. INS dispersions in (c) toluene and (d) water.

2.3.5 Bulk and Surface Characterization

Infrared spectroscopy. FTIR spectroscopy was used to characterize the surface chemistry of the as-synthesized hexaniobate nanoscrolls (Figure 2.10). The exfoliating agent used in the fabrication of conventional nanoscrolls was Bu_4NOH (TBAOH). In the fabrication of SNS and INS, both TBAOH and $C_{18}H_{37}N$ (oleylamine) were used. In the FTIR spectra in Figure 2.10, absorption bands around ~1600 to 1630 cm^{-1} and ~720 cm^{-1} were found in all the samples, attributed to the N-H bending vibration and the $–NH_2$ wagging vibration, respectively.[28] The absorption bands located between ~ 2960 cm^{-1} and ~2857 cm^{-1} represent the symmetric and asymmetric C-H stretching modes.[29] Also, the peaks in the range of 1500-1300 cm^{-1} is ascribed to CH_2 bending. Evidence for the hydroxyl group in the spectrum of the conventionally prepared nanoscrolls and SNS is provided by the broad band between 3100-3550 cm^{-1} (Figure 2.10a and b), which is likely from the hydroxyl groups of TBAOH ($C_{16}H_{37}NO \cdot 30H_2O$). The stretching vibrations of O-H are essentially gone in INS sample (Figure 2.10c). This indicates that there are little or no hydroxyl groups on the surface of the intercalated nanoscrolls.

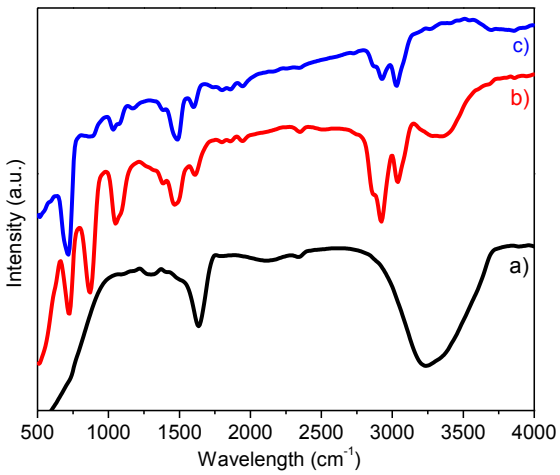

Figure 2.10. FTIR spectra of (a) nanoscrolls prepared in conventional aqueous method, (b) SNS, and (c) INS.

X-ray photoelectron spectroscopy (XPS). XPS was used to investigate the surface of conventional (aqueous) NS, SNS and INS. Analysis (Figure 2.11) indicates the presence of nitrogen, niobium, oxygen and carbon on the surface as would be expected for the oleylamine and tetrabutylammonium species on a niobate nanoscroll. The peaks of N 1s at 398 and 407 eV confirm the presence of nitrogen functionalities on the surface of all the three samples. Nitrogen atomic concentration was slightly higher in the case of the INS, which can be attributed to the excess oleylamine used in the synthesis (Table 2.3). Figure 2.11b shows the XPS spectra of Nb 3d in the nanoscroll sample with binding energies of 207, 210 corresponding to Nb $3d_{5/2}$ and Nb $3d_{3/2}$, respectively; these energies are in good agreement with the previously reported values.[30] XPS spectrum of O 1s (532 eV) and C 1s (285 eV) are shown in Figures 2.11c and d, respectively, which are attributed to the hydrocarbon component of the surfactant.

Table 2.3: XPS atomic concentrations (% ± 0.1%)

Element	Conventional	SNS	INS
N	1.60	2.2	2.67
Nb	3.14	4.07	4.62
C	73.65	72.92	72.17
O	21.61	20.81	20.55

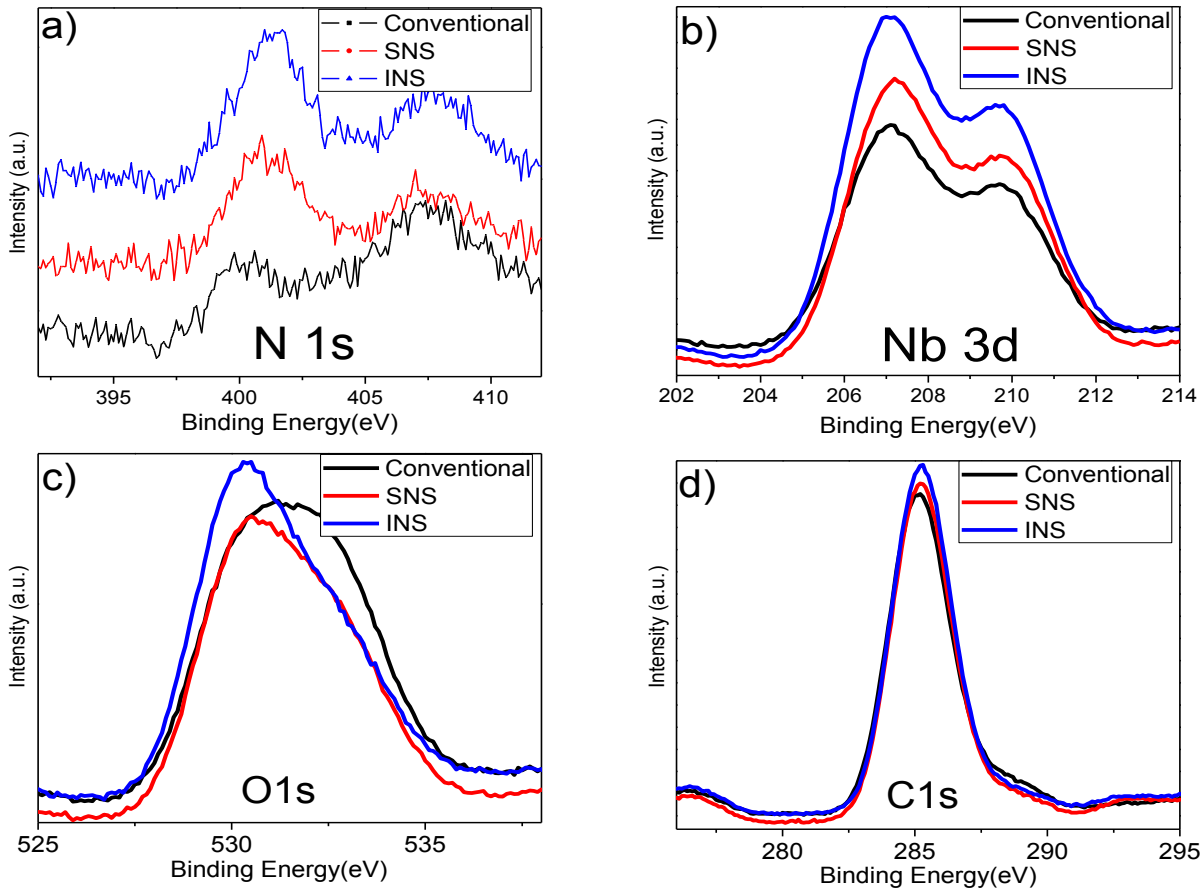

Figure 2.11. XPS spectrum show the surface structure of nanoscrolls synthesized in conventional aqueous method, SNS and INS. XPS spectrum of (a) N 1s from the amine functionalities, (b) Nb 3d from the $–NbO_6$, (c) O 1s, and (d) C 1s from the surface hydrocarbon atmosphere.

X-ray Absorption Near-edge structure (XANES) Spectroscopy. The oxygen K-edge in the nanoscroll samples has been investigated by XANES spectroscopy. XANES is sensitive to the atomic bonding and can detect even very small changes. Figure 2.12 displays the oxygen K-edge XANES spectra of hexaniobate nanoscrolls. All the spectra correspond to the O K-edge XANES spectrum of hexaniobate and the energies are in good agreement with previous reports.[31] The peak at 532 eV is usually called the "pre-peak" which can be seen clearly in all three

nanoscroll samples. The line shapes of other peaks of O *K*-edge are similar in all three samples, which confirm that the atomic bonding is identical.

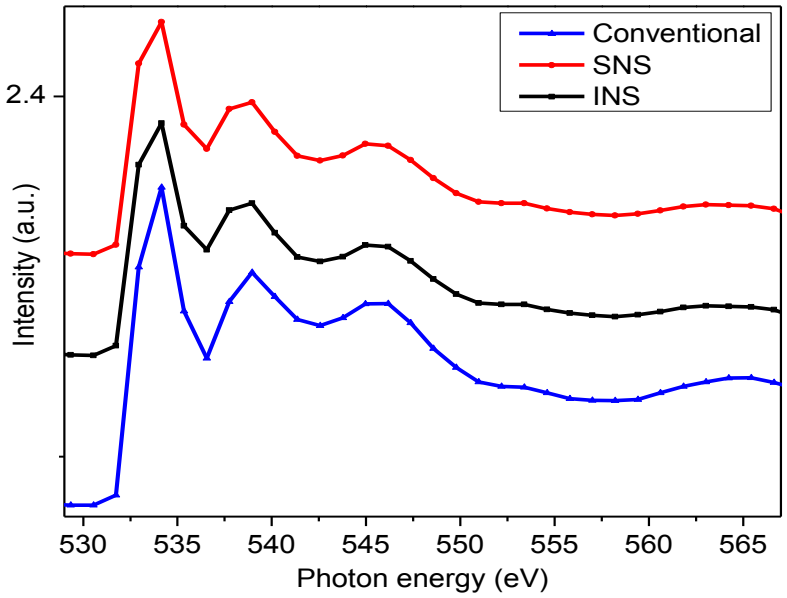

Figure 2.12. Oxygen K-edge X-ray absorption spectra of hexaniobate samples.

Thermal analysis. The thermal stability of the SNS and INS materials were examined by thermogravimetric analysis (TGA) and differential thermal analysis (DTA). TGA of the SNS shows an initial mass loss between 40 and 100 °C of ~1.06%, with a ~15% mass loss up to 450 °C, which was due to the loss of the TBA^+ and surface oleylamine groups (Figure 2.13a). On the other hand, TGA of the INS shows comparatively larger mass loss between 180 and 450 °C of ~38%, which is attributable to the greater amount of oleylamine present in the interlayer region (Figure 2.13c). Formula weights of TBAOH ($C_{16}H_{37}NO{\cdot}30H_2O$) and oleylamine are 799.93 g/mol and 267.49 g/mol, respectively. The endothermic peaks in the case of SNS and INS are attributable to the decomposition of the SNS and INS samples the weight loss of the amine molecules retained on the surface and in the interlayers of nanoscrolls (Figures 2.13b and d).

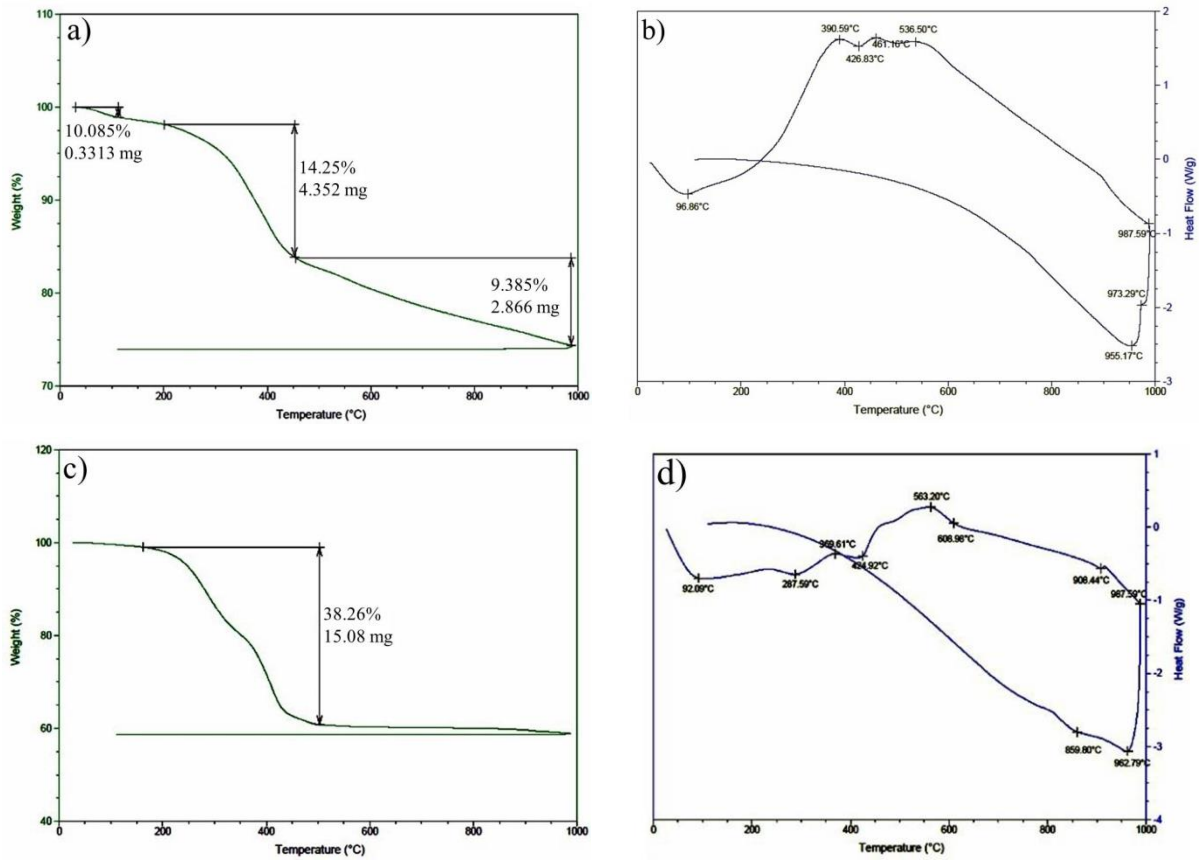

Figure 2.13. The TGA/DSC profile of the (a, b) SNS and (c, d) INS respectively.

2.4. Discussion

Solvothermal methods allow for the rapid, high yield synthesis of hexaniobate nanoscrolls. Exfoliation occurs when the interlayer spacing of the hexaniobate crystallites increases until a point where the total crystallite collapses into individual layers. In potassium hexaniobate ($K_4Nb_6O_{17}$), K^+ can be readily replaced with a proton by acid exchange and the resulting products can then be exfoliated to fabricate nanoscrolls. The exfoliated nanosheets are very anisotropic and have thickness of 1–2 nm. The high asymmetry of the hexaniobate layers allows the nanosheets to curl only in one orientation.[10]

The exfoliation of a proton exchanged hexaniobate crystallites can be performed by aqueous and non-aqueous methods. When the aqueous method is used, the interlayer hydrogen ions can be exchanged with TBA^+ causing the hexaniobate crystallites to exfoliate in water, and the exfoliated individual sheets can then produce nanoscrolls (Figure 2.1).[1c, 19e-g, 32] This process occurs between 4 to 10 days due to the mild reaction conditions and lack of external temperatures and pressures. Nanoscrolls prepared in aqueous media usually have less rigid morphology. While there are previous reports on the hexaniobate nanoscroll fabrication via aqueous methods,[1c, 19e-g, 32] the solvothermal approach presented herein is much more flexible in that the nanoscrolls are prepared with tunable dimensions.[33] Before examining the hexaniobate nanoscrolls in more detail, it is important to discuss the importance of the solvothermal method.

The effectiveness of solvothermal techniques is well established for the synthesis of a variety of nanomaterials where higher temperatures and pressures can translate to improved conditions for the production of the different targets.[34] The solvothermal approach allows for more controlled variation of reaction parameters (type of solvent, surfactant, intercalant, temperature, etc.). This is important for the development of these materials in various applications. In the fabrication of nanoscrolls, the solvothermal method has a great impact through its favorable reaction conditions allowed by the higher temperatures and pressures. This translates to rapid exfoliation and nanoscroll formation. Further, the more rigorous conditions allow for layer flexibility such that highly commensurate, rigid structures can be achieved.

Figure 2.14 shows the synthetic procedure used in the formation of hexaniobate nanoscrolls. Unlike conventional aqueous methods, this approach is rapid (< 6 hrs), can produce bulk materials, and does so in high yield (~100%). By promoting the reaction of the proton-exchanged hexaniobate with TBAOH and OAm in toluene under solvothermal conditions,

nanoscrolls can readily be produced. Further, unlike the aqueous method, this solvothermal route results in nanoscrolls with higher morphological uniformity. Final product forms hexaniobate colloidal nanoscroll suspensions.

One of the significant aspects of the solvothermal approach is the possibility of varying architecture in a controlled fashion. Here, nanoscrolls can be readily fabricated with tunable dimensions (SNS and INS). The architectures of the SNS and INS are dictated by the amount of OAm used in the reaction mixture. The wall thicknesses and interwall diameters vary due to the presence of surfactant on the surfaces of the nanoscroll walls (Figure 2.3 and 2.4).

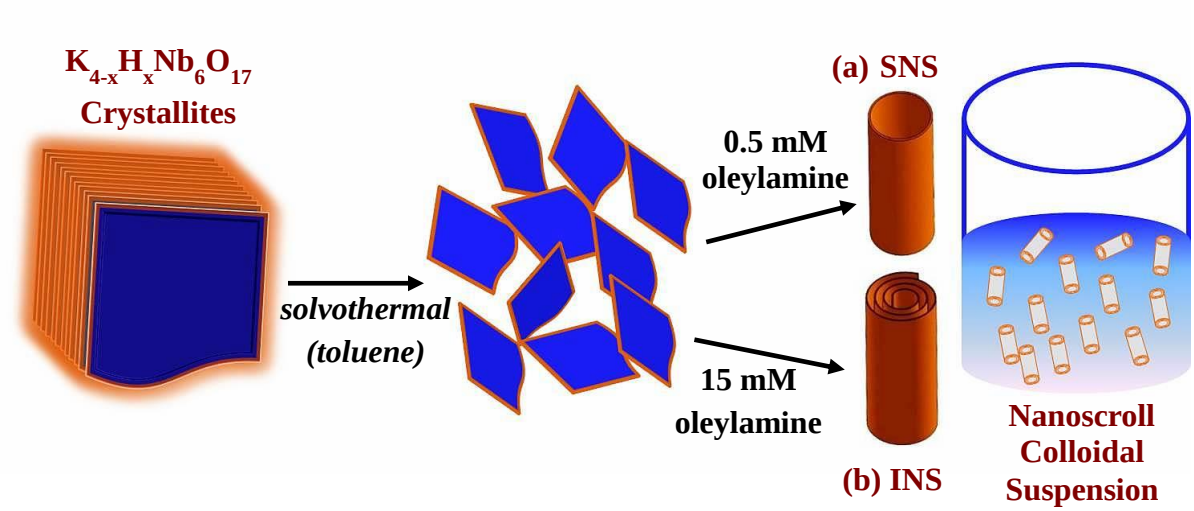

Figure 2.14. A schematic representing rapid solvothermal fabrication of simple (SNS) and intercalated (INS) nanoscrolls from $H_xK_{4-x}Nb_6O_{17}$ crystallites in toluene. (a) Low concentrations of oleylamine produce SNS. (b) Higher concentrations of oleylamine produce INS. (SNS and INS cartoons were drawn by SolidWorks software)

Clear evidence is shown for the tunability in interwall diameters. By using intercalants with different chain lengths the interwall diameters can readily be tuned. Nanoscrolls with series of intercalants including CTAB, propylamine, benzylamine or octylamine can readily be achieved (Figure 2.8). This process of tunability supports the proposed interwall structure (Figure 2.15).

Another important result demonstrated by this method is the surface functionalization (Figure 2.9). Both INS and SNS can be dispersed in polar and non-polar solvents. The OAm surface groups in the as-prepared nanoscrolls allow these materials to be readily dispersed in non-polar solvents (e.g. toluene). The hydrophobic OAm surface groups can be displaced by TBA^+, allowing the nanoscrolls to be suspended in hydrophilic solvents.

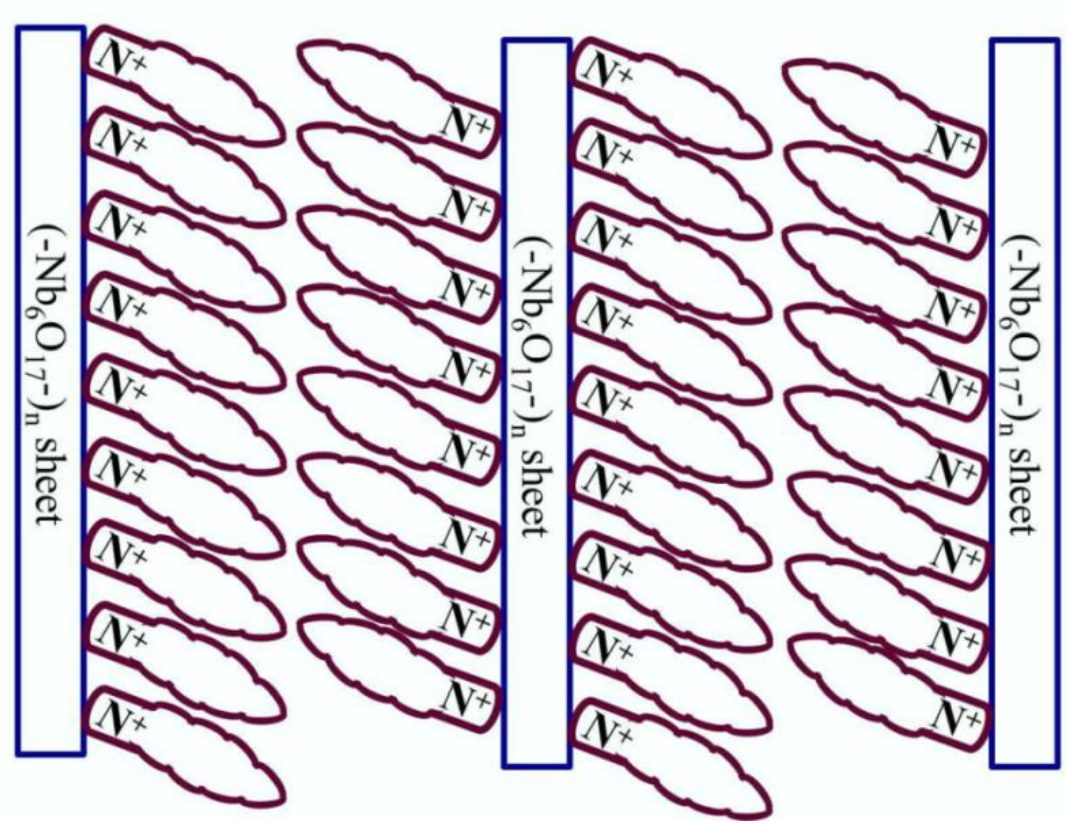

Figure 2.15. Expected wall structure of the intercalated hexaniobate nanoscrolls with alkylamine molecules as interlayer spacer.

Typical hexaniobate crystal sizes are as much as 50 μm on an edge. Hexaniobate crystallites exfoliate into individual nanosheets dissociates at certain crystallographic planes and convolve into nanoscrolls. When a single-layer $(–Nb_6O_{17}–)_n$ sheet rolls up, alkylamine molecules are already adsorbed on both sides of the sheet and then reside in the interlayer spaces of the

nanoscrolls. It was often found that instead of convolution occurring after the individual hexaniobate nanosheets separate from the main crystallite, the scrolling occurs while nanosheets are still attached to the crystallite surface, then at some point in the process, the scroll detaches from the surface (Figure 2.7b). This transformation of nanosheets into nanoscrolls takes 4 to 6 h (Figure 2.7). Nanoscrolls have well-defined interlayer morphological features at longer reaction times (12h). Figure 2.15 shows the possible wall-structure of the intercalated hexaniobate nanoscrolls with alkylamine molecules as interlayer spacer.

Building on this chemistry, it may then be possible fabricate novel nanocomposites with tunable dimensions. The prospect of exfoliating layers from various layered inorganic materials opens up a variety of new nanofabrication opportunities. These colloidal nanoscrolls are considered as among the newer building blocks for advanced materials assembly. Hexaniobate nanoscrolls have already been used to make peapod structures[14] – the availability of methods for making bulk nanoscrolls will positively impact the production of such composites as well as other composites where nanomaterials are attached to surfaces.

2.5. Conclusions

We have demonstrated an effective solvothermal synthetic approach that leads to the formation of bulk quantities of high-quality simple (SNS) and intercalated nanoscrolls (INS). The interlayer spacing of the nanoscrolls can be easily tuned by varying the relative amount and chain lengths of the primary alkylamines. It is expected that this flexible synthetic approach can be extended to the exfoliation and scrolling of several other layered oxide materials. Moreover, the inorganic/organic complex nanoscrolls examined in this study could find direct applications in water splitting through the production of stable, high surface area, catalytically active

composites.[2, 15, 24a, 35] Efforts were made to utilize this method in capturing nanoparticles for the formation of nanopeapod structures; these efforts are highlighted in Chapter 3.[19, 24]

2.6. References

1. (a) Viculis, L. M.; Mack, J. J.; Kaner, R. B., A chemical route to carbon nanoscrolls. *Science* **2003,** *299* (5611), 1361-1361; (b) Cao, J.; Musfeldt, J. L.; Mazumdar, S.; Chernova, N. A.; Whittingham, M. S., Pinned low-energy electronic excitation in metal-exchanged vanadium oxide nanoscrolls. *Nano Letters* **2007,** *7* (8), 2351-2355; (c) Maeda, K.; Eguchi, M.; Youngblood, W. J.; Mallouk, T. E., Niobium Oxide Nanoscrolls as Building Blocks for Dye-Sensitized Hydrogen Production from Water under Visible Light Irradiation. *Chemistry of Materials* **2008,** *20* (21), 6770-6778; (d) Xie, X.; Ju, L.; Feng, X. F.; Sun, Y. H.; Zhou, R. F.; Liu, K.; Fan, S. S.; Li, Q. L.; Jiang, K. L., Controlled Fabrication of High-Quality Carbon Nanoscrolls from Monolayer Graphene. *Nano Letters* **2009,** *9* (7), 2565-2570; (e) Golberg, D., NANOMATERIALS Exfoliating the inorganics. *Nature Nanotechnology* **2011,** *6* (4), 200-201.
2. Saito, R.; Fujita, M.; Dresselhaus, G.; Dresselhaus, M. S., ELECTRONIC-STRUCTURE OF GRAPHENE TUBULES BASED ON C-60. *Physical Review B* **1992,** *46* (3), 1804-1811.
3. Hamilton, E. J. M.; Dolan, S. E.; Mann, C. M.; Colijn, H. O.; McDonald, C. A.; Shore, S. G., PREPARATION OF AMORPHOUS BORON-NITRIDE AND ITS CONVERSION TO A TURBOSTRATIC, TUBULAR FORM. *Science* **1993,** *260* (5108), 659-661.
4. Li, Y. D. D.; Li, X. L. L.; He, R. R. R.; Zhu, J.; Deng, Z. X. X., Artificial lamellar mesostructures to WS2 nanotubes. *Journal of the American Chemical Society* **2002,** *124* (7), 1411-1416.
5. Feldman, Y.; Wasserman, E.; Srolovitz, D. J.; Tenne, R., HIGH-RATE, GAS-PHASE GROWTH OF MOS2 NESTED INORGANIC FULLERENES AND NANOTUBES. *Science* **1995,** *267* (5195), 222-225.
6. Richter, C.; Schmuttenmaer, C. A., Exciton-like trap states limit electron mobility in TiO2 nanotubes. *Nature Nanotechnology* **2010,** *5* (11), 769-772.
7. Ma, R. Z.; Bando, Y.; Sasaki, T., Directly rolling nanosheets into nanotubes. *Journal of Physical Chemistry B* **2004,** *108* (7), 2115-2119.
8. Shi, L.; Xu, Y. M.; Li, Q., Controlled growth of lead oxide nanosheets, scrolled nanotubes, and nanorods. *Crystal Growth & Design* **2008,** *8* (10), 3521-3525.
9. Ye, C. H.; Bando, Y.; Shen, G. Z.; Golberg, D., Formation of crystalline SrAl2O4 nanotubes by a roll-up and post-annealing approach. *Angewandte Chemie-International Edition* **2006,** *45* (30), 4922-4926.
10. Saupe, G. B.; Waraksa, C. C.; Kim, H. N.; Han, Y. J.; Kaschak, D. M.; Skinner, D. M.; Mallouk, T. E., Nanoscale tubules formed by exfoliation of potassium hexaniobate. *Chem. Mater.* **2000,** *12* (6), 1556-1562.
11. Schaak, R. E.; Mallouk, T. E., Prying apart Ruddlesden-Popper phases: Exfoliation into sheets and nanotubes for assembly of perovskite thin films. *Chemistry of Materials* **2000,** *12* (11), 3427-3434.
12. Uma, S.; Raju, A. R.; Gopalakrishnan, J., BRIDGING THE RUDDLESDEN-POPPER AND THE DION-JACOBSON SERIES OF LAYERED PEROVSKITES - SYNTHESIS OF

LAYERED OXIDES, A2-XLA2TI3-XNBXO10 (A=K, RB), EXHIBITING ION-EXCHANGE. *Journal of Materials Chemistry* **1993,** *3* (7), 709-713.
13. (a) Lieber, C. M., One-dimensional nanostructures: Chemistry, physics & applications. *Solid State Communications* **1998,** *107* (11), 607-616; (b) Feng, S. H.; Xu, R. R., New materials in hydrothermal synthesis. *Accounts of Chemical Research* **2001,** *34* (3), 239-247.
14. Yao, Y.; Chaubey, G. S.; Wiley, J. B., Fabrication of Nanopeapods: Scrolling of Niobate Nanosheets for Magnetic Nanoparticle Chain Encapsulation. *J. Am. Chem. Soc.* **2012,** *134* (5), 2450-2452.
15. Sayama, K.; Yase, K.; Arakawa, H.; Asakura, K.; Tanaka, A.; Domen, K.; Onishi, T., Photocatalytic activity and reaction mechanism of Pt-intercalated K4Nb6O17 catalyst on the water splitting in carbonate salt aqueous solution. *Journal of Photochemistry and Photobiology a-Chemistry* **1998,** *114* (2), 125-135.
16. Domen, K.; Kudo, A.; Shibata, M.; Tanaka, A.; Maruya, K.; Onishi, T., NOVEL PHOTOCATALYSTS, ION-EXCHANGED K4NB6O17, WITH A LAYER STRUCTURE. *Journal of the Chemical Society-Chemical Communications* **1986,** (23), 1706-1707.
17. Bizeto, M. A.; Shiguihara, A. L.; Constantino, V. R. L., Layered niobate nanosheets: building blocks for advanced materials assembly. *Journal of Materials Chemistry* **2009,** *19* (17), 2512-2525.
18. Gasperin, M.; Lebihan, M. T., HYDRATION MECHANISM OF LAMELLAR ALKALINE NIOBATES WITH THE FORMULA A4NB4O17(A=K, RB, CS). *Journal of Solid State Chemistry* **1982,** *43* (3), 346-353.
19. (a) Du, G. H.; Peng, L. M.; Chen, Q.; Zhang, S.; Zhou, W. Z., Imaging helical potassium hexaniobate nanotubes. *Applied Physics Letters* **2003,** *83* (8), 1638-1640; (b) Shiguihara, A. L.; Bizeto, M. A.; Constantino, V. R. L., Chemical Modification of Niobium Layered Oxide by Tetraalkylammonium Intercalation. *Journal of the Brazilian Chemical Society* **2010,** *21* (7), 1366-1376; (c) Kiba, S.; Haga, J.; Hashimoto, S.; Nakato, T., Adsorptive and Photocatalytic Removal of Phenol by Layered Niobates Organically Modified Through Intercalation and Silylation. *Journal of Nanoscience and Nanotechnology* **2010,** *10* (12), 8341-8348; (d) Wei, Q. M.; Nakato, T., Preparation of a layered hexaniobate-titania nanocomposite and its photocatalytic activity on removal of phenol in water. *Journal of Porous Materials* **2009,** *16* (2), 151-156; (e) Maeda, K.; Eguchi, M.; Lee, S. H. A.; Youngblood, W. J.; Hata, H.; Mallouk, T. E., Photocatalytic Hydrogen Evolution from Hexaniobate Nanoscrolls and Calcium Niobate Nanosheets Sensitized by Ruthenium(II) Bipyridyl Complexes. *J. Phys. Chem. C* **2009,** *113* (18), 7962-7969; (f) Sarahan, M. C.; Carroll, E. C.; Allen, M.; Larsen, D. S.; Browning, N. D.; Osterloh, F. E., K4Nb6O17-derived photocatalysts for hydrogen evolution from water: Nanoscrolls versus nanosheets. *Journal of Solid State Chemistry* **2008,** *181* (7), 1678-1683; (g) Bizeto, M. A.; Constantino, V. R. L., Porphyrin inclusion into hexaniobate nanoscrolls. *Microporous and Mesoporous Materials* **2005,** *83* (1-3), 212-218.
20. Du, G. H.; Yu, Y.; Peng, L. M., Hexaniobate nanotubes with variable interlayer spacings. *Chem. Phys. Lett.* **2004,** *400* (4-6), 536-540.
21. (a) Wang, X.; Zhuang, J.; Peng, Q.; Li, Y. D., A general strategy for nanocrystal synthesis. *Nature* **2005,** *437* (7055), 121-124; (b) Deng, Z. X.; Li, L. B.; Li, Y. D., Novel inorganic-organic-layered structures: Crystallographic understanding of both phase and morphology formations of one-dimensional CdE (E = S, Se, Te) nanorods in ethylenediamine. *Inorganic Chemistry* **2003,** *42* (7), 2331-2341; (c) Wang, C.; Deng, Z. X.; Zhang, G. H.; Fan, S. S.; Li,

Y. D., Synthesis of nanocrystalline TiO2 in alcohols. *Powder Technology* **2002,** *125* (1), 39-44; (d) Rajamathi, M.; Seshadri, R., Oxide and chalcogenide nanoparticles from hydrothermal/solvothermal reactions. *Current Opinion in Solid State & Materials Science* **2002,** *6* (4), 337-345.

22. (a) Wu, L.; Bi, J. H.; Li, Z. H.; Wang, X. X.; Fu, X. Z., Rapid preparation of Bi2WO6 photocatalyst with nanosheet morphology via microwave-assisted solvothermal synthesis. *Catalysis Today* **2008,** *131* (1-4), 15-20; (b) Zhang, L. Z.; Djerdj, I.; Cao, M. H.; Antonietti, M.; Niederberger, M., Nonaqueous sol-gel synthesis of a nanocrystalline InNbO4 visible-light photocatalyst. *Advanced Materials* **2007,** *19* (16), 2083-+; (c) Lotsch, B. V.; Doblinger, M.; Sehnert, J.; Seyfarth, L.; Senker, J.; Oeckler, O.; Schnick, W., Unmasking melon by a complementary approach employing electron diffraction, solid-state NMR spectroscopy, and theoretical calculations-structural characterization of a carbon nitride polymer. *Chemistry-a European Journal* **2007,** *13* (17), 4969-4980; (d) Kumar, G. A.; Chen, C. W.; Ballato, J.; Riman, R. E., Optical characterization of infrared emitting rare-earth-doped fluoride nanocrystals and their transparent nanocomposites. *Chemistry of Materials* **2007,** *19* (6), 1523-1528; (e) Murugan, A. V.; Sonawane, R. S.; Kale, B. B.; Apte, S. K.; Kulkarni, A. V., Microwave-solvothermal synthesis of nanocrystalline cadmium sulfide. *Materials Chemistry and Physics* **2001,** *71* (1), 98-102; (f) Yu, S. H.; Yang, J.; Han, Z. H.; Zhou, Y.; Yang, R. Y.; Qian, Y. T.; Zhang, Y. H., Controllable synthesis of nanocrystalline CdS with different morphologies and particle sizes by a novel solvothermal process. *Journal of Materials Chemistry* **1999,** *9* (6), 1283-1287; (g) Wang, W. Z.; Geng, Y.; Yan, P.; Liu, F. Y.; Xie, Y.; Qian, Y. T., Synthesis and characterization of MSe (M = Zn, Cd) nanorods by a new solvothermal method. *Inorganic Chemistry Communications* **1999,** *2* (3), 83-85.
23. (a) Walton, R. I., Subcritical solvothermal synthesis of condensed inorganic materials. *Chemical Society Reviews* **2002,** *31* (4), 230-238; (b) Qian, Y. T., Solvothermal synthesis of nanocrystalline III-V semiconductors. *Advanced Materials* **1999,** *11* (13), 1101-+.
24. (a) Ikeda, S.; Tanaka, A.; Shinohara, K.; Hara, M.; Kondo, J. N.; Maruya, K. I.; Domen, K., Effect of the particle size for photocatalytic decomposition of water on Ni-loaded K4Nb6O17. *Microporous Materials* **1997,** *9* (5-6), 253-258; (b) Miyamoto, N.; Nakato, T., Liquid crystalline nature of K4Nb6O17 nanosheet sols and their macroscopic alignment. *Advanced Materials* **2002,** *14* (18), 1267-+; (c) Miyamoto, N.; Nakato, T., Liquid crystalline nanosheet colloids with controlled particle size obtained by exfoliating single crystal of layered niobate K4Nb6O17. *Journal of Physical Chemistry B* **2004,** *108* (20), 6152-6159.
25. (a) Nakato, T.; Ueda, H.; Hashimoto, S.; Terao, R.; Kameyama, M.; Mouri, E., Pickering Emulsions Prepared by Layered Niobate K4Nb6O17 Intercalated with Organic Cations and Phytocatalytic Dye Decomposition in the Emulsions. *Acs Applied Materials & Interfaces* **2012,** *4* (8), 4338-4347; (b) Ekambaram, S.; Yanagisawa, M.; Uchida, S.; Fujishiro, Y.; Sato, T., Synthesis and photocatalytic property of hectorite/(Pt,TiO2) and H4Nb6O17/(Pt,TiO2) nanocomposites. *Molecular Crystals and Liquid Crystals* **2000,** *341*, 1017-1022; (c) Kim, Y. I.; Atherton, S. J.; Brigham, E. S.; Mallouk, T. E., SENSITIZED LAYERED METAL-OXIDE-SEMICONDUCTOR PARTICLES FOR PHOTOCHEMICAL HYDROGEN EVOLUTION FROM NONSACRIFICIAL ELECTRON-DONORS. *Journal of Physical Chemistry* **1993,** *97* (45), 11802-11810.
26. Du, G. H.; Chen, Q.; Yu, Y.; Zhang, S.; Zhou, W. Z.; Peng, L. M., Synthesis, modification and characterization of K4Nb6O17-type nanotubes. *Journal of Materials Chemistry* **2004,** *14* (9), 1437-1442.

27. Wu, B. H.; Guo, C. Y.; Zheng, N. F.; Xie, Z. X.; Stucky, G. D., Nonaqueous Production of Nanostructured Anatase with High-Energy Facets. *Journal of the American Chemical Society* **2008,** *130* (51), 17563-17567.
28. Kisner, A.; Lenk, S.; Mayer, D.; Mourzina, Y.; Offenhausser, A., Determination of the Stability Constant of the Intermediate Complex during the Synthesis of Au Nanoparticles Using Aurous Halide. *Journal of Physical Chemistry C* **2009,** *113* (47), 20143-20147.
29. Gunasekaran, S.; Sailatha, E.; Seshadri, S.; Kumaresan, S., FTIR, FT Raman spectra and molecular structural confirmation of isoniazid. *Indian Journal of Pure & Applied Physics* **2009,** *47* (1), 12-18.
30. Pian, X. T.; Lin, B. Z.; Chen, Y. L.; Kuang, J. D.; Zhang, K. Z.; Fu, L. M., Pillared Nanocomposite TiO2/Bi-Doped Hexaniobate with Visible-Light Photocatalytic Activity. *J. Phys. Chem. C* **2011,** *115* (14), 6531-6539.
31. Byeon, S. H.; Kim, H. J.; Kim, D. K.; Hur, N. H., Synthesis, structure, magnetic properties, and XANES spectra of reduced niobate RbNaxCa2Nb3O10. *Chemistry of Materials* **2003,** *15* (2), 383-389.
32. (a) Eguchi, M.; Angelone, M. S.; Yennawar, H. P.; Mallouk, T. E., Anisotropic alignment of lamellar potassium hexaniobate microcrystals and nanoscrolls in a static magnetic field. *J. Phys. Chem. C* **2008,** *112* (30), 11280-11285; (b) Shiguihara, A. L.; Bizeto, M. A.; Constantino, V. R. L., Exfoliation of layered hexaniobate in tetra(n-butyl) ammonium hydroxide aqueous solution. *Colloids and Surfaces a-Physicochemical and Engineering Aspects* **2007,** *295* (1-3), 123-129; (c) Bizeto, M. A.; Alves, W. A.; Barbosa, C. A. S.; Ferreira, A.; Constantino, V. R. L., Evaluation of hexaniobate nanoscrolls as support for immobilization of a copper complex catalyst. *Inorganic Chemistry* **2006,** *45* (16), 6214-6221.
33. Adireddy, S.; Yao, Y.; He, J.; Wiley, J. B., Rapid solvothermal fabrication of hexaniobate nanoscrolls. *Materials Research Bulletin* **2013,** *48* (9), 3236-3241.
34. (a) Yang, H. G.; Liu, G.; Qiao, S. Z.; Sun, C. H.; Jin, Y. G.; Smith, S. C.; Zou, J.; Cheng, H. M.; Lu, G. Q., Solvothermal Synthesis and Photoreactivity of Anatase TiO2 Nanosheets with Dominant {001} Facets. *J. Am. Chem. Soc.* **2009,** *131* (11), 4078-4083; (b) Ma, S. Q.; Sun, D. F.; Simmons, J. M.; Collier, C. D.; Yuan, D. Q.; Zhou, H. C., Metal-organic framework from an anthracene derivative containing nanoscopic cages exhibiting high methane uptake. *J. Am. Chem. Soc.* **2008,** *130* (3), 1012-1016; (c) Li, H. X.; Bian, Z. F.; Zhu, J.; Zhang, D. Q.; Li, G. S.; Huo, Y. N.; Li, H.; Lu, Y. F., Mesoporous titania spheres with tunable chamber stucture and enhanced photocatalytic activity. *J. Am. Chem. Soc.* **2007,** *129* (27), 8406-+; (d) Chen, X. M.; Tong, M. L., Solvothermal in situ metal/ligand reactions: A new bridge between coordination chemistry and organic synthetic chemistry. *Accounts of Chemical Research* **2007,** *40* (2), 162-170; (e) Zhang, J. P.; Lin, Y. Y.; Huang, X. C.; Chen, X. M., Copper(I) 1,2,4-triazolates and related complexes: Studies of the solvothermal ligand reactions, network topologies, and photoluminescence properties. *J. Am. Chem. Soc.* **2005,** *127* (15), 5495-5506; (f) Rao, C. N. R.; Deepak, F. L.; Gundiah, G.; Govindaraj, A., Inorganic nanowires. *Progress in Solid State Chemistry* **2003,** *31* (1-2), 5-147; (g) Chen, W.; Wang, J. Y.; Chen, C.; Yue, Q.; Yuan, H. M.; Chen, J. S.; Wang, S. N., Photoluminescent metal-organic polymer constructed from trimetallic clusters and mixed carboxylates. *Inorganic Chemistry* **2003,** *42* (4), 944-946; (h) Patzke, G. R.; Krumeich, F.; Nesper, R., Oxidic nanotubes and nanorods - Anisotropic modules for a future nanotechnology. *Angewandte Chemie-International Edition* **2002,** *41* (14), 2446-2461; (i) Cao, R.; Sun, D. F.; Liang, Y. C.; Hong, M. C.; Tatsumi, K.; Shi, Q., Syntheses and characterizations of three-

dimensional channel-like polymeric lanthanide complexes constructed by 1,2,4,5-benzenetetracarboxylic acid. *Inorganic Chemistry* **2002,** *41* (8), 2087-2094; (j) Lo, S. M. F.; Chui, S. S. Y.; Shek, L. Y.; Lin, Z. Y.; Zhang, X. X.; Wen, G. H.; Williams, I. D., Solvothermal synthesis of a stable coordination polymer with copper-I-copper-II dimer units: Cu-4{1,4-C6H4(COO)(2)}(3)(4,4 '-bipy)2 (n). *J. Am. Chem. Soc.* **2000,** *122* (26), 6293-6294.

35. (a) Sayama, K.; Tanaka, A.; Domen, K.; Maruya, K.; Onishi, T., PHOTOCATALYTIC DECOMPOSITION OF WATER OVER PLATINUM-INTERCALATED K4NB6O17. *Journal of Physical Chemistry* **1991,** *95* (3), 1345-1348; (b) Sayama, K.; Arakawa, H.; Domen, K., Photocatalytic water splitting on nickel intercalated A(4)Ta(x)Nb(6-x)O(17) (A=K, Rb). *Catalysis Today* **1996,** *28* (1-2), 175-182.

Chapter 3

High Yield Solvothermal Synthesis of Magnetic Peapod Nanocomposites via the Capture of Preformed Nanoparticles in Scrolled Nanosheets*

3.1 Introduction

Among one-dimensional nanomaterials, nanoscrolls are especially unique due to an interesting convolved architecture.[1] Such structures offer the potential for tunability beyond simple nanotubes – like tubes, the structures have outer and inner shell components, but unlike them, the scrolls can possess flexibility in their diameter as well as an interlayer structure that is open to further modification.[2] A wide range of materials are known to form nanoscrolls including graphene,[1a] BN,[3] WS_2,[4] MoS_2,[5] TiO_2,[6] V_2O_5,[7] and $K_4Nb_6O_{17}$.[8] Such scrolled structures have already received attention in technologically significant areas such as heterogeneous catalysis, drug-delivery systems, intercalation, ion-exchange, photo-degradation, hydrogen storage, gas sensors, and solar energy conversion.[9]

Fabrication of new nanocomposites holds both fundamental and practical importance in catalysis,[10] magnetic and optical devices,[11] fuel cells,[12] sensors,[13] templates for nanoparticle (NP) assembly,[14] and photonics.[15] Various methods have been developed for the preparation of nanocomposites, such as those based on vapor-liquid-solid (VLS),[16] chemical reduction,[17] co-electrodeposition,[18] atomic layer deposition (ALD),[19] wet-chemical route,[20] and electron beam lithography.[21]

*This chapter was adapted from: Adireddy S.; Carbo, C.E.,; Yao Y.; Vargas J.M.; Spinu L; Wiley, J. B., High yield solvothermal synthesis of magnetic peapod nanocomposites via the capture of preformed nanoparticles in scrolled nanosheets. *Chemistry of Materials* **2013** (Just Accepted)

Some of these methods, however, can be costly, time consuming, and not readily scalable for bulk synthesis. The controlled convolution of exfoliated nanosheets offers a new synthetic paradigm for composite formation.[22] Exploiting the exfoliation/scrolling process, various molecular functionalities could be introduced to fabricate novel composite architectures, which would be laborious or even unobtainable by conventional methods.

The cooperative behavior of nanocomposites is determined by the geometrical arrangement of the building units in combination with the intrinsic properties of each constituent.[23] Interactions between different components can give rise to a series of new or enhanced characteristics, such as stronger magnetic response, unusual electron transport, enhanced quantum yields, etc.[24] Furthermore, unique combinations of nanomaterials can serve as model systems to explore fundamental classical and quantum coupling interactions[25] and the development of a detailed understanding of structure-property relations in multifunctional nanostructures may prove invaluable for the rational design of new composites with targeted technologically significant applications.[26]

One dimensional NP chains can be prepared by a variety of techniques including oriented aggregation,[27] electric–dipolar interactions,[28] solution-phase template assembly,[29] and magnetic dipole moments.[28d, 30] Recent work in our group resulted in the *in situ* formation of nanopeapod (NPP)-like structures containing chains of cobalt NPs.[14] Building on this initial study, we have developed a convenient and controllable protocol for the bulk synthesis of NPP composites using a solvothermal approach. During this treatment, exfoliated hexaniobate nanosheets scroll around highly ordered chains of preformed NPs to produce the target NPP structures. Herein we demonstrate the effectiveness of this technique through the synthesis of a series of magnetic

ferrites where the 1D NP chains show a clear enhancement in magnetic response. It should be noted that preliminary results from this study were included in a recent proceedings.[31]

3.2 Experimental

Materials. K_2CO_3 (99%) and Nb_2O_5 (99%) were acquired from Alfa Aesar. Benzyl ether (99%), cobalt(II) acetylacetonate (97%), 1,2-hexadecanediol, hexane (anhydrous, 95%), iron(III) acetylacetonate (97%), iron(III) oxide (hydrated; catalyst grade, 30–50 mesh), manganese(II) acetylacetonate (98%), nickel(II) acetylacetonate (95%), 1-octadecene (90%), octyl ether (99%), oleic acid (99.8%, anhydrous), oleylamine (>70%), Phenyl ether (99%), tetrabutylammonium hydroxide 30-hydrate (TBAOH) (97%), and toluene (99.8%, anhydrous) were purchased from Sigma-Aldrich. Pure grade ethanol (Pharmco-Aaper, 200 Proof, absolute) was used in all preparations.

3.2.1 Niobate Nanosheets

Synthesis of $K_4Nb_6O_{17}$ crystallites.

K_2CO_3 and Nb_2O_5 (in the molar ratio of 1.0:1.4) were ground and heat treated in an alumina crucible at 900 °C for 1h before continuing to heat at 1050 °C for another 24 h.[8] The white product was washed several times with milli-Q (18.2 MΩ cm^{-1} at 25 °C) water and acetone and then dried overnight at 80 °C.

Acid-exchanged $K_4Nb_6O_{17}$.

$H_xK_{4-x}Nb_6O_{17}$ was obtained by stirring 0.15 g of $K_4Nb_6O_{17}$ powder with 15 mL of a 3 M HCl solution at 50 °C for 4 days.[8] The white product was washed with milli-Q water and acetone and dried at 80 °C.

3.2.2 Magnetic Nanoparticle Synthesis

Magnetic Fe_3O_4 NPs.

Magnetic NPs with different capping groups, various shapes, and diameters from 6 to 20 nm were synthesized according to published reports.[32] Oleylamine (OAm) capped 9 nm Fe_3O_4 NPs were used predominately in the fabrication and characterization of NPPs.

Synthesis of spherical OAm-capped Fe_3O_4 NPs. Monodispersed OAm-capped ~9 nm Fe_3O_4 NPs were synthesized according to a modified procedure from Xu et al.[32a] Nanocrystals were synthesized in a three-neck flask equipped with a thermocouple, heating mantle and magnetic stirrer. $Fe(acac)_2$ (1 mmol), benzyl ether (4 mL) and OAm (6 mL) were stirred under N_2 and the mixture was dehydrated by heating it to 110 °C for 1 h. Then the solution was further heated to 300 °C at the rate of 10 °C/min, and held at this temperature for 1h before cooling to room temperature. Black-brown iron oxide NPs were precipitated on addition of acetone, isolated from solution, and then redispersed in toluene. The precipitation–redispersal procedure was repeated several times to obtain pure Fe_3O_4 NPs. Finally, the OAm capped-Fe_3O_4 NPs (yield ~100 mg) were dispersed in toluene.

Synthesis of spherical oleic acid (OAc)-capped Fe_3O_4 NPs. Monodispersed OAc-capped Fe_3O_4 NPs with average diameters ~9 nm and ~20 nm were synthesized according to the method of Yu et al.[32b] Fe_3O_4 NPs (9 nm) were synthesized when 2 mmol of iron(III) oxide hydrate fine powder was mixed with OAc (8 mmol), octadecene (5 g), and heated to 320 °C under a blanket of N_2 for 45 mins. Larger 20 nm Fe_3O_4 NPs can easily be prepared by simply increasing the amount of OAc to 12 mmol and reaction time to 1h. As-synthesized OAc capped-Fe_3O_4 NPs (yield ~ 140 mg) were re-dispersed in toluene.

Seed mediated growth of monodispersed Fe_3O_4 NPs. Monodispersed magnetic NPs can be prepared using the synthetic protocol reported by Sun et al.[33] In a typical synthesis of ~6 nm Fe_3O_4 NPs, $Fe(acac)_3$ (2 mmol), 1,2-hexadecanediol (10 mmol), OAc (6 mmol) and OAm (6 mmol) were dissolved in 20 mL of benzyl ether. The solution was heated to 200 °C for 30 min under N_2 atmosphere, then the reaction temperature raised to reflux (300 °C) for another 2 h. After the reaction, the solution was cooled to room temperature. The black-brown mixture was isolated with the addition of 30 mL ethanol, followed by centrifugation. The Fe_3O_4 NPs (yield ~ 180 mg) were dispersed in toluene to be used as seed crystals to grow larger NPs. An ~80 mg sample of the 6 nm Fe_3O_4 NPs was then used to grow 9 nm, 12 nm, 14 nm, 16 nm and 18 nm Fe_3O_4 NPs.

Synthesis of monodispersed MFe_2O_4 (M = Mn, Co, and Ni) NPs.

Again under the conditions utilized above,[33] reaction of $Fe(acac)_3$ with $Mn(acac)_2$, $Co(acac)_2$ or $Ni(acac)_2$ led to 7 nm $MnFe_2O_4$, 5 nm and 10 nm $CoFe_2O_4$, 7 nm $NiFe_2O_4$ NPs, respectively; all these samples could be readily dispersed in toluene. As-synthesized MFe_2O_4 NPs (yield ~180 mg) were re-dispersed in toluene.

3.2.3 Synthesis of Magnetic NP@hexaniobate Nanopeapods

A 20 mg sample of magnetic NPs dispersed in toluene (8 mL) was added to the mixture of 5 mL (15 mmol) OAm, 100 mg of $H_xK_{4-x}Nb_6O_{17}$, and 0.15 g (0.19 mmol) TBAOH. The solution was magnetically stirred for 2 h and transferred to a 23 mL Teflon-lined stainless steel autoclave (Parr, model 4749, 1800 psig). The sealed autoclave was heated to 220 °C for 6 h and then cooled to room temperature. The resulting brown precipitate was washed with a mixture of 15 mL toluene and 30 mL ethanol before being isolated via centrifugation. The product was then

redispersed in 35 mL toluene and further centrifugation (3000 rpm, 3 min) was carried out to remove any residual free magnetic NPs.

3.2.4 Characterization

For transmission electron microscopy (TEM) measurements, toluene dispersed samples were drop cast onto a 200 mesh carbon-coated copper grid and heated in a drying oven at 60 °C overnight. The morphology of the materials was characterized on a JEOL 2010 TEM operated at an accelerating voltage of 200 kV with a Gatan slow scan CCD camera. The unit was also equipped with an EDAX Genesis energy dispersive spectroscopy (EDS) system for elemental analysis. High-resolution TEM (HRTEM) and selected area electron diffraction (SAED) measurements were performed with FEI TECNAI G2 F30 FEG TEM (300 kV). Magnetic hysteresis loops were obtained at room temperature in a Princeton AGM-VSM vibrating sample magnetometer at a maximum magnetic field of 20 kOe on powder samples contained in standard gel capsules. Temperature dependent magnetization measurements were carried out with a Quantum Design superconducting quantum interference device (SQUID) between 4 K and 300 K in a 20 Oe magnetic field on powder samples contained in gel capsules; both zero-field cooling (ZFC) and field cooling (FC) experiments were performed.

3.3 Results

A series of Fe_3O_4 NPs were prepared separately, mixed with hexaniobate crystallites, and treated solvothermally in toluene above 200 °C to rapidly make Fe_3O_4@hexaniobate NPPs in high yield (Figure 3.1).

The Fe_3O_4 NPs were synthesized according to a modified literature procedure[32a] and exhibit spherical shape with an average diameter of ~9 nm; representative TEM and HRTEM images of Fe_3O_4 NPs are presented in Figures 3.2a and 3.2b with a size distribution diagram

shown in the inset of Figure 3.2a. The experimental procedure used in the formation of the NPPs is highlighted in Figure 3.1. Figures 3.2c and 3.2d present the morphology of typical NPP samples. TEM images exhibit clear dark and bright contrast differences between the Fe_3O_4 NPs and the hexaniobate nanoscrolls. NPPs form with different lengths, typically varying between 0.1 μm and 1 μm and the host nanoscroll structures consist of 2 to 6 layers with an interlayer spacing of ~3.2 nm and outer diameters ranging from 30-55 nm. The inner diameter is dictated by the size of the NP; for 9 nm NPs, this results in an inner diameter of about 12-13 nm. Each of the NPPs typically contain 40-100 NPs with an interparticle space of about 2-3 nm. Elemental analysis with EDS confirmed that the NPPs contain Fe and Nb (Figure 3.2d, inset).

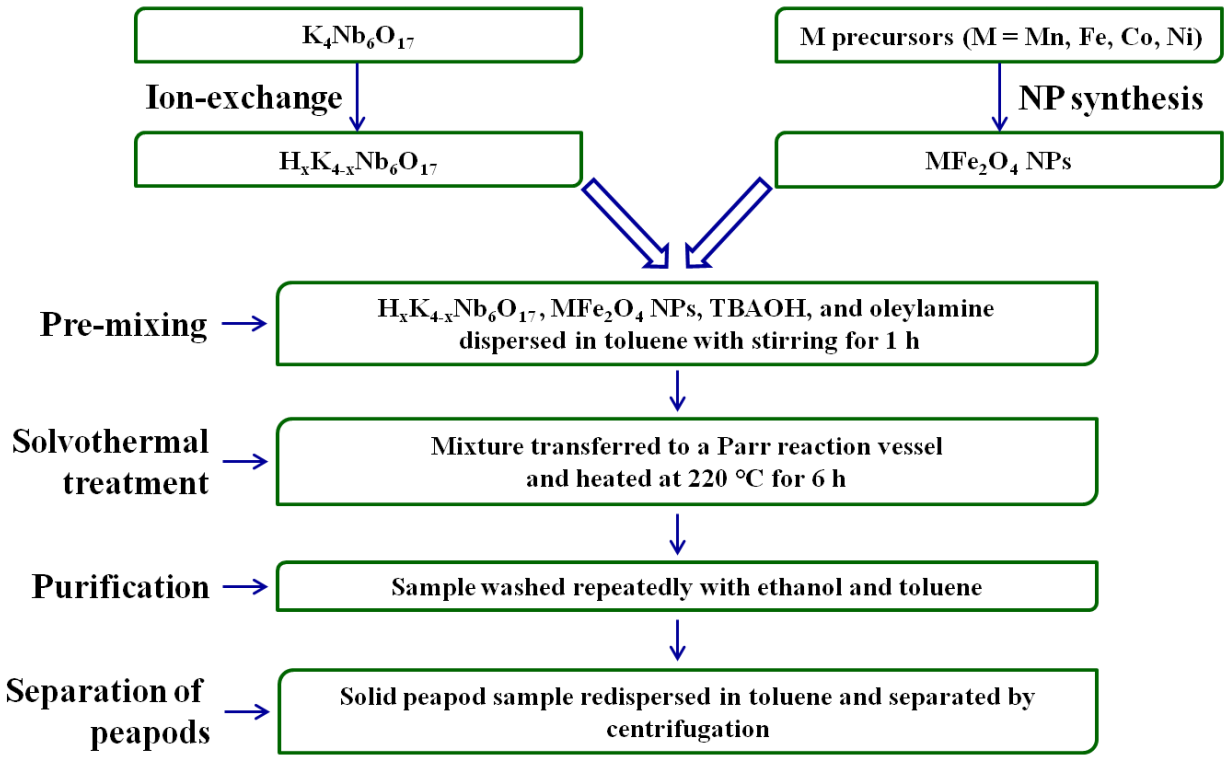

Figure 3.1. Flow chart for the fabrication of MFe_2O_4@hexaniobate NPPs.

The versatile synthetic strategy used here produces NPP structures in high yield. Figure 3.3 shows a series of low magnification TEM images highlighting a representative sample. Yields were evaluated by analyzing the filling fraction of 500 different NPPs. Figure 3.3b

presents a pie-chart of the filling fraction of the set. Almost half are over 95% filled with NPs and over two-thirds are at least 80% filled. TEM images (Figures 3.3c, 3.3d and 3.3e) highlight the uniform filling in various regions of sample.

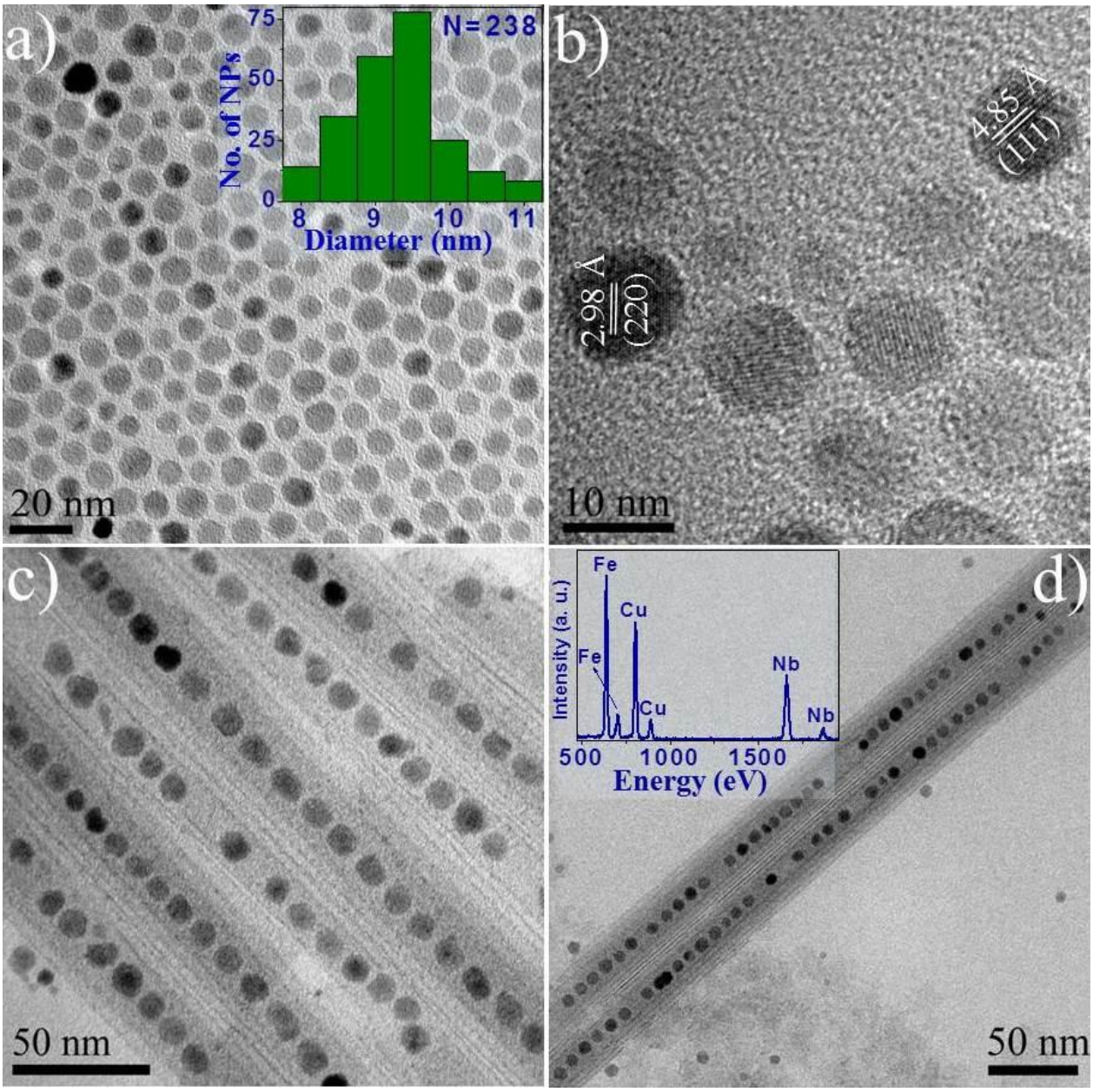

Figure 3.2. (a, b) TEM and HRTEM images of Fe_3O_4 NPs. (c, d) TEM images of Fe_3O_4@hexaniobate NPPs [Inset, Figure d) EDS spectrum, Cu peaks from TEM grid].

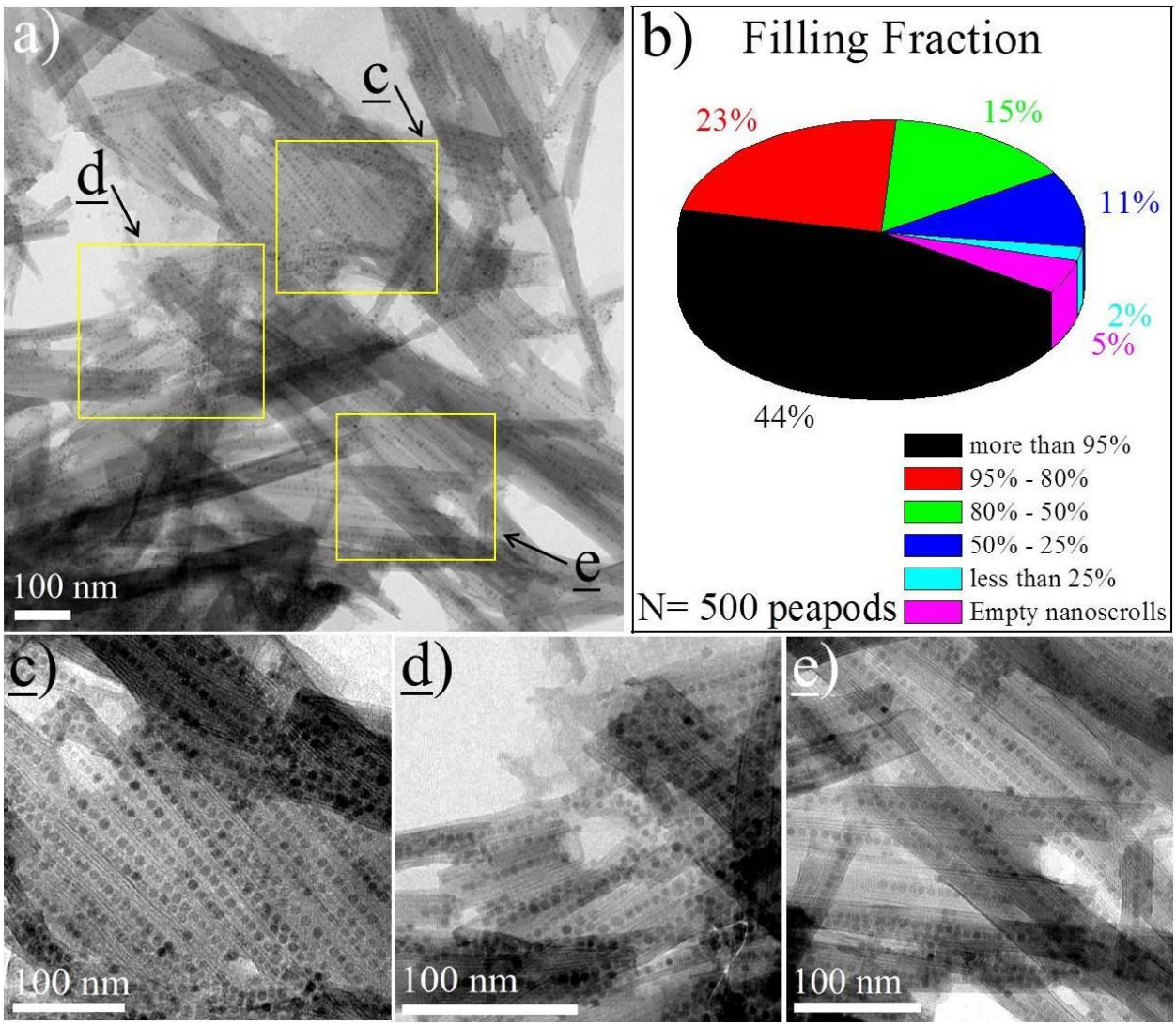

Figure 3.3. (a) Low-magnification TEM image of a representative sample of Fe_3O_4@hexaniobate NPPs; (b) Pie chart representing the filling fraction of 500 NPPs; (c, d, e) TEM images demonstrating uniform NPP filling.

Control experiments were performed to determine the optimal NP sizes that can be captured within the hexaniobate nanosheets. Reactions with monodispersed Fe_3O_4 NP samples of 9, 14, 16 and 18 nm were all examined. With 9 nm NPs, high-quality NPPs were observed (Figure 3.4a). Similarly 14 nm NPs were also readily captured by this method (Figure 3.4b). Reactions with 16 nm and 18 nm NPs, however, showed almost no evidence for encapsulation; TEM (Figures 3.4c and 3.4d) illustrated the inefficient encapsulation of hexaniobate nanoscrolls

when larger NPs sizes were reacted. These results show that the NPP formation is NP size dependent and that the upper limit under these reaction conditions is around 14 nm. In terms of a lower limit, reactions with polydispersed NP samples showed NPPs with NP's as small as 4 nm (Figure 3.5).

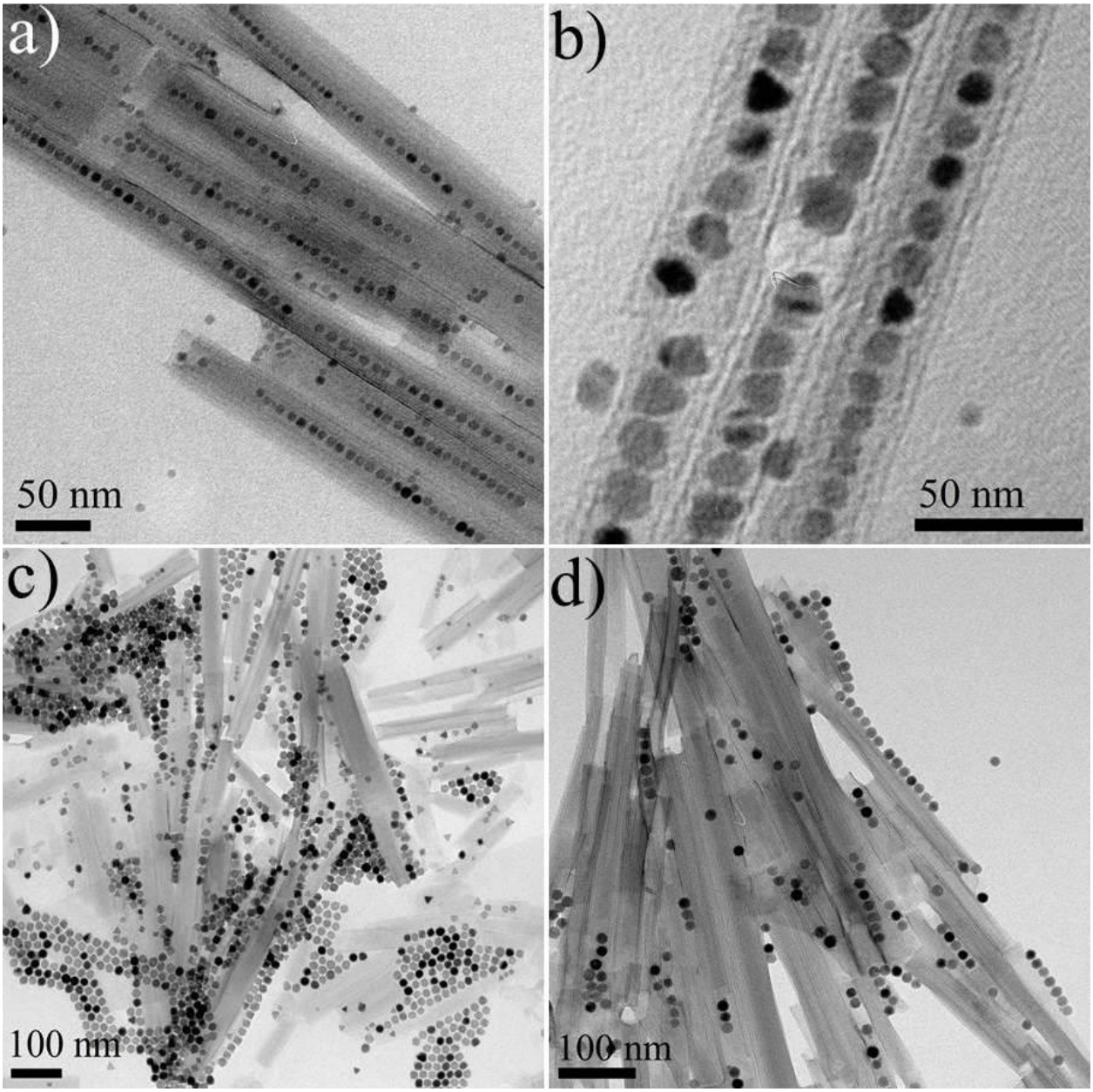

Figure 3.4. (a, b) TEM image showing the encapsulation of 9 nm and 14 nm Fe_3O_4@hexaniobate NPPs respectively; (c, d) TEM images demonstrating the inefficient encapsulation of 16 nm and 18 nm Fe_3O_4 NPs.

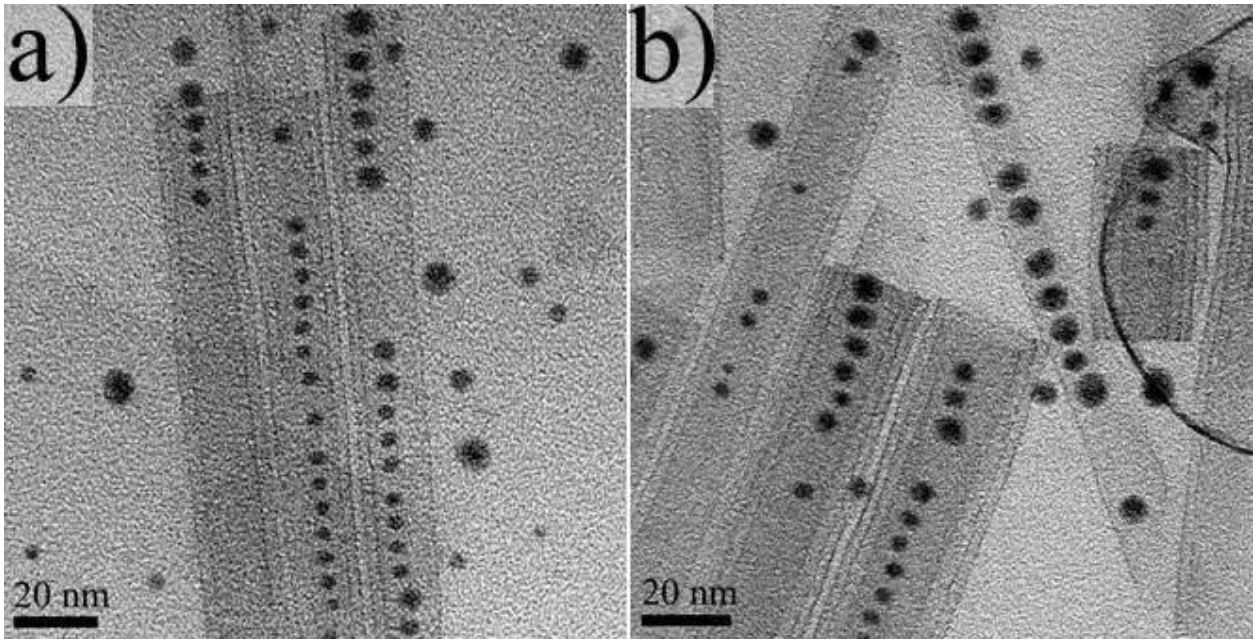

Figure 3.5. (a, b) TEM images showing NPPs with small NPs.

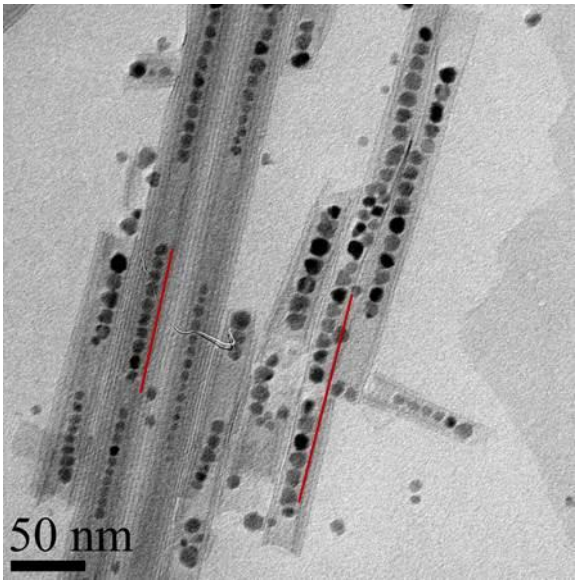

Figure 3.6. TEM image showing the size selective encapsulation of 9 and 12 nm Fe_3O_4 NPs in hexaniobate nanoscrolls. (Solid lines (red) highlight two regions exhibiting size segregation.)

Mixed NP samples were also examined. In these experiments, clear evidence for size separation was seen. When combinations of 9 nm and 12 nm Fe_3O_4 NPs were treated, the NPs segregated either into separate NPPs, or occasionally within different sections of the same NPP.

Figure 3.6 presents a series of NPPs exhibiting size selective NP encapsulation. Similar segregations can also be seen in polydispersed samples (Figure 3.7).

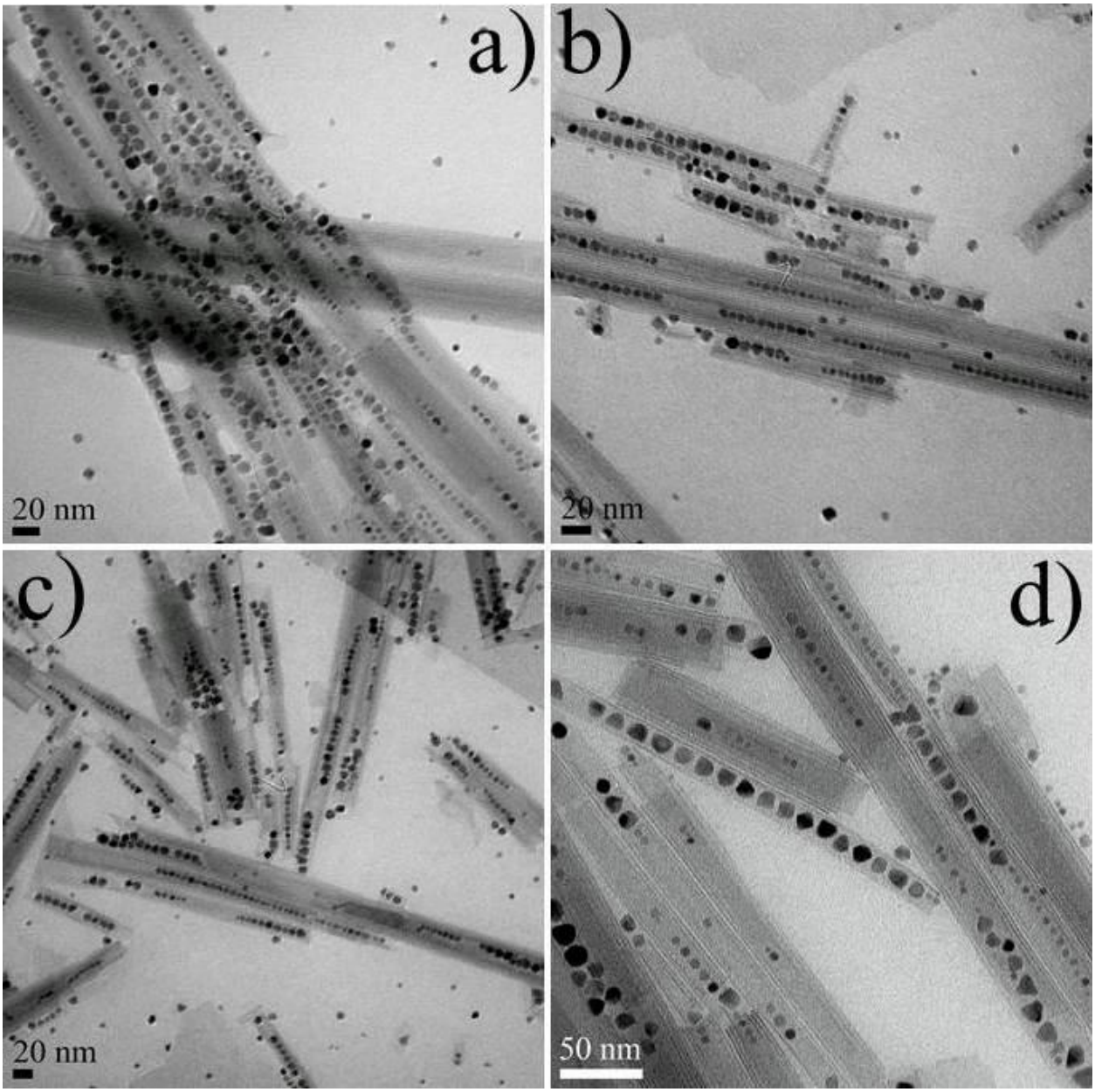

Figure 3.7. TEM images of the Fe_3O_4@hexaniobate NPPs showing the size selective separation of NPs, (a, b, c) polydispersed Fe_3O_4 NPs encapsulated separately in the hexaniobate nanoscrolls; (d) polydispersed $CoFe_2O_4$ NP encapsulation in hexaniobate nanoscrolls.

This approach for the fabrication of NPPs is not limited to just the OAm surfactant or Fe_3O_4 NPs. When OAc-coated Fe_3O_4 NPs were used, NPs are easily captured to form NPPs

(Figure 3.8a). And, reactions with other metal ferrites NPs, $MnFe_2O_4$, $CoFe_2O_4$, and $NiFe_2O_4$, also result in NPPs (Figures 3.8b, 3.8c and 3.8d, respectively). Note, the lack of monodispersity in the $CoFe_2O_4$ sample serves to further highlight size selectivity in these systems where large NPs (~10 nm) are readily segregated from other smaller (~4 - 6 nm) NPs (Figure 3.8c).

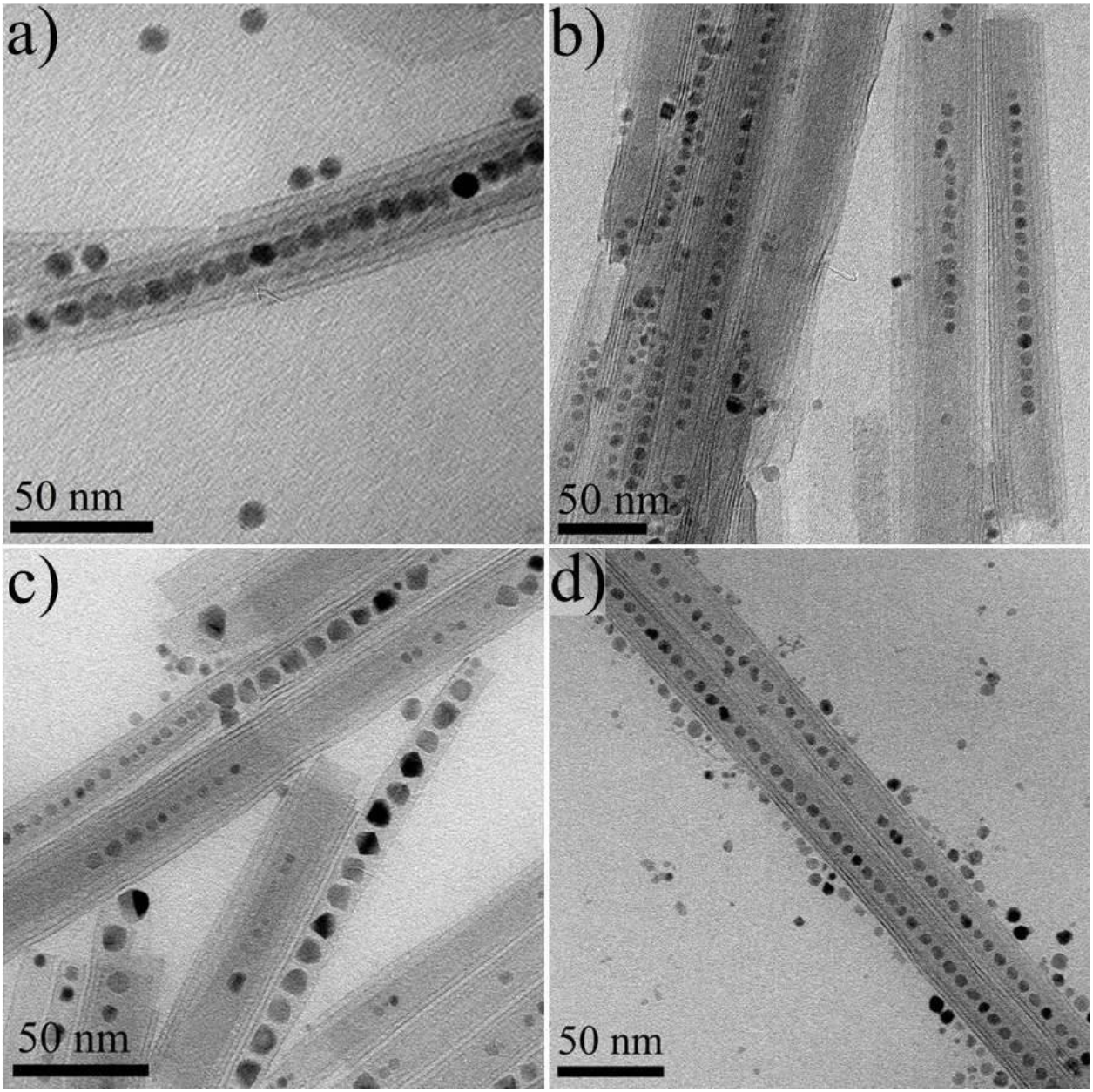

Figure 3.8. (a) The TEM image showing the encapsulation of OAc-coated Fe_3O_4 NPs, (b, c, d) $MnFe_2O_4$, $CoFe_2O_4$, $NiFe_2O_4$ NPs@hexaniobate NPPs**.**

NPP production depends on several factors such as the presence of TBAOH, the amount and type of surfactant, and reaction temperature. In the present study, TBAOH acts as an exfoliating agent while oleylamine plays a dual role as both intercalant and surfactant. When either of these reagents is completely removed from the synthesis, NPPs will not form. To better understand the role of the primary amine chain length in NPP formation, experiments were performed with propylamine and octylamine instead of oleylamine; in the case of propylamine, NPPs were not produced, while with octylamine, NPPs were produced, but only in very low yields (Figure 3.9). With respect to reaction temperatures, it was found that solvothermal reactions needed to be carried out above 180 °C to achieve effective NP encapsulation; syntheses performed at lower temperatures (120 - 150 °C) showed only moderate levels of encapsulation (4 to 5 NPs per scroll).

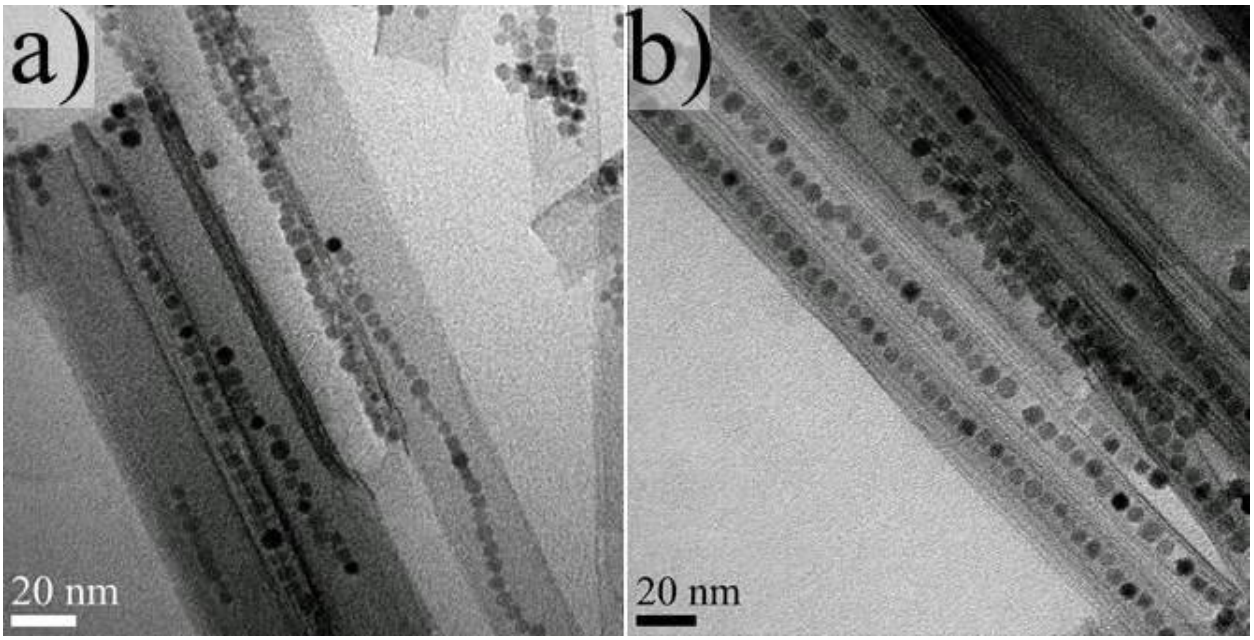

Figure 3.9. TEM images showing the effect of intercalant chain length on the fabrication of Fe_3O_4@hexaniobate nanocomposites, (a) the NP chains formed on top of the hexaniobate nanosheets when propylamine (amine with smaller chain lengths) was used as an intercalant; (b) NP chains were encapsulated inside the hexaniobate nanoscrolls when octylamine was used instead of propylamine.

To better gauge the stability of these materials with respect to NP retention, NPP samples were sonicated for various times. After sonicating samples at intervals up to an hour, the NPP architectures were found to remain intact, with no significant release of NPs or disturbance of NPP architecture detected.

Another set of experiments were performed to test whether NPPs would readily form through the insertion of ferrite NPs into preformed nanoscrolls. Combinations of free NPs and nanoscrolls were treated either at room temperature or under solvothermal conditions. In both cases, only a few NPs were able to insert into the scrolls. Greater than 95% of the scrolls remained empty and those few showing NP uptake had only about 1-5 NPs on average (Figure 3.10).

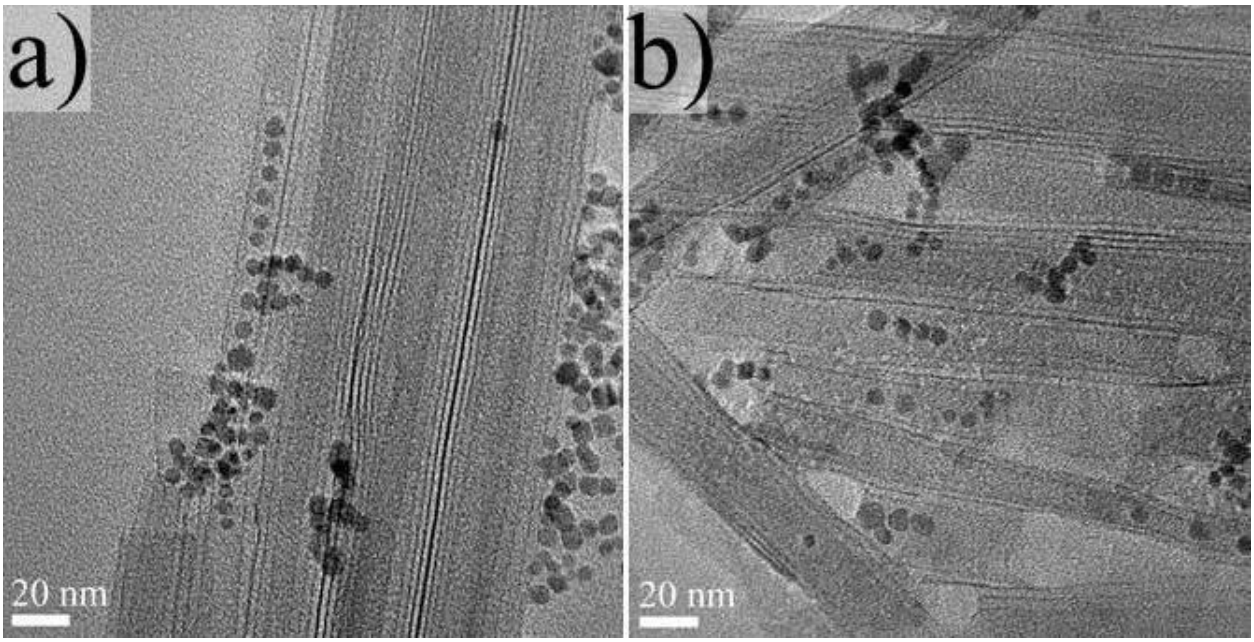

Figure 3.10. TEM images showing almost no encapsulation when preformed hexaniobate nanoscrolls were reacted with NPs. Reaction were carried out at a) room temperature or b) under solvothermal conditions at 220 °C.

Magnetic Characterization. The coercivity of NPP encased magnetic NPs was expected to be greater than that of the free NPs due to the coupling of magnetic dipoles along chains of ferrite NPs. Figure 3.11 shows the room temperature magnetic hysteresis loops of the powder samples of both free 9 nm Fe_3O_4 NPs and Fe_3O_4@hexaniobate nanoscrolls. Clear evidence for magnetic coupling is observed where the coercivity of the NPP sample (H_C = 95 Oe) is almost 4 times greater than that of the free NPs (H_C = 26 Oe).

Variable temperature magnetization effects also show clear differences between free NPs and peapods. Figure 3.11b presents ZFC and FC measurements on both free 9 nm Fe_3O_4 NPs and the corresponding Fe_3O_4 NPPs. The NP sample shows behavior typical for monodispersed NP samples with a ZFC maximum at about 43 K and an irreversible temperature, defined as the temperature at which the ZFC and FC curves separate, at 100 K. In the Fe_3O_4 NPP sample, both the ZFC maximum and the irreversible temperature values shift, to 74 K and 214 K, respectively. These shifts in the maximum and irreversible temperatures are consistent with strong particle-particle interactions within the nanopeapods – dipolar coupling of adjacent NPs results in nanowire-like magnetic anisotropy, leading to the broadening of the ZFC curve and the dramatic increase in the irreversible temperature. It should be noted that a significant diamagnetic contribution is present in these samples as highlighted by the negative magnetization in the ZFC curves below 50 K; this is due to the surfactant groups in the NP sample and the surfactant and non-magnetic scrolled niobate nanosheets in the peapod sample.

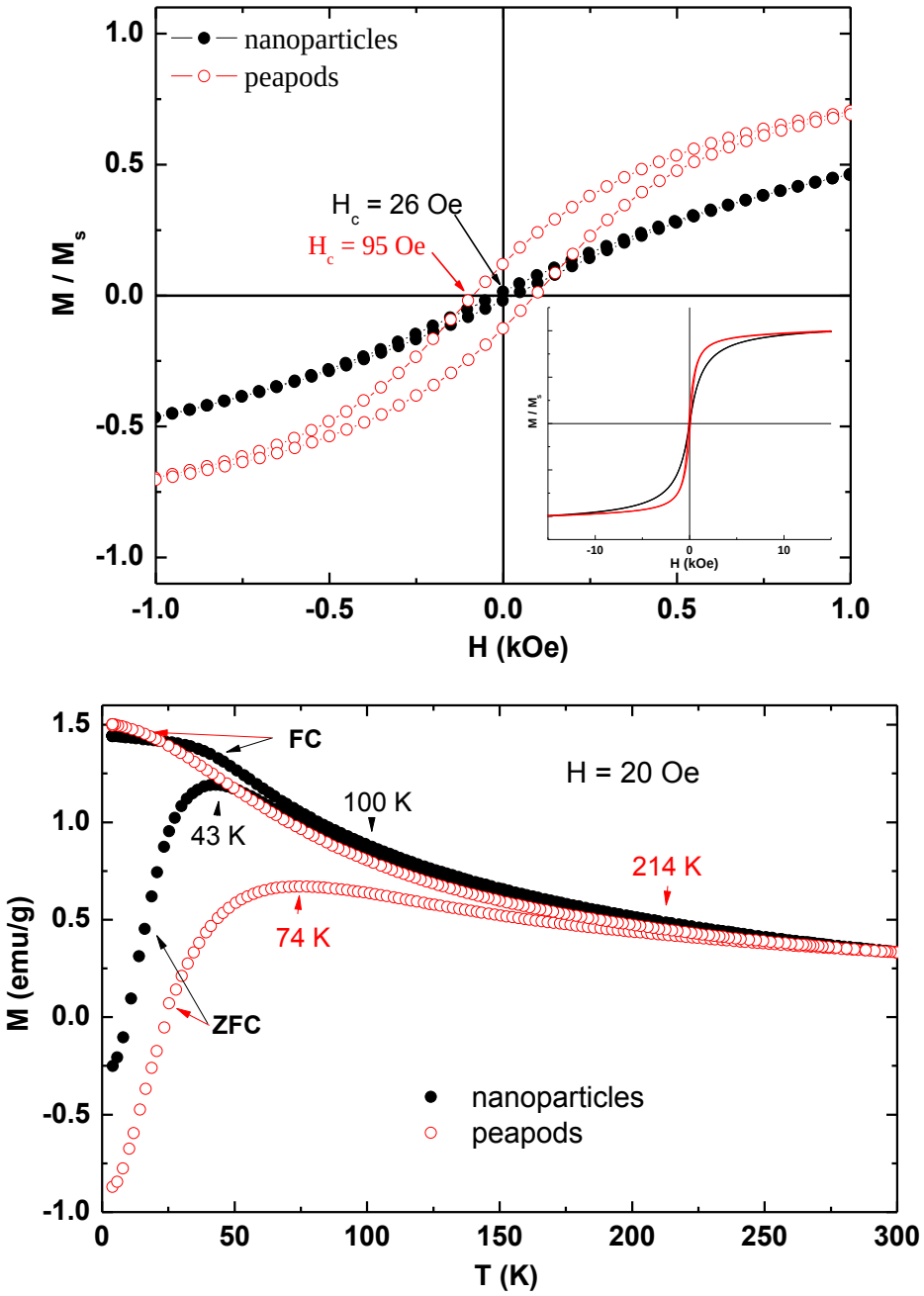

Figure 3.11. Magnetic measurements on powder samples of Fe_3O_4 NPs (filled circles) and Fe_3O_4 NPPs (open circles). (a) Room temperature VSM showing variation in magnetization as a function of field strength. (b) Variable temperature magnetization (SQUID) measurements including ZFC and FC data. ZFC maxima are indicated at 43 K and 73 K and irreversible temperatures at 100 K and 214 K for the NP and NPP samples, respectively. (Note: the magnetization data for the NPP sample was adjusted (x 6) for data comparison.)

3.4 Discussion

The approach described here presents an effective solvothermal method for the formation of NPPs. These composites can be readily obtained building on the solvothermal fabrication of hexaniobate nanoscrolls.[34] While we have reported previously on the *in situ* formation of cobalt metal NPPs,[14] the solvothermal approach is much more flexible in that the NPs are made separately before they are combined and captured within hexaniobate nanoscrolls, allowing for much greater control over the NPPs in terms of NP composition and dimensions. Further, unlike the *in situ* method, this new approach results in NPPs with higher NP loadings and allows for their rapid production in high yield; 95% of the nanoscrolls have some NP encapsulation, over two-thirds of the nanoscrolls are at least 80% filled with NPs and almost half (44%) are more than 95% full. Figure 3.12 shows the scheme used for the fabrication of MFe_2O_4@hexaniobate NPPs from MFe_2O_4 NPs and $H_xK_{4-x}Nb_6O_{17}$ crystallites via a solvothermal method.

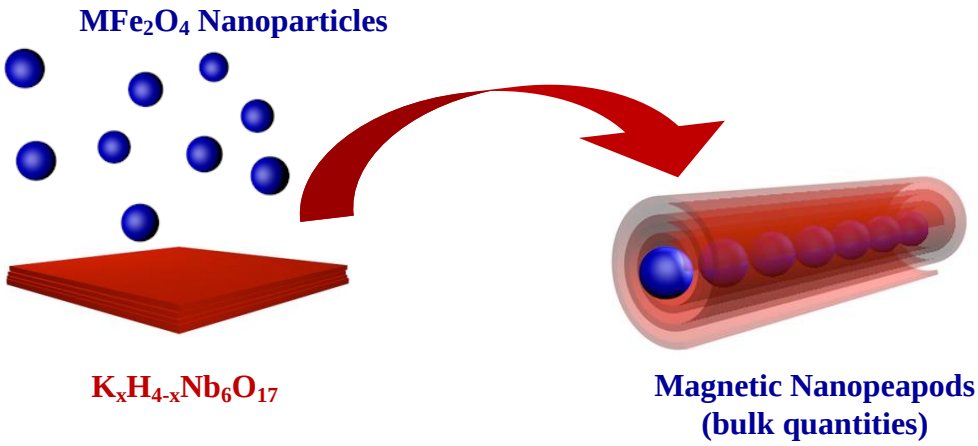

Figure 3.12. General scheme for the fabrication of MFe_2O_4@hexaniobate NPPs from MFe_2O_4 NPs and $H_xK_{4-x}Nb_6O_{17}$ crystallites via a solvothermal method. (Cartoons were drawn by Cinema 4D software)

Several factors are important to the success of this method. TBAOH clearly is needed to aid in the exfoliation of the nanosheets and the surfactant (OAm) is critical for functionalization of both the NPs and nanoscrolls. OAc also works well, indicating that there is some flexibility for variation of the surfactant head group. Shortening the length of the aliphatic chain does, however, have an adverse impact in that shorter chains result in only limited success in the fabrication of NPP structures (Figure 3.9). Temperature too, plays a key role where reactions at < 180 °C show only moderate levels of encapsulation; this is likely related to the formation of the nanoscrolls under solvothermal conditions where higher temperatures are needed to produce higher yields.[34]

Before discussing the NPPs in more detail, it is important to consider scroll formation. In our investigations on bulk hexaniobate nanoscroll synthesis.[34] it would appear that instead of the nanoscrolls arising from individual exfoliated nanosheets, they develop on the surface of larger crystallites and break off. Time dependent studies show evidence for partial formation of nanoscrolls on the surface of nanosheets (Figure 3.13) and typical hexaniobate crystallite sizes are as much as 50 μm on an edge, but resulting nanoscrolls are much smaller in length. These observations are consistent with a mechanism involving scrolling and detachment. The factors influencing the size of a nanoscroll likely consist of many interrelated components including structural defects on the nanosheets themselves, stresses created in the sheet during the scrolling/ detachment process, the scrolling rate, as well as the impact of temperature, pressure and solvation.

With respect to the topology of NPPs, variation is seen in the both length and inner and outer diameters. The NPPs lengths, typically ranging from 0.1 to 1 μm, are much smaller than the average hexaniobate crystallite. This behavior is consistent with the nanoscroll detachment

mechanism described above. The inner diameters of the NPPs with mid-sized NPs (≥ 9 nm) are dictated by the diameters of the NPs captured in the scroll. This is different than what is seen in the solvothermal synthesis of plain nanoscrolls, where the scroll inner diameters routinely vary between *ca.* 20 and 45 nm.[34] For the Fe_3O_4@hexaniobate NPPs containing 9 nm NPs (Figure 3.2c), the inner diameter averages about 13 nm; the greater diameter breadth is due to the presence of surfactant on the surfaces of NP and nanoscroll. For smaller NPs (e.g. 5 nm), the diameter of the scrolls are also about 12-13nm (Figure 3.5). This may indicate an intrinsic limit in curvature for the scroll such that the smallest accessible inner diameter is dictated by allowed limits in local Nb-O-Nb bond angles between adjacent NbO_6 octahedra. The outer diameter of the NPPs shows a larger range of variation; this is simply determined by the number of layers (turns) of the scroll, which on average is about 3 layers, but typically ranges from 2 to 6. In terms of interparticle distances, as shown in Figure 3.2 for example, one can see that the separation between individual NPs and between the NPs and the scroll wall (Figure 3.2c) is ca. 2 nm. These distances are similar to those seen in the self-assembly of free NPs (Figure 3.2a). The surface of the NPs and the surfaces of the nanosheets are both functionalized with OAm. The height of this ligand is about 2 nm,[35] indicating that in both the NPP and self-assembled structures, interdigitation is likely occurring due to favorable inter-chain interactions.[36]

This solvothermal approach is quite effective in the synthesis of NPPs and similar methods can be used in the formation of bulk nanoscrolls.[34] The question then arises as to the mechanism for NP encapsulation within the nanoscrolls. Clearly, it is not random capture; if this was occurring, the numbers of encased NPs would be much less, polydispersed NP samples would produce polydispersed NP-containing NPPs, and one might expect to see NPs not only in the core but also within the interlayer regions outside the core. The efficiency of entrapment

then indicates some degree of preorganization of the NPs on the surface of niobate crystallites prior to scrolling. In our previous *in situ* studies, those resulting in the low yield preparation of cobalt metal containing NPPs,[14] microscopic evidence showed preorganization of NPs parallel to the edges of various hexaniobate crystallites. This supported the idea that the NPs pre-organized before capture, possibly along a step edge on the niobate nanosheets. Interactions between NPs, due to favorable interactions of surface groups (e.g. OAm) and/or of magnetic dipoles, would support attraction between adjacent NPs to form chains. Then on scrolling, organized NPs could be captured. It is certainly also possible that the NPs aid in the scrolling step; the fact that the inner diameters of the NPPs match those of the functionalized NPs, as opposed to a range of sizes seen in pure nanoscroll fabrication,[34] lends some support to this idea. An alternative mechanism could be that as the nanoscroll starts to form, then NPs are attracted to the resulting cleft produced in the initial curvature. A third consideration would be the pre-formation of the nanoscrolls, followed by the insertion of NPs; experiments at room temperature and under solvothermal conditions, however, do not support this mechanism in that very few NPs were taken up by preformed nanoscrolls (Figure 3.10). In any case, modeling studies on the scrolling process and NP capture mechanisms may help to elucidate more energetically favorable assembly pathways.[37]

Interestingly, the NPs captured via this solvothermal method show an upper size limit of about 14 nm. In the *in situ* approach,[14] which involved the decomposition of cobalt carbonyl in high boiling point solvents at $\leq$ 150 °C under flowing nitrogen, larger NPs > 40 nm could be captured, though not in high yield. Also, typically the oxide shells of the NPPs were usually only one layer thick. This difference in behavior likely has something to do with the lower reaction temperatures and pressures used in the *in situ* method as well as nanosheet detachment and

preorganization steps occurring under these conditions. Under the more rigorous solvothermal conditions reported herein, the larger sized NPs may not readily preorganize on crystallite surfaces.

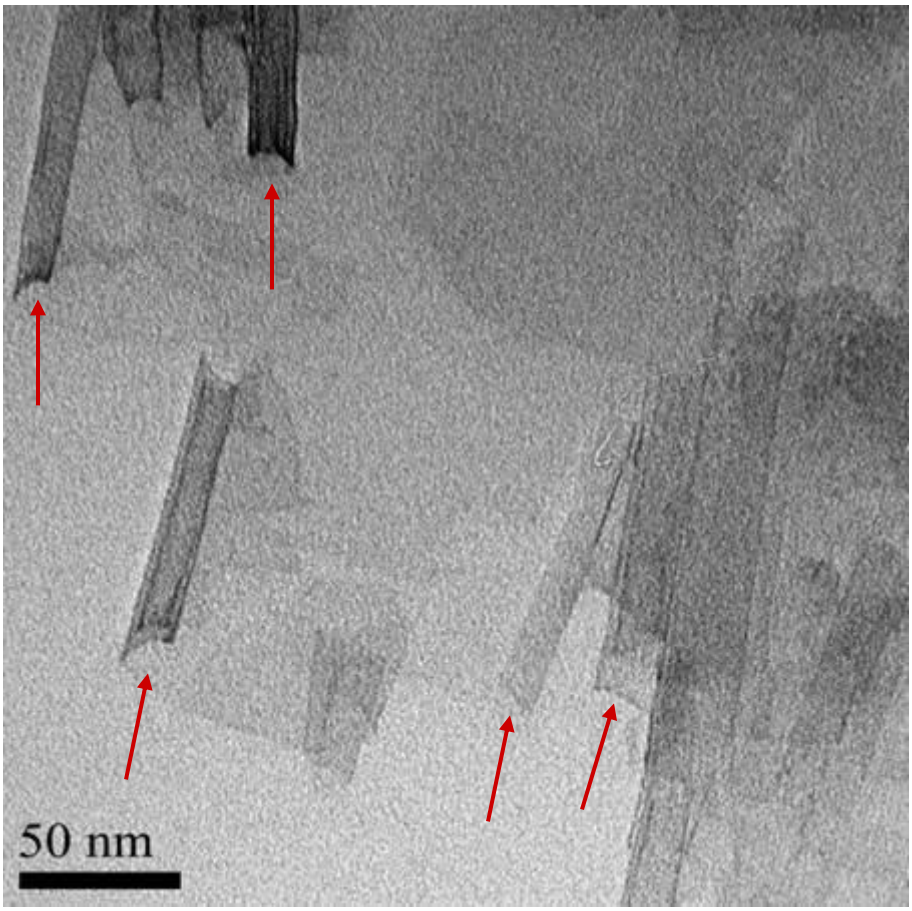

Figure 3.13. TEM images showing partially scrolled hexaniobate nanosheets after 3 h of solvothermal treatment at 220 °C. Arrows point to some of the emerging scrolls.

Another important result demonstrated by this method is the ability of the scrolling process to show selectivity for NPs of similar diameters. Both sets of monodispersed NPs (9 nm and 12 nm) and polydispersed samples were treated. Clear evidence is seen for size segregation, typically into different NPPs (Figure 3.6), but sometimes into different regions of the same NPP (Figures 3.6 and 3.8c). This process of size selectivity is again likely related to a preorganization step on the surface of the nanosheet. It is known that the energetics for the close-packed assembly of NPs are favored by NPs of similar sizes.[28f, 38] Clearly, this plays a role here possibly

in the preorganization along the cleft of a scrolling nanosheet. Building on this chemistry, one can envision the development of strategies for segregating and separating monodispersed NPs from polydispersed NP samples.

3.5 Conclusions

One of the especially significant aspects of NPPs is the possibility of encapsulating NPs in nanoscrolls to enhance or vary the properties of the NPs. In this study we organized magnetic NPs where the resulting chains showed a clear increase in coercivity. One can expect that other types of NPs or NP combinations (e.g. magnetic, electronic, optical, and/or catalytic) can be captured to create composites with enhanced or even new properties (metamaterials). Further, while this study focused on hexaniobate nanosheets, the development of similar chemistries exploiting other nanosheets including graphene,[15a, 39] transition metal dichalcogenides,[40] or vanadates[41] can be envisioned. One could then design and fabricate important combinations of nanomaterials for potential applications in areas such solar conversion, thermoelectrics, catalysis, and multiferroics.[42]

3.6 References

1. (a) Xia, D.; Xue, Q. Z.; Xie, J.; Chen, H. J.; Lv, C.; Besenbacher, F.; Dong, M. D., Fabrication of Carbon Nanoscrolls from Monolayer Graphene. *Small* **2010,** *6* (18), 2010-2019; (b) Maeda, K.; Eguchi, M.; Youngblood, W. J.; Mallouk, T. E., Niobium Oxide Nanoscrolls as Building Blocks for Dye-Sensitized Hydrogen Production from Water under Visible Light Irradiation. *Chemistry of Materials* **2008,** *20* (21), 6770-6778; (c) Kobayashi, Y.; Hata, H.; Salama, M.; Mallouk, T. E., Scrolled sheet precursor route to niobium and tantalum oxide nanotubes. *Nano Letters* **2007,** *7* (7), 2142-2145; (d) Rurali, R.; Coluci, V. R.; Galvao, D. S., Prediction of giant electroactuation for papyruslike carbon nanoscroll structures: First-principles calculations. *Physical Review B* **2006,** *74* (8); (e) Pan, H.; Feng, Y.; Lin, J., Ab initio study of electronic and optical properties of multiwall carbon nanotube structures made up of a single rolled-up graphite sheet. *Physical Review B* **2005,** *72* (8); (f) Grundmann, M., Nanoscroll formation from strained layer heterostructures. *Applied Physics Letters* **2003,** *83* (12), 2444-2446.
2. (a) Sidorov, A. N.; Slawinski, G. W.; Jayatissa, A. H.; Zamborini, F. P.; Sumanasekera, G. U., A surface-enhanced Raman spectroscopy study of thin graphene sheets functionalized with gold and silver nanostructures by seed-mediated growth. *Carbon* **2012,** *50* (2), 699-705;

(b) O'Dwyer, C.; Lavayen, V.; Tanner, D. A.; Newcomb, S. B.; Benavente, E.; Gonzalez, G.; Torres, C. M. S., Reduced Surfactant Uptake in Three Dimensional Assemblies of VOx Nanotubes Improves Reversible Li+ Intercalation and Charge Capacity. *Advanced Functional Materials* **2009,** *19* (11), 1736-1745; (c) Lee, J.; Cho, S.; Hwang, Y.; Cho, H. J.; Lee, C.; Choi, Y. M.; Ku, B. C.; Lee, H.; Lee, B.; Kim, D.; Kim, S. H., Application of fullerene-added nano-oil for lubrication enhancement in friction surfaces. *Tribology International* **2009,** *42* (3), 440-447; (d) O'Dwyer, C.; Lavayen, V.; Newcomb, S. B.; Benavente, E.; Santa Ana, M. A.; Gonzalez, G.; Torres, C. M. S., Atomic layer structure of vanadium oxide nanotubes grown on nanourchin structures. *Electrochemical and Solid State Letters* **2007,** *10* (4), A111-A114; (e) Chen, Q.; Peng, L. M., Structure and applications of titanate and related nanostructures. *International Journal of Nanotechnology* **2007,** *4* (1-2), 44-65; (f) Zhang, L.; Dong, L. X.; Bell, D. J.; Nelson, B. J.; Schoenenberger, C.; Gruetzmacher, D., Fabrication and characterization of freestanding Si/Cr micro- and nanospirals. *Microelectronic Engineering* **2006,** *83* (4-9), 1237-1240; (g) Schumacher, O.; Mendach, S.; Welsch, H.; Schramm, A.; Heyn, C.; Hansen, W., Lithographically defined metal-semiconductor-hybrid nanoscrolls. *Applied Physics Letters* **2005,** *86* (14); (h) Zhang, L.; Golod, S. V.; Deckardt, E.; Prinz, V.; Grutzmacher, D., Free-standing Si/SiGe micro- and nano-objects. *Physica E-Low-Dimensional Systems & Nanostructures* **2004,** *23* (3-4), 280-284; (i) Prinz, V. Y., Precise semiconductor nanotubes and nanoshells fabricated on (110) and (111) Si and GaAs. *Physica E-Low-Dimensional Systems & Nanostructures* **2004,** *23* (3-4), 260-268; (j) Prinz, V. Y.; Seleznev, V. A.; Gutakovsky, A. K.; Chehovskiy, A. V.; Preobrazhenskii, V. V.; Putyato, M. A.; Gavrilova, T. A., Free-standing and overgrown InGaAs/GaAs nanotubes, nanohelices and their arrays. *Physica E* **2000,** *6* (1-4), 828-831.

3. Hamilton, E. J. M.; Dolan, S. E.; Mann, C. M.; Colijn, H. O.; McDonald, C. A.; Shore, S. G., PREPARATION OF AMORPHOUS BORON-NITRIDE AND ITS CONVERSION TO A TURBOSTRATIC, TUBULAR FORM. *Science* **1993,** *260* (5108), 659-661.
4. Li, Y. D. D.; Li, X. L. L.; He, R. R. R.; Zhu, J.; Deng, Z. X. X., Artificial lamellar mesostructures to WS2 nanotubes. *Journal of the American Chemical Society* **2002,** *124* (7), 1411-1416.
5. Feldman, Y.; Wasserman, E.; Srolovitz, D. J.; Tenne, R., HIGH-RATE, GAS-PHASE GROWTH OF MOS2 NESTED INORGANIC FULLERENES AND NANOTUBES. *Science* **1995,** *267* (5195), 222-225.
6. Richter, C.; Schmuttenmaer, C. A., Exciton-like trap states limit electron mobility in TiO2 nanotubes. *Nature Nanotechnology* **2010,** *5* (11), 769-772.
7. Corr, S. A.; Grossman, M.; Furman, J. D.; Melot, B. C.; Cheetham, A. K.; Heier, K. R.; Seshadri, R., Controlled Reduction of Vanadium Oxide Nanoscrolls: Crystal Structure, Morphology, and Electrical Properties. *Chemistry of Materials* **2008,** *20* (20), 6396-6404.
8. Saupe, G. B.; Waraksa, C. C.; Kim, H. N.; Han, Y. J.; Kaschak, D. M.; Skinner, D. M.; Mallouk, T. E., Nanoscale tubules formed by exfoliation of potassium hexaniobate. *Chemistry of Materials* **2000,** *12* (6), 1556-1562.
9. (a) Golberg, D.; Bando, Y.; Tang, C. C.; Zhi, C. Y., Boron nitride nanotubes. *Advanced Materials* **2007,** *19* (18), 2413-2432; (b) Viculis, L. M.; Mack, J. J.; Kaner, R. B., A chemical route to carbon nanoscrolls. *Science* **2003,** *299* (5611), 1361-1361; (c) Shi, L.; Xu, Y. M.; Li, Q., Controlled growth of lead oxide nanosheets, scrolled nanotubes, and nanorods. *Crystal Growth & Design* **2008,** *8* (10), 3521-3525; (d) Lieber, C. M., One-dimensional nanostructures: Chemistry, physics & applications. *Solid State Communications* **1998,** *107*

(11), 607-616; (e) Feng, S. H.; Xu, R. R., New materials in hydrothermal synthesis. *Accounts of Chemical Research* **2001,** *34* (3), 239-247.
10. (a) Kudo, A.; Tanaka, A.; Domen, K.; Maruya, K.; Aika, K.; Onishi, T., PHOTOCATALYTIC DECOMPOSITION OF WATER OVER NIO-K4NB6O17 CATALYST. *Journal of Catalysis* **1988,** *111* (1), 67-76; (b) Zou, Z. G.; Ye, J. H.; Sayama, K.; Arakawa, H., Direct splitting of water under visible light irradiation with an oxide semiconductor photocatalyst. *Nature* **2001,** *414* (6864), 625-627; (c) Zeng, T. Q.; Chen, W. W.; Cirtiu, C. M.; Moores, A.; Song, G. H.; Li, C. J., Fe3O4 nanoparticles: a robust and magnetically recoverable catalyst for three-component coupling of aldehyde, alkyne and amine. *Green Chemistry* **2010,** *12* (4), 570-573.
11. Lal, S.; Link, S.; Halas, N. J., Nano-optics from sensing to waveguiding. *Nature Photonics* **2007,** *1* (11), 641-648.
12. (a) Steele, B. C. H.; Heinzel, A., Materials for fuel-cell technologies. *Nature* **2001,** *414* (6861), 345-352; (b) Xu, C. W.; Wang, H.; Shen, P. K.; Jiang, S. P., Highly ordered Pd nanowire arrays as effective electrocatalysts for ethanol oxidation in direct alcohol fuel cells. *Adv. Mater.* **2007,** *19* (23), 4256-+.
13. Kong, J.; Franklin, N. R.; Zhou, C. W.; Chapline, M. G.; Peng, S.; Cho, K. J.; Dai, H. J., Nanotube molecular wires as chemical sensors. *Science* **2000,** *287* (5453), 622-625.
14. Yao, Y.; Chaubey, G. S.; Wiley, J. B., Fabrication of Nanopeapods: Scrolling of Niobate Nanosheets for Magnetic Nanoparticle Chain Encapsulation. *J. Am. Chem. Soc.* **2012,** *134* (5), 2450-2452.
15. (a) Geim, A. K.; Novoselov, K. S., The rise of graphene. *Nature Materials* **2007,** *6* (3), 183-191; (b) Sgobba, V.; Guldi, D. M., Carbon nanotubes-electronic/electrochemical properties and application for nanoelectronics and photonics. *Chemical Society Reviews* **2009,** *38* (1), 165-184; (c) Wang, C. G.; Chen, J.; Talavage, T.; Irudayaraj, J., Gold Nanorod/Fe3O4 Nanoparticle "Nano-Pearl-Necklaces" for Simultaneous Targeting, Dual-Mode Imaging, and Photothermal Ablation of Cancer Cells. *Angewandte Chemie-International Edition* **2009,** *48* (15), 2759-2763.
16. (a) Wu, J. S.; Dhara, S.; Wu, C. T.; Chen, K. H.; Chen, Y. F.; Chen, L. C., Growth and optical properties of self-organized AU(2)Si nanospheres pea-podded in a silicon oxide nanowire. *Adv. Mater.* **2002,** *14* (24), 1847-1850; (b) Hu, M. S.; Chen, H. L.; Shen, C. H.; Hong, L. S.; Huang, B. R.; Chen, K. H.; Chen, L. C., Photosensitive gold-nanoparticle-embedded dielectric nanowires. *Nature Materials* **2006,** *5* (2), 102-106.
17. Sun, B. Y.; Sato, Y.; Suenaga, K.; Okazaki, T.; Kishi, N.; Sugai, T.; Bandow, S.; Iijima, S.; Shinohara, H., Entrapping of exohedral metallofullerenes in carbon nanotubes: (CsC60)(n)@SWNT nano-peapods. *J. Am. Chem. Soc.* **2005,** *127* (51), 17972-17973.
18. Liu, L. F.; Lee, W.; Scholz, R.; Pippel, E.; Gosele, U., Tailor-made inorganic nanopeapods: Structural design of linear noble metal nanoparticle chains. *Angewandte Chemie-International Edition* **2008,** *47* (37), 7004-7008.
19. Qin, Y.; Liu, L. F.; Yang, R. B.; Gosele, U.; Knez, M., General Assembly Method for Linear Metal Nanoparticle Chains Embedded in Nanotubes. *Nano Letters* **2008,** *8* (10), 3221-3225.
20. Hunyadi, S. E.; Murphy, C. J., Tunable one-dimensional silver-silica nanopeapod architectures. *J. Phys. Chem. B* **2006,** *110* (14), 7226-7231.
21. Wei, Q. H.; Su, K. H.; Durant, S.; Zhang, X., Plasmon resonance of finite one-dimensional Au nanoparticle chains. *Nano Letters* **2004,** *4* (6), 1067-1071.

22. (a) Tang, Z. Y.; Kotov, N. A.; Magonov, S.; Ozturk, B., Nanostructured artificial nacre. *Nature Materials* **2003,** *2* (6), 413-U8; (b) Ray, S. S.; Okamoto, M., Polymer/layered silicate nanocomposites: a review from preparation to processing. *Progress in Polymer Science* **2003,** *28* (11), 1539-1641; (c) Kickelbick, G., Concepts for the incorporation of inorganic building blocks into organic polymers on a nanoscale. *Progress in Polymer Science* **2003,** *28* (1), 83-114; (d) Manias, E.; Touny, A.; Wu, L.; Strawhecker, K.; Lu, B.; Chung, T. C., Polypropylene/Montmorillonite nanocomposites. Review of the synthetic routes and materials properties. *Chemistry of Materials* **2001,** *13* (10), 3516-3523; (e) Kruk, M.; Jaroniec, M., Gas adsorption characterization of ordered organic-inorganic nanocomposite materials. *Chemistry of Materials* **2001,** *13* (10), 3169-3183; (f) Wang, Z.; Pinnavaia, T. J., Hybrid organic-inorganic nanocomposites: Exfoliation of magadiite nanolayers in an elastomeric epoxy polymer. *Chemistry of Materials* **1998,** *10* (7), 1820-1826; (g) Giannelis, E. P., Polymer layered silicate nanocomposites. *Advanced Materials* **1996,** *8* (1), 29-&; (h) Aksay, I. A.; Trau, M.; Manne, S.; Honma, I.; Yao, N.; Zhou, L.; Fenter, P.; Eisenberger, P. M.; Gruner, S. M., Biomimetic pathways for assembling inorganic thin films. *Science* **1996,** *273* (5277), 892-898; (i) Vaia, R. A.; Vasudevan, S.; Krawiec, W.; Scanlon, L. G.; Giannelis, E. P., NEW POLYMER ELECTROLYTE NANOCOMPOSITES - MELT INTERCALATION OF POLY(ETHYLENE OXIDE) IN MICA-TYPE SILICATES. *Advanced Materials* **1995,** *7* (2), 154-156.
23. (a) Ramanathan, T.; Abdala, A. A.; Stankovich, S.; Dikin, D. A.; Herrera-Alonso, M.; Piner, R. D.; Adamson, D. H.; Schniepp, H. C.; Chen, X.; Ruoff, R. S.; Nguyen, S. T.; Aksay, I. A.; Prud'homme, R. K.; Brinson, L. C., Functionalized graphene sheets for polymer nanocomposites. *Nature Nanotechnology* **2008,** *3* (6), 327-331; (b) Balazs, A. C.; Emrick, T.; Russell, T. P., Nanoparticle polymer composites: Where two small worlds meet. *Science* **2006,** *314* (5802), 1107-1110; (c) Veprek, S., The search for novel, superhard materials. *Journal of Vacuum Science & Technology A* **1999,** *17* (5), 2401-2420; (d) Zhao, D.; Yang, P.; Melosh, N.; Feng, J.; Chmelka, B. F.; Stucky, G. D., Continuous mesoporous silica films with highly ordered large pore structures. *Advanced Materials* **1998,** *10* (16), 1380-+; (e) Suryanarayana, C., NANOCRYSTALLINE MATERIALS. *International Materials Reviews* **1995,** *40* (2), 41-64; (f) Lan, T.; Pinnavaia, T. J., CLAY-REINFORCED EPOXY NANOCOMPOSITES. *Chemistry of Materials* **1994,** *6* (12), 2216-2219; (g) Sanchez, C.; Julian, B.; Belleville, P.; Popall, M., Applications of hybrid organic-inorganic nanocomposites. *Journal of Materials Chemistry* **2005,** *15* (35-36), 3559-3592; (h) Sanchez, C.; Soler-Illia, G.; Ribot, F.; Lalot, T.; Mayer, C. R.; Cabuil, V., Designed hybrid organic-inorganic nanocomposites from functional nanobuilding blocks. *Chemistry of Materials* **2001,** *13* (10), 3061-3083; (i) Giannelis, E. P.; Krishnamoorti, R.; Manias, E., Polymer-silicate nanocomposites: Model systems for confined polymers and polymer brushes. *Polymers in Confined Environments* **1999,** *138*, 107-147; (j) Messersmith, P. B.; Giannelis, E. P., SYNTHESIS AND CHARACTERIZATION OF LAYERED SILICATE-EPOXY NANOCOMPOSITES. *Chemistry of Materials* **1994,** *6* (10), 1719-1725; (k) Huang, Z. M.; Zhang, Y. Z.; Kotaki, M.; Ramakrishna, S., A review on polymer nanofibers by electrospinning and their applications in nanocomposites. *Composites Science and Technology* **2003,** *63* (15), 2223-2253; (l) Alexandre, M.; Dubois, P., Polymer-layered silicate nanocomposites: preparation, properties and uses of a new class of materials. *Materials Science & Engineering R-Reports* **2000,** *28* (1-2), 1-63; (m) Wong, E. W.;

Sheehan, P. E.; Lieber, C. M., Nanobeam mechanics: Elasticity, strength, and toughness of nanorods and nanotubes. *Science* **1997,** *277* (5334), 1971-1975.
24. (a) Wang, Y.; Zhang, H. J.; Lu, L.; Stubbs, L. P.; Wong, C. C.; Lin, J. Y., Designed Functional Systems from Peapod-like Co@Carbon to Co3O4@Carbon Nanocomposites. *Acs Nano* **2010,** *4* (8), 4753-4761; (b) Okazaki, T.; Bandow, S.; Tamura, G.; Fujita, Y.; Iakoubovskii, K.; Kazaoui, S.; Minami, N.; Saito, T.; Suenaga, K.; Iijima, S., Photoluminescence quenching in peapod-derived double-walled carbon nanotubes. *Physical Review B* **2006,** *74* (15); (c) Chikkannanavar, S. B.; Luzzi, D. E.; Paulson, S.; Johnson, A. T., Synthesis of peapods using substrate-grown SWNTs and DWNTs: An enabling step toward peapod devices. *Nano Letters* **2005,** *5* (1), 151-155.
25. (a) Bandow, S.; Hiraoka, T.; Yumura, T.; Hirahara, K.; Shinohara, H.; Iijima, S., Raman scattering study on fullerene derived intermediates formed within single-wall carbon nanotube: from peapod to double-wall carbon nanotube. *Chemical Physics Letters* **2004,** *384* (4-6), 320-325; (b) Hornbaker, D. J.; Kahng, S. J.; Misra, S.; Smith, B. W.; Johnson, A. T.; Mele, E. J.; Luzzi, D. E.; Yazdani, A., Mapping the one-dimensional electronic states of nanotube peapod structures. *Science* **2002,** *295* (5556), 828-831; (c) Berber, S.; Kwon, Y. K.; Tomanek, D., Microscopic formation mechanism of nanotube peapods. *Physical Review Letters* **2002,** *88* (18).
26. (a) Hsieh, C. H.; Chou, L. J.; Lin, G. R.; Bando, Y.; Golberg, D., Nanophotonic Switch: Gold-in-Ga2O3 Peapod Nanowires. *Nano Letters* **2008,** *8* (10), 3081-3085; (b) White, D. W. R., PEAPOD regulates lamina size and curvature in Arabidopsis. *Proceedings of the National Academy of Sciences of the United States of America* **2006,** *103* (35), 13238-13243.
27. (a) Gazit, O.; Cohen, Y.; Tannenbaum, R., Periodic nanocomposites: A simple path for the preferential self-assembly of nanoparticles in block-copolymers. *Polymer* **2010,** *51* (10), 2185-2190; (b) Ng, C. H. B.; Yang, J. X.; Fan, W. Y., Synthesis and self-assembly of one-dimensional sub-10 nm Ag nanoparticles with cyclodextrin. *J. Phys. Chem. C* **2008,** *112* (11), 4141-4145; (c) Zhi, Z. L.; Murakami, Y.; Morita, Y.; Hasan, Q.; Tamiya, E., Multianalyte immunoassay with self-assembled addressable microparticle array on a chip. *Analytical Biochemistry* **2003,** *318* (2), 236-243.
28. (a) Li, M.; Johnson, S.; Guo, H. T.; Dujardin, E.; Mann, S., A Generalized Mechanism for Ligand-Induced Dipolar Assembly of Plasmonic Gold Nanoparticle Chain Networks. *Advanced Functional Materials* **2011,** *21* (5), 851-859; (b) Kuo, C. W.; Wang, C. R. C., Absorption Spectral Simulation of the End-to-End Linked Gold Nanorods Chain Structure. *Current Nanoscience* **2010,** *6* (6), 619-625; (c) Talapin, D. V.; Shevchenko, E. V.; Murray, C. B.; Titov, A. V.; Kral, P., Dipole-dipole interactions in nanoparticle superlattices. *Nano Letters* **2007,** *7* (5), 1213-1219; (d) Lalatonne, Y.; Richardi, J.; Pileni, M. P., Van der Waals versus dipolar forces controlling mesoscopic organizations of magnetic nanocrystals. *Nature Materials* **2004,** *3* (2), 121-125; (e) Atay, T.; Song, J. H.; Nurmikko, A. V., Strongly interacting plasmon nanoparticle pairs: From dipole-dipole interaction to conductively coupled regime. *Nano Letters* **2004,** *4* (9), 1627-1631; (f) Murray, C. B.; Kagan, C. R.; Bawendi, M. G., Synthesis and characterization of monodisperse nanocrystals and close-packed nanocrystal assemblies. *Annual Review of Materials Science* **2000,** *30*, 545-610.
29. (a) Jiang, J.; Chae, B.; Jeong, S. K.; Min, B. K.; Kim, S. H.; Piao, L.; Yoon, S., Assembling Ag nanoparticles into morphology controlled secondary structures on loosely packed self-assembled monolayers. *Journal of Colloid and Interface Science* **2013,** *394*, 639-642; (b) Bhattacharjee, R. R.; Mandal, T. K., Polymer-mediated chain-like self-assembly of

functionalized gold nanoparticles. *Journal of Colloid and Interface Science* **2007,** *307* (1), 288-295.

30. (a) Wang, H.; Chen, Q. W.; Sun, Y. B.; Wang, M. S.; Sun, L. X.; Yan, W. S., Synthesis of Necklace-like Magnetic Nanorings. *Langmuir* **2010,** *26* (8), 5957-5962; (b) Zhang, F.; Wang, C. C., Fabrication of one-dimensional iron oxide/silica nanostructures with high magnetic sensitivity by dipole-directed self-assembly. *J. Phys. Chem. C* **2008,** *112* (39), 15151-15156; (c) Seipenbusch, M.; Toneva, P.; Peukert, W.; Weber, A. P., Impact fragmentation of metal nanoparticle agglomerates. *Particle & Particle Systems Characterization* **2007,** *24* (3), 193-200; (d) Richardi, J.; Motte, L.; Pileni, M. P., Mesoscopic organizations of magnetic nanocrystal: the influence of short-range interactions. *Current Opinion in Colloid & Interface Science* **2004,** *9* (1-2), 185-191; (e) Deng, J. G.; He, C. L.; Long, X. P.; Peng, Y. X.; Li, P.; Chan, A. S. C., Preparation and characterization of magnetic Fe3O4- polypyrrole nanoparticles. *Acta Polymerica Sinica* **2003,** (3), 393-397.
31. Adireddy, S.; Yao, Y.; Vargas, J. M.; Spinu, L.; Wiley, J. B., New Nanocomposites - Controlled Capture of Nanoparticles in Scrolled Nanosheets. *Nanotechnology 2013: Advanced Materials, CNTs, Particles, Films and Composites* **2013,** *1*, 526.
32. (a) Xu, Z. C.; Shen, C. M.; Hou, Y. L.; Gao, H. J.; Sun, S. S., Oleylamine as Both Reducing Agent and Stabilizer in a Facile Synthesis of Magnetite Nanoparticles. *Chemistry of Materials* **2009,** *21* (9), 1778-1780; (b) Yu, W. W.; Falkner, J. C.; Yavuz, C. T.; Colvin, V. L., Synthesis of monodisperse iron oxide nanocrystals by thermal decomposition of iron carboxylate salts. *Chemical Communications* **2004,** (20), 2306-2307.
33. Sun, S. H.; Zeng, H.; Robinson, D. B.; Raoux, S.; Rice, P. M.; Wang, S. X.; Li, G. X., Monodisperse MFe2O4 (M = Fe, Co, Mn) nanoparticles. *J. Am. Chem. Soc.* **2004,** *126* (1), 273-279.
34. Adireddy, S.; Yao, Y.; He, J.; Wiley, J. B., Rapid solvothermal fabrication of hexaniobate nanoscrolls. *Materials Research Bulletin* (0).
35. Chen, M.; Feng, Y. G.; Wang, X.; Li, T. C.; Zhang, J. Y.; Qian, D. J., Silver nanoparticles capped by oleylamine: Formation, growth, and self-organization. *Langmuir* **2007,** *23* (10), 5296-5304.
36. (a) He, J. B.; Kanjanaboos, P.; Frazer, N. L.; Weis, A.; Lin, X. M.; Jaeger, H. M., Fabrication and Mechanical Properties of Large-Scale Freestanding Nanoparticle Membranes. *Small* **2010,** *6* (13), 1449-1456; (b) Pocovi-Martinez, S.; Frances-Soriano, L.; Zaballos-Garcia, E.; Scaiano, J. C.; Gonzalez-Bejar, M.; Perez-Prieto, J., CO2 switchable nanoparticles: reversible water/organic-phase exchange of gold nanoparticles by gas bubbling. *Rsc Advances* **2013,** *3* (15), 4867-4871.
37. (a) Perim, E.; Galvao, D. S., The structure and dynamics of boron nitride nanoscrolls. *Nanotechnology* **2009,** *20* (33); (b) Braga, S. F.; Coluci, V. R.; Legoas, S. B.; Giro, R.; Galvao, D. S.; Baughman, R. H., Structure and dynamics of carbon nanoscrolls. *Nano Letters* **2004,** *4* (5), 881-884.
38. (a) Shevchenko, E. V.; Talapin, D. V.; Kotov, N. A.; O'Brien, S.; Murray, C. B., Structural diversity in binary nanoparticle superlattices. *Nature* **2006,** *439* (7072), 55-59; (b) Wang, Z. L., Transmission electron microscopy of shape-controlled nanocrystals and their assemblies. *Journal of Physical Chemistry B* **2000,** *104* (6), 1153-1175; (c) Sun, S. H.; Murray, C. B.; Weller, D.; Folks, L.; Moser, A., Monodisperse FePt nanoparticles and ferromagnetic FePt nanocrystal superlattices. *Science* **2000,** *287* (5460), 1989-1992; (d) Storhoff, J. J.; Lazarides, A. A.; Mucic, R. C.; Mirkin, C. A.; Letsinger, R. L.; Schatz, G. C., What controls the optical

properties of DNA-linked gold nanoparticle assemblies? *J. Am. Chem. Soc.* **2000,** *122* (19), 4640-4650; (e) Li, M.; Schnablegger, H.; Mann, S., Coupled synthesis and self-assembly of nanoparticles to give structures with controlled organization. *Nature* **1999,** *402* (6760), 393-395.

39. (a) Novoselov, K. S.; Geim, A. K.; Morozov, S. V.; Jiang, D.; Katsnelson, M. I.; Grigorieva, I. V.; Dubonos, S. V.; Firsov, A. A., Two-dimensional gas of massless Dirac fermions in graphene. *Nature* **2005,** *438* (7065), 197-200; (b) Novoselov, K. S.; Geim, A. K.; Morozov, S. V.; Jiang, D.; Zhang, Y.; Dubonos, S. V.; Grigorieva, I. V.; Firsov, A. A., Electric field effect in atomically thin carbon films. *Science* **2004,** *306* (5696), 666-669; (c) Thess, A.; Lee, R.; Nikolaev, P.; Dai, H. J.; Petit, P.; Robert, J.; Xu, C. H.; Lee, Y. H.; Kim, S. G.; Rinzler, A. G.; Colbert, D. T.; Scuseria, G. E.; Tomanek, D.; Fischer, J. E.; Smalley, R. E., Crystalline ropes of metallic carbon nanotubes. *Science* **1996,** *273* (5274), 483-487.
40. (a) Whittingham, M. S., Lithium batteries and cathode materials. *Chemical Reviews* **2004,** *104* (10), 4271-4301; (b) Winter, M.; Besenhard, J. O.; Spahr, M. E.; Novak, P., Insertion electrode materials for rechargeable lithium batteries. *Advanced Materials* **1998,** *10* (10), 725-763; (c) Rapoport, L.; Bilik, Y.; Feldman, Y.; Homyonfer, M.; Cohen, S. R.; Tenne, R., Hollow nanoparticles of WS2 as potential solid-state lubricants. *Nature* **1997,** *387* (6635), 791-793; (d) Friend, R. H.; Yoffe, A. D., ELECTRONIC-PROPERTIES OF INTERCALATION COMPLEXES OF THE TRANSITION-METAL DICHALCOGENIDES. *Advances in Physics* **1987,** *36* (1), 1-94; (e) Wilson, J. A.; Disalvo, F. J.; Mahajan, S., CHARGE-DENSITY WAVES AND SUPERLATTICES IN METALLIC LAYERED TRANSITION-METAL DICHALCOGENIDES. *Advances in Physics* **1975,** *24* (2), 117-201.
41. (a) Elchebly, M.; Payette, P.; Michaliszyn, E.; Cromlish, W.; Collins, S.; Loy, A. L.; Normandin, D.; Cheng, A.; Himms-Hagen, J.; Chan, C. C.; Ramachandran, C.; Gresser, M. J.; Tremblay, M. L.; Kennedy, B. P., Increased insulin sensitivity and obesity resistance in mice lacking the protein tyrosine phosphatase-1B gene. *Science* **1999,** *283* (5407), 1544-1548; (b) Pope, M. T.; Muller, A., POLYOXOMETALATE CHEMISTRY - AN OLD FIELD WITH NEW DIMENSIONS IN SEVERAL DISCIPLINES. *Angewandte Chemie-International Edition in English* **1991,** *30* (1), 34-48; (c) Swarup, G.; Cohen, S.; Garbers, D. L., INHIBITION OF MEMBRANE PHOSPHOTYROSYL-PROTEIN PHOSPHATASE-ACTIVITY BY VANADATE. *Biochemical and Biophysical Research Communications* **1982,** *107* (3), 1104-1109; (d) Cantley, L. C.; Josephson, L.; Warner, R.; Yanagisawa, M.; Lechene, C.; Guidotti, G., VANADATE IS A POTENT (NA,K)-ATPASE INHIBITOR FOUND IN ATP DERIVED FROM MUSCLE. *Journal of Biological Chemistry* **1977,** *252* (21), 7421-7423.
42. (a) Li, X. Q.; Zhang, T. Y.; Gu, S. W.; Kang, S. Z.; Li, G. D.; Mu, J., Reduced graphene oxide/potassium niobate composite nanoscrolls with enhanced photocatalytic activity for dye degradation. *Separation and Purification Technology* **2013,** *108*, 139-142; (b) Feng, K.; Tang, B. B.; Wu, P. Y., "Evaporating" Graphene Oxide Sheets (GOSs) for Rolled up GOSs and Its Applications in Proton Exchange Membrane Fuel Cell. *Acs Applied Materials & Interfaces* **2013,** *5* (4), 1481-1488; (c) Zhang, Y.; Evans, J. R. G., Morphologies developed by the drying of droplets containing dispersed and aggregated layered double hydroxide platelets. *Journal of Colloid and Interface Science* **2013,** *395*, 11-17; (d) Semenenko, D. A.; Itkis, D. M.; Kulova, T. L.; Yashuk, T. S.; Skundin, A. M.; Goodilin, E. A.; Tretyakov, Y. D., Fabrication of microporous cathode materials containing polyaniline-vanadia self-

scrolled nanoribbons. *Electrochimica Acta* **2012,** *63*, 329-334; (e) Tzanakis, I.; Hadfield, M.; Henshaw, I.; Garland, N.; Khan, Z., Experimental Sliding Performance of Composite Tip Seal with High-Carbon Steel Plate under Lubricated Conditions Applied to Scroll Expander Systems. *Tribology Transactions* **2011,** *54* (4), 505-513; (f) Yella, A.; Mugnaioli, E.; Therese, H. A.; Panthofer, M.; Kolb, U.; Tremel, W., Synthesis of Fullerene- and Nanotube-Like SnS2 Nanoparticles and Sn/S/Carbon Nanocomposites. *Chemistry of Materials* **2009,** *21* (12), 2474-2481; (g) Benchabane, S.; Khelif, A.; Rauch, J. Y.; Robert, L.; Laude, V., Evidence for complete surface wave band gap in a piezoelectric phononic crystal. *Physical Review E* **2006,** *73* (6); (h) Laude, V.; Wilm, M.; Benchabane, S.; Khelif, A., Full band gap for surface acoustic waves in a piezoelectric phononic crystal. *Physical Review E* **2005,** *71* (3); (i) Carpi, F.; De Rossi, D., Improvement of electromechanical actuating performances of a silicone dielectric elastomer by dispersion of titanium dioxide powder. *Ieee Transactions on Dielectrics and Electrical Insulation* **2005,** *12* (4), 835-843; (j) Shastry, S.; Srinivasan, G.; Bichurin, M. I.; Petrov, V. M.; Tatarenko, A. S., Microwave magnetoelectric effects in single crystal bilayers of yttrium iron garnet and lead magnesium niobate-lead titanate. *Physical Review B* **2004,** *70* (6); (k) Zilker, S. J., Materials design and physics of organic photorefractive systems. *Chemphyschem* **2000,** *1* (2), 72-87; (l) Rao, Y.; Qu, J. M.; Marinis, T.; Wong, C. P., A precise numerical prediction of effective dielectric constant for polymer-ceramic composite based on effective-medium theory. *Ieee Transactions on Components and Packaging Technologies* **2000,** *23* (4), 680-683; (m) Haertling, G. H., Ferroelectric ceramics: History and technology. *Journal of the American Ceramic Society* **1999,** *82* (4), 797-818; (n) Sugawara, Y.; Onitsuka, K.; Yoshikawa, S.; Xu, Q. C.; Newnham, R. E.; Uchino, K., METAL CERAMIC COMPOSITE ACTUATORS. *Journal of the American Ceramic Society* **1992,** *75* (4), 996-998.

Chapter 4

A general method for the fabrication of hexaniobate-based nanocomposites

4.1 Introduction

Solvothermal-exfoliation of layered inorganic materials has become an effective and promising method to achieve a wide range of novel functional nanopeapod-type (NPP) composites.[1] Recently, NPPs that combine various components, in one hybrid entity have emerged as an interesting class of multifunctional materials.[2] The geometry-dependent physical properties of NPPs make them highly attractive platforms for the various applications.[2i]

Clever combinations of different functional nanomaterials can enable the development of multifunctional nanocomposites for various applications. For example, noble metal NPs show localized surface plasmon resonance (LSPR) and they have been used for both cancer diagnosis and therapies.[3] Their nanoarchitectures can function as contrast agents, carriers for drug delivery, and transducers for the photothermal destruction of tumor cells.[4] Magnetic NPs also have been varied applications such as recycling of expensive catalysts, pharmaceutics, magnetic resonance imaging, drug delivery, ferrofluids, data storage and magnetics.[5]

Additionally, quantum dot (QD) nanostructures have been intensively studied and used as imaging tools with exceptional optical properties including strong photoluminescence, robust photostability, broad spectral absorption, and tunable emission spectra.[6] QDs have also been used as a light harvesting semiconductor NPs and investigated as sensitizers for wide band-gap semiconductors.[7] Because of all these applications, the development of a general strategy to

fabricate novel nanocomposites by combining various semiconducting, metallic or magnetic NPs has been one of great interest.[5f, 8]

Many researchers have worked to fabricate hybrid materials from the exfoliated hexaniobate ($H_xK_{4-x}Nb_6O_{17}$) nanosheets for the purpose of harvesting sunlight in the visible region for energy production.[9] Various methods have been used for the fabrication of hexaniobate based nanocomposites.[9d, 10] For example, TiO_2/Bi-doped hexaniobate composites have been synthesized via solid-state reaction and a subsequent exfoliation-restacking route.[11] Such nanocomposites showed good photocatalytic activity in the degradation of methylene blue under visible light irradiation. Sarac et al. decorated the surface of hexaniobate nanoscrolls with CdTe QD and investigated their photoelectrochemical properties.[12] These results show that the QD-hexaniobate nanocomposite can work as an efficient visible light harvester for solar applications and authors suggest potential applications in water splitting.[12] While exhibiting interesting properties, the composites display limited morphological uniformity and the methods used in their fabrication are not appropriate to a wide variety of materials combinations or large-scale production for industrial applications.

Hexaniobate, $K_4Nb_6O_{17}$ has the unique ability to exfoliate and structurally transform into an energetically favorable nanoscroll geometry to relieve built-in strain.[9a] Due to this scrolling behavior, NPs can be readily captured (Chapter 3), which may be advantageous in catalysis, magnetic devices,[13] fuel cells,[14] sensors,[15] templates for nanoparticle (NP) assembly,[10d] and photonics.[16]

The combination of hexaniobate, metals (oxides) NPs, and QDs are interesting for the construction of multifunctional NPPs. It has been recently shown that by using different amounts of surfactants, the nanoscroll architecture can be manipulated (Chapter 2).[17] Unique interactions

between the NP cores and hexaniobate shells over nanometer length scale may enhance various properties. However, there are very few reports focusing on the structurally uniform NPP structures.

Novel synthetic approaches have been developed through which a series of important geometrical parameters can be tailored in a controllable manner so as to combine nanosheets with metal (oxide) NPs, and quantum dots in various dimensions. NPPs or NP decorated nanosheets can be fabricated by mixing the pre-made NPs with the layered inorganic crystallites and heat treating the reaction mixture in the presence of exfoliating agents and surfactants via a non-aqueous solvothermal method. A modified synthetic approach to fabricate bi-functional (Au-Fe_3O_4-hexaniobate) NPP structures is also demonstrated. These hexaniobate-based nanocomposites exhibit excellent synthetic flexibility as well as, size, and shape selectivity. Furthermore, the highly interdisciplinary combination of materials incorporated into the NPPs make them especially promising for applications in solar conversion.

4.2 Experimental

Materials. Benzyl ether (99%), 1,2-hexadecanediol, hexane (anhydrous, 95%), iron(III) acetylacetonate (97%), benzyl alcohol (99%), 1-octadecene (90%), octyl ether (99%), oleic acid (99.8%, OAc), oleylamine (>70%, OAm), phenyl ether (99%), tetrabutylammonium hydroxide 30-hydrate (TBAOH) (97%), titanium (IV) isopropoxide (97%) and toluene (99.8%, anhydrous) were purchased from Sigma-Aldrich. K_2CO_3 (99%) and Nb_2O_5 (99%) were acquired from Alfa Aesar. Pure grade ethanol (Pharmco-Aaper, 200 Proof, absolute) was used in all preparations.

4.2.1 Niobate Nanosheets

Synthesis of $K_4Nb_6O_{17}$ crystallites.

$K_4Nb_6O_{17}$ was synthesized by the solid-state reaction of K_2CO_3 and Nb_2O_5 (in the molar ratio of 1.0:1.4) in air at 900 °C for 1h before continuing to heat at 1050 ^oC for another 24 h.[9a] A slight excess of K_2CO_3 was used to compensate for the loss of volatile potassium oxide species. The product was washed 2 times with *ca.* 200 mL milli-Q water and 50 mL acetone and dried overnight at 80 °C.

Synthesis of $H_xK_{4-x}Nb_6O_{17}$.

Experimental conditions were used similar to Saupe et al.[10] The proton-exchange form of hexaniobate, $H_xK_{4-x}Nb_6O_{17}$ was obtained by treating 0.15 g of $K_4Nb_6O_{17}$ powder with 15 mL of a 3 M HCl solution at 50 °C for 4 days. As-synthesized product was thoroughly washed 2 times with ca. 200 mL of milli-Q water and 50 mL acetone and dried overnight at 80 °C. $TBA_xH_{4-x}Nb_6O_{17}$ nanoscrolls were prepared by stirring the 0.1 g of $H_xK_{4-x}Nb_6O_{17}$ powder in 20 mL of aqueous TBAOH solution (15 mM, pH = 11) at 45 °C for 10 days.

Solvothermal preparation of intercalated multi-walled nanoscrolls (INS).

The reaction solution was prepared by mixing $H_xK_{4-x}Nb_6O_{17}$ (0.10 g), 0.15 g (0.19 mmol) TBAOH and 5 mL OAm (~15 mmol) in 8 mL of toluene. (Reactions can readily be scaled up to 0.50 g.) This mixture was magnetically stirred for 1 hour and transferred into a Teflon-lined stainless steel autoclave (Parr, model 4749, 1800 psig, 23 mL). The autoclave was maintained at 220 °C for 6 h and then cooled down to room temperature. The resulting white precipitate was washed with 50 mL ethanol and centrifuged for 5 min to remove excess intercalating agents.

4.2.2 Nanoparticles

Synthesis of TiO_2 NPs.

Quasi monodispersed TiO_2 NPs were synthesized using methods similar to Wu et al.[18] A reaction solution was prepared by mixing and titanium isopropoxide (0.5 mL), OAm (2 mL), OAc (2 mL) in 10 mL of benzyl alcohol. This mixture was magnetically stirred for 10 min and transferred into a Teflon-lined stainless steel autoclave (Parr, model 4749, 1800 psig, 23 mL). The autoclave was maintained at 180 °C for 24 h and then cooled down to room temperature. The resulting pale yellow, milky suspensions were precipitated by absolute ethanol and separated via centrifugation. The products were purified by three successive cycles of dispersion in toluene, precipitation with ethanol, and centrifugation (3000 rpm, 10 min). The TiO_2 NPs (yield ~ 80 mg) were dispersed in toluene.

Synthesis of Quantum dots.

Semiconducting metal sulfide QDs such as CdS and ZnS were synthesized according to a modified procedure from Hyeon et al.[19] CdSe NPs were prepared by a protocol similar to that reported by Li et al.[20]

Synthesis of cadmium sulfide NPs. Monodispersed CdS NPs were synthesized in a three-neck flask equipped with thermocouple, heating mantle and magnetic stirrer. The mixture of $CdCl_2$ (0.5 mmol) and OAm (5 mL) was heated at 90 °C to generate Cd-OAm complexes. Sulfur (3 mmol) was dissolved in 2.5 mL of OAm and injected into Cd-OAm solution at room temperature. This mixture was further heated to 140 °C and held at this temperature for 20 h before cooling to room temperature. CdS NPs nanocrystals were separated by adding excess ethanol followed by centrifugation. Collected CdS NPs (yield ~ 25 mg) were dispersed in toluene.

Synthesis of Zinc sulfide NPs. Reaction mixture was prepared by mixing $ZnCl_2$ (1 mmol), OAm (5 mL), and trioctylphosphine oxide (1.15 g) in 100 mL flask and magnetically stirred under N_2 flow. Zinc-OAm solution was prepared by heating the reaction mixture at 170 °C for 1h. Sulfur (3 mmol) was dissolved in 1.25 mL of OAm and injected into Zn-OAm solution at room temperature. This mixture was further heated to 320 °C at the rate of 10 °C/min and held at this temperature for 1 h before cooling to room temperature. ZnS NPs nanocrystals were separated by adding excess ethanol followed by centrifugation. Collected ZnS NPs (yield ~ 25 mg) were dispersed in toluene.

Synthesis of Cadmium Selenide NPs. A Se stock solution was prepared by heating the mixture of Se powder (0.0784 g) and octadecene (15 mL) at 280 °C for half an hour. A transparent Cd-precursor solution was prepared by heating $Cd(Ac)_2 \cdot 2H_2O$ (0.266 g) to 5 mL of OAc at 120 °C for 1h. Cadmium solution was swiftly added to the Se stock solution and reaction temperature was quickly raised to 260 °C and held at this temperature for 40 min before cooling down to room temperature. CdSe NPs were separated by adding excess ethanol followed by centrifugation. Collected CdSe NPs (yield ~ 40 mg) were dispersed in toluene.

Synthesis of silver NPs.

Ag NPs were synthesized according to a modified procedure from Sun et al.[21] NPs were synthesized in a three-neck flask equipped with thermocouple, heating mantle, and magnetic stirrer. $AgNO_3$ (1 mmol) and 10 mL of OAm were mixed and magnetically stirred under N_2 flow. The mixture was dehydrated by heating it to 110 °C for 30 min and further heated to 180 °C at the rate of 10 °C/min, and held at this temperature for 30 min before cooling down to room temperature. The blue-brown Ag NPs were separated by adding excess ethanol followed by centrifugation. Collected Ag NPs (yield ~ 25 mg) were dispersed in toluene.

Synthesis of gold NPs.

Au NPs were prepared by a protocol similar to that reported by Saruyama et al.[22] NPs were synthesized in a round bottom flask equipped with thermocouple, heating mantle and magnetic stirrer. $HAuCl_4.4H_2O$ (0.05 mmol, 20.5 mg), hexane (3 mL), OAc (0.5 mmol, 160 µL) and OAm (0.5 mmol, 165 µL) were magnetically stirred. The solution was heated to 50 °C, and held at this temperature for 1 day before cooling to room temperature. The pink Au NPs (yield ~ 5 mg) were purified with an excess of ethanol.

4.2.3 Synthesis of Nanopeapods with Various Metal Oxide and Metal Chalcogenide NPs

Synthesis of NPs@hexaniobate NPPs.

A 20 mg sample of NPs (TiO_2, CdS, CdSe, ZnS and Ag) dispersed in toluene (8 mL) toluene was added to the mixture of 5 mL (15 mmol) OAm, $H_xK_{4-x}Nb_6O_{17}$ (100 mg), and 0.15 g (0.19 mmol) TBAOH. The above prepared reaction solution was magnetically stirred for 2 h and transferred to a 23 mL Teflon-lined stainless steel autoclave (Parr, model 4749, 1800 psig). The sealed autoclave was heated to 220 °C for 6 h and then cooled to room temperature. The resulting precipitate was washed with a mixture of 15 mL toluene and 30 mL ethanol before being isolated via centrifugation. The product was then redispersed in 35 mL toluene and further centrifugation (3000 rpm, 3 min) was applied to remove any residual free NPs.

4.2.4 Modification of Nanosheets and Nanoscrolls

Silver decorated hexaniobate nanosheets and nanoscrolls.

A 20 mg sample of 10 nm Ag NPs dispersed in 8 mL toluene was added to the mixture of 0.1 g $H_xK_{4-x}Nb_6O_{17}$, 5 mL (15 mmol) OAm, and 0.15 g (0.19 mmol) TBAOH. The reaction solution was magnetically stirred for 2 h and transferred to a 23 mL Teflon-lined stainless steel

autoclave (Parr, model 4749, 1800 psig). The sealed autoclave was heated to 150 °C for various reaction times and then cooled to room temperature. When the reaction was conducted for 6 h, Ag decorated nanosheets were fabricated. Increasing the reaction time to 16 h led to the fabrication of Ag decorated nanoscrolls. In both cases, the resulting precipitate was washed with a mixture of 15 mL toluene and 30 mL ethanol before being isolated via centrifugation. The product was then redispersed in 35 mL toluene and further centrifugation (3000 rpm, 3 min) was applied to remove any residual free NPs.

Synthesis of Au@hexaniobate NPPs from preformed hexaniobate nanoscrolls.

Au@hexaniobate NPPs were synthesized in a two-step method. First, intercalated multi-walled hexaniobate nanoscrolls (INS) were fabricated according to the protocol similar to Adireddy et al. (Chapter 2).[17] In a typical experiment, the reaction solution was prepared by mixing $H_xK_{4-x}Nb_6O_{17}$ (0.1g), 0.15 g (0.19 mmol) TBAOH and 5 mL OAm (~15 mmol) in 8 mL of toluene. This mixture was magnetically stirred for 1 h and transferred into a Teflon-lined stainless steel autoclave (Parr, model 4749, 1800 psig, 23 mL). The autoclave was maintained at 220 °C for 6 h and then cooled down to room temperature. The resulting white precipitate (INS) was washed with 50 mL ethanol and centrifuged for 5 min to remove excess intercalating agents, and then dried under 60 °C.

Au@ hexaniobate NPPs can be synthesized by combining INS (20 mg), $HAuCl_4.\ 4H_2O$ (20.5 mg, 0.05 mmol), hexane (3 mL), OAc (160 µL, 0.5 mmol), and OAm (165 µL, 0.5 mmol) and magnetically stirred. The solution was heated to 50 °C, and held at this temperature for 1 day before cooling to room temperature. The pale pink Au@hexaniobate NPPs were purified with an excess of ethanol.

4.2.5 Gold Insertion into Preformed Nanopeapod Structures

Synthesis of Au-Fe_3O_4@hexaniobate NPPs from preformed Fe_3O_4@hexaniobate NPPs.

Au-Fe_3O_4@hexaniobate NPPs were synthesized in a two-step method. First, partially filled Fe_3O_4@hexaniobate NPPs were fabricated. In a method similar to that described in Chapter 3, a 10 mg sample of magnetic NPs dispersed in 8 mL toluene was added to the mixture of 100 mg $H_xK_{4-x}Nb_6O_{17}$, 5 mL (15 mmol) OAm, and 0.15 g (0.19 mmol) TBAOH. The reaction solution was magnetically stirred for 2 h and transferred to a 23 mL Teflon-lined stainless steel autoclave (Parr, model 4749, 1800 psig). The sealed autoclave was heated to 220 °C for 6 h and then cooled to room temperature. The resulting brown precipitate (partially filled Fe_3O_4@hexaniobate NPPs) was washed with a mixture of 15 mL toluene and 30 mL ethanol before being isolated via centrifugation. The product was then redispersed in 35 mL toluene and further centrifugation (3000 rpm, 3 min) was applied to remove any residual free magnetic NPs.

Partially filled Fe_3O_4@hexaniobate NPPs (20 mg), $HAuCl_4$ $4H_2O$ (20.5 mg, 0.05 mmol), hexane (3 mL), OAc (160 µL, 0.5 mmol) and OAm (165 µL, 0.5 mmol) were mixed and magnetically stirred. The solution was heated to 50 °C, and held at this temperature for 1 day before cooling to room temperature. The pale pink Au-Fe_3O_4@hexaniobate NPPs were purified with an excess of ethanol.

4.2.6 Characterization

The morphologies of the products were characterized with a TEM JEOL 2010 operated at an accelerating voltage of 200 kV with a Gatan slow scan CCD camera. The unit is equipped with EDAX genesis energy dispersive spectroscopy (EDS) system. For transmission electron microscopy (TEM) measurements, toluene dispersed samples were drop cast onto a 200 mesh carbon-coated copper grid and heated in a drying oven at 60 °C overnight. High-angle annular

dark-field scanning TEM (HAADF-STEM) and EDS mapping measurements were carried out using FEI TECNAI G2 F30 FEG TEM (300 kV). X-ray powder diffraction data were collected on a Philips X-Pert PW 3020 MPD equipped with a curved graphite monochromator, at an accelerating voltage and current of 40 kV and 40 mA, respectively. Absorption spectra were recorded (in the reflectance mode) by using a Cary 500 UV-Vis spectrophotometer.

4.3 Results

A series of NPs (TiO_2, CdS, CdSe, ZnS, Ag, Au, and Fe_3O_4,) were prepared separately, mixed with hexaniobate nanosheets, and treated solvothermally in toluene above 150 °C to make novel nanocomposites. Various different types of hexaniobate based nanocomposites were fabricated in the presence of organic media. This approach readily produces NPP structures in high yields. Unreacted nanosheets or nanoscrolls and free NPs can be removed with a simple centrifugation step. To confirm the formation of nanocomposites with desired composition, EDS analysis was performed during TEM measurements.

4.3.1 Nanopeapods

TiO_2@hexaniobate NPPs.

NPPS were synthesized by the encapsulation of TiO_2 NPs. Elongated titania NPs were obtained by the method of Wu et al..[18] Figure 4.1a presents a TEM image of the TiO_2 NPs. The crystalline phase of the as-synthesized NPs was identified by XRD characterization. Figure 4.1b shows the XRD pattern of the TiO_2 NPs, in which all diffraction peaks match well with the crystal structure of the anatase TiO_2 NPs [JCPDS No. 01-0562].[23]

Reactions with TiO_2 NPs and hexaniobate nanosheets resulted in high-quality NPPs. Figure 4.1c and 4.1d present representative TEM images of TiO_2@hexaniobate NPPs.

Experiments were performed to determine the optimal NP shapes and sizes that can be captured within the hexaniobate nanosheets. Particle morphology affected the efficiency of encapsulation. TiO_2 rod-like NPs with the dimensions of *ca.* 6.5 nm diameter and 12 nm lengths were predominately captured. TEM images (Figures 4.1c and 4.1d) illustrate almost no encapsulation for the NPs with other dimensions. The different sized TiO_2 NPs serve to highlight shape selectivity in these systems.

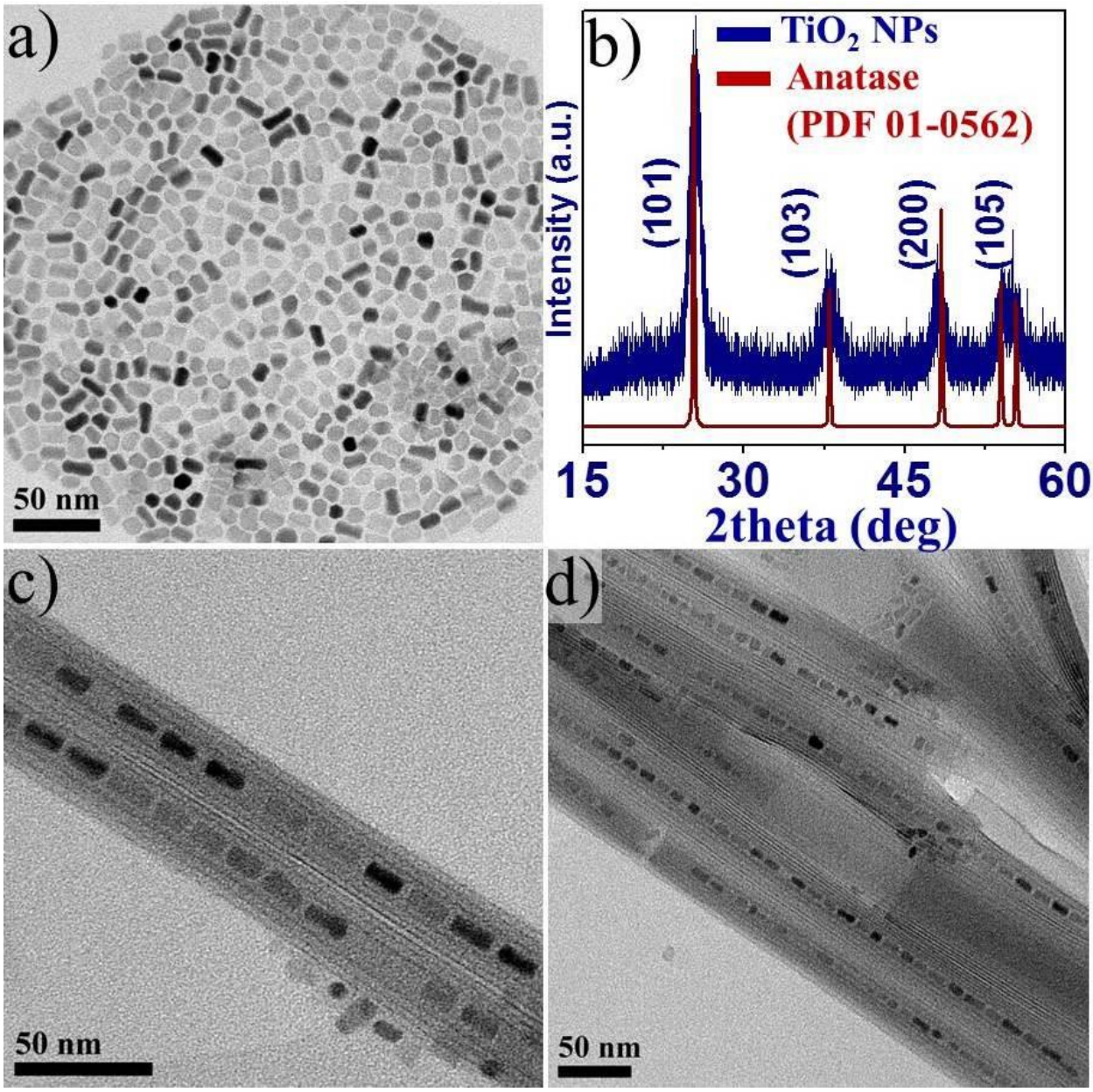

Figure 4.1. TEM image of (a) TiO_2 NPs, (b) XRD pattern of TiO_2 NPs, and (c,d) TEM images of TiO_2@hexaniobate NPPs.

QDs@hexaniobate NPPs.

NPP structures were readily obtained with CdS, ZnS, and CdSe QDs. The organic-capped QDs were synthesized according to a modified literature procedure.[19-20] As-synthesized monodispersed QDs were suspended in toluene and combined with TBAOH, OAm, hexaniobate

crystallites, and heat treated at 220 °C via solvothermal method. QDs@hexaniobate NPPs formed within 6 hrs. NPPs can be easily seen by TEM (Figure 4.2).

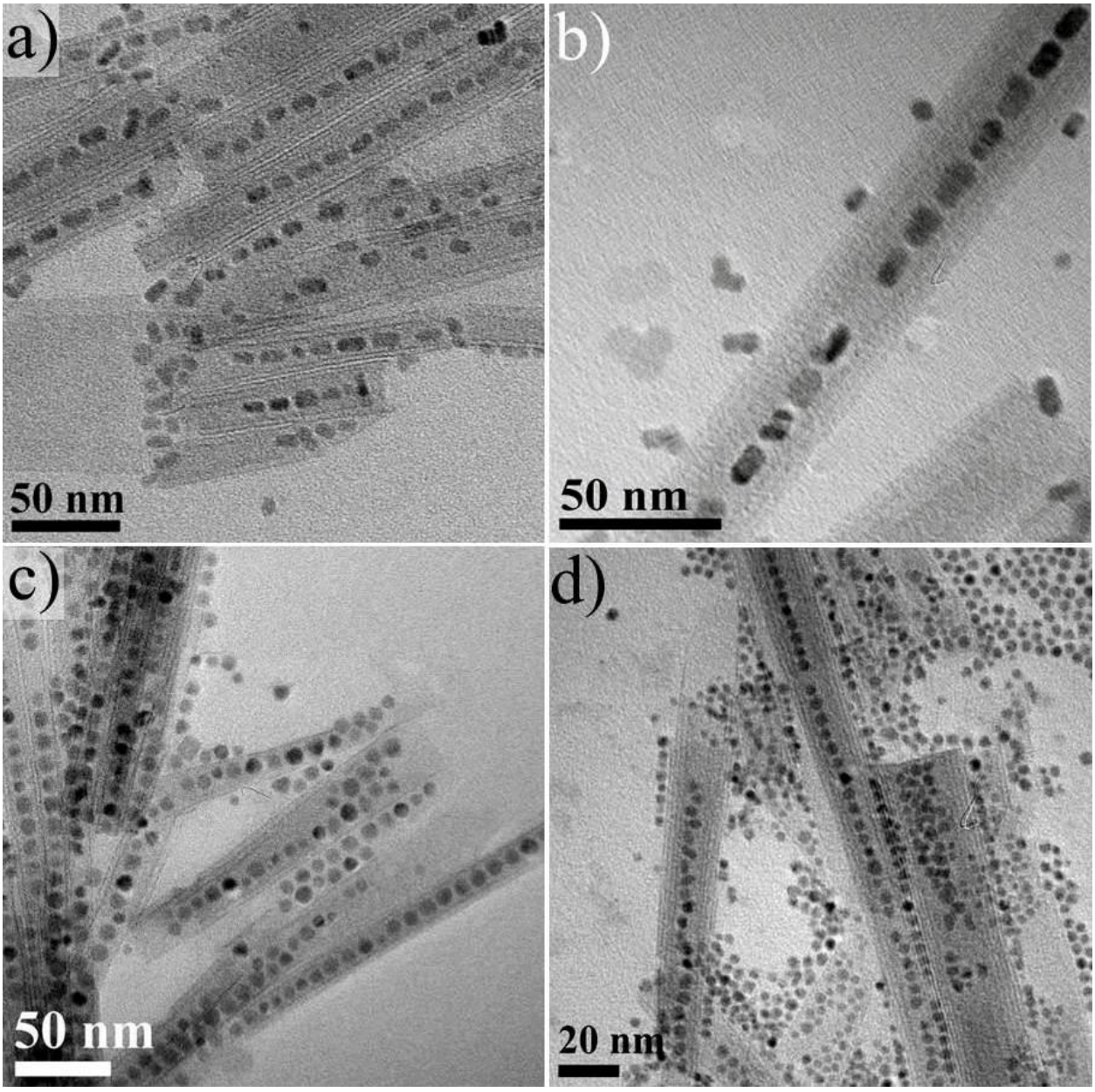

Figure 4.2. TEM images of (a, b) CdS@hexaniobate NPPs, (c) ZnS@hexaniobate NPPs, and (d) CdSe@hexaniobate NPPs.

QDs can be observed clearly inside the hexaniobate nanoscrolls as black dots in the bright field images of the NPPs (Figure 4.2). Figures 4.2a and 4.2b highlight the morphology of typical CdS@hexaniobate NPPs samples. Like in the TiO_2@hexaniobate NPPs, rod-like NPs are

readily captured by this method. TEM images of NPPs show contrast differences between the CdS NPs and the hexaniobate nanoscrolls. ZnS@hexaniobate NPPs are shown Figure 4.2c. Each of the hexaniobate nanoscrolls is almost filled with the spherical ZnS QDs. The versatile synthetic strategy can also be extended to CdSe QDs; Figure 4.2d shows low magnification TEM images highlighting a representative CdSe@hexaniobate sample.

4.3.2 Ag NP Modified Hexaniobate Nanostructures

Nanocomposite materials containing Ag NPs are accessible. Ag NPs prepared by a one-pot synthesis have spherical shape with a narrow size distribution and average diameter of 10 nm (Figure 4.3a).[21] The NPs were combined with hexaniobate nanosheets under various reaction conditions. In these systems, Ag NPs can be attached to the nanosheets before scrolling (Figure 4.3b), attached to the surfaces of the nanoscrolls (Figure 4.3c), and/or incorporated into the scrolled nanosheets to produce NPP structures (Figure 4.3d). The morphology and composition of the products has been investigated by TEM and EDS, respectively. The nanocomposites are composed of Ag and hexaniobate (Figure 4.3). The geometries of nanocomposites can readily be tuned by applying different reaction conditions. For example, lower temperatures (150 °C - 6h) resulted in simple nanosheets whose surface is decorated (Figure 4.3b). Using the same reaction temperature but longer reaction times (150 °C - 16h) resulted in nanoscrolls with a surface coating of Ag NPs (Figure 4.3c). Higher temperatures with shorter reaction times (220 °C - 6h) resulted in NPP-type morphologies (Figure 4.3d) with no NPs attached to the surface of the scrolls. In all the products, the Ag NPs retained their narrow size distribution irrespective of the temperature changes; this is likely attributable to the presence of surfactants in the reaction mixture. Elemental analyses with EDS also confirmed that the nanocomposites are composed of Ag and Nb as major components (Insets: Figures 4.1b, 4.1c and 4.1d).

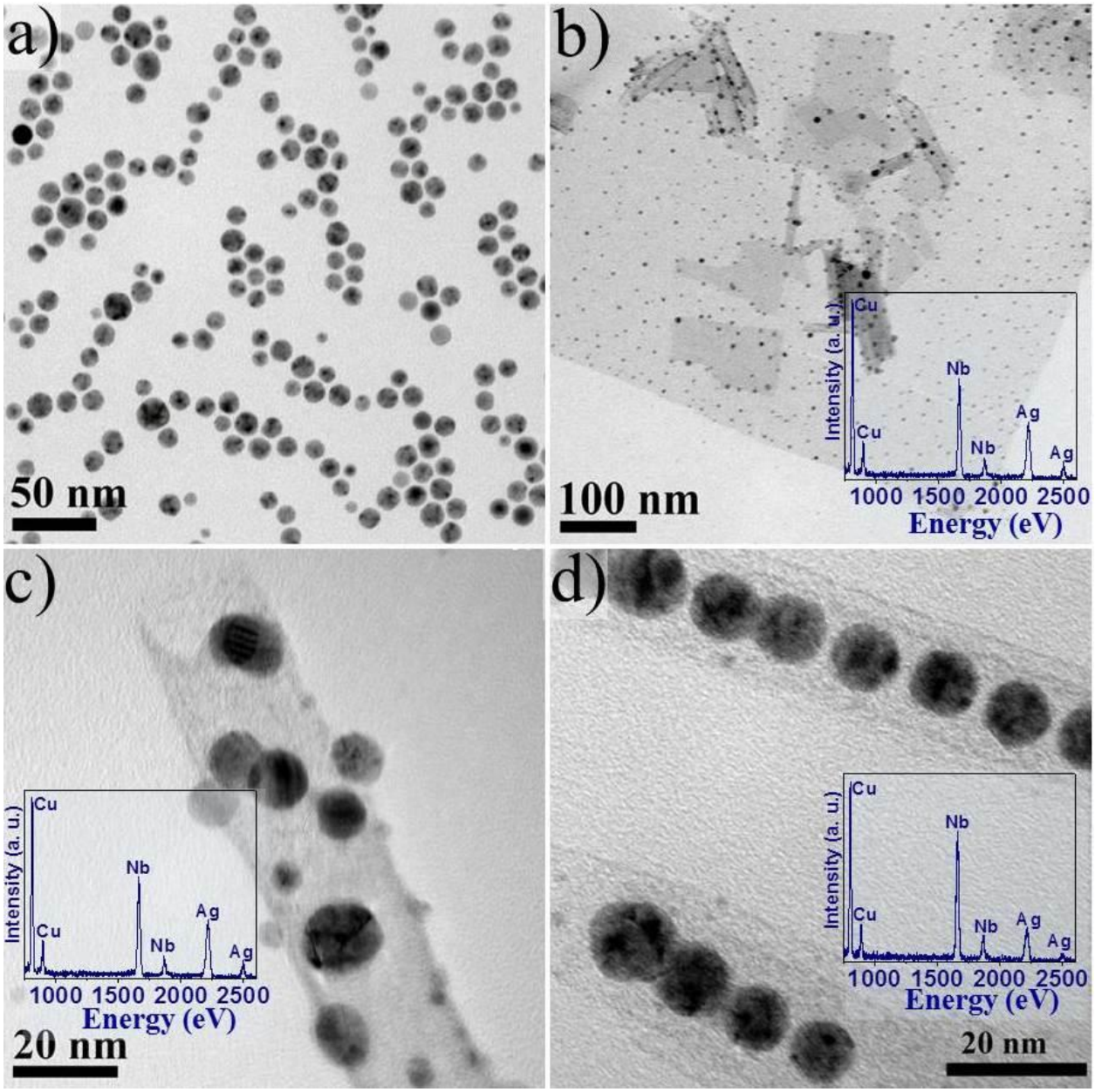

Figure 4.3. TEM images of (a) Ag NPs; (b) Ag functionalized hexaniobate nanosheet prepared at 150 °C in 6h; (c) Ag functionalized hexaniobate nanoscroll prepared at 150 °C in 16h; (d) Ag@hexaniobate NPPs prepared at 220 °C in 16h. [Insets: respective EDS data; The Cu-related peaks are from the TEM grid.].

4.3.3 *In situ* Growth of Au NPs in Preformed Hexaniobate Nanoscrolls

Well-defined intercalated multi-walled hexaniobate nanoscrolls (INS) consisting of 2 to 6 layers with a wall thickness of about 1.1 nm and an interlayer spacing of ~3.2 nm were readily obtained after the solvothermal treatment (Chapter 2).[24] Examples of these nanoscrolls are shown in Figure 4.4.

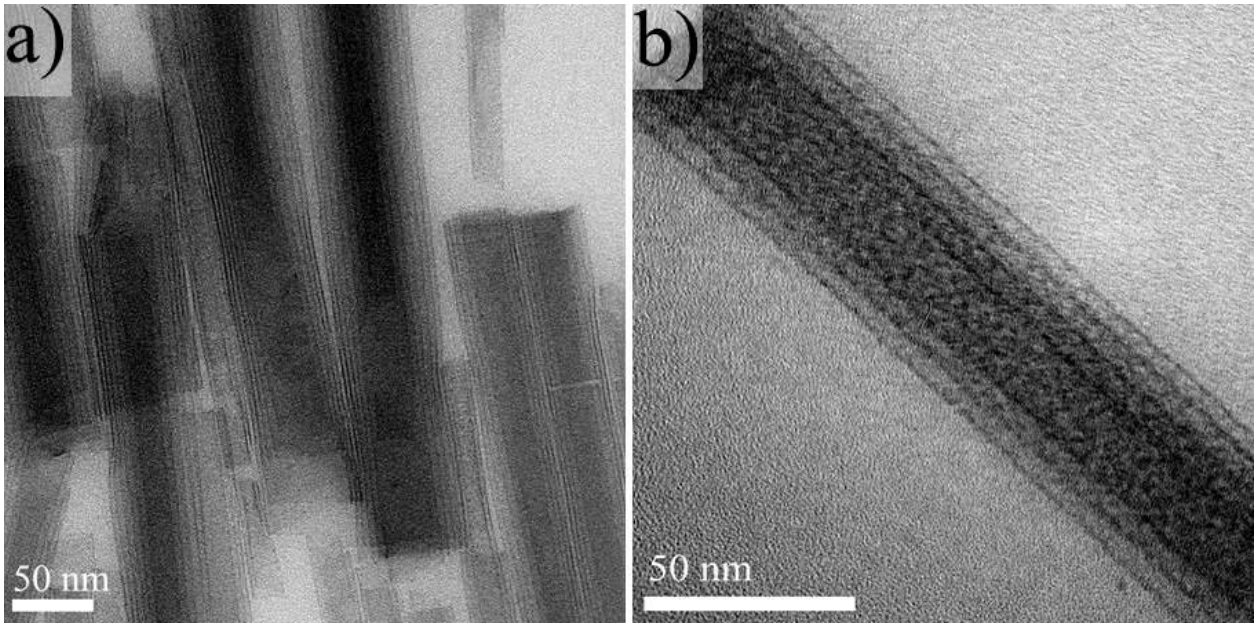

Figure 4.4. (a, b) TEM micrographs of INS, showing multi-walled architecture, which were used as templates to grow Au NP chains.

Au NPs can be readily synthesized *in situ* by reducing Au^{3+} in a solution of hexane with OAm as a reducing agent and surfactant, at 50 °C.[22] The Au NPs have the diameters around 10 nm (Figure 4.5a). To make NPP structures, the same reaction was done in the presence of OAm-intercalated multi-walled hexaniobate nanoscrolls (INS). TEM images demonstrate that the product was dominated by uniform Au NP chains inside the hexaniobate nanoscrolls. High contrast between the Au and hexaniobate nanoscrolls was distinctly observed in the TEM images

(see Figure 4.5b, 4.5c, and 4.5d). EDS analysis confirmed the composition of these NPPs where a single NPP showed only Au and Nb as major components (Inset: Figure 4.5d).

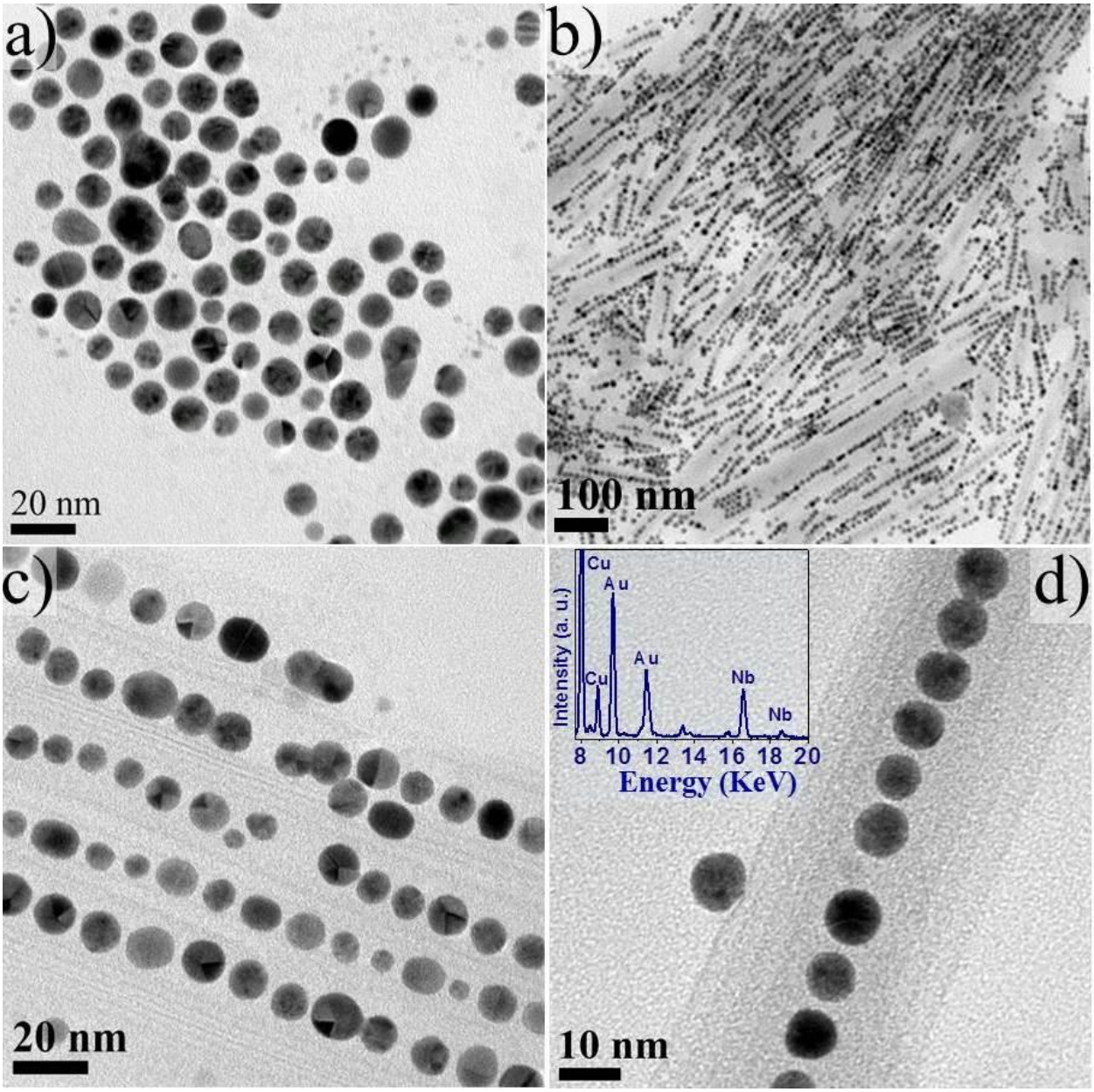

Figure 4.5. TEM images of (a) Au NPs and (b, c, d) TEM images of Au@hexaniobate NPPs [Inset (d): respective EDS data, Cu from TEM grid].

4.3.4 Bifunctional NPPs Through *in situ* Growth of Au NPs in Partially-Filled Fe_3O_4@hexaniobate NPPs

Uniform Au-Fe_3O_4@hexaniobate NPP composites were synthesized. Initially, by decreasing the concentration of Fe_3O_4 NPs in the reaction mixture for the synthesis of Fe_3O_4@hexaniobate NPPs (Chapter 3), partially filled peapod nanoscrolls were prepared - this produced NPPs with significant open space within the peapod structure (Figure 4.6).

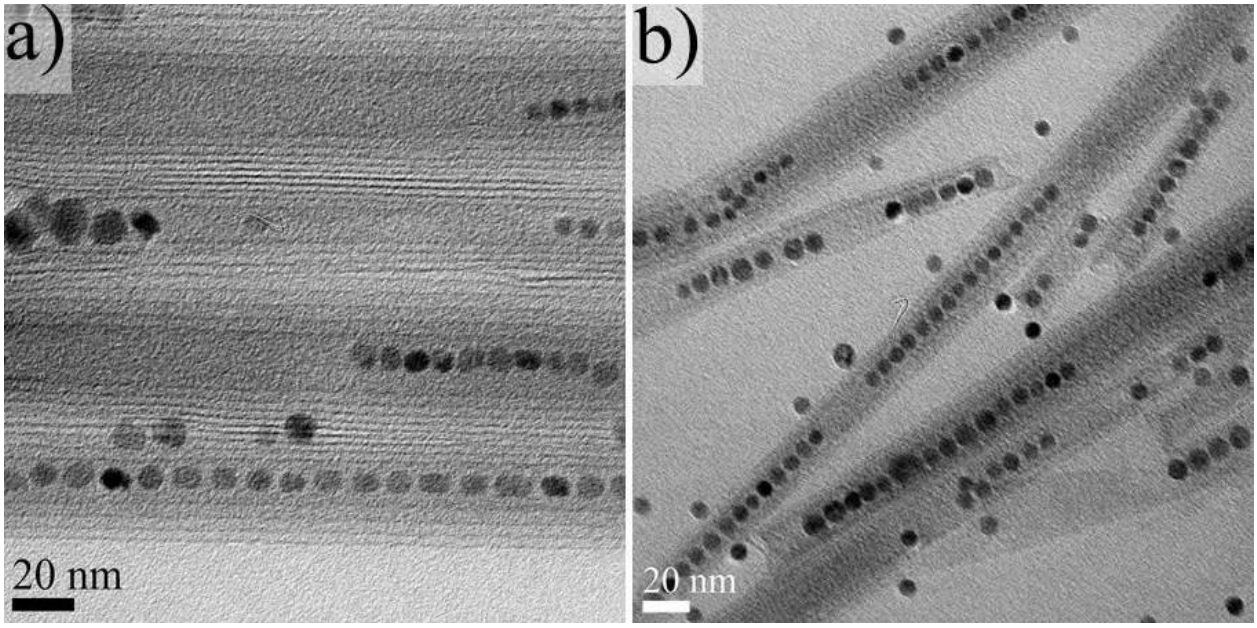

Figure 4.6. (a, b) TEM images of the partially filled Fe_3O_4@hexaniobate NPPs showing the empty spaces in the hexaniobate nanoscrolls that were later used as templates to grow Au NPs

In situ treatment with gold, as described above, readily leads to NPPs with both Au and Fe_3O_4 NPs. These Au-Fe_3O_4@hexaniobate NPP structures were examined with TEM, HAADF-STEM and EDS elemental mapping. The TEM images (Figure 4.7a, 4.7b) indicate that Au-Fe_3O_4@hexaniobate bi-functional NPPs were successfully obtained. Clear contrast is seen between the dark gold and lighter Fe_3O_4 NPs. HAADF-STEM and EDS analysis provide more definitive confirmation. High contrast between the cores Au (white) and Fe_3O_4 (dark gray) NPs

was observed in the HAADF-STEM images (Figure 4.7c). The outline of the hexaniobate shell, though not as well pronounced, can also be seen (dark gray). Panels d, e, f and g of Figure 4.7 are the elemental mapping images of the Au, Fe and Nb; the cyan for Au, orange for Fe, and purple represents Nb, respectively. These results clearly support the formation of Au-Fe_3O_4 NP core and hexaniobate shell.

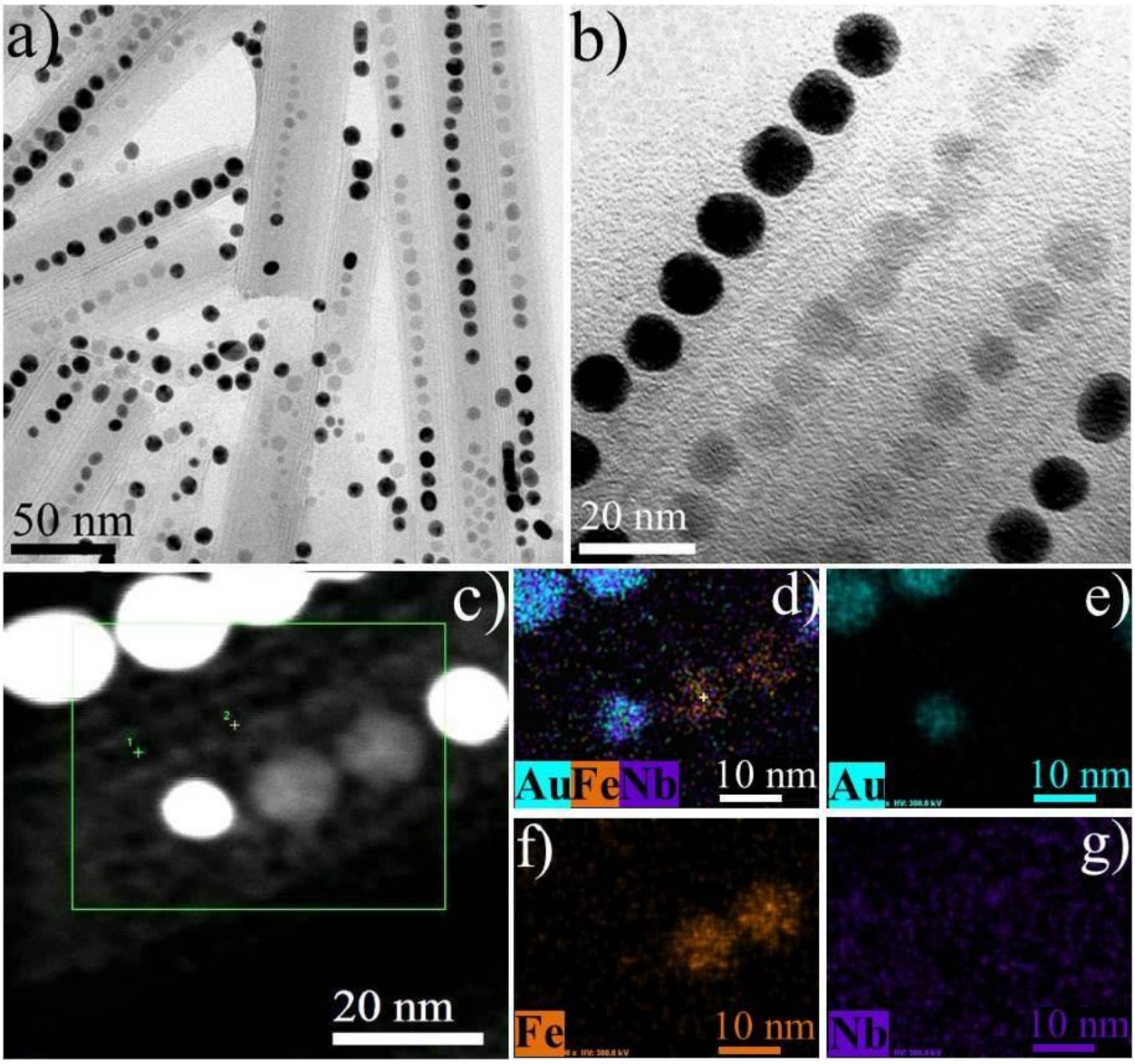

Figure 4.7. TEM images of (a, b) Au-Fe3O4@hexaniobate NPP structures; c) HAADF-STEM image. EDX elemental mapping analysis of bi-functional NPPs; d) Au, Fe and Nb; e) Au (cyan color); f) Fe (orange color); g) Nb (purple color).

4.3.5 UV-Vis Measurements

To further understand the nature of nanoscrolls and NPPs, UV-Vis absorption spectra were collected. UV−Vis spectra of nanoscrolls show no peak in the visible region (Figure 4.8a), which is attributable to the wide band-gap of hexaniobate.[12] The effect of Ag and Au on the nanoscrolls was investigated in toluene. For NP sizes of approximately 10 nm, Ag and Au NPs are known to absorb via a surface plasmon resonance (SPR) at ca. 420 nm and 520 nm, respectively.[25] The SPR of Ag, Ag@hexaniobate, Au, Au@hexaniobate, and Au-Fe_3O_4@hexaniobate nanostructures are shown in Figures 4.8b and 4.8c, for the Ag and Au materials, respectively. Originating from their unique chemical composition and morphology, Ag@hexaniobate, Au@hexaniobate, and Au-Fe_3O_4@hexaniobate NPPs show unique optical properties. As shown in Figure 4.8b and 4.8c, OAm-capped Ag and Au NPs in toluene solution showed an SPR peak at 420 nm and 524 nm, respectively. The peak position of the plasmon resonance band is known to depend on the dielectric properties of the surrounding media and NP morphology.[26] Encapsulation of Ag and Au NP chains with a hexaniobate nanoscroll was anticipated to shift the SPR of Ag and Au NPs to higher wavelengths due to interaction between metal NP chains.[27] In the case of Ag@hexaniobate, a broad peak at 430 nm appears in the UV−Vis absorption spectrum (Figure 4.8b). An absorbance peaks at ~530 nm and 538 nm are observed for the Au@hexaniobate and Au- Fe_3O_4@hexaniobate NPPs, respectively (Figure 4.8c). Figure 4.8 clearly demonstrates the difference between absorption peaks with and without noble metals. The light harvesting ability of nanoscrolls in the visible light region was enhanced by the noble metals.

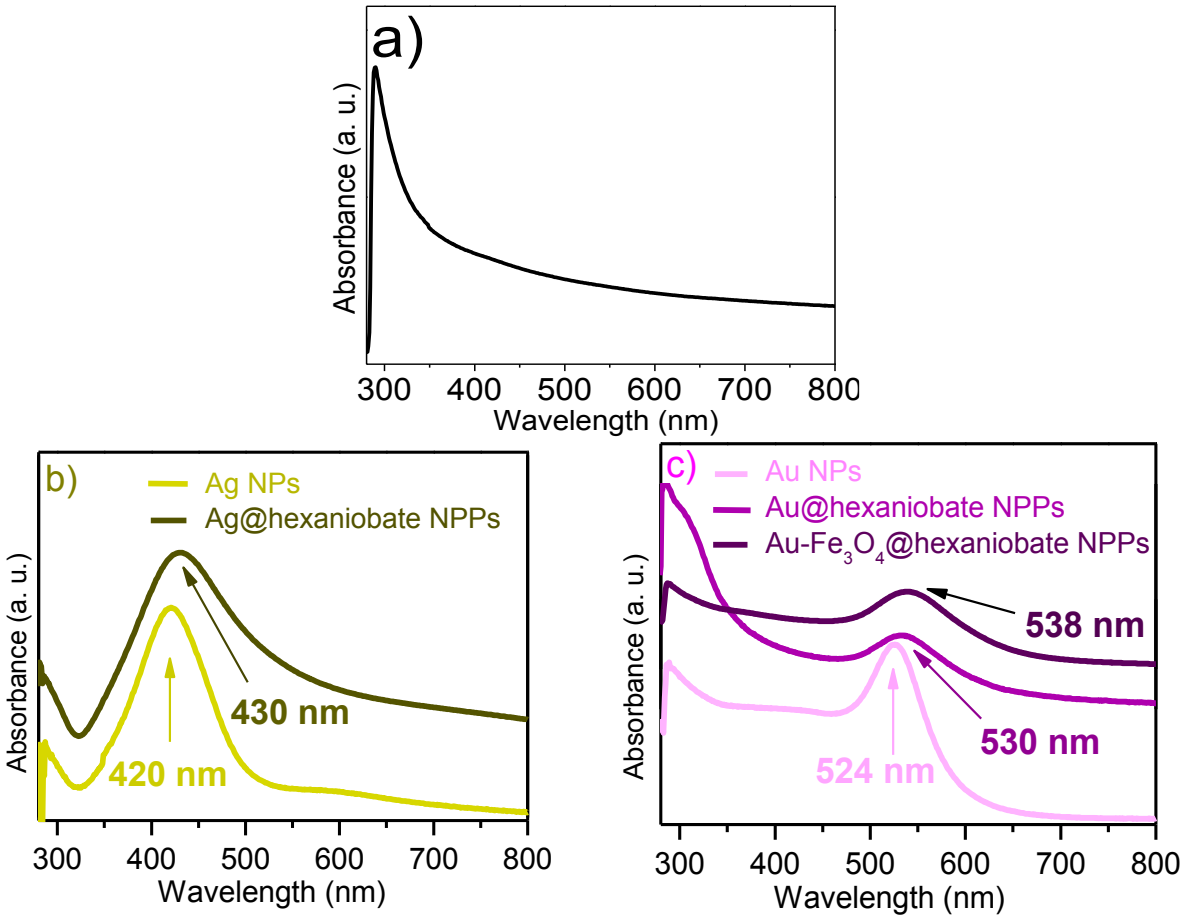

Figure 4.8. UV−Vis absorption spectrum of (a) hexaniobate nanoscrolls, (b) Ag NPs and Ag@hexaniobate NPPs, and (c) Au NPs, Au@hexaniobate NPPs, and Au-Fe_3O_4@hexaniobate NPPs.

These results show that optical properties of the hexaniobate nanoscrolls can be further tuned by combining them with differently sized noble metals (alloys); this could offer great potential toward plasmonic catalysis.

4.4 Discussion

If useful NP capturing methods are to be developed, the synthetic route needs to allow the addition of different reagents for the controlled exfoliation to capture the NP chains of desired materials combinations; that is, the fabrication must be simplified by a sufficient number of different synthetic modifications to permit a morphologically uniform construction of novel

nanomaterials. One of the versatile soft-solution methods for the encapsulation of Co NPs in hexaniobate nanoscrolls was published by Yao et al. nearly two years ago.[10d] Unlike other early work, it focused on the controlled capturing of NP chains of Co via an *in situ* thermal decomposition of Co followed by simultaneous encapsulation by exfoliated hexaniobate nanosheets. Even though it is a very useful method for the encapsulation of magnetic NPs, this method may not be applicable to pre-formed NPs.

But to be pertinent to our understanding of future hexaniobate-based industrial applications, synthetic routes need to be applied not only to Co, but to other NP combinations—an impossible task a few years ago simply because most researchers attempted to use aqueous exfoliation route where hydrophobic NPs could not be introduced during the week-long scrolling process. The challenge of how to fabricate novel hexaniobate-based nanoarchitectures can be addressed by considering that such solvothermally exfoliated hexaniobate nanosheets can capture inside pore structures. Recent synthetic advances have made it possible to synthesize and characterize hexaniobate nanoscrolls (Chapter 2).[24] However, it is still impossible to obtain reliable experimental thermodynamic data on the encapsulation potential of hexaniobate nanoscrolls when NPs with two or more sizes are present under operating conditions.

Shape selectivity. Shape selectivity is an important advance towards the separation of particles with specific morphology from polydispersed NP colloidal suspensions. The explanation for the shape selective encapsulation associated with solvothermal scrolling of exfoliated hexaniobate nanosheets is not clear. It is known that the inner diameter of the nanoscroll is usually determined by the size of the particles within the pores, therefore the scrolling occurs around sets of particles. For this to effectively occur, there has to be a driving force that selects NPs of one shape (or size) over another. Further, the process has to be able to

dynamic, so that if irregular particles are inadvertently incorporated, they have time to be rejected from the ordered array. For a thorough understanding of shape selectivity, we need to understand the effect of surface groups and particle facets on the various kinetic and thermodynamic effects that can influence the encapsulation capabilities of hexaniobate nanoscrolls. Simulation and modeling studies on the scrolling process and NP capture mechanisms may also help to elucidate more energetically favorable assembly pathways.[28]

NPP formation. Encapsulation of various NP chains in the exfoliated hexaniobate nanosheets via solvothermal method is one of the most efficient methods for the fabrication of NPPs where the properties of two or more components can be combined. The experimental procedure used in the formation of the NPP is highlighted in Figure 4.9. This approach readily produces NPPs structures in high yields.

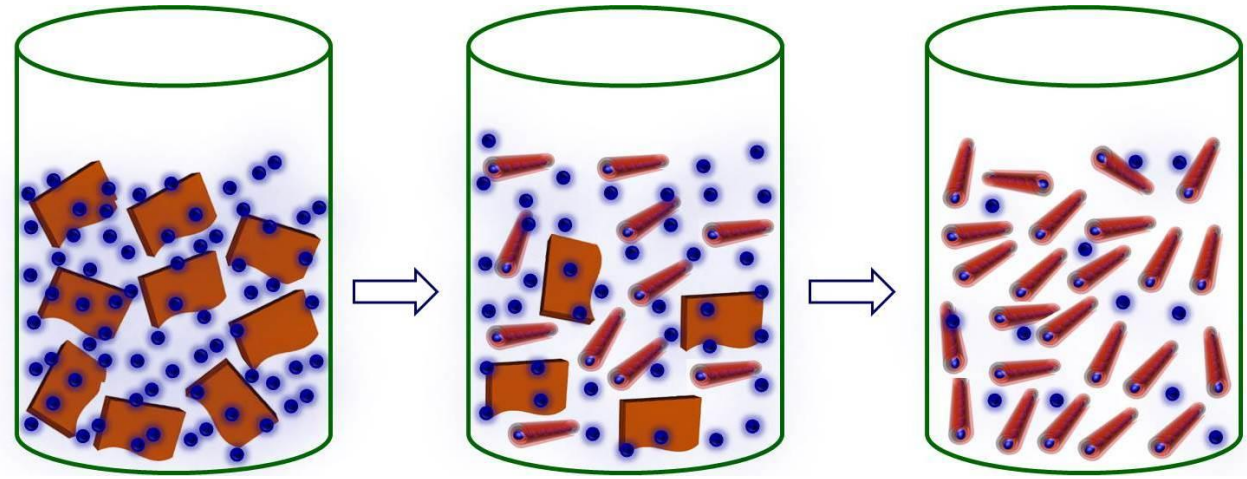

Figure 4.9. General scheme for the fabrication of metal (oxide) NPs or QDs to produce NP@hexaniobate NPPs via a solvothermal method. Three reaction vessels show three stages of the NPPs fabrication [left to right, before solvothermal treatment, intermediate step (220 °C–4h) and after solvothermal treatment (220 °C–6h), respectively].

Controlled solvothermal treatments generate a hexaniobate shell around the NP cores. In this method, pre-synthesized uniform metal (oxides) NPs or QDs stabilized with OAm were combined with hexaniobate crystallite, TBAOH, and toluene. Subsequent solvothermal treatment

at specific temperatures under controlled reaction conditions resulted in the production of NPs encapsulated in hexaniobate nanoscrolls. This synthetic method could be generally applied to fabricate nanocomposites with various dimensions and compositions. For example, as shown in Figure 4.3b and 4.3c, Ag NP decorated hexaniobate nanotubes (1D) and nanosheets (2D) could be readily fabricated.

This method enabled systematic selection of NPs with specific morphology. Surface modified TiO_2 NPs were successfully encapsulated inside hexaniobate nanoscrolls, demonstrating the wide-spread applicability of this fabrication strategy. The TiO_2 NPs with slight morphological changes enabled us to observe the shape selective encapsulation of hexaniobate. Rod-shaped TiO_2 NPs with the dimensions of *ca.* 6.5 nm diameter and 12 nm lengths were predominately captured (Figure 4.1a). NPs with other sizes were not captured during the solvothermal treatment. This observation highlighted the shape selective encapsulation capabilities of hexaniobate. These results demonstrate that hexaniobate is a novel candidate for the separating of polydispersed NPs. This shape selective concept of hexaniobate is not limited to TiO_2 NPs and should be easily applicable to other NP systems.

This highly reproducible synthetic process can serve as a standard protocol for the fabrication of NPPs for various materials. For example, this method was successfully applied to the encapsulation of QDs (Figure 4.2). In addition to the ability to control the morphology of TiO_2 NPs and QDs (Figures 4.1c, 4.1d, 4.2a, and 4.2b), this method also provides a means for Ag NP decoration of hexaniobate sheets and scrolls under various reaction conditions. Ag NPs can be readily attached on nanosheets before scrolling (Figure 4.3b), attached to the surfaces of the nanoscrolls (Figure 4.3c), and/or incorporated into the scrolled nanosheets to produce NPP

structures (Figure 4.3d). The experimental procedure used in the formation of the Ag-hexaniobate nanocomposites is highlighted in Figure 4.10.

Ag modification. In pursuing such research, usually different temperatures and times must be employed because higher temperatures (≥200 °C) always favor the peapod formation due to the rapid exfoliation and scrolling mechanism. Therefore, Ag-decorated nanosheets and scrolls were fabricated at 150 °C. Shorter reaction times (6h) favored Ag-decorated hexaniobate nanosheets (Figure 4.3b) and longer times (16h) produced nanoscrolls with a surface coating of Ag NPs (Figure 4.3c). The formation of such nanocomposites, instead of NPPs, indicates that exfoliation at lower temperature (150 °C - 6h) is slower and attached Ag NPs restrict the scroll formation, but longer reaction times (≥16h) at 150 °C facilitate the scroll formation. Furthermore, the anchored OAm molecules are much more abundant on the exfoliated nanosheets, which may allow an easy coupling of the Ag NPs to the individual nanosheets, owing to the interdigitation among these surfactant molecules.[29] To the best of our knowledge, this is the first fabrication process for producing Ag-hexaniobate nanocomposites with three different morphologies.

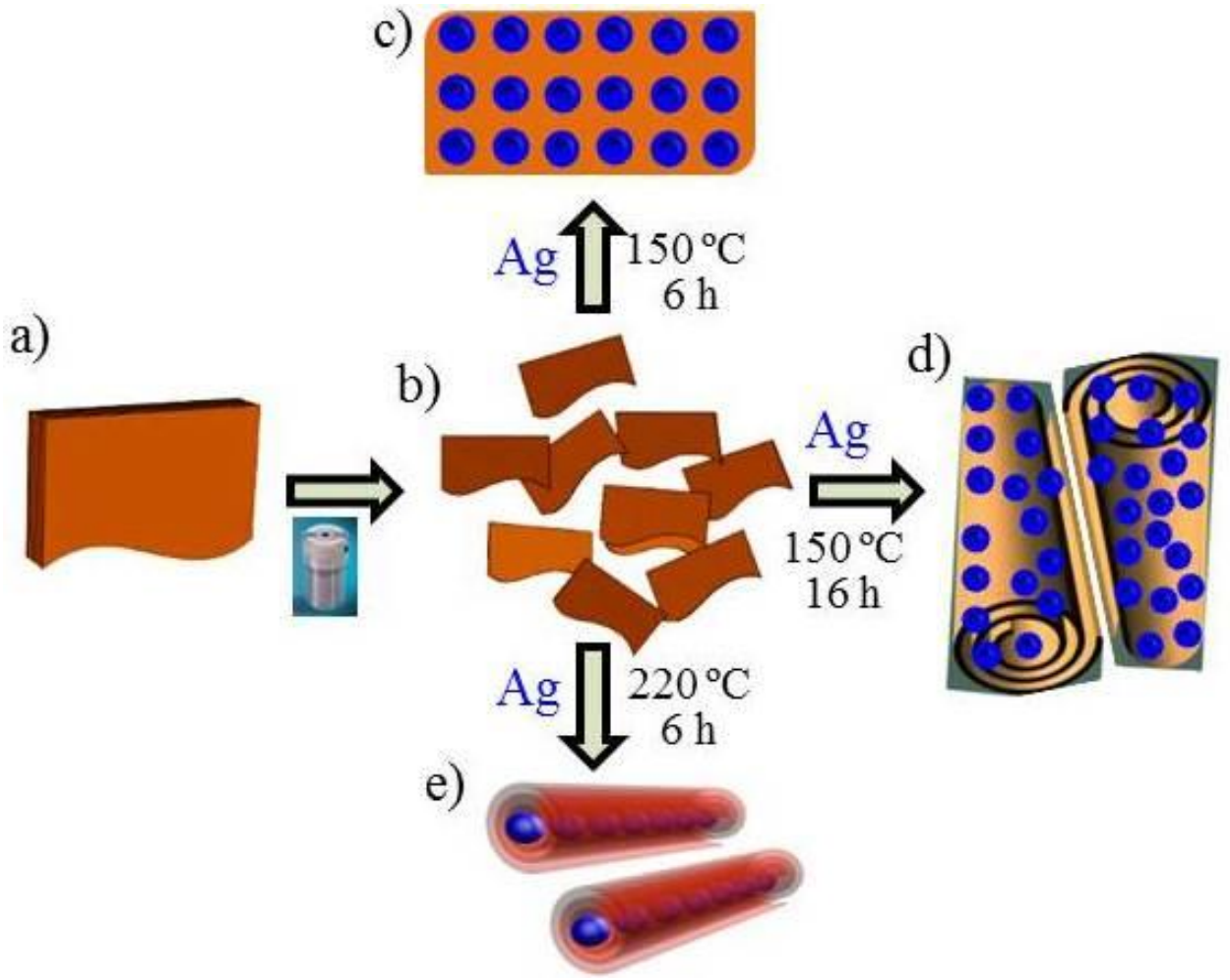

Figure 4.10. Schematic for the fabrication of Ag-hexaniobate nanocomposites via a solvothermal method. Cartoons show a) hexaniobate crystallites, b) exfoliated nanosheets, c) Ag NP decoration of hexaniobate sheets, d) Ag NP decoration of hexaniobate nanoscrolls, and e) Ag@hexaniobate NPPs (Peapod cartoons were drawn by Cinema 4D software).

Au NPP from performed nanoscrolls. By promoting the reaction of the proton-exchanged hexaniobate with TBAOH and OAm in toluene under solvothermal conditions, nanoscrolls can readily be produced with higher morphological uniformity (Chapter 2).[24] Such nanoscrolls can be successfully used as templates to grow Au NP chains (Figure 4.4). The experimental procedure used in the formation of the Au-hexaniobate NPPs is highlighted in Figure 4.11. Uniform Au@hexaniobate NPPs were successfully fabricated by filling the empty space with Au NPs in each nanoscroll (Figure 4.5). OAm is responsible for the reduction of Au^{3+}

ions. The reduction of Au^{3+} to Au^0, that is, in the presence of OAm, has already been reported.[22] Hiramatsu et al. used OAm as a surfactant and reducing agent to produce gold and silver NPs with adjustable sizes in large scale.[30] According to the model proposed by La Mer and Dinegar for colloidal particle nucleation and growth, nucleation occurs when ion concentration reaches supersaturation.[31] In our case, the initially formed gold atoms may thus self-nucleate to form a fixed number of seeds, and gold NPs then grow inside and outside of the hexaniobate nanoscroll by diffusion-driven deposition of gold atoms onto these existing seeds. This mechanism is similar to the previous reports by Hiramatsu et al..[30] The resulting Au@hexaniobate NPPs are structurally uniform. Free gold NPs can then be removed by a simple centrifugation step.

Bi-functional Au-Fe_3O_4@hexaniobate NPPs. Partially filled Fe_3O_4@hexaniobate NPPs can be readily synthesized by solvothermally treating the reaction mixture containing Fe_3O_4 NPs, hexaniobate crystallites, OAm, and toluene at 220 °C (Figure 4.6). By modifying the synthetic method, uniform Au-Fe_3O_4@hexaniobate NPPs can also be successfully fabricated (Figure 4.7). The experimental procedure used in the formation of the bi-functional Au- Fe_3O_4@hexaniobate NPPs is highlighted in Figure 4.11. By decreasing the concentration of Fe_3O_4 NPs in the reaction mixture, partially filled Fe_3O_4@hexaniobate NPPs were synthesized to ensure that there is some space to grow the Au NPs in each nanoscroll, Au-Fe_3O_4@hexaniobate NPPs cores were grown inside the nanoscrolls by filling the gaps.

Although recent years have seen some progress in our ability to synthesize and characterize multi-functional nanomaterials, it is at present still not very easy to image nanocomposites with significant contrast difference among various building blocks under operating conditions. Recently, the use of STEM EDS chemical mapping has become possible,

so as to indicate the presence of each of the element in the multi-component NPP systems (Figure 4.7d-g).

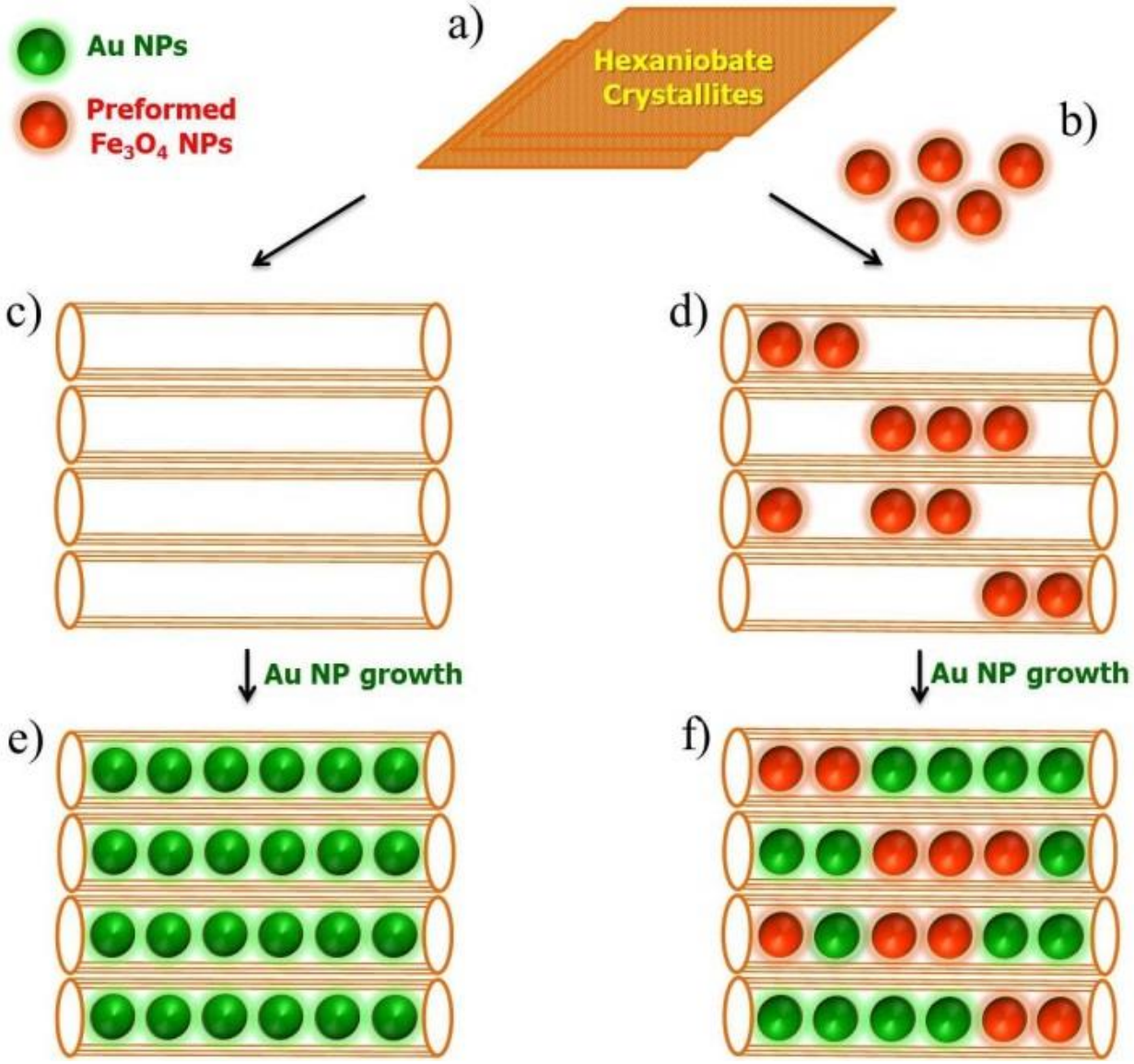

Figure 4.11. Schematic representation of *in situ* growth of Au NPs in preformed nanoscrolls and partially filled Fe_3O_4@hexaniobate NPPs. Cartoon show a) hexaniobate crystallites, b) preformed Fe_3O_4 NPs, c) INS, d)partially filled Fe_3O_4@hexaniobate NPPs, e) Au@hexaniobate NPPs, and f) Au- Fe_3O_4@hexaniobate bi-functional NPPs.

Because Fe_3O_4@hexaniobate NPPs are composed of superparamagnetic Fe_3O_4 NP cores, they may be used not only as a drug delivery vehicle but also as a magnetic resonance (MR)

imaging contrast agent. By immobilizing the Au NPs inside the Fe_3O_4@hexaniobate NPPs, multi-functional nanocomposites can be readily prepared, possibly rendering them useful as transducers for the photothermal destruction of tumor cells.[32] The resulting monodispersed NPPs maintain structural uniformity, which is highly desirable for various applications.

SPR effects. The Ag@hexaniobate, Au@hexaniobate, and Au-Fe_3O_4@hexaniobate nanostructures showed unique optical properties (Figures 4.8c, 4.8e, and 4.8f, respectively). Encapsulation of Ag and Au NP chains within a hexaniobate nanoscroll resulted in a shift in SPR to higher wavelengths.[27] Noble metal@hexaniobate NPPs absorbed light in the visible region. The enhanced light harvesting properties of nanoscrolls are expected to be especially useful in designing future solar-powered photocatalysts.

4.5 Conclusions

In this chapter, we demonstrated several successful synthetic strategies for the preparation novel nanocomposites by adding metal (oxide) NPs and quantum dots to hexaniobate nanoscrolls via a facile non-aqueous solvothermal method. This method was successfully extended to the fabrication of novel bi-functional Au-Fe_3O_4@hexaniobate NPPs. This ability further demonstrates the extensive tunability available in NPP systems where one can direct nanocomponents to both inside and outside of the nanoscrolls so that a variety of magnetic, optical, catalytic and electronic properties can be developed to make new important, technologically significant nanocomposite constructs. UV-Vis analysis revealed that the NPP structures work as an efficient visible light harvester and could be effective systems for solar applications like water splitting. The long-range morphological uniformity, properties, chemical identity and composition of these nanocomposites were investigated by TEM, HAADF-STEM

and EDS. Currently, new combinations of hybrid materials for photocatalytic applications are being investigated.

4.6 References

1. (a) Sato, Y.; Suenaga, K.; Bandow, S.; Iijima, S., Site-dependent migration behavior of individual cesium ions inside and outside C-60 fullerene nanopeapods. *Small* **2008,** *4* (8), 1080-1083; (b) Kang, J. W.; Hwang, H. J., Schematics and simulations of nanomemory device based on nanopeapods. *Materials Science & Engineering C-Biomimetic and Supramolecular Systems* **2005,** *25* (5-8), 843-847; (c) Kim, G.; Son, Y. W.; Cho, Y.; Han, S.; Ihm, J., Field emission of carbon nanotubes and electronic structure of carbon nanopeapods. *Current Applied Physics* **2002,** *2* (1), 57-60; (d) Hangarter, C. M.; Lee, Y. I.; Hernandez, S. C.; Choa, Y. H.; Myung, N. V., Nanopeapods by Galvanic Displacement Reaction. *Angewandte Chemie-International Edition* **2010,** *49* (39), 7081-7085; (e) Sohi, A. N.; Naghdabadi, R., Torsional buckling of carbon nanopeapods. *Carbon* **2007,** *45* (5), 952-957; (f) Shimada, T.; Ohno, Y.; Suenaga, K.; Okazaki, T.; Kishimoto, S.; Mizutani, T.; Taniguchi, R.; Kato, H.; Cao, B. P.; Sugai, T.; Shinohara, H., Tunable field-effect transistor device with metallofullerene nanopeapods. *Japanese Journal of Applied Physics Part 1-Regular Papers Brief Communications & Review Papers* **2005,** *44* (1A), 469-472; (g) Rols, S.; Cambedouzou, J.; Chorro, M.; Schober, H.; Agafonov, V.; Launois, P.; Davydov, V.; Rakhmanina, A. V.; Kataura, H.; Sauvajol, J. L., How confinement affects the dynamics of C(60) in carbon nanopeapods. *Physical Review Letters* **2008,** *101* (6); (h) Liu, L. F.; Lee, W.; Scholz, R.; Pippel, E.; Gosele, U., Tailor-made inorganic nanopeapods: Structural design of linear noble metal nanoparticle chains. *Angewandte Chemie-International Edition* **2008,** *47* (37), 7004-7008; (i) Trave, A.; Ribeiro, F. J.; Louie, S. G.; Cohen, M. L., Energetics and structural characterization of C-60 polymerization in BN and carbon nanopeapods. *Physical Review B* **2004,** *70* (20); (j) Sun, B. Y.; Inoue, T.; Shimada, T.; Okazaki, T.; Sugai, T.; Suenaga, K.; Shinohara, H., Synthesis and characterization of Eu-metallofullerenes from Eu@C-74 to Eu@C-90 and their nanopeapods. *Journal of Physical Chemistry B* **2004,** *108* (26), 9011-9015; (k) Lu, J.; Nagase, S.; Zhang, S.; Peng, L. M., Strongly size-dependent electronic properties in C-60-encapsulated zigzag nanotubes and lower size limit of carbon nanopeapods. *Physical Review B* **2003,** *68* (12).
2. (a) Hsin, Y. L.; Lin, C. F.; Liang, Y. C.; Hwang, K. C.; Horng, J. C.; Ho, J. A. A.; Lin, C. C.; Hwu, J. R., Microwave arcing induced formation and growth mechanisms of core/shell metal/carbon nanoparticles in organic solutions. *Advanced Functional Materials* **2008,** *18* (14), 2048-2056; (b) Kataura, H.; Maniwa, Y.; Abe, M.; Fujiwara, A.; Kodama, T.; Kikuchi, K.; Imahori, H.; Misaki, Y.; Suzuki, S.; Achiba, Y., Optical properties of fullerene and non-fullerene peapods. *Applied Physics a-Materials Science & Processing* **2002,** *74* (3), 349-354; (c) Okada, S.; Saito, S.; Oshiyama, A., Energetics and electronic structures of encapsulated C-60 in a carbon nanotube. *Physical Review Letters* **2001,** *86* (17), 3835-3838; (d) Hsieh, C. H.; Chou, L. J.; Lin, G. R.; Bando, Y.; Golberg, D., Nanophotonic Switch: Gold-in-Ga2O3 Peapod Nanowires. *Nano Letters* **2008,** *8* (10), 3081-3085; (e) Chen, P. H.; Hsieh, C. H.; Chen, S. Y.; Wu, C. H.; Wu, Y. J.; Chou, L. J.; Chen, L. J., Direct Observation of Au/Ga2O3 Peapodded Nanowires and Their Plasmonic Behaviors. *Nano Letters* **2010,** *10* (9), 3267-3271; (f) Lai, Y. F., Effects of synthesis parameters on the growth of magnesium oxide

nanowries by vapor-liquid-solid mechanism at low temperatures. *Acta Physica Sinica* **2010,** *59* (12), 8814-8819; (g) Lai, Y. F.; Chaudouet, P.; Charlot, F.; Matko, I.; Dubourdieu, C., Magnesium oxide nanowires synthesized by pulsed liquid-injection metal organic chemical vapor deposition. *Applied Physics Letters* **2009,** *94* (2); (h) Zhou, W. W.; Sun, L.; Yu, T.; Zhang, J. X.; Gong, H.; Fan, H. J., The morphology of Au@MgO nanopeapods. *Nanotechnology* **2009,** *20* (45); (i) Qin, Y.; Lee, S. M.; Pan, A.; Gosele, U.; Knez, M., Rayleigh-instability-induced metal nanoparticle chains encapsulated in nanotubes produced by atomic layer deposition. *Nano Letters* **2008,** *8* (1), 114-118.

3. (a) Jain, P. K.; Huang, X. H.; El-Sayed, I. H.; El-Sayed, M. A., Noble Metals on the Nanoscale: Optical and Photothermal Properties and Some Applications in Imaging, Sensing, Biology, and Medicine. *Accounts of Chemical Research* **2008,** *41* (12), 1578-1586; (b) Hutter, E.; Fendler, J. H., Exploitation of localized surface plasmon resonance. *Advanced Materials* **2004,** *16* (19), 1685-1706; (c) Haes, A. J.; Van Duyne, R. P., A nanoscale optical blosensor: Sensitivity and selectivity of an approach based on the localized surface plasmon resonance spectroscopy of triangular silver nanoparticles. *J. Am. Chem. Soc.* **2002,** *124* (35), 10596-10604; (d) Malinsky, M. D.; Kelly, K. L.; Schatz, G. C.; Van Duyne, R. P., Chain length dependence and sensing capabilities of the localized surface plasmon resonance of silver nanoparticles chemically modified with alkanethiol self-assembled monolayers. *J. Am. Chem. Soc.* **2001,** *123* (7), 1471-1482.
4. (a) Bock, C.; Paquet, C.; Couillard, M.; Botton, G. A.; MacDougall, B. R., Size-selected synthesis of PtRu nano-catalysts: Reaction and size control mechanism. *J. Am. Chem. Soc.* **2004,** *126* (25), 8028-8037; (b) Sarikaya, M.; Tamerler, C.; Jen, A. K. Y.; Schulten, K.; Baneyx, F., Molecular biomimetics: nanotechnology through biology. *Nature Materials* **2003,** *2* (9), 577-585.
5. (a) Shevchenko, E. V.; Talapin, D. V.; Kotov, N. A.; O'Brien, S.; Murray, C. B., Structural diversity in binary nanoparticle superlattices. *Nature* **2006,** *439* (7072), 55-59; (b) Mornet, S.; Vasseur, S.; Grasset, F.; Duguet, E., Magnetic nanoparticle design for medical diagnosis and therapy. *Journal of Materials Chemistry* **2004,** *14* (14), 2161-2175; (c) Katz, E.; Willner, I., Integrated nanoparticle-biomolecule hybrid systems: Synthesis, properties, and applications. *Angewandte Chemie-International Edition* **2004,** *43* (45), 6042-6108; (d) Gao, X. H.; Cui, Y. Y.; Levenson, R. M.; Chung, L. W. K.; Nie, S. M., In vivo cancer targeting and imaging with semiconductor quantum dots. *Nature Biotechnology* **2004,** *22* (8), 969-976; (e) Nam, J. M.; Thaxton, C. S.; Mirkin, C. A., Nanoparticle-based bio-bar codes for the ultrasensitive detection of proteins. *Science* **2003,** *301* (5641), 1884-1886; (f) Zeng, H.; Li, J.; Liu, J. P.; Wang, Z. L.; Sun, S. H., Exchange-coupled nanocomposite magnets by nanoparticle self-assembly. *Nature* **2002,** *420* (6914), 395-398; (g) Haynes, C. L.; Van Duyne, R. P., Nanosphere lithography: A versatile nanofabrication tool for studies of size-dependent nanoparticle optics. *Journal of Physical Chemistry B* **2001,** *105* (24), 5599-5611; (h) Kang, Y. S.; Risbud, S.; Rabolt, J. F.; Stroeve, P., Synthesis and characterization of nanometer-size Fe3O4 and gamma-Fe2O3 particles. *Chem. Mat.* **1996,** *8* (9), 2209-&; (i) Yu, H.; Chen, M.; Rice, P. M.; Wang, S. X.; White, R. L.; Sun, S. H., Dumbbell-like bifunctional Au-Fe3O4 nanoparticles. *Nano Lett.* **2005,** *5* (2), 379-382; (j) Yavuz, C. T.; Mayo, J. T.; Yu, W. W.; Prakash, A.; Falkner, J. C.; Yean, S.; Cong, L. L.; Shipley, H. J.; Kan, A.; Tomson, M.; Natelson, D.; Colvin, V. L., Low-field magnetic separation of monodisperse Fe3O4 nanocrystals. *Science* **2006,** *314* (5801), 964-967; (k) Wang, J.; Chen, Q. W.; Zeng, C.; Hou, B. Y., Magnetic-field-induced growth of single-crystalline Fe3O4 nanowires. *Adv. Mater.*

2004, *16* (2), 137-+; (l) Taberna, L.; Mitra, S.; Poizot, P.; Simon, P.; Tarascon, J. M., High rate capabilities Fe3O4-based Cu nano-architectured electrodes for lithium-ion battery applications. *Nature Materials* **2006,** *5* (7), 567-573; (m) Bazylinski, D. A.; Heywood, B. R.; Mann, S.; Frankel, R. B., FE3O4 AND FE3S4 IN A BACTERIUM. *Nature* **1993,** *366* (6452), 218-218.

6. (a) Alivisatos, A. P., Semiconductor clusters, nanocrystals, and quantum dots. *Science* **1996,** *271* (5251), 933-937; (b) Murray, C. B.; Norris, D. J.; Bawendi, M. G., SYNTHESIS AND CHARACTERIZATION OF NEARLY MONODISPERSE CDE (E = S, SE, TE) SEMICONDUCTOR NANOCRYSTALLITES. *J. Am. Chem. Soc.* **1993,** *115* (19), 8706-8715; (c) Michalet, X.; Pinaud, F. F.; Bentolila, L. A.; Tsay, J. M.; Doose, S.; Li, J. J.; Sundaresan, G.; Wu, A. M.; Gambhir, S. S.; Weiss, S., Quantum dots for live cells, in vivo imaging, and diagnostics. *Science* **2005,** *307* (5709), 538-544; (d) Burda, C.; Chen, X. B.; Narayanan, R.; El-Sayed, M. A., Chemistry and properties of nanocrystals of different shapes. *Chemical Reviews* **2005,** *105* (4), 1025-1102.
7. (a) Loss, D.; DiVincenzo, D. P., Quantum computation with quantum dots. *Physical Review A* **1998,** *57* (1), 120-126; (b) Chan, W. C. W.; Nie, S. M., Quantum dot bioconjugates for ultrasensitive nonisotopic detection. *Science* **1998,** *281* (5385), 2016-2018; (c) Bruchez, M.; Moronne, M.; Gin, P.; Weiss, S.; Alivisatos, A. P., Semiconductor nanocrystals as fluorescent biological labels. *Science* **1998,** *281* (5385), 2013-2016.
8. (a) Moniruzzaman, M.; Winey, K. I., Polymer nanocomposites containing carbon nanotubes. *Macromolecules* **2006,** *39* (16), 5194-5205; (b) Samir, M.; Alloin, F.; Dufresne, A., Review of recent research into cellulosic whiskers, their properties and their application in nanocomposite field. *Biomacromolecules* **2005,** *6* (2), 612-626; (c) Ray, S. S.; Okamoto, M., Polymer/layered silicate nanocomposites: a review from preparation to processing. *Progress in Polymer Science* **2003,** *28* (11), 1539-1641; (d) Bulte, J. W. M.; Douglas, T.; Witwer, B.; Zhang, S. C.; Strable, E.; Lewis, B. K.; Zywicke, H.; Miller, B.; van Gelderen, P.; Moskowitz, B. M.; Duncan, I. D.; Frank, J. A., Magnetodendrimers allow endosomal magnetic labeling and in vivo tracking of stem cells. *Nature Biotechnology* **2001,** *19* (12), 1141-1147; (e) Gangopadhyay, R.; De, A., Conducting polymer nanocomposites: A brief overview. *Chemistry of Materials* **2000,** *12* (3), 608-622; (f) Suryanarayana, C., NANOCRYSTALLINE MATERIALS. *International Materials Reviews* **1995,** *40* (2), 41-64; (g) Woan, K.; Pyrgiotakis, G.; Sigmund, W., Photocatalytic Carbon-Nanotube-TiO2 Composites. *Advanced Materials* **2009,** *21* (21), 2233-2239; (h) Ramanavicius, A.; Ramanaviciene, A.; Malinauskas, A., Electrochemical sensors based on conducting polymer-polypyrrole. *Electrochimica Acta* **2006,** *51* (27), 6025-6037; (i) Lira-Cantu, M.; Krebs, F. C., Hybrid solar cells based on MEH-PPV and thin film semiconductor oxides (TiO2, Nb2O5, ZnO, CeO(2)and CeO2-TiO2): Performance improvement during long-time irradiation. *Solar Energy Materials and Solar Cells* **2006,** *90* (14), 2076-2086; (j) Long, Y. Z.; Chen, Z. J.; Duvail, J. L.; Zhang, Z. M.; Wan, M. X., Electrical and magnetic properties of polyaniline/Fe3O4 nanostructures. *Physica B-Condensed Matter* **2005,** *370* (1-4), 121-130; (k) Bakueva, L.; Musikhin, S.; Hines, M. A.; Chang, T. W. F.; Tzolov, M.; Scholes, G. D.; Sargent, E. H., Size-tunable infrared (1000-1600 nm) electroluminescence from PbS quantum-dot nanocrystals in a semiconducting polymer. *Applied Physics Letters* **2003,** *82* (17), 2895-2897; (l) Wang, H.; Xu, J. Z.; Zhu, J. J.; Chen, H. Y., Preparation of CuO nanoparticles by microwave irradiation. *Journal of Crystal Growth* **2002,** *244* (1), 88-94; (m) Godovsky, D. Y., Device applications of polymer-nanocomposites. In *Biopolymers/Pva*

Hydrogels/Anionic Polymerisation Nanocomposites, Abe, A., Ed. 2000; Vol. 153, pp 163-205.

9. (a) Saupe, G. B.; Waraksa, C. C.; Kim, H. N.; Han, Y. J.; Kaschak, D. M.; Skinner, D. M.; Mallouk, T. E., Nanoscale tubules formed by exfoliation of potassium hexaniobate. *Chemistry of Materials* **2000,** *12* (6), 1556-1562; (b) Kudo, A.; Sayama, K.; Tanaka, A.; Asakura, K.; Domen, K.; Maruya, K.; Onishi, T., NICKEL-LOADED K4NB6O17 PHOTOCATALYST IN THE DECOMPOSITION OF H2O INTO H-2 AND O-2 - STRUCTURE AND REACTION-MECHANISM. *Journal of Catalysis* **1989,** *120* (2), 337-352; (c) Kudo, A.; Tanaka, A.; Domen, K.; Maruya, K.; Aika, K.; Onishi, T., PHOTOCATALYTIC DECOMPOSITION OF WATER OVER NIO-K4NB6O17 CATALYST. *Journal of Catalysis* **1988,** *111* (1), 67-76; (d) Domen, K.; Kudo, A.; Shibata, M.; Tanaka, A.; Maruya, K.; Onishi, T., NOVEL PHOTOCATALYSTS, ION-EXCHANGED K4NB6O17, WITH A LAYER STRUCTURE. *Journal of the Chemical Society-Chemical Communications* **1986,** (23), 1706-1707.
10. (a) Sayama, K.; Tanaka, A.; Domen, K.; Maruya, K.; Onishi, T., PHOTOCATALYTIC DECOMPOSITION OF WATER OVER PLATINUM-INTERCALATED K4NB6O17. *Journal of Physical Chemistry* **1991,** *95* (3), 1345-1348; (b) Miyamoto, N.; Yamamoto, H.; Kaito, R.; Kuroda, K., Formation of extraordinarily large nanosheets from K4Nb6O17 crystals. *Chemical Communications* **2002,** (20), 2378-2379; (c) Sayama, K.; Arakawa, H.; Domen, K., Photocatalytic water splitting on nickel intercalated A(4)Ta(x)Nb(6-x)O(17) (A=K, Rb). *Catalysis Today* **1996,** *28* (1-2), 175-182; (d) Yao, Y.; Chaubey, G. S.; Wiley, J. B., Fabrication of Nanopeapods: Scrolling of Niobate Nanosheets for Magnetic Nanoparticle Chain Encapsulation. *J. Am. Chem. Soc.* **2012,** *134* (5), 2450-2452.
11. Pian, X. T.; Lin, B. Z.; Chen, Y. L.; Kuang, J. D.; Zhang, K. Z.; Fu, L. M., Pillared Nanocomposite TiO2/Bi-Doped Hexaniobate with Visible-Light Photocatalytic Activity. *J. Phys. Chem. C* **2011,** *115* (14), 6531-6539.
12. Sarac, F. E.; Yilmaz, C.; Acar, F. Y.; Unal, U., CdTe quantum dot sensitized hexaniobate nanoscrolls and their photoelectrochemical properties. *Rsc Advances* **2012,** *2* (27), 10182-10184.
13. Lal, S.; Link, S.; Halas, N. J., Nano-optics from sensing to waveguiding. *Nature Photonics* **2007,** *1* (11), 641-648.
14. (a) Steele, B. C. H.; Heinzel, A., Materials for fuel-cell technologies. *Nature* **2001,** *414* (6861), 345-352; (b) Xu, C. W.; Wang, H.; Shen, P. K.; Jiang, S. P., Highly ordered Pd nanowire arrays as effective electrocatalysts for ethanol oxidation in direct alcohol fuel cells. *Adv. Mater.* **2007,** *19* (23), 4256-+.
15. Kong, J.; Franklin, N. R.; Zhou, C. W.; Chapline, M. G.; Peng, S.; Cho, K. J.; Dai, H. J., Nanotube molecular wires as chemical sensors. *Science* **2000,** *287* (5453), 622-625.
16. (a) Geim, A. K.; Novoselov, K. S., The rise of graphene. *Nature Materials* **2007,** *6* (3), 183-191; (b) Sgobba, V.; Guldi, D. M., Carbon nanotubes-electronic/electrochemical properties and application for nanoelectronics and photonics. *Chemical Society Reviews* **2009,** *38* (1), 165-184; (c) Wang, C. G.; Chen, J.; Talavage, T.; Irudayaraj, J., Gold Nanorod/Fe3O4 Nanoparticle "Nano-Pearl-Necklaces" for Simultaneous Targeting, Dual-Mode Imaging, and Photothermal Ablation of Cancer Cells. *Angewandte Chemie-International Edition* **2009,** *48* (15), 2759-2763.
17. Adireddy, S.; Yao, Y.; He, J.; Wiley, J. B., Rapid solvothermal fabrication of hexaniobate nanoscrolls. *Materials Research Bulletin* (0).

18. Wu, B. H.; Guo, C. Y.; Zheng, N. F.; Xie, Z. X.; Stucky, G. D., Nonaqueous Production of Nanostructured Anatase with High-Energy Facets. *Journal of the American Chemical Society* **2008,** *130* (51), 17563-17567.
19. Joo, J.; Na, H. B.; Yu, T.; Yu, J. H.; Kim, Y. W.; Wu, F. X.; Zhang, J. Z.; Hyeon, T., Generalized and facile synthesis of semiconducting metal sulfide nanocrystals. *J. Am. Chem. Soc.* **2003,** *125* (36), 11100-11105.
20. Liu, L. P.; Zhuang, Z. B.; Xie, T.; Wang, Y. G.; Li, J.; Peng, Q.; Li, Y. D., Shape Control of CdSe Nanocrystals with Zinc Blende Structure. *J. Am. Chem. Soc.* **2009,** *131* (45), 16423-16429.
21. Wang, C.; Yin, H. G.; Chan, R.; Peng, S.; Dai, S.; Sun, S. H., One-Pot Synthesis of Oleylamine Coated AuAg Alloy NPs and Their Catalysis for CO Oxidation. *Chemistry of Materials* **2009,** *21* (3), 433-435.
22. Saruyama, M.; Kanehara, M.; Teranishi, T., Drastic Structural Transformation of Cadmium Chalcogenide Nanoparticles Using Chloride Ions and Surfactants. *J. Am. Chem. Soc.* **2010,** *132* (10), 3280-+.
23. Han, X.; Wang, X.; Xie, S.; Kuang, Q.; Ouyang, J.; Xie, Z.; Zheng, L., Carbonate ions-assisted syntheses of anatase TiO2 nanoparticles exposed with high energy (001) facets. *Rsc Advances* **2012,** *2* (8), 3251-3253.
24. Adireddy, S.; Yao, Y.; He, J.; Wiley, J. B., Rapid solvothermal fabrication of hexaniobate nanoscrolls. *Materials Research Bulletin* **2013,** *48* (9), 3236-3241.
25. (a) Chan, G. H.; Zhao, J.; Hicks, E. M.; Schatz, G. C.; Van Duyne, R. P., Plasmonic properties of copper nanoparticles fabricated by nanosphere lithography. *Nano Letters* **2007,** *7* (7), 1947-1952; (b) Haes, A. J.; Zou, S. L.; Schatz, G. C.; Van Duyne, R. P., Nanoscale optical biosensor: Short range distance dependence of the localized surface plasmon resonance of noble metal nanoparticles. *Journal of Physical Chemistry B* **2004,** *108* (22), 6961-6968; (c) Chen, D. H.; Chen, C. J., Formation and characterization of Au-Ag bimetallic nanoparticles in water-in-oil microemulsions. *Journal of Materials Chemistry* **2002,** *12* (5), 1557-1562; (d) Rivas, L.; Sanchez-Cortes, S.; Garcia-Ramos, J. V.; Morcillo, G., Mixed silver/gold colloids: A study of their formation, morphology, and surface-enhanced Raman activity. *Langmuir* **2000,** *16* (25), 9722-9728; (e) Cepak, V. M.; Martin, C. R., Preparation and stability of template-synthesized metal nanorod sols in organic solvents. *Journal of Physical Chemistry B* **1998,** *102* (49), 9985-9990; (f) Grabar, K. C.; Freeman, R. G.; Hommer, M. B.; Natan, M. J., PREPARATION AND CHARACTERIZATION OF AU COLLOID MONOLAYERS. *Analytical Chemistry* **1995,** *67* (4), 735-743.
26. (a) Wilson, O. M.; Scott, R. W. J.; Garcia-Martinez, J. C.; Crooks, R. M., Synthesis, characterization, and structure-selective extraction of 1-3-nm diameter AuAg dendrimer-encapsulated bimetallic nanoparticles. *J. Am. Chem. Soc.* **2005,** *127* (3), 1015-1024; (b) Pillalamarri, S. K.; Blum, F. D.; Tokuhiro, A. T.; Bertino, M. F., One-pot synthesis of polyaniline - Metal nanocomposites. *Chemistry of Materials* **2005,** *17* (24), 5941-5944; (c) Zhao, M. Q.; Crooks, R. M., Intradendrimer exchange of metal nanoparticles. *Chemistry of Materials* **1999,** *11* (11), 3379-3385.
27. Ghosh, S. K.; Pal, T., Interparticle coupling effect on the surface plasmon resonance of gold nanoparticles: From theory to applications. *Chemical Reviews* **2007,** *107* (11), 4797-4862.
28. (a) Perim, E.; Galvao, D. S., The structure and dynamics of boron nitride nanoscrolls. *Nanotechnology* **2009,** *20* (33); (b) Braga, S. F.; Coluci, V. R.; Legoas, S. B.; Giro, R.;

Galvao, D. S.; Baughman, R. H., Structure and dynamics of carbon nanoscrolls. *Nano Letters* **2004,** *4* (5), 881-884.
29. (a) He, J. B.; Kanjanaboos, P.; Frazer, N. L.; Weis, A.; Lin, X. M.; Jaeger, H. M., Fabrication and Mechanical Properties of Large-Scale Freestanding Nanoparticle Membranes. *Small* **2010,** *6* (13), 1449-1456; (b) Pocovi-Martinez, S.; Frances-Soriano, L.; Zaballos-Garcia, E.; Scaiano, J. C.; Gonzalez-Bejar, M.; Perez-Prieto, J., CO2 switchable nanoparticles: reversible water/organic-phase exchange of gold nanoparticles by gas bubbling. *Rsc Advances* **2013,** *3* (15), 4867-4871.
30. Hiramatsu, H.; Osterloh, F. E., A simple large-scale synthesis of nearly monodisperse gold and silver nanoparticles with adjustable sizes and with exchangeable surfactants. *Chemistry of Materials* **2004,** *16* (13), 2509-2511.
31. Regev, O.; Backov, R.; Faure, C., Gold nanoparticles spontaneously generated in onion-type multilamellar vesicles. Bilayers-Particle coupling imaged by Cryo-TEM. *Chemistry of Materials* **2004,** *16* (25), 5280-5285.
32. (a) De, M.; Ghosh, P. S.; Rotello, V. M., Applications of Nanoparticles in Biology. *Advanced Materials* **2008,** *20* (22), 4225-4241; (b) Huang, X. H.; Jain, P. K.; El-Sayed, I. H.; El-Sayed, M. A., Gold nanoparticles: interesting optical properties and recent applications in cancer diagnostic and therapy. *Nanomedicine* **2007,** *2* (5), 681-693; (c) Sharma, P.; Brown, S.; Walter, G.; Santra, S.; Moudgil, B., Nanoparticles for bioimaging. *Advances in Colloid and Interface Science* **2006,** *123*, 471-485; (d) Wang, L. Y.; Luo, J.; Fan, Q.; Suzuki, M.; Suzuki, I. S.; Engelhard, M. H.; Lin, Y. H.; Kim, N.; Wang, J. Q.; Zhong, C. J., Monodispersed core-shell Fe3O4@Au nanoparticles. *Journal of Physical Chemistry B* **2005,** *109* (46), 21593-21601; (e) Pellegrino, T.; Kudera, S.; Liedl, T.; Javier, A. M.; Manna, L.; Parak, W. J., On the development of colloidal nanoparticles towards multifunctional structures and their possible use for biological applications. *Small* **2005,** *1* (1), 48-63; (f) Gillen, G.; Roberson, S., Preliminary evaluation of an SF5+ polyatomic primary ion beam for analysis of organic thin films by secondary ion mass spectrometry. *Rapid Communications in Mass Spectrometry* **1998,** *12* (19), 1303-1312; (g) Narayanaswamy, R.; Young, M. A.; Parkhurst, E.; Ouellette, M.; Kerr, M. E.; Ho, D. M.; Elder, R. C.; Bruce, A. E.; Bruce, M. R. M., SYNTHESIS, STRUCTURE, AND ELECTRONIC SPECTROSCOPY OF NEUTRAL, DINUCLEAR GOLD(I) COMPLEXES - GOLD(I)-GOLD(I) INTERACTIONS IN SOLUTION AND IN THE SOLID-STATE. *Inorganic Chemistry* **1993,** *32* (11), 2506-2517.

Chapter 5

Conclusions

In this dissertation, synthesis of various morphologically uniform hexaniobate-based nanocomposites has been described via non-aqueous solvothermal reactions. Initially, we have developed an effective solvothermal synthetic approach that led to the formation of bulk quantities of high-quality simple (SNS) and intercalated nanoscrolls (INS). The exfoliation/scrolling process was investigated using time-temperature dependent experiments, revealing the formation of nanoscrolls. In contrast to the former aqueous methods of exfoliation and scrolling of individual nanosheets, our new non-aqueous solvothermal methods provide unique means for nanocomposites fabrication. This strategy was successfully utilized in capturing nanoparticles for the formation of nanopeapod-type (NPP) structures. Such morphologically controlled novel nanocomposites should be critical in the development of new nanocomposites for future energy applications. This finding marks an important contribution to the fabrication of future hexaniobate-based photocatalysts.

This solvothermal synthetic method represents a new strategy for control of in NPP fabrication with advantages including; (1) flexibility in combining the pea and pod components independently, (2) controlled chemical composition and tunable surface functionalization of NPPs, and (3) wide range applicability to the controlled encapsulation of various magnetic and non-magnetic NPs. The effectiveness of such encapsulation has been highlighted by showing the morphologies of eight new NPPs. This approach should not only lead to products with improved properties, but also provide an opportunity to design new nanostructures with potential applications in many fields. Further, beyond the systems studied in this dissertation, there are

numerous other materials that could be incorporated into new nanocomposites following similar routes.

NPPs comprised of hexaniobate-encapsulated NP chains were produced through a versatile solvothermal process in high yields. This method allows for control of reaction temperature and time, type of surfactant, and solvents to improve the overall yield and morphology of NPPs. While the solvothermal experimental results provided insights about the encapsulation process, additional open-air non-aqueous experiments at 50 °C were needed to observe the *in-situ* Au NP growth. NP morphology was found to be another key parameter since particle size determines the inner scroll diameter, and the filling fraction of NPPs was highly sensitive to the NP size and shape. It is likely that NPs that are captured initially serve as size and shape determining agents for the NPP formation. The encapsulation process was investigated by TEM, revealing the morphological uniformity of wide-variety of NPPs. STEM EDS experiments were performed to investigate the chemical identities of building blocks in multi-functional architectures.

This approach was successfully applied to the fabrication of eight new hexaniobate based nanocomposites. Scrolling nanosheets successfully encapsulated MFe_2O_4 (Fe_3O_4, $CoFe_2O_4$, $NiFe_2O_4$, and $ZnFe_2O_4$), TiO_2, CdS, CdSe, Zns, Ag, Au and Au-Fe_3O_4 NP chain to form NPPs. The increased coercivity in magnetic NPPs was highlighted in Chapter 3, confirming the contribution of improved magnetic interactions in the longer NP chains. Shape selectivity has been highlighted by TiO_2@hexaniobate NPPs. This ability further demonstrated the extensive tunability available in NPP systems where one can fabricate Ag-hexaniobate nanocomposites. The resulting products are almost exclusively Ag modified hexaniobate nanosheets and nanoscrolls in addition to Ag-hexaniobate NPPs. This method was also successfully extended to

the fabrication of novel bi-functional Au-Fe_3O_4@hexaniobate NPPs (Chapter 4). In this approach, the non-aqueous method was applied to *in situ* growth of Au NPs inside the Fe_3O_4@hexaniobate NPPs. The size of Au NPs was observed to be similar to Fe_3O_4 NPs which were already present inside the nanoscroll. Our methods should allow for possible improvement in the photocatalytic properties of hexaniobate.

As the preceding discussion has clearly shown, the non-aqueous solvothermal approach to fabricating—and even *in situ* growth—shape and size selectivity in exfoliated hexaniobate nanosheets is based on a number of simple synthetic steps. But the success of the approach, as illustrated by the specific NP combinations mentioned in this dissertation, emboldens us to conclude that a fairly simple but versatile and cost-effective solvothermal synthetic approach will produce materials with great morphological uniformity. At present, the methods that enable nanoscroll fabrications involve a significant tunability, for they are not suitable for capturing a wide-variety of non-polar NPs, nor high-temperature or pressure based reaction conditions. Future experiments will investigate the effects of more than three different NP combinations and how their relative sizes affect encapsulation, and additional thermodynamic and kinetic modeling may be needed in order to predict the interparticle interactions.

The series of solvothermal synthetic procedures summarized in this account are readily applicable and highly reproducible for the large-scale synthesis of NPPs. In the future, obtaining a detailed understanding of NPP formation mechanism will lead to the fabrication of various nanocomposites with controlled morphology, and chemical composition. In particular, the synthesis of uniform NPPs with larger (≥15 nm) NPs is still very much a challenge. Controlled capturing of various NP chains can provide means for precisely tailoring optical, electronic, and

mechanical properties as well as controlling quantum and classical coupling interactions, ultimately leading to the optimization of photocatalytic and magnetic applications of NPPs.

The synthetic routes described in this dissertation are not only important to understanding some underlying details of advanced materials assembly, but have broader implications in developing magnetically separable future photo-catalytic devices that seek to integrate hexaniobate-based components with magnetic, plasmonic, and quantum dot building blocks. If effective materials assembly is accomplished and successfully used to produce novel photocatalysts that allow us to produce renewable green energy more efficiently instead of increasingly scarce fossil fuels. We expect that these series of versatile synthetic approaches will be invaluable in this regard as well, by delivering increasingly detailed synthetic insights into the nucleation, crystal growth and assembly of nanomaterials building blocks that might eventually allow us to rationally direct and control these processes such that they form desired new nanoarchitectures. With the development of more novel synthetic strategies to direct the fabrication of highly-ordered nanoscale materials, it is expected that hexaniobate-based assembly will play a crucial role in the future of optical, magnetic, and electronic devices.

Appendix

Additional Information

Experimental Details for Figure A.1.: Ferromagnetic resonance (FMR) measurements were performed on a Bruker EMX spectrometer operating at 9.44 GHz (X-band) with a modulation field frequency of 100 kHz, an amplitude of H_{mod} = 3 Oe and operating microwave power (P) of 0.35 mW. In a typical experiment, the magnetic field was driven from H = 0 Oe to 8 kOe, with a sweep time (τ) of ~ 41 s (195 Oe/s). A commercial nitrogen gas flow cryostat was used in the temperature range of 100 - 300 K. The cavity itself was kept at room temperature and its quality factor did not change upon cooling. The samples were prepared as colloidal solutions in toluene (freezing point ~ 178 K), and supported in commercial fused silica EPR tube. Frozen samples were prepared by two different experimental protocols; in the zero-field-cooling (ZFC) experiment the sample was frozen in the absence of an applied magnetic field and in the field-cooling (FC) experiment the sample was frozen in a persistent magnetic field of 8 kOe.

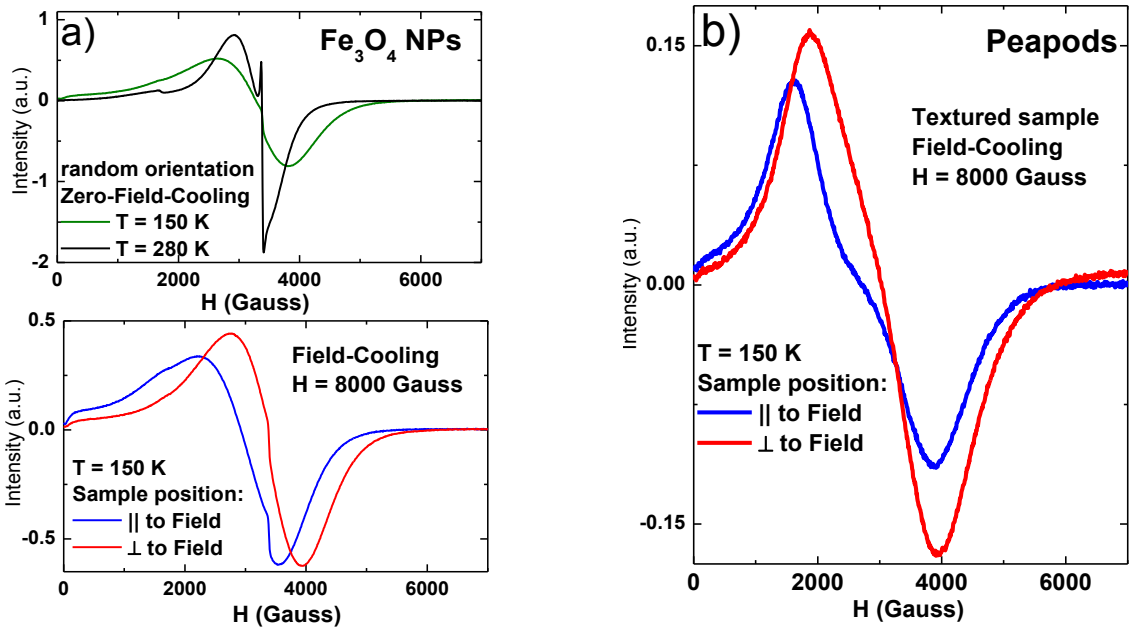

Figure A.1. (a) FMR, X-band (9.44 GHz) spectra of the colloidal Fe_3O_4 NPs measured in ZFC and FC conditions. In the FC condition, the spectra were collected with magnetic field parallel and perpendicular to the frozen magnetic axis of the sample; (b) FMR spectra of the Fe_3O_4 NPs inside of the nanoscrolls at 150 K, with magnetic field applied parallel and perpendicular to the nanochannels.

Experimental Details for Figure A.2.: X-ray photoelectron spectra (XPS) were collected by Kratos AXIS 165 instrument at Material Characterization Center, Louisiana State University (LSU). X-ray absorption near-edge spectroscopy (XANES) measurements were carried out at the variable line spacing plane grating monochromator (VLSPGM) beamline with an operational photon energy range between 200 eV and 1000 eV at the Center for Advanced Microstructures & Devices (CAMD) synchrotron. Samples were mounted inside a ultrahigh-vacuum chamber and the absorption measured via sample current (total electron yield mode).

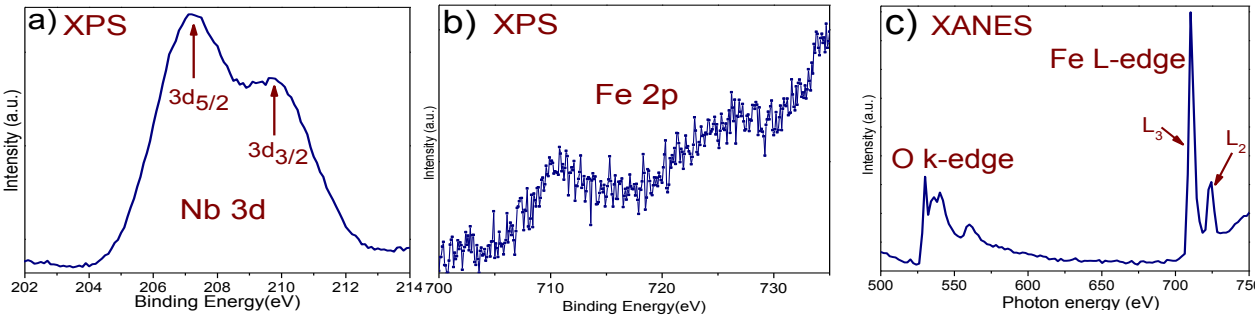

Figure A.2. XPS spectrum of nanopeapods (a) Nb 3d; (b) Fe 2p; (c) XANES data for Fe $L_{3,2}$-edge

VITA

Shivaprasad Reddy Adireddy was born in Suryapet, in the state of Telangana, India. He is the eldest son of Mr. Venkat Reddy and Mrs. Achamma. He was admitted into the Bachelor of Science program at Osmania University (OU), Hyderabad, India, with mathematics, physics, and chemistry as his majors. He graduated in May 2005 and joined Master's program at OU, organic chemistry major. He obtained master's degree from OU in May 2007. In August 2008, he was admitted into the graduate program in Advanced Materials research institute (AMRI), Department of Chemistry at the University of New Orleans, New Orleans, LA, USA. He obtained Master's degree in Materials Chemistry in spring 2011 and was accepted in Prof. John B. Wiley's research group in November 2011 for pursuing a Ph.D. in Nanomaterials Chemistry.